FEASIBILITY OF FLUXLESS SMELTING OF TITANIFEROUS MAGNETITE ORE IN A PILOT-PLANT OPEN-ARC DC FURNACE

by

Isabella Johanna Geldenhuys

Thesis presented in partial fulfilment
of the requirements for the Degree

of

MASTER OF ENGINEERING
EXTRACTIVE METALLURGICAL ENGINEERING

in the Faculty of Engineering
at Stellenbosch University

Supervisor

Professor Guven Akdogan

Co-Supervisor

Dr Quinn Reynolds

March 2020

DECLARATION

By submitting this thesis electronically, I declare that the entirety of the work contained therein is my own, original work, that I am the sole author thereof (save to the extent explicitly otherwise stated), that reproduction and publication thereof by Stellenbosch University will not infringe any third party rights and that I have not previously in its entirety or in part submitted it for obtaining any qualification.

Date: *March 2020*

PLAGIARISM DECLARATION

1. Plagiarism is the use of ideas, material and other intellectual property of another's work and to present it as my own.

2. I agree that plagiarism is a punishable offence because it constitutes theft.

3. I also understand that direct translations are plagiarism.

4. Accordingly, all quotations and contributions from any source whatsoever (including the internet) have been cited fully. I understand that the reproduction of text without quotation marks (even when the source is cited) is plagiarism.

5. I declare that the work contained in this assignment, except where otherwise stated, is my original work and that I have not previously (in its entirety or in part) submitted it for grading in this module/assignment or another module/assignment.

March 2020

ABSTRACT

Titaniferous magnetite (titanomagnetite) is nominally defined as magnetite deposits containing more than one mass percent of titanium dioxide (TiO_2). Titanomagnetite deposits are known for being difficult to process; this is primarily due to the complex nature of the mineral compounds that make up the ore. The complex mineralisation means chemical upgrading processes are needed to derive economic value from the ore. While titanomagnetite deposits are widely processed for the recovery of vanadium, or vanadium and iron, titanium is not commercially recovered. The current study reviews the feasibility to extract iron and vanadium while producing a high-titanium slag via fluxless smelting in an open-arc direct current (DC) furnace. The study evaluated the technical feasibility via a pilot-scale study and furthermore considered the viability of the titania-rich furnace slag produced during the study, as a potential feedstock for the production of pigment and metal. Fluxless smelting could offer an opportunity to unlock all three valuable commodities from South Africa's Bushveld Complex, the largest known deposit of its kind in the world. The demise of Highveld Steel and Vanadium has created an opportunity to implement the best available technology for this complex ore, leveraging the know-how and experiences of the ilmenite smelting industry in South Africa.

A pilot-scale DC furnace was operated continuously for 17 days at power levels of up to 1.3 MW. During the smelting test, 108 tons of titaniferous magnetite concentrate was processed. Smelting of the concentrate involved a simple recipe which comprised of concentrate and low-ash anthracite fed to the furnace in the desired proportion to achieve the targeted metallurgical result, namely an undiluted titania-rich slag and a vanadium-bearing iron product. The test demonstrated that slag composition by virtue of the degree of reduction could be optimised for the desired specification, namely slag containing at least 85% TiO_2. Due to the nature of open-arc smelting, the furnace can be operated to optimise metallurgy and is not constrained with respect to the operating power. Slag containing 89% TiO_2 was consistently produced demonstrating the production of high-grade titania slag in the absence of fluxes. Phase chemically the slags were found to be dominated by the presence of an M_3O_5 phase (where M = Fe, Ti, Mg, Al and Mn), which is also typical of high-titania slags produced from the smelting of ilmenite. The compositional invariance observed for industrial ilmenite slags was established to also apply to the slags produced during the current study. Slags produced from titaniferous magnetite deposits will compete with higher grade titania feedstocks. The fact that the slags produced during the study resembled industrial slags is encouraging. A flowsheet was developed based on the outcomes from the pilot test, namely a mass and energy balance for fluxless smelting of titaniferous magnetite in a DC furnace. A detailed benchmarking study would be required to assess the economic viability in a highly competitive market.

The results from the study supported the premise that the comprehensive processing of vanadium-bearing titaniferous magnetite deposits is technically feasible. The outcomes provide valuable insights into the behaviour of a fluxless titaniferous magnetite smelting process, presents a foundation for future work, and improves the general understanding of the requirements, challenges and benefits of fluxless smelting of titanomagnetite ores.

OPSOMMING

Titaanhoudende magnetiet (titanomagnetiet) word nominaal gedefinieer as magnetietdepositos wat meer as een massa persent van titaniumdioksied (TiO_2) bevat. Titanomagnetietdepositos is bekend om moeilik te wees om te prosesseer; dis hoofsaaklik as gevolg van die komplekse aard van die mineraalsamestellings waaruit die erts bestaan. Die komplekse mineralisasie beteken chemiese opgraderingprosesse word benodig om ekonomiese waarde uit die erts te verkry. Terwyl titanomagnetietdepositos algemeen geprosesseer word vir die herwinning van vanadium, of vanadium en yster, is titanium nog nie kommersieel herwin nie. Die huidige studie beoordeel die uitvoerbaarheid daarvan om yster en vanadium te ekstraheer terwyl ’n hoë titaniumslak via flukslose smelting in ’n oopboog direkte stroom (DC) oond geproduseer word. Die studie evalueer die tegniese uitvoerbaarheid via ’n loodsskaalstudie en het verder die lewensvatbaarheid van die titaniumryke oondslak geproduseer deur die studie oorweeg as ’n potensiële voermateriaal vir die produksie van pigment en metaal. Flukslose smelting kan ’n geleentheid skep om al drie waardevolle kommoditeite uit Suid-Afrika se Bosveld Kompleks te ontsluit, die grootste bekende deposito van sy soort in die wêreld. Die ondergang van *Highveld Steel and Vanadium* het ’n geleentheid geskep om die beste beskikbare tegnologie vir hierdie komplekse erts te implementeer, wat die kennis en ondervinding van die ilmenietsmeltingindustrie in Suid-Afrika gebruik.

’n Loodsskaal DC-oond is aaneenlopend vir 17 dae by kragvlakke van tot en met 1.3 MW bedryf. Tydens die smeltingtoets is 108 ton titaanhoudende magnetietkonsentraat geprosseseer. Smelting van die konsentraat het ’n eenvoudiger resep behels wat bestaan het uit konsentraat en lae-as antrasiet in die oonde gevoer in die gewenste proporsie om die doelwit metallurgiese resultaat te kry, naamlik ’n onverdunde titania-ryke slak en ’n vanadium-draende yster produk. Die toets het gedemonstreer dat slakkomposisie op grond van die grade van reduksie geoptimeer kan word vir die gewenste spesifikasie, naamlik slak wat ten minste 85% TiO_2 bevat. As gevolg van die aard van oopboogsmelting, kan die oond bedryf word om metallurgie te optimeer en is nie beperk ten opsigte van die bedryfskrag nie. Slak wat 89% TiO_2 bevat, is konstant geproduseer wat die produksie van hoë-graad titaniaslak in die afwesigheid van flukse demonstreer. Fase chemies is die slak gevind om gedomineer te wees deur die teenwoordigheid van ’n M_3O_5- fase (waar M = Fe, Ti, Mg, Al en Mn), wat ook tipies is van hoë titaniaslakke geproduseer uit die smelting van ilmeniet. Die komposisionele onveranderlike waargeneem vir industriële ilmenietslakke is vasgestel om ook op die slakke geproduseer in die huidige studie, toepaslik te wees. Slakke geproduseer uit titaanhoudende magnetietdepositos sal kompeteer met hoër graad titaniavoermateriaal. Die feit dat die slakke geproduseer in die studie aard na die industriële slakke, is bemoedigend. ’n Vloeidiagram is ontwikkel gebaseer op die uitkomste van hierdie loodstoets, naamlik ’n massa- en energiebalans vir flukslose smelting van titaanhoudende magnetiet in ’n DC-oond. ’n Gedetaileerde normstudie word benodig om die ekonomiese lewensvatbaarheid in ’n hoogs kompeterende mark te assesseer.

Die resultate van die studie ondersteun die veronderstelling dat die omvattende prosessering van vanadiumhoudende titaanhoudende magenetietdepositos tegnies uitvoerbaar is. Die uitkomstes lewer waardevolle insig in die gedrag van ’n flukslose titaanhoudende magnetietsmeltingsproses, lewer ’n fondasie vir toekomstige werk, en verbeter die algemene verstaan van die vereistes, uitdagings en voordele van flukslose smelting van titanomagnetietertse.

To Carl, because the vastness of space and time
is bearable only through love.

ACKNOWLEDGEMENTS

There are a number of people without whom this thesis might not have been written, and to whom I am greatly indebted on the journey of life. I am grateful to colleagues for sharing their ideas and inspiring me to have my own. There are too many to mention all by name, but I would like to particularly thank Tom Curr, Nic Barcza, Rodney Jones, Glen Denton and Markus Erwee for the role they played in my journey.

MINTEK's financial support for this study is gratefully acknowledged. This project would not have been possible without the assistance, and hard work of the shift workers that supported me throughout the pilot-plant campaign. The support from my supervisors are gratefully acknowledged.

TABLE OF CONTENTS

LIST OF FIGURES

LIST OF TABLES

1 INTRODUCTION

The background, aim and purpose of this thesis are described as an introduction to what is a broad topic, namely the pyrometallurgical processing of titaniferous ores.

This thesis specifically focuses on aspects of fluxless smelting of titaniferous magnetite in a direct current (DC) electric arc furnace as a potential technical solution for comprehensive utilisation of titaniferous magnetite ore from South Africa's Bushveld Complex.

Fluxless smelting has the potential benefit of efficiently recovering iron, vanadium as well as titanium. Current smelting practices recover iron and vanadium while discarding the slag as waste, namely as a diluted titania-containing slag. The slag dumps generated through the current fluxed smelting approaches have created a significant environmental legacy for countries such as South Africa and China, while also not recovering the full potential value from the ore.

1.1 BACKGROUND AND GENERAL STATEMENT OF THE PROBLEM

The reasons why this thesis of interest to industry is briefly introduced and described as an introduction to the topic.

The Bushveld Complex is a large and complex deposit in South Africa on which a number of industries are built. The total aerial extent of Bushveld limbs exceeds 65 000 km². The Bushveld Complex hosts well over half the world's resources in chromium and platinum group metals (PGM). Vanadium is present in the magnetite's coarse-grained mafic rocks (Cawthorn *et al.*, 2005). The Bushveld Complex is said to constitute about 30% of known vanadium ore deposits (U.S. Geological Survey, 2017) and the abundance and scale of this titaniferous deposit represent a long-term opportunity for South Africa.

Efficient recovery of titanium from titaniferous magnetite ores continues to remain a promising, yet unrealised opportunity, despite significant occurrences of titaniferous magnetite (titanomagnetite) deposits worldwide, and the existence of established industrial-scale practices. Current smelting processes only recover iron and vanadium, while the bulk of the titanium content is discarded as waste slag (Fischer, 1975; Reynolds, 1985; Rohrmann, 1985; U.S. Geological Survey, 2016). In cases where the mineralogy allows, a small fraction of ilmenite is recovered during the ore preparation phase (before smelting), but the degree of recovery of titanium via this method is reportedly low due to the mineralogical characteristics of titanomagnetite ores (Chen & Chu, 2014a).

Titaniferous magnetite ore is predominantly processed via either blast furnace technology in ore-based ironmaking in China and Russia. The use of conventional blast furnace technology to process titaniferous magnetite is generally accepted as a challenging smelting practice. Without significant interventions, the hearth and tuyeres can block with highly refractory titanium carbide that is produced due to the very reducing conditions in a blast furnace. Russian and Chinese producers have been optimising the integration of titaniferous magnetite into blast furnaces since the 1960s. Successful blast furnace operations typically blend the magnetite with a good quality iron ore to dilute the titanium oxide to reduce the risk of hearth precipitation and thus subsequent operational challenges (Killick & Miller, 2014; Steinberg *et al.*, 2011). The conventional rotary kiln-electric furnace (RKEF) process is widely used for oxide ore smelting processes such as nickel, and in the 1960s, South Africa's Highveld Steel and Vanadium (Highveld Steel) and New Zealand Steel both adopted this technology principle for processing of vanadium-bearing titaniferous ores. In an RKEF flowsheet, the purpose of the kilns is to prereduce the relevant metal oxide using a low-cost energy source, such as pulverised coal, prior to smelting to lower the overall electrical energy requirement. In a typical RKEF process, the objective is to maximise the metallization of the metal of interest prior to smelting. For titaniferous magnetite ores, this translates to producing vanadium-rich pig iron via reductive smelting in the electric furnace; the vanadium is recovered post-taphole from the metal as a vanadium-rich slag. Highveld and New Zealand Steel adopted different approaches with respect to the pretreatment and the electric smelting operation, albeit both alternating current (AC) furnace technology. New Zealand Steel selected partially open bath operation, and foamy slag practises, while Highveld Steel implemented submerged-arc smelting mode (Hukkanen & Walden, 1985; Rohrmann, 1985; Steinberg *et al.*, 2011).

Smelting practices and a number of process facets relating to processing titaniferous magnetite ore via pyrometallurgical means are evaluated to present the case for producing a high-titania slag from titaniferous magnetite in an open-arc direct current (DC) furnace. The aim of the study is to evaluate the potential to extract not only the iron and vanadium but also to generate slag that can be used as a titania slag feedstock for the production of pigment or metal. The intent is to assess whether the slag produced via fluxless smelting in a DC furnace, could be an acceptable feedstock for beneficiation, despite being produced from a low-grade titania feedstock.

The goal of the current study is to evaluate the feasibility of fluxless smelting of the titaniferous magnetite ore in a DC arc furnace, as an alternative to current processing technologies for titaniferous magnetite ore, and potentially unlock this complex and abundant resource comprehensively.

1.2 Significance of the Research

In 2015 EVRAZ Highveld Steel and Vanadium closed down after about 50 years of processing titaniferous magnetite to recover primarily iron and vanadium (EVRAZ Highveld Steel and Vanadium, 2015; Rohrmann, 1985; Steinberg *et al.*, 2011). Large quantities of titania-bearing waste slag remains an environmental legacy for years to come. The impact of this closure is not easily quantified, but as a result, this well-endowed resource is currently mostly dormant. The loss of this smelting capacity is significant for both the local and global markets. In the context of the South African economy, the job losses alone are devastating. The current research presents a potential solution that could efficiently unlock the wealth of the Bushveld Complex for the country and potentially provide a long-term sustainable technology solution to process titaniferous magnetite in South Africa.

Inefficient processing of titaniferous magnetite, via the current smelting practices, results in an enormous environmental legacy. The Highveld Steel slag dump, for example, consists of about 45 million tons of slag (Avertana, 2017). The slag stockpile produced from the blast furnaces at Panzhihua is estimated by Chen et al. (2014b) to contain in excess of 70 million tons of slag (Liu et al. (2008) reported that the slag dumps contained 50 million tons in 2008). These numbers indicate that the Panzhihua site in China produced 20 million tons of waste slag in about 6 years or about 3 million tons of slag per annum. The slag dumps, located on the riverbanks of the Jinsha River, are a significant environmental legacy, apart from the fact that the resource is inefficiently processed. The unrecovered vanadium and titanium, and residual iron are locked in a highly diluted discard slag. The Highveld Steel slag dump, located near Emalahleni, Mpumalanga, also remains an environmental challenge, and it is said that the Department of Environmental Affairs has grave concerns about this liability and is enforcing that sale of assets includes a strategy to manage the dump. Thus far, no entity has been willing to take on the legacy of the slag dump as part of proposals to rescue parts of the complex (EVRAZ Highveld Steel and Vanadium, 2015).

The Bushveld Complex remains one of the world's most significant deposits of vanadiferous titanomagnetite, and the current study aims to assess the potential to unlock this deposit efficiently via a pilot smelting study. The test study demonstrated the feasibility of fluxless smelting of titaniferous magnetite ore, in an open-arc DC pilot plant furnace.

1.3 Thesis Delineation

The first sections consider available literature in the context of the objective of this study and summarise the nature, occurrence and abundance of titaniferous magnetite deposits, processing methods and perspectives on the three commodities of interest.

The pilot smelting study, which provides the experimental basis of this work, is presented following the conclusion of the literature review and development of a contextualised overview of smelting. The pilot study includes ad description of the design and construction of a pilot-scale furnace.

The experimental methodology, including characterisation of feed and products, is described, which includes a high-level summary of the furnace operation and operating conditions.

The results are discussed in the context of the research question, namely the feasibility of fluxless smelting of titaniferous magnetite in a direct current pilot-plant furnace.

The slag quality produced during the pilot study is evaluated in the context of the potential use as feedstock to the pigment industry, and finally, a flowsheet is proposed to extract iron, vanadium and titanium from titaniferous magnetite deposits using fluxless smelting in an open-arc furnace.

1.4 Definitions

Direct current open-arc furnace (DC furnace or DC arc furnace) refers to a pyrometallurgical vessel that comprises a cylindrical steel shell with a roof that is typically conical. It is lined inside with a refractory material in order to contain the molten materials being processed. The furnace usually has a centrally located graphite electrode, usually the cathode, and an anode embedded in the hearth (refractory lined base of the furnace); the metal in the furnace is in electrical contact with the anode. Energy is supplied to the furnace by an open plasma arc that impacts on the upper surface of the molten material (Jones *et al.*, 2011).

Sulfur is used as the preferred spelling based on the current convention ("Editorial: So long sulphur", 2009; Langslow, 1988).

The following definitions, abbreviations and nomenclature are used throughout, additional definitions are provided in the text.

ton	1 metric ton (1000 kg)
Fe_3O_4	magnetite
$FeTiO_3$	ilmenite
$Fe^{2+}(Fe^{3+},Ti^{3+})_2O_4$	titaniferous magnetite or titanomagnetite
TiO_2	rutile, titanium dioxide or titania
$\overline{x}$	mean or average
σ	standard deviation
tpa	ton per annum
DC	direct current
AC	alternating current

2 REVIEW OF RELATED LITERATURE

This section outlines an overview of the nature and occurrence of titaniferous magnetite deposits, as well as an overview of the pyrometallurgical processing practices associated with these ores.

The nature and occurrence of titaniferous (titania-bearing) magnetite deposits are well-known to be numerous and significant in size, especially in South Africa, where the dominance of the Bushveld Complex is a vital feature of the country's bountiful natural resources. Extraction of iron and vanadium from titaniferous magnetite ores is a well-established and mature technology, but complete utilisation, which includes recovering titanium and minimising environmental impact, has proved to be a multifaceted and frustrating challenge throughout the world.

Titanomagnetite ore is of importance to South Africa as one the world's most significant deposits of vanadiferous titanomagnetite is located in the well-known Bushveld Complex. The Bushveld Complex is said to constitute about 30% of known vanadium land-based deposits (U.S. Geological Survey, 2017).

2.1 THE NATURE AND OCCURRENCE OF TITANOMAGNETITE

Titaniferous magnetite (or titanomagnetite) ore is generically defined as being a magnetite ore containing more than one mass per cent titanium dioxide (TiO_2). Characteristically these ores are also vanadium-bearing (vanadiferous) and known to vary significantly in composition, with complex mineralisation (Fischer, 1975). Most titanomagnetite ores are low in sulfur and phosphorous and are therefore of interest as a source of iron. The global supply of low-phosphorous iron ores is declining (Dippenaar, 2005) and titanomagnetite has the potential to become increasingly important as iron ore in the future.

Vanadiferous titanomagnetite ores are widely reported to represent the bulk of primary ore-based feedstock of vanadium in the world. Vanadium recovery is an added incentive to process titanomagnetite ores. These ores are also frequently cited by researchers to be a potential source of titanium (as oxide); however, none of the current pyrometallurgical processes recovers titanium as a product from the smelting process. Most of the processes dilute titanium, via additives, to enable processing of the ore. Fluxing aims to optimise the recovery of iron and vanadium. The diluted titania slag is discarded to slag dumps, as a waste (Fischer, 1975; Roskill Information Services, 2010; U.S. Geological Survey, 2016).

Titanomagnetite ores exhibit what is referred to as presenting with a classic oxidation profile down to the water table (ranging from weathered to unweathered ore and containing within this profile, varying degrees of weathering). The changing mineralogical profile results in a wide range of behaviours or responses during metallurgical processing, especially as ores change from unweathered to highly weathered, oxidised ore (Cawthorn *et al.*, 2005; Connelly *et al.*, 2008; Fischer, 1975). The bulk chemical composition of these ores is also varied. Fischer (1975) reported the grade of the ores as follows: Fe content ranging from 16% to 60%, TiO_2 from 1.5% to 38% and V_2O_5 from 0.1% to 2%. The complex mineralisation of the ores results in limited upgrading potential (removal of gangue minerals to produce a higher grade concentrate, typically through physical beneficiation).

Methods commonly associated with iron ore or beach sand deposits usually do not provide significant upgrading benefit when applied to titanomagnetite ores. The reason for this limitation is due to the mineralisation of these ores. The primary metals in titanomagnetite, namely iron and titanium, occur within the structure as a mixture of magnetite (Fe_3O_4 or $FeO.Fe_2O_3$) and ilmenite ($FeTiO_3$), the latter is embedded within this mixture, usually in the form of finely dispersed granules, grains or thin layers (Fischer, 1975). Fine grinding does consequently not quantitatively unlock the constituent minerals. Some deposits allow for the recovery of a small fraction of titanium as an ilmenite concentrate, and some titania is recovered before smelting of the bulk ore. Recovery of ilmenite is typically not always feasible due to the complex mineralisation of the association of the minerals. Panzhihua (China) reportedly recovers about 25% titanium before smelting the magnetite ore in blast furnaces (Chen *et al.*, 2015).

As a result of the complex mineralogy and the physical variability, titanomagnetite ores are generally regarded as difficult to process, especially if compared to traditional iron ore or beach sand (containing ilmenite). Comprehensive utilisation of these ores thus requires the application of both physical and chemical methods. Despite these challenges, titanomagnetite is widely processed to recover iron and vanadium.

2.2 SIGNIFICANT DEPOSITS

Deposits of titanomagnetite are found in significant quantities throughout the world, generally reported via mineral inventory reports for vanadium (Fischer, 1975; Goldberg *et al.*, 1992). As most titaniferous magnetite deposits are vanadiferous, the data is a fair proxy of vanadium ore deposits throughout the world. Figure 2-1 shows the general global locations of vanadiferous magnetite deposits. It is clear that these ores are broadly distributed throughout the world (Goldberg *et al.*, 1992).

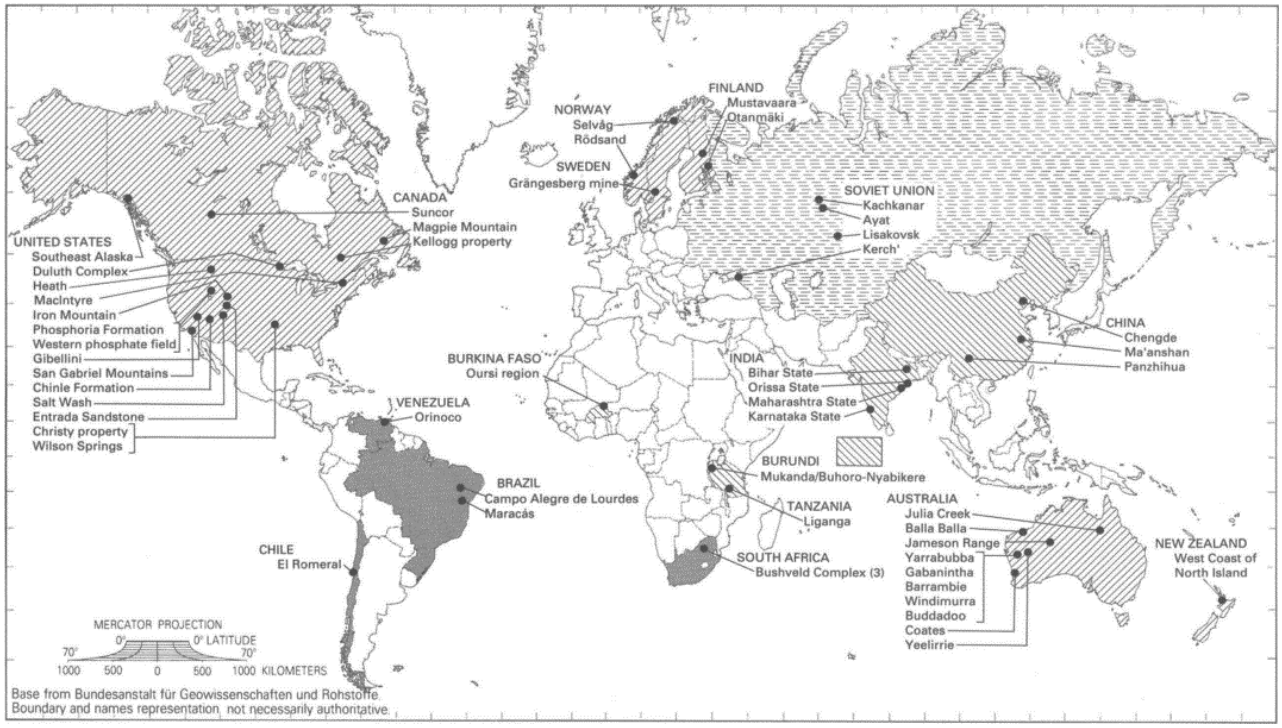

Figure 2-1. General global locations of significant deposits of vanadiferous titanomagnetite (Goldberg et al., 1992)

By far, the largest known vanadiferous titanomagnetite deposit is hosted in the Main Zone of the Bushveld Complex (Cawthorn *et al.*, 2005). Substantial and expanding resources are also documented in the Panzhihua Complex in Sichuan Province, China (Pang *et al.*, 2010) and the Windimurra Complex, Australia (reportedly second in volume to the Bushveld Complex) (Ivanic *et al.*, 2010). Most of these resources feature vanadium-rich magnetite, and many also contain inter-grown or spatially associated ilmenite (Peck & Huminicki, 2016). Typical vanadium grades are about 0.5% V_2O_5, but individual deposit grades range from about 0.1% to 1.7%.

Table 2-1: Significant titanomagnetite deposits grouped by primary mineralogy of the ore

Deposit	Primary ore mineralogy
Tellnes (Norway) Lac Tio (Canada)	Hemo-ilmenite or titanomagnetite with or without apatite (Pang *et al.*, 2010)
Bushveld (South Africa) Windimurra (Australia)	Titanomagnetite with or without apatite (Pang *et al.*, 2010)
Panzhihua (China) Hongge (China)	Titanomagnetite with or without ilmenite (Pang *et al.*, 2010)
Kachkanar (Russia)	Titanomagnetite with or without ilmenite or apatite (Badmatsyrenova & Orsoev, 2005)
Waikato North Head (New Zealand)	Titanomagnetite beach sands (Goldberg *et al.*, 1992)

Titanomagnetite deposits are what is regarded as magmatic iron-titanium deposits. It is noteworthy to highlight that Norwegian and Canadian hard-rock ilmenite deposits (processed to titania-rich slags via smelting) are also classified as magmatic iron-titanium deposits. Table 2-1 summarises the most significant titanomagnetite deposits by the primary mineralogy of the ore as described by Pang et al. (2010); Table 2-1 includes a reference to the hard rock ilmenite deposits for reference (Badmatsyrenova & Orsoev, 2005; Goldberg *et al.*, 1992; Pang *et al.*, 2010).

2.3 Economic Importance and Context

The early history and the current practices highlight that the origins of titaniferous magnetite processing are rooted in ironmaking. In South Africa, evidence exists of smelting practices that date back to at least the second millennium of the Late Iron Age (Killick & Miller, 2014). History shows that the processing challenges of these ores should not be underestimated. As stated previously, titaniferous magnetite is frequently reported to be a source of iron, vanadium and titania; thus, this premise warrants a brief comparison with competing resources. It may be concluded that the incentive and importance of titaniferous magnetite ore may be overstated due to size (abundance) of the deposits rather than the quality.

2.3.1 Iron ore

Titaniferous magnetite ores exhibit widely varied compositions, ranging from 16% to 60% Fe, 1.5% to 38% TiO_2 and 0.1% to 2% V_2O_5 (Fischer, 1975). A general, simplified classification of iron ore, adapted from Taylor et al. (1988), defines iron ores as follows:

1. High-grade: Iron content of 63% or higher. Typically these ores only require simple, and inexpensive beneficiation, either via washing and screening, or washing, screening, and heavy-medium separation.
2. Medium-grade: Iron content of 55% to 63%. Medium-grade ores are not upgraded further due to the nature of the dissemination of the gangue in the ore.
3. Low-grade: Ore containing approximately 20% to 47% iron is defined as low-grade. Low-grade ores are milled in order to liberate the iron minerals from the host rock, and usually undergo one or more beneficiation process like magnetic, high-intensity magnetic, or flotation steps, or a combination of these (depending on the physical and chemical properties of the ore) to facilitate upgrading.

Compared to the general definitions, titanomagnetite ores can be categorised as low- or possibly medium-grade iron ores with an inconvenient, and complicated association with titania. The titania generally occurs within the crystal lattice of the magnetite, thus limiting the options for beneficiation of the magnetite (Taylor *et al.*, 1988). The inability to separate the ilmenite from the magnetite means that there is a limit to upgrading the iron content through physical means.

2.3.2 Titania feedstock

As a primary titania feedstock, titaniferous magnetite is also not a viable or competitive option. Any process aimed at extracting titania from low-grade ores (and slags) needs to compete at least with furnace slag produced from ilmenite smelters. This reality restricts potential process options to extract titanium from low-grade materials, and while the slag from current titanomagnetite smelting operations contains a significant economic value on paper at least, these low-grade titania slags cannot easily compete with slag produced by ilmenite smelters.

Ilmenite (nominally $FeTiO_3$), the most abundant titanium mineral, containing from about 35% to 65% TiO_2 accounts for about 89% of the world's consumption of titania minerals. The widely varied compositions of ilmenite deposits are a consequence of geological alterations, which can result in the concentration of TiO_2 in ilmenite. In nature, the ore occurs with other minerals and impurities such as MgO, CaO, SiO_2, MnO in the mineral which can result in ilmenite with TiO_2 content lower than 52.6% (pure stoichiometric ilmenite). Ilmenite is found in either rock or sand-based deposits. The TiO_2 in hard-rock deposits range from 8% to 37%. Generally, it is feasible to upgrade ilmenite deposits substantially through physical upgrading processes.

The Bushveld Complex contains relatively high concentrations of titania and can be compared with some hard rock deposits (U.S. Geological Survey, 2014). The mineralogical composition of the titanomagnetite ore limits upgraded with the aim of reducing the titania content. Hard rock mineral processing is used in cases where ilmenite occurs in rock deposits and not in the form of mineral sands. This type of processing is used in Canada and Norway. The ilmenite product from these two instances is smelted to produce pig iron and high-titania slag, but unlike the beach sands, the hard rock deposits tend to be lower in grade prior to smelting. There is thus similarity between hard-rock ilmenite deposits and the titaniferous magnetite deposit in the Bushveld Complex. Ilmenite is upgraded via reductive smelting in an electric furnace to produce titania-rich slag, typically containing about 75 to 86 mass % TiO_2. Ilmenite slags (either

from hard rock or beach sands) are mostly used in the pigment industry. Of interest in the current study is pyrometallurgical processing or smelting of titaniferous minerals to produce titania-rich slag from atypical titania deposits. Typically the titania content of slag produced via smelting of ilmenite in South Africa contains about 80 to 85 mass % of TiO_2 (Gous, 2006; Williams & Steenkamp, 2006).

2.3.3 Vanadium

Vanadium is a passenger commodity in the context of smelting titanomagnetite. If vanadium is the primary desired outcome, direct processing of ore, without the intermediate process of ironmaking, is possible. These technologies are excluded from the current review as iron and titanium are targeted.

In recent years, efficient extraction of iron, vanadium and titanium from titaniferous magnetite deposits has been the topic of numerous published research studies. A marked increase in research publications was noted during the process of collating potential reference materials. The dramatic increase in interest, quantitatively indicated through the high number of publications, can be linked to the increase in ironmaking capacity in China, where titaniferous magnetite is an abundant resource. Both iron and vanadium are primarily consumed in the manufacturing of steel alloys. It is well-established that steel consumption can be used as an indication of economic growth or decline. In the ever-changing environment of globalisation, the economic health and status of the Chinese economy have become a key to many economic indicators. Steel production and consumption are however still an indicator of the health of the global economy (Pariser *et al.*, 2018).

The World Steel Association represents over 160 steel producers (including 9 of the world's 10 largest steel companies). The association publishes data related to the steel industry activities, including annual output data of world crude steel via an annual publication “World Steel in Figures” (World Steel Association, 2018). The data is useful in that the contribution of China to the production of crude steel is tracked separately. Figure 2-2 (data World Steel Association, 2018, own presentation) shows the dramatic increase in global output during the early 2000s. Chinese expansion projects during this period were of a scope and scale never seen before. The trend for annual total world crude steel output and the contribution from China from 2006 to 2017 is presented to support the increase in vanadium and iron production capacity; it is worth noting that since about 2013, China produces 50% of crude steel output by doubling its production output in a mere decade to 800 million tons. During the same period, the rest of the world (by difference) remained more or less on par in terms of output.

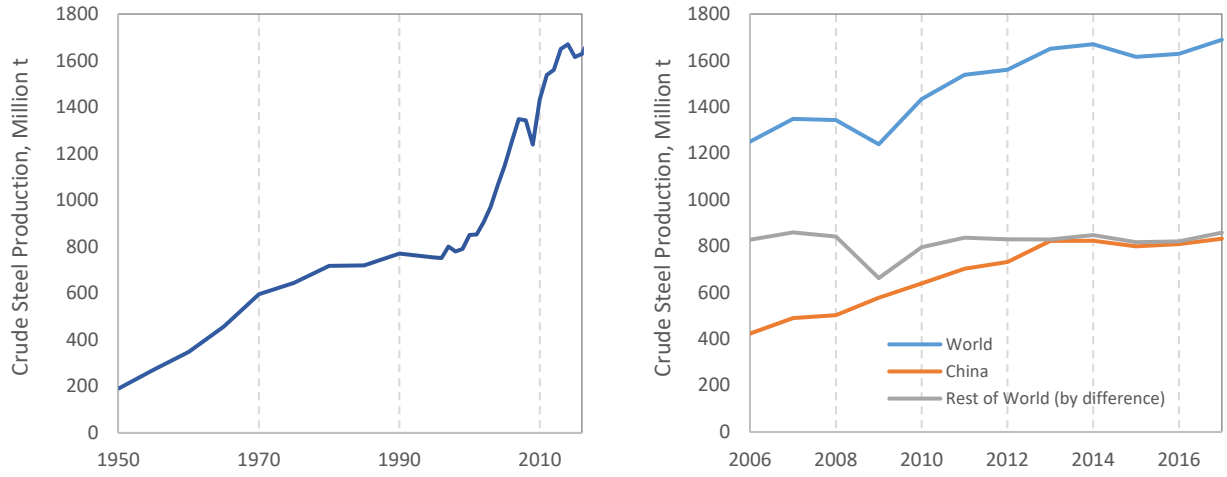

Figure 2-2: World crude steel production from 1950 to 2017 (left) and Chinese crude steel production from 2006 to 2017, contrasted with the rest of the world (right)

Vanadium is co-recovered as vanadium pentoxide from the iron product during the processing of vanadiferous titanomagnetite, principally through an oxidative process after smelting. Although the recovery of vanadium is basically achieved via the same chemical reactions, Russian, Chinese and South African processes vary in practical execution; the three countries associated with the majority of mine production of vanadium from titanomagnetite. New Zealand contributes small volumes of mine production of raw materials but does not process the pentoxide (intermediate vanadium rich slag is exported to China for processing). The dominant process is the recovery of vanadium from an intermediate product between ironmaking and steelmaking.

Vanadium deportment is favoured to the iron product, where it is usually extracted from metal before the production of the finished steel, whether or not the finished steel will contain vanadium. A vanadium extraction step is therefore

added to the steelmaking process. Hot metal (vanadium-bearing iron) from the ironmaking process is oxidised and a slag, typically containing between 10% and 25% V_2O_5, is produced. The vanadium content varies depending on the process used to recover vanadium from the iron as well as the grade of the ore and vanadium recoveries (Hukkanen & Walden, 1985; Kelly, 1993; Moskalyk & Alfantazi, 2003; Steinberg *et al.*, 2011). The vanadium-bearing slags produced at Highveld Steel typically contained about 20 to 22% V_2O_5 (the plant is no longer in operation). Slags from Nizhny Tagil (Russia) range from 12 to 18% V_2O_5, while the slags from major Chinese co-producers like Panzhihua and Chengde are thought to be 10 to 15% V_2O_5 (Roskill Information Services, 2010; Taylor *et al.*, 2005). The vanadium-rich slag is treated via a roast-leach process, the end product of either consisting of vanadate or vanadium oxide depending on the specific plant. Between 50 and 60% of the world's primary vanadium units are recovered in this manner. The vanadium-bearing feed is then processed via conventional alkali roast-leach processes to produce V_2O_5 flake. (Bauer *et al.*, 2012; Roskill Information Services, 2010).

The co-occurrence of vanadium and titaniferous magnetite means that vanadium is a factor in the processing of titanomagnetite and may even be described as an incentive to process these ores in lieu of good quality iron ores. Japan, Europe and the USA recover vanadium from secondary sources available throughout the world, and these sources are said to be substantial. Recycling of vanadium is still relatively small in scale, mainly associated with reprocessing vanadium catalysts into new catalysts. Vanadium associated with steel scrap processing is usually lost to slag, where it is present in uneconomic low concentrations for recovery (Kelly, 1993; Roskill Information Services, 2010).

Vanadium production significantly increased from the mid-1950s with the mining and processing of titanomagnetite ore either directly from the ore for vanadium extraction, or to produce vanadium-containing pig iron from which an oxidation slag, highly enriched in vanadium is produced. Process development began in Finland, followed by South Africa and some smaller producers in Norway and Chile (Bauer *et al.*, 2012). Titanomagnetite ores have also been mined in the former Soviet Union and China in large quantities since the early 1960s and 1970s, respectively (Fu *et al.*, 2011; Fu & Xie, 2011; Smirnov *et al.*, 2000).

A review of relevant literature reveals that the vanadium market is complex, dynamic and diverse. The majority of vanadium production is consumed by the steel industry, and the economics of vanadium is therefore closely associated with drivers linked to the steel industry. Vanadium is mainly used as an alloying element in the steel industry, and about 85% of vanadium produced is used in the manufacture of steel while non-ferrous alloy production consumes about 9% of production (Bauer *et al.*, 2012). The United States Geological Survey (USGS) (U.S. Geological Survey, 2016) reports world vanadium reserves to be in the region of 15 million tons with Russia, China and South Africa accounting for about 87% of these known reserves. Despite being considered as a minor element in many deposits, it is a rather abundant one, and recovery of vanadium from titanomagnetite is technologically speaking feasible for even the low-grade deposits (0.1 to 2% V_2O_5) (Fischer, 1975). Secondary vanadium sources in crude oils are challenging to estimate; thus, global resources are likely understated. Secondary production of vanadium from fly ash, petroleum residues, slag, and spent catalysts have also increased, which also contributed towards a market oversupply situation in more recent times and is likely to continue to put pressure on vanadium prices as over-supply conditions are expected to prevail (U.S. Geological Survey, 2017).

Alternate applications for vanadium are enthusiastically described by the industry interest group Vanitec, and it is suggested that alternative applications such as energy storage, may change the market fundamentals in the future (Vanitec, 2017). Vanadium production capacity experienced significant growth in the early 2000s as a result of extensive capacity expansion projects, most notably in China. China became, and remains, the dominant producer of vanadium with an annual production of more than double nearest rivals South Africa and Russia. (Roskill Information Services, 2010; U.S. Geological Survey, 2016, 2017). Before this substantial increase in production capacity in China, South Africa had been the leading producer of vanadium, but the closure of Highveld Steel severely impacted South Africa's vanadium output.

2.3.4 Economic context

Increased capacity in ironmaking industry in China, the increased availability of secondary sources of vanadium, the global economic downturn, and uncertainty about the potential applications of vanadium all contributed to commodity volatility, which most likely contributed to the ultimate demise of EVRAZ Highveld Steel and Vanadium in 2015. Cost of production simultaneously increased dramatically, and while Highveld Steel had access to a world-class resource, the ageing and inefficient technology could not survive the modern era. Titanomagnetite can be described as a source of low-to-medium-grade iron ore (with vanadium co-produced during iron-making), or a low-to-medium-grade titania feedstock (with vanadium and iron co-produced). This differentiation is applied in the current study. Both scenarios offer the opportunity to sweeten the pot through co-production of vanadium as either option allows for recovery of vanadium via the iron production stream. The factors highlighted in this section show that without an efficient technology, the goal of comprehensive utilisation of titaniferous magnetite deposits cannot be realised.

2.4 History of Titaniferous Magnetite Processing

The earliest evidence of processing of titanomagnetite ores dates back to the Late Iron Age, with more recent instances dating back to the 1860s (Killick & Miller, 2014; Singewald, 1913). Electric smelting emerged in the 1960s, but processing is currently still dominated by blast furnace technology. It was also during the 1960s that vanadium became more prominent and incentivised the processing of titanomagnetite. The history of titaniferous magnetite processing highlights that the origins of titaniferous magnetite processing are rooted in ironmaking dating back in South Africa to at least the second millennium of the Late Iron Age.

The titanium industry is young in comparison to the ironmaking industry. Pigment production started in the 1920s and titanium metal extraction only developed in the 1950s via the Kroll Process (Gambogi & Gerdemann, 2013; Jones & Egerton, 2012).

Archaeometallurgy is the study of the history and prehistoric use and production of metals (Killick & Fenn, 2012). This may seem an extraordinary feature of a pyrometallurgical background study, but history and cross-disciplinary perspectives, often reveal alternative insights. In the case of ironmaking from titanomagnetite ore, the historical perspective highlights that for hundreds of years, titanomagnetite has been viewed as a type of iron ore, albeit it challenging to process. The ore was only processed if no alternative iron source was available. A brief history of titanomagnetite smelting is included to illustrate this perspective.

Examples of early processing of titanomagnetite ore to produce iron are well-described by Killick and Miller (2014). The Killick and Miller study is the first published study to report the smelting of high-titanium iron ore from an archaeometallurgy perspective. The authors also describe evidence of direct smelting of titanomagnetite ores from the Late Iron Age (the Late Iron Age is defined as the period ranging from about 1000 to 1880 cal. CE). Evidence shows that the early settlers in the northern Lowveld exploited the abundant mineral resources, producing and mining copper and iron at many sites. The incidences of iron smelting are described as unique, not only in the context of African iron smelting archaeology but also in the context global bloomery type smelting technology of this age. The uniqueness refers to the prominence of relatively high titania (titanium oxide-containing) slags recovered from iron furnaces in this area. The early ironmakers were forced to adapt to produce iron from the readily available titanomagnetite. The reduction of magnetite to iron metal is much slower than similarly sized lumps of iron ore (Manamela & Pistorius, 2005; Park & Ostrovski, 2003). Titanium in titanomagnetite stabilises the spinel structure, and as a result, ore fines had to be processed to ensure that adequate reduction of iron was achieved in the short shafts of the bloomery furnaces (only about 1 m high). The Lowveld bloomery furnaces processed titanomagnetite and magnetite with less than 3 mass % silica, which required significant fluxing with silica to lower the liquidus of the slag. Slags recovered from iron furnaces from the region contained 12 to 25 mass % TiO_2.

A modern blast furnace is significantly more productive and efficient than these early examples of smelting, but the early ironmakers demonstrated the basic metallurgical principles and challenges associated with processing titanomagnetite, quite well. Unlike in modern blast furnaces, where operators have to guard against the formation of titanium nitrides and carbides and viscous slags due to the very reducing conditions, the conditions in these furnaces were relatively mild, and as a result, reduction of TiO_2 did not occur at all (Mcrae *et al.*, 1969; Zhang *et al.*, 2007). The early settlers were likely attracted to the northern Lowveld region due to copper and salt (from saline springs) and not by the vast quantities of titanomagnetite and magnetite, but these settlers would have needed iron. Through experimentation, they adapted bloomery smelting methods to produce their much-needed iron.

Singewald (1913) describes early endeavours processing titanomagnetite ores in England, Norway, Sweden and the United States dating back to the 1860s. These blast furnace operations were challenging and found not to be economically competitive. High-grade non-titaniferous iron ores were readily available to ironmakers, and operators avoided processing titaniferous ores as much as possible.

James et al. (2002) reviewed slag taken from the site of the Albemarle Iron Works in the United States. The slag was analysed with modern analytical techniques to establish why the blast furnace at the Albemarle site never produced any usable iron. A cold blast furnace, to produce cast iron, was constructed and put into operation in September of 1771 but closed permanently in June of 1772. No usable iron was ever produced despite several subsequent attempts to restart the furnace. The reason for this failure was not apparent at the time. It was more than a hundred years later, in 1882, that an analysis of ore from the mine revealed that the iron ore contained significant titanium. In 1977 it was conclusively established that the ore processed at Albemarle was indeed titaniferous magnetite which would have caused tremendous operational problems. Most prominent would have been very viscous slags limiting the separation of the iron from the slag (James *et al.*, 2002).

The first instances of electric smelters being applied to the processing of titaniferous magnetite date back to the 1960s. South Africa and New Zealand both implemented technology to smelt titaniferous ores via electric furnace processes to

recover iron and vanadium (Kelly, 1993; Rohrmann, 1985; Steinberg *et al.*, 2011). In Russia and China, blast furnace processes were being adapted more or less during the same time as the emergence of electric smelting, aiming to treat these ores via the traditional ironmaking technology instead of using electric smelting (Moskalyk & Alfantazi, 2003). The world was a different place in the 1960s with both Russia and China very isolated from the western world and South Africa and New Zealand geographically isolated, and in the case of South Africa, economically and politically isolated at the time. The two electric smelting sites were both supported by the respective governments with the geopolitical aspects likely playing a substantive role in both countries. The stated objective was to create a local iron and steel industry. These factors explain the variations in the emergence of titanomagnetite processing.

The exploitation of titanomagnetite has received a lot of attention over the past 100 years due to the fact that these ores represent a significant proportion of exploitable reserves in the context of vanadium and iron. The United States Bureau of Mines published an overview report in 1913. In the report, the chemical and economic value of titaniferous magnetite deposits of the United States is reviewed (Singewald, 1913). A topic of interest featured in the 1913 Singewald report, is an in-depth study aiming to remove the titanium from the ore via physical means and the author concludes, as is now well-established, upgrading the ore via physical means is not achievable. Upgrading refers to the extraction of all three metals of interest.

Despite published over a hundred years ago, the Singewald report is surprisingly current. The author states that practices were changing and blast furnace operations were already accepting lower grade ores. The report concluded that processing of feed with more than 1 mass % TiO_2 was found to be uneconomical at the time of the report. The author reflected on the state of technology and expressed the following opinion on electric smelting of titaniferous magnetite ore *"Electric smelting of iron ores is still in its infancy, and its full possibilities have not yet been demonstrated. Electric smelting is of special interest in this connection since there is a confident feeling in many quarters that herein lies the hope of utilisation of the titaniferous ores."* (Singewald, 1913: 15)

The increased interest in titanium recovery from titanomagnetite is likely as a result of growing global awareness that resources are limited, and the drive to mitigate and reduce the environmental impact of minerals processing and metal production. Currently, all the smelters processing titanomagnetite ore are still creating slag dump sites. The slags are highly diluted, which makes it challenging to recover the left-over vanadium and the titanium economically.

Smelting of titanomagnetite ore to produce iron is a well-established industrial practice, dominated by the following geographical regions, China (Panzhihua), Russia (Kachkanar), South Africa (Bushveld Complex) and New Zealand (Waikato North Head). These regions are associated with substantial deposits of vanadium-bearing titanomagnetite deposits, and it is therefore expected that processing would be focussed as such. Extraction processes of vanadium and iron from titanomagnetite ores are well described in the literature, and several excellent review papers comprehensively describe the relevant processes.

- Rohrmann (1985) and Steinberg et al. (2011) summarise processing of South African titaniferous magnetite ore. Both authors provide detailed process information regarding the vanadium and ironmaking processes. Rohrmann (1985) is indeed a classic reference with regards to vanadium processing and extraction in South Africa.
- Moskalyk & Alfantzi (2003) comprehensively reviewed global vanadium extraction processes, and the survey features detailed process descriptions of extractive processes of vanadium as well as descriptions of the different approaches employed by producers in China, Russia and South Africa.
- Taylor et al. (2005) prepared a comprehensive overview of the extractive metallurgy relating to vanadiferous titanomagnetite ores, and this comprehensive summary is of specific interest as it includes descriptions of practices in China and Russia where blast furnaces are predominantly used to process these ores.
- Kelly (1993) summarises the development and modifications of the New Zealand Steel processing plant. The paper provides an overview of the improvements at the site since start-up.
- Russian process descriptions of smelting practices in the area of interest are relatively scarce. Lazutkin et al. (2001) provides a rare summary of slag and feed compositions of Russian vanadiferous titanomagnetite ores as processed in Russian blast furnaces.

The TiO_2 content of the slag from titanomagnetite smelting operations ranges from 10 to 40 mass % TiO_2. Ironmaking slags from titanomagnetite smelting are generally described via the TiO_2-SiO_2-Al_2O_3-MgO-CaO slag system, regardless of whether the ore is processed in a blast or electric furnace.

A practice of blending the magnetite with iron ore is commonly used to dilute titania in the feed. Operational problems are reported if the feed to the blast furnaces is not managed very carefully (Steinberg *et al.*, 2011). The difficulties reported include poor burden permeability and low productivity. A number of operational problems can occur if the impact of titanium oxide in the feed is not adequately managed, amongst others foaming slag, a build-up in the hearth and blocking of tuyers are main issues listed as concerns for a blast furnace operators. If not managed, long periods of idling may be required to clear build-up or accretions (James *et al.*, 2002; Smirnov *et al.*, 2000).

Slag from these processes, as a result of the fluxing and blending strategies, are low-grade titaniferous slags. The primary objective of these practices is to maximise iron production and recovery of vanadium, unlike the case of ilmenite smelting where the titaniferous slag is upgraded through the removal of iron with significant efforts made to minimise contaminants. For titanomagnetite ores, fluxes, binders and reductants (via the ash content), is intentionally added to dilute the titania content and to act as a slag modifier. The aim is to improve operability and recoveries (Pistorius & Kotzé, 2009). Based on the generalised descriptions by the various authors listed previously, the next graphic is presented (Figure 2-3) as a generalised flowsheet description (adapted from Hukkanen & Walden, 1985).

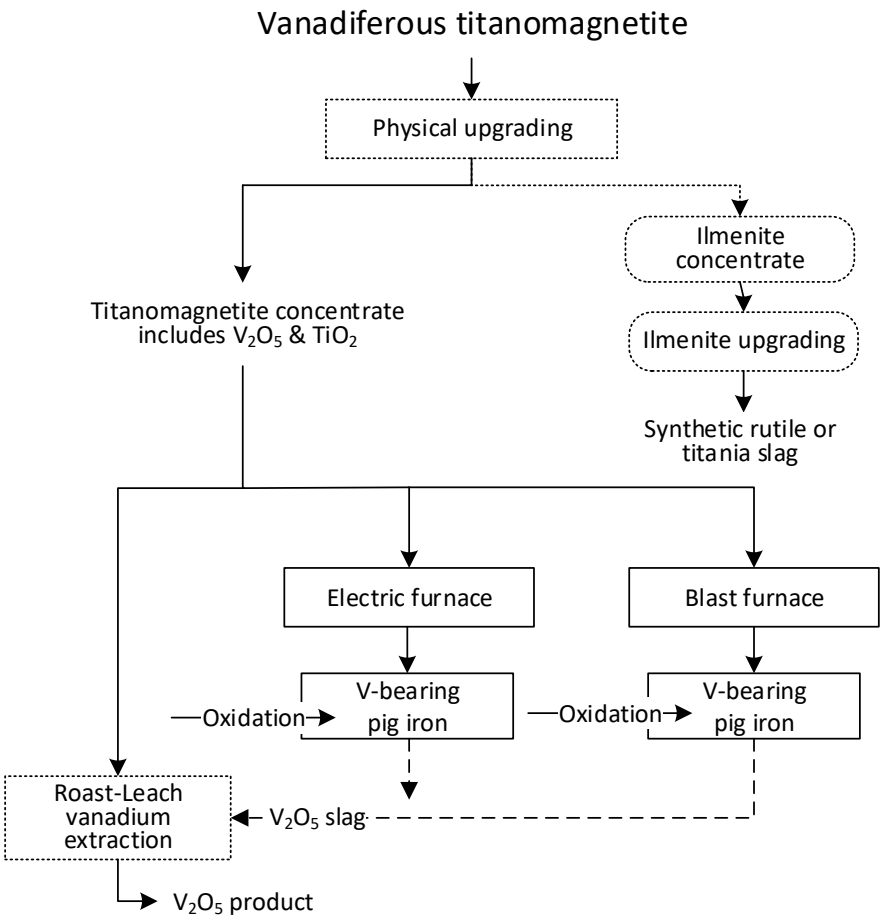

Figure 2-3: Generalised flowsheet of vanadiferous titanomagnetite processing practices (adapted from Hukkanen & Walden, 1985)

Titanomagnetite is not currently an established titanium feedstock mainly due to the associated complexity, the relatively low grade, and the abundance of other titanium feedstocks. These factors indicate that a process to comprehensively process titanomagnetite will need to be efficient to be economically viable.

2.5 Current Industrial Smelting Practices

In the next sections, descriptions for the primary smelting processes are presented. The ore of interest is naturally the South African Bushveld deposit even though Highveld Steel is no longer operational. Two examples of blast furnace operations are included to illustrate the scale of current processing capacities and provide context for the background review. The primary focus in this section is to compare the operational strategies of prominent producers and to compare the slag compositions (and ore grades) from the different regions. Table 2-2 summarises the relative smelting capacities as well as the generalised process, and products.

Table 2-2: Summary of titaniferous magnetite smelting capacities

Plant	Process description	Capacity, crude steel per annum[1]	Products
Highveld Steel & Vanadium (South Africa)[2]	Rotary kilns, originally submerged-arc electric furnaces moved to open-arc electric furnaces (from 2006)	777 000 tons	FeV, steel, vanadium slag
New Zealand Steel (New Zealand)	Multi-hearth furnaces, rotary kilns, electric arc furnaces (multi-hearth furnaces developed since1972)	850 000 tons	Concentrated ore, steel, vanadium slag
Nizhniy Tagil Metallurgical Plant (NTMK) (Russia)	Blast furnace route	4.3 million tons	Concentrated ore, V_2O_5, FeV, steel
Chengde Xinghua Vanadium Chemical Company (Pangang, China)	Blast furnace route (with pelletizing)	7.5 million tons	V_2O_5, FeV, vanadium slag, steel
Panzhihua Iron and Steel Company (China)	Blast furnace route	8.4 million tons	V_2O_5, FeV, steel, vanadium slag

Note 1: Capacity data from the World Steel Association 2010; Note 2: Highveld Steel not in operation since 2015

2.5.1 South Africa – Highveld Steel and Vanadium

The Highveld Steel and Vanadium Corporation (Highveld Steel), renamed as EVRAZ Highveld Steel and Vanadium Company in 2007 (after EVRAZ took over the control as a shareholder from Anglo American) started smelting ore from the Mapochs Mine in 1968 following an implementation programme initiated in 1960. (Rohrmann, 1985; Steinberg *et al.*, 2011).

The original process flowsheet for Highveld Steel, known as the Rotary Kiln-Electric Furnace (RKEF) process, comprised of co-current rotary kilns (for prereduction of the concentrate), from which concentrate was fed into submerged-arc furnaces, producing vanadium-bearing pig iron and waste slag. The use of an RKEF flowsheet is a well-established technology in the industry, and at the time, the use of conventional blast furnace technology had been regarded as being too high risk due to the high concentration of titanium in the Bushveld Complex ores.

The selected process route was based on development work conducted by Dr William Bleloch, dating back to 1934. Dr Bleloch pioneered recovery of iron from the Bushveld magnetite ore proposing the use of South Africa's "atypical iron ore" via "electrometallurgy" - the use of electric-arc furnaces to recover metals. His work halted as a result of World War II, but in the post-war years, he turned his attention back to metallurgy and in particular electric smelting projects. In 1948 he oversaw the smelting of 100 tons of Bushveld magnetite in Norway, and through this test demonstrated the successful production of pig iron and recovery of vanadium. His visionary work was published in March 1949 in the Journal of the Chemical, Metallurgical and Mining Society of South Africa, entitled "The electric smelting of iron ores for the production of alloy irons and steels and the recovery of chromium and vanadium" (Bleloch, 1949). It took nearly 30 years for his dream of smelting South African magnetite ore to be implemented. His proposed approached as implemented by Highveld Steel processed titanomagnetite ore for nearly 50 years.

The furnace operation remained unchanged until the late 1990s when Highveld Steel started a series of studies to identify opportunities to address operational problems that had been part of the process, since inception (typical issues for submerged-arc furnaces), namely:

- Difficulties in controlling slag chemistry and thus vanadium recovery
- Operational instability due to the furnace operation being overly dependent on the characteristics of the feed from the kiln which was prone to variability
- Burden conductivity being high. A consequence of submerged-arc mode operation at Highveld - low electrode resistance which limited the power input.

Highveld Steel converted four of the furnaces from submerged-arc into open-arc mode over a period of about 6 years (a process started in 2004), thereby eliminating the dependence of the power input on the burden and slag composition. The conversion yielded the expected overall operational improvements. The change in operating mode resulted in (Steinberg *et al.*, 2011) improved vanadium recovery, lower coal consumption, electrode consumption, and energy consumption, and the ability to use less-reactive coal and to process more fine ore directly in the smelting process.

It is important to note that the listed factors are also valid when processing high-titania ores in a DC open-arc furnace (Geldenhuys, 2017; Jones & Geldenhuys, 2011). The conversion to open-arc smelting, in light of the reported benefits to the process, is an essential link to the topic of the work herein. The independence of power input is also a feature of open-arc DC furnace smelting technology (Geldenhuys, 2017; Jones *et al.*, 2011). The ability to independently dial in the

power input means that the process can be optimised for metallurgy and not for electrical properties (as would be the case for submerged-arc smelting). This is a critical requirement for ilmenite smelting. Due to the highly conductive nature of high-titania slags, an open-arc operation is the preferred embodiment.

The benefits of open-arc smelting in a DC furnace and the listed benefits are similar to benefits listed by Steinberg et al. (2011); described in "Some myths about DC arc furnaces" by Jones et al. (2011). An open-arc operation, however, requires that the power-to-feed balance control is managed well as the buffer created by a burden is no longer available to absorb minor power or feed imbalances. Steinberg et al. (2011) and Geldenhuys (2017) both describe the importance of this issue, highlighting the fact that the additional degree of freedom afforded by operating with an open arc means that the quality of the feed input control or the power-to-feed balance, becomes critically important. As part of the upgrade, mainly the roof design, Highveld Steel had to upgrade and modify control systems, operating practices and feed systems to address these issues. Steinberg et al. (2011) also indicated the intention to investigate implementing a calcining step before the rotary kilns (as implemented by New Zealand Steel in the 70s).

It is somewhat perplexing why the change from submerged- to open-arc was only implemented nominally in the new millennium, especially in light of the fact that Highveld Steel's only compatriot, New Zealand Steel and all ilmenite smelting operations, are open-arc processes. During the 1960s when both Highveld and New Zealand Steel pioneered electric smelting of prereduced titaniferous magnetite ores, New Zealand Steel selected open-arc smelting technology (via a shielded arc which incorporated a foamy slag practice), while Highveld Steel opted for a submerged-arc smelting mode, which relies on the slag properties to heat the melt. An objective review of the industry shows that no other electric furnace in which titaniferous ore is processed (whether it is magnetite or ilmenite) operate in submerged-arc mode. High-titania content drastically increases slag conductivity, and open-arc mode is thus the more logical embodiment, regardless of whether it is AC or DC powered.

The smelting operation at Highveld Steel had to flux the slags substantially to modify the slag properties, and one of the first changes after the conversions to open-arc mode was indeed a dramatic reduction in fluxing (resulting in considerable energy and recovery improvements). While the reason for the late adoption of what is a more appropriate and efficient smelting mode is not fully expanded on in literature, the shift to an open-arc operation was vindicated by the dramatic improvements the smelting operations reported by Steinberg et al. (2011).

The cause of the unfortunate demise of what was a flagship company in South Africa is a complicated matter and subject to many personal opinions and speculation. The ore from the Bushveld Complex is rich in vanadium (relative to most deposits the grades are high, especially the vanadium). Highveld Steel relied heavily on the economic benefits of recovering vanadium as a co-product.

The impact of the closure of Highveld Steel in 2015 (EVRAZ Highveld Steel and Vanadium, 2015), combined with China's continued dominance as a vanadium producer, and the emergence of secondary sources of vanadium, is a subject of much debate amongst analysts (Roskill Information Services, 2010; U.S. Geological Survey, 2016, 2017). The cost of electricity in South Africa dramatically increased since 2007, which also coincided with China's dramatically expansion drive - from 2007 to 2015 electricity tariffs increased by 300% (PowerOptimal, 2015). The impact of such a dramatic change in input costs cannot be discounted, but likely was not the only cause for the demise of the company. In April 2015, the Highveld Steel was placed under business rescue, and the smelters have been decommissioned (EVRAZ Highveld Steel and Vanadium, 2015). Commodity volatility, decline in demand due to the global commodity downturn, cost of electricity and the ageing infrastructure likely all contributed towards the demise.

Typical analysis of the feed composition processed by Highveld Steel is presented in Table 2-3 (Rohrmann, 1985; Steinberg *et al.*, 2011). The relative amounts of oxides such as CaO, MgO, FeO, SiO_2, TiO_2 and Al_2O_3, to a large extent is an indication of the physical properties of molten slags, such as liquidus and viscosity, factors which determine the operability of the process. Table 2-4 and Table 2-5 present the slag and metal composition, as tapped from the furnaces at Highveld Steel from two references, representing the two historical operating regimes (submerged-arc and open-arc operation).

Table 2-3: Chemical composition of Highveld Steel titanomagnetite feed

	Fe_{Total}	FeO	Fe_2O_3	Al_2O_3	CaO	MgO	SiO_2	TiO_2	V_2O_5	MnO	Cr_2O_3
*	54.8	16.5	60.0	4.8	0.10	1.6	2.0	12.7	1.65	0.3	0.40
**	53 - 57			2.5-3.5			1.0-1.8	12-15	1.4-1.9		0.15-0.6

(*) Steinberg et al. (2011); (**) Rohrmann (1985)

Table 2-4: Chemical composition of Highveld Steel slag, mass %

FeO	SiO_2	Al_2O_3	MgO	CaO	MnO	TiO_2	V_2O_5	Cr_2O_3	S	
1.0	16.2	18.0	14.1	14.1	0.40	35.6	0.90	0.20	-	(Steinberg *et al.*, 2011: 706)
-	22.0	14.0	15.0	17.0	-	32.0	0.90	-	0.17	(Rohrmann, 1985: 148)

Table 2-5: Chemical composition of Highveld Steel iron, mass %

Fe	C	V	Ti	Si	Mn	Cr	
94.5	3.2	1.29	0.20	0.20	0.20	0.34	(Steinberg *et al.*, 2011: 706)
94.3	3.5	1.22	0.20	0.20	0.25	0.30	(Rohrmann, 1985: 148), Fe by difference

Highveld Steel slag dump contains reportedly about 45 million tons of waste slag (Avertana, 2017) produced over about 50 years of operation. Efforts continue to extract value from the dump, including the titanium for pigment production. The slags produced from titaniferous magnetite ores either via electric or blast furnace smelting are often referred to as 'steelmaking slag' despite not being typical steelmaking slags. As discussed previously, millions of tons of low-grade titania-bearing slag are produced annually, adding to enormous stockpiles of discard slag already in existence around the world. These slags can contain from about 9 to 53 mass % TiO_2 (Hassell *et al.*, 2016). It is clear that these slag dumps will need to be reprocessed eventually.

A wide range of options has been considered to recover value from the low-grade slag. Some examples are selective nitriding and chlorination processes, to produce $TiCl_4$ (various embodiments), production of Si-Ti alloy in a DC furnace and a variety of leach recovery processes, using sulfuric acid, to highlight a few. The proposed processes combine various techniques including hydrometallurgical extraction, direct reduction (via fluidized beds, rotary kilns or rotary hearth furnaces) and electric smelting (Chen *et al.*, 2011; Fu & Xie, 2011; Guo *et al.*, 2014; Hu *et al.*, 2013). However, these methods typically suffer from low-recovery and/or high input cost and process complexity.

While there is clearly significant ongoing effort to extract the value from the ore more effectively, and to deal with the stockpiled slag dumps to reduce the environmental impact, there is currently no commercial process that is actively processing significant quantities of low-grade titania slags (Avertana, 2017; Chen *et al.*, 2015; Goso *et al.*, 2016; Liu *et al.*, 2008; Steinberg *et al.*, 2011; Yuan *et al.*, 2007; Zhang *et al.*, 2007).

The Bushveld Complex is, however, one of the largest deposits of vanadiferous magnetite, and the future of this resource is therefore of utmost importance to the mining and minerals industry in South Africa. Vanadium and titanium are in the context of titaniferous magnetite processing complicated partners or passengers, but it is still true that perhaps, like the early settlers in the Lowveld (Killick & Miller, 2014), the need to adapt is the key to success.

2.5.2 New Zealand – New Zealand Steel

Titanomagnetite concentrate (referred to as 'ironsand' in this region) is processed in New Zealand to recover iron and vanadium at the New Zealand Steel Limited (New Zealand Steel) smelting complex. New Zealand Steel was incorporated in 1965 by the New Zealand Government and later became BHP New Zealand Steel Limited (Kelly, 1993; New Zealand Steel, 2018); New Zealand Steel demerged from BHP in 2002. The iron concentrate processed by New Zealand Steel is mined from the Waikato North Head site, south of Auckland, as well as from the Tahāroa deposit on the west coast of the North Island of New Zealand. The mined ores are subjected to fairly typical minerals concentration processes in order to improve the iron and vanadium grades through rejection of gangue. The gangue elements are however mostly locked in solid solution in the magnetic lattice, as is typical for titanomagnetite deposits. Typical chemical composition of the concentrate (per Kelly, 1993), is presented in Table 2-6. The gangue elements (elements other than iron) are typical for titanomagnetite ores. Compared to Highveld Steel, New Zealand ore is significantly lower in titanium and vanadium.

Table 2-6: Chemical analysis of primary New Zealand Steel ironsand concentrate

Fe_{Total}	Al_2O_3	CaO	MgO	SiO_2	TiO_2	H_2O	V_2O_3	MnO	K_2O	P
58	3.7	0.67	3.0	2.9	7.8	3.4	0.46	0.57	0.07	0.04

The original plant was designed to produce 150 000 ton per annum of continuously cast billets using local sub-bituminous coal. The reduction process would produce reduced sponge iron that would be melted in electric furnaces together with scrap. The reduction technology consisted of a coal-based direct reduced ironmaking process using rotary kilns to produce the direct reduced iron (DRI). The technology is widely used and known as the SL/RN (Stelco-

Lurgi/Republic Steel-National Lead). The SL/NR process is known for being able to process a wide range of iron-bearing ores and can also process either lumpy ore, pellets, finely sized iron-bearing feedstocks (including ilmenite). Carbon (in solid form) is used to produce hot or cold DRI by feeding the coal together with the iron ore to a rotary kiln wherein the coal is gasified, and the iron ore is reduced. The SL/RN technology is widely used in developing countries due to robustness and flexibility as well as the ability to use low-quality coal. The process generates significant amounts of residual gas, which can be used for power generation or other process needs. Notably, coal consumption is considerably higher than for a blast furnace and the energy efficiency of individual plants depends on how efficient the residual gas is incorporated into the plant (Kelly, 1993; Lepinski, 2000).

New Zealand Steel initially fed green unfired titanomagnetite pellets directly to the rotary kiln while coal was injected into the kiln. Kelly (1993) describes that various process improvements were needed to overcome challenges on the plant. It was found that the green pellets deteriorated significantly in the kiln, resulting in excessive fines generation. The waste gas handling system could not handle the excess dust, which limited the throughput of the reduction step. Coal injection was found to be unsuccessful, with poor temperature control resulting in accretion problems in the kilns. In 1972, the plant resorted to feeding iron concentrate directly (abandoning the pellets) and the iron concentrate was no longer milled. At the same time, coal injection was abandoned, and coal was fed together with the unmilled ore concentrate. Although the operation immediately improved to the plant was still operating below design capacity. The bottleneck remained the high waste gas volumes and velocities as a result of the combustion of volatiles from the coal causing excessive dust losses from the kilns. To address this issue, the plant implemented charring of the coal, before feeding the reductant to the kiln. This led to the development of the multi-hearth furnaces, currently in use at New Zealand Steel (Kelly, 1993; Richards & Davies, 1980).

It is worth noting that one of the conclusions in the Steinberg et al. (2011) publication was that the Highveld Steel plant needed to improve the efficiency of prereduction and that multi-hearth furnaces were being evaluated at the time. Perhaps if the process changes were introduced earlier, Highveld Steel might still be in operation today. According to Kelly (1993), the energy released as part of the charring step is used to preheat the concentrate, and the overall productivity of the kilns improved about 35% as a result. Primary concentrate is mixed together with limestone ($CaCO_3$) and coal before being fed to multi-hearth furnaces where volatiles from the coal is used to generate heat. In the multi-hearth furnaces, the feed is dried, preheated and the coal is charred. The waste gas from the multi-hearth furnaces is used to generate electricity on the plant.

The hot feed, at about 650°C, is fed to the rotary kilns, where the reduction of iron is achieved. The hot reduced iron is fed to the two electric furnaces (tapping slag at about 1550°C and metal at about 1475°C). The CaO produced in the kiln from the limestone, added with the coal, serves as the primary flux in the smelter. The flux is used to modify the slag composition to attain the desired slag fluidity, but also produces a slag with diluted titania content. The next two tables, Table 2-7 and Table 2-8, present the slag and metal composition as tapped from the furnaces at New Zealand Steel (Kelly, 1993).

Table 2-7: Chemical composition of New Zealand Steel slag, mass %

Fe_{total}	SiO_2	Al_2O_3	MgO	CaO	MnO	TiO_2	S	V_2O_3
0.98	18.3	17.0	13.3	15.5	1.3	32.3	0.12	0.18

Table 2-8: Chemical composition of New Zealand Steel iron, mass %

Fe	C	V	Ti	Si	Mn	S	P
~95	3.2	0.45	0.23	0.28	0.44	0.037	0.09

Vanadium rich slag is a by-product of the ironmaking process at New Zealand Steel, but unlike the Highveld Steel flowsheet, the vanadium slag produced during post-taphole processing is exported to China for vanadium recovery (Taylor *et al.*, 2005).

2.5.3 China – Panzhihua Iron and Steel Corporation

The Panzhihua area in China is well-known for iron, vanadium, titanium, cobalt, and nickel resources. Taylor et al. (2005) list China's known deposits of titanium and vanadium to account for about 35% and 12% of world reserves respectively, ranking third after Russia and South Africa. The Panzhihua titanomagnetite deposit accounts for more than 90% of the titanium reserves in China which is the likely driver for the intense research focus from Chinese (Li *et al.*, 2006; Liu *et al.*, 2008; Yuan *et al.*, 2007). The average composition of titanomagnetite ore from this area is reported to contain about 40% Fe, 13% TiO_2 and 0.4% V_2O_5.

Chinese titanomagnetite is processed in blast furnaces. The Panzhihua Iron and Steel Corporation is one such complex. The process resembles a conventional ironmaking process, adapted to cope with the higher than typical titania content of titaniferous magnetite ores. The operators overcome process challenges through blending (mixing in iron ore) and fluxing strategies to dilute the titanium dioxide content of the sintered feed to manageable levels. The typical problems associated with the processing of titanomagnetite concentrate in a blast furnace are overcome by modifying the feed to attain a slag with suitable properties (such as slag viscosity and liquidus) (Taylor *et al.*, 2005). The Panzhihua blast furnace process follows the typical processing route described as part of the generic flowsheet depicted in Figure *2-3* presented earlier. Zhang et al. (2007) report the ore processed by Panzhihua to contain 10.6% TiO_2 and 0.3% V_2O_5, which Steinberg et al. (2011) stated is comparable to the ore processed by Highveld Steel (a typical TiO_2 grade of about 12.7% is reported). According to Taylor et al. (2005), the Panzhihua area's titanomagnetite ore has the following average composition before and after physical upgrading; see Table 2-9.

Table 2-9: Composition of Panzhihua ore and concentrate, mass %

	Fe_{total}	SiO_2	Al_2O_3	MgO	CaO	TiO_2	V_2O_5	CoO	NiO	S	P
Ore	39.8	6.5	5.14	3.06	26.5	13.3	0.39	0.02	0.02	0.61	-
Concentrate	51.6	4.7	4.58	3.09	1.43	12.7	0.58	-	-	0.56	0.025

Worth noting is the change in the gangue composition. It is known that Panzhihua recovers a fraction of ilmenite concentrate from the titanomagnetite ore - no detailed processing information was accessible to interrogate the recoveries of the ore dressing circuit, but it is likely that the objective of the processing is to maximise Fe (and V) content and to minimise TiO_2 before smelting in the blast furnaces. These objectives are not supported by the natural mineralisation of the ore, as is typical for titaniferous magnetite deposits (Rohrmann, 1985).

In South Africa, the Tivani Project (Ferrox Holdings is the majority owner) in the Limpopo province, reportedly have also found titanomagnetite from the Rooiwater Complex to be amenable to the recovery of ilmenite. The project was announced in 2012, with minimal movement in further development over the last few years, but it is noteworthy due to the difference between the ore mined by Highveld Steel where the mineralisation of the ore does not allow for the extraction of ilmenite (Reynolds, 1985). It is clear that the particular mineralisation of a deposit should be understood well to maximise the potential.

According to Liu et al. (2008) more than 3 million tons of the blast furnace slag, containing about 22% to 25% TiO_2 and about 2% to 6% metallic iron, are produced on an annual basis at Panzhihua (Chen & Chu, 2014b). The slag dumps are located on the riverbanks of the Jinsha River and apart from the fact that the resource is inefficiently processed, is a growing environmental concern. The sheer scale of production at the Panzhihua site and the similarities to the Bushveld Complex are worth noting. Table 2-10 summarises the chemical composition of slag from the Panzhihua Steel process from three different sources, namely Taylor et al. (2005), Zhang et al. (2007) and Zhou et al. (2015). The authors reported typical chemical compositions of the blast furnace slag, and these are generally in agreement. The metal composition from the blast furnace is reported in Table 2-11 via Taylor et al. (2005).

Table 2-10: Chemical composition of Panzhihua blast furnace slag, mass %

Fe_{met}	FeO	SiO_2	Al_2O_3	MgO	CaO	MnO	TiO_2	Ti_2O_3	S	V_2O_5	Others	Note
	1.1	25.3	15.2	7.2	29.0		22.2			0.22		a
2.5	1.7	24.4	13.8	8.5	26.5	0.5	16.9	4.1	0.7		0.5	b
-	1.8	26.0	13.5	7.7	27.9	0.7	20.5					c

a (Taylor *et al.*, 2005) basicity of 1.15; b (Zhang *et al.*, 2007); c (Zhou *et al.*, 2015);

Table 2-11: Chemical composition of Panzhihua Steel iron, mass %

$Fe_{dif.}$	C	V	Ti	Si	S	P	Reference
93.4	4.3	0.32	1.17	0.1	0.05	0.07	(Taylor *et al.*, 2005)

dif. = Fe calculated by difference

Chen et al. (2014b) report recoveries of respectively iron, vanadium and titanium via the Panzhihua blast furnace to be 70%, 47%, and 25%, respectively. Note however that the titanium is recovered via preconcentration efforts from which a small proportion of the titanium is extracted as an ilmenite concentrate; the titanium is not recovered via the blast

furnace smelting step. It is not clear where the boundaries for this mass balance is drawn, but it is indicative of the overall efficiency of the blast furnace process.

2.5.4 Russia – Nizhniy Tagil Metallurgical Plant

The Kachkanar mountain deposit is the most significant titanomagnetite deposit in Russia with vanadium reserves indicated to be in the region of 9 to 12 million tons (Fischer, 1975; Lazutkin *et al.*, 2001). The ore composition is reported to contain about 16% Fe, 1.5% TiO_2 and 0.1% to 1.2% V_2O_5 (Moskalyk & Alfantazi, 2003; Taylor *et al.*, 2005). Compared to the South African ores from the Bushveld Complex, the Kachkanar deposit is much lower in titania, which would make the ore less challenging to process in a blast furnace, if compared to the Chinese ores. EVRAZ Nizhniy Tagil Metallurgical Plant (NTMK) is one of the oldest steel production and mining centres in Russia with a history dating back to 1725. NTMK became part of the EVRAZ Group in 2000, which also eventually was the last owner Highveld Steel before the demise of the company in 2015 (Lazutkin *et al.*, 2001; Smirnov *et al.*, 2000).

According to Lazutkin et al. (2001), research into processing titanomagnetite ores in blast furnace was already well advanced as early as 1925, stating that Russian metallurgists had developed a blast furnace smelting process to produce vanadium-bearing pig iron and titanium-bearing slag. They also report that the titania-bearing slag was used as feedstock for the paint industry. Unfortunately, no definitive support literature was found to support the comment or to provide further technical insight. Based on the low starting grade, and the fact that the smelting technology is a blast furnace, the recovery of titanium was likely quite complicated, with large quantities of waste generation due to the high concentration of gangue components.

Smirnov et al. (2000) summarise progress made since the introduction of titanomagnetite to the blast furnace process. The authors introduce the process as follows: *"The lower efficiency of smelting vanadium pig iron is attributable to a specific feature of the blast-furnace process when the charge contains Kachkanar titanomagnetite ores. This feature is related to the presence of titanium in the ores."* The authors also refer to the *"harmful effects of titanium"* to further illustrate the context.

JSC (Joint Stock Company) Kachkanarskiy produces vanadium-bearing iron ore pellets and agglomerate which serves as feedstock for the steelworks of NTMK. The composition of the concentrate produced by Kachkanarskiy is reported as containing 61.3% to 64.9% Fe, about 3% TiO_2, and 0.57% to 0.66% V_2O_5, prior to pelletizing and sintering (Moskalyk & Alfantazi, 2003).

Lazutkin et al. (2001) articulate the challenges associated with blast furnaces as follows: *"While noting the definite improvements that have been made to the blast-furnace smelting of titanomagnetites, we must still concur with the assessment of Academician M.A. Pavlov: Titanomagnetites cannot be as easily smelted as conventional ores – this much must be acknowledged beforehand."* The quote again highlights the challenging nature of smelting titania-bearing ores in a blast furnace.

The current NTMK blast furnaces were commissioned in the early 2000s (2005 to 2006) and produce a vanadium-bearing iron product (Infomine Research Group, 2014). The operation at NTMK reportedly produces iron with 0.15% Si, 0.2% Ti and V of up to 0.55% (Taylor *et al.*, 2005). Limited operational data for the Russian operations are available in the public domain. The operating regime of the Russian process is however much closer to conventional iron ore processing due to the much lower TiO_2 content of the feed, and the ore is less likely to be economically processed for titanium recovery.

2.5.5 Fluxless smelting of titaniferous ores (ilmenite smelting)

Smelting of ilmenite, a titaniferous ore, is essentially an iron extraction process (concentrating the titanium oxide in the slag by removing the iron oxide through reductive smelting), but unlike the titanomagnetite operations, ilmenite smelters are not principally ironmakers. Iron is an economic boon, rather than the object of the process. In addition, the feed is intentionally processed in the absence of additives and contaminants. Iron is removed from the oxide ore by reduction to metallic iron. The reaction takes place in the liquid state at a temperature of around 1650°C. The unique characteristic of ilmenite smelting is that the process yields titania-rich furnace slag as the primary produce and iron as a metal by-product; usually, slag is a discard stream in ferro-alloy smelting. In some cases, some of the iron is reduced to the metallic state in a pretreatment step (solid-state reduction). Benefits of prereduction include lower energy consumption in the furnace (lower electrical requirement), and due to the significant reduction of iron in the pretreatment step, incidences of foaming slag is reduced as less reaction gas is produced in the furnace (Gilman & Taylor, 2001; Pistorius, 2008; Stanaway, 1994a; Zhang *et al.*, 2011).

The iron extraction process offers little opportunity for removal of minor impurities which may naturally be present in the titanium-bearing mineral. The quality (and grade) of the feedstock determines the quality of the end product that can be produced. This holds true regardless of whether the titania feedstock is hard rock ilmenite, beach sands, or

titaniferous magnetite the grade of the ore processed, which is related to the degree that the rock ore or mineral sand deposit is amenable to upgrading. Slag producers have some wiggle room to increase product grade, mainly through reducing the iron oxide content of the slag. Although it is possible to reduce virtually all the iron oxide from the slag, consequences include: a dramatic increase in slag viscosity, increased energy consumption and operational challenges, amongst others. The remaining oxides are proportionally concentrated in the slag with the titania. Starting concentrations of deleterious elements are thus dependent on the precursor feedstock being processed. Some furnace slags are further upgraded via proprietary leaching processes resulting in what is referred to as upgraded slag (UGS).

The most prominent ilmenite smelting furnaces are configured in the following ways:

- A rectangular six-in-line AC (alternating current) electric arc furnace; as used by Quebec Iron and Titanium Corporation (QIT) at Sorel in Canada, and by Richards Bay Minerals (RBM) at Richards Bay in South Africa. Six pre-baked graphite electrodes are used, and ilmenite and reductant are fed into the furnace through a complex assembly of feed ports in the furnace roof (Sun *et al.*, 2012; Williams & Steenkamp, 2006). RBM yields about 25% of titanium feedstocks (titania slag and rutile), 33% of the global zircon output and 25% of the global high purity pig iron (Rio Tinto, 2016)
- A circular AC electric arc furnace; as used by TiZir Titanium and Iron (formerly known as Tinfos) at Tyssedal in Norway. This furnace has three self-baking Søderberg electrodes, and a number of feed ports are used to feed prereduced ilmenite (in pellet form) and coal into the furnace (Rosenqvist, 1992).
- A circular DC (direct current) electric arc furnace; as used by Namakwa Sands, located at Vredenburg in South Africa, and by KZN Sands located at Empangeni in South Africa. The ilmenite and anthracite fed via feed ports on the roof, generally located around the graphite electrode (Gous, 2006; Williams & Steenkamp, 2006). Namakwa Sands produces 10% of the world's zircon, 5% of global pig iron and 8% of the world's titanium dioxide (Cloete, 2014).

Table 2-12 summarises the current furnace slag producers, with capacity and feedstock information compared to the product grade. The data presented in the table is assembled from a broad selection of publications as listed previously.

Table 2-12: Furnaces slag production capacities for primary ilmenite smelters worldwide

Company	Country	Stated capacity, tpa	Feedstock			Slag product
			TiO_2	FeO	Type	TiO_2 grade
QIT [a]	Canada	1.2 million	34%	53%	rock	77 to 80%, & upgraded slag 95%
RBM [b]	SA	1.05 million	49%	-	roasted sand	85%
Namakwa Sands [c]	SA	180 000	47%	47%	sand	86%
KZN Sands [d]	SA	250 000	49%	-	sand	85%
TTI [e]	Norway	200 000	44% 51%	46%	rock sand	75%
CYMCO Xinli [f]	China	85 000	-	-	sand	87%

(a) Rio Tinto Fer et Titane formerly Quebec Iron &Titanium (QIT) Fer et Titane; (b) Richards Bay Minerals (a subsidiary of Rio Tinto);
(c) Tronox Namakwa Sands; (d) Tronox KZN Sands formerly Ticor; (e) TiZir Titanium and Iron (TTI) formerly TINFOS, (Tyssedal, Norway)
(f) Yunnan Xinli Non-ferrous Metals Company Ltd wholly owned by China Yunnan Metallurgical Company (CYMCO)

The new DC smelters in Saudi Arabia, the Jazan smelters, have been marred by significant start-up delays. National Titanium Dioxide Company (Cristal) has invested heavily in this facility, but recently Cristal and Tronox announced their intention to merge. Tronox is currently providing expert support to the Cristal; start-up has been shifted to late 2019 (the Cristal operation has been struggling since 2015 to reach production capacity) (Perks, 2018).

Figure 2-4 summarises the various processes related to the processing of ilmenite and rutile (high titania ores) to produce titania pigment and titanium metal, including upgrading via smelting (Filippou & Hudon, 2009; adapted from Stanaway, 1994b, fig. 1).

Slags produced by various industrial smelters are processed either directly as feedstock to the two primary pigment processes, namely the sulfate and the chloride processes, or alternatively upgraded to meet the specifications of the chloride process. The challenge with the gangue components contained in titania feedstocks (other than FeO and TiO_2) is the impact these components have on the operability of the post-taphole processes. These components impact product quality, contribute to the environmental footprint of the pigment production process and also increase operating cost and process complexity.

It is technically feasible to upgrade ilmenite (without smelting), but it would not be economical due to the large volume of iron waste that would be produced. Upgrading technologies are mostly an iron removal step, and in the case of ilmenite, smelting is the most effective way of removing iron from iron-rich titaniferous ores. It is important to note that smelting offers only a minimal opportunity for the removal of minor impurities which may naturally be present in the titanium-bearing mineral.

The quality (and grade) of the feedstock to a large degree determines the quality of the end product that can be produced. It is no different whether the slag is produced from ilmenite or titanomagnetite ores. The co-production of iron is a significant economic and environmental advantage of the smelting processes if compared to pigment processes where iron is rejected as waste material, for example. The iron product is also usually a good quality product and thus sought after for speciality applications. About 30% of the feedstock for the pigment industry is produced via smelting of ilmenite minerals in Canada and South Africa (Filippou & Hudon, 2009).

Table 2-13 summarises the titania content of the relevant feedstocks depicted in Figure 2-4.

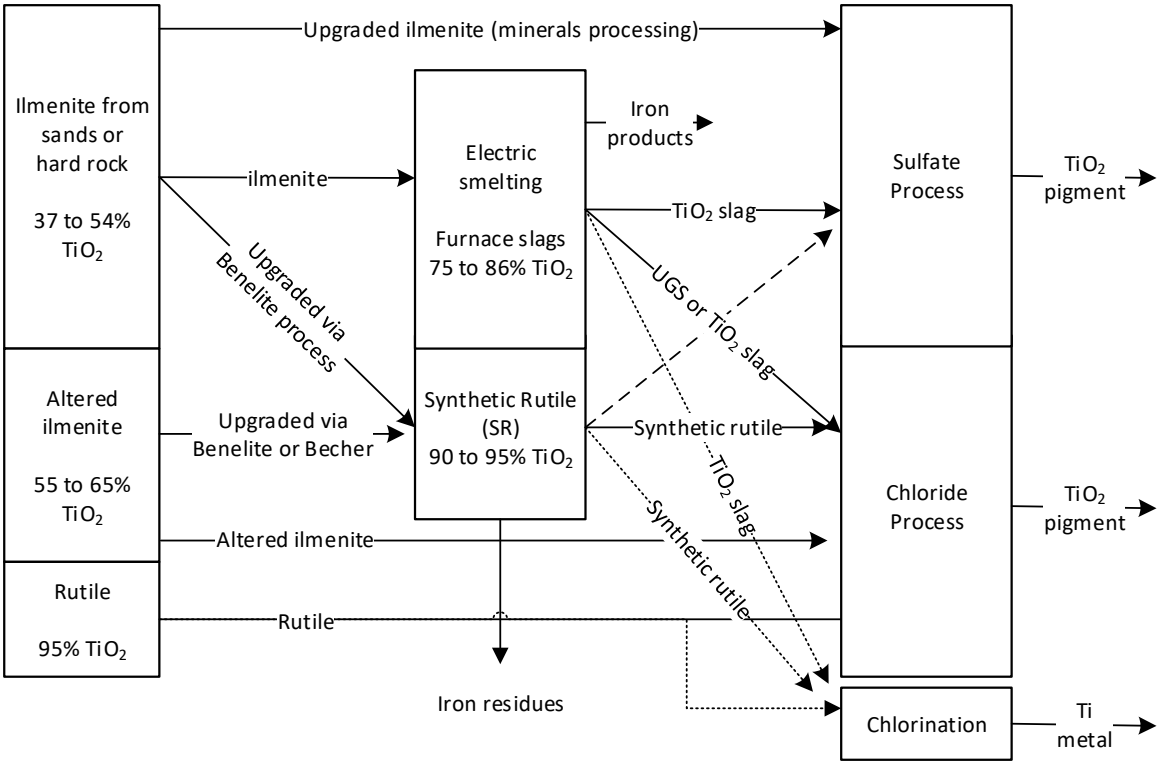

Figure 2-4: Summarised representation of titania feedstock processing options - adapted from Stanaway (1994b)

Table 2-13: Titania grade of various types of titania feedstocks, mass %

Material	TiO_2 content	Type
Ilmenite	37 – 54%	Naturally occurring
Leucoxene (altered ilmenite)	55 – 65%	
Rutile	95%	
Furnace slags	75 – 86%	Upgraded
Upgraded slag (UGS)	95%	
Synthetic Rutile (SR)	90 – 93%	

2.6 BACKGROUND AND CURRENT PRACTICES - CONCLUSION

The review of the relevant literature provides an overview of the smelting technologies currently in use provide useful background and context for the proposed technology solution. The subject is broad, and complex, due to the relatively low-grades of the three commodities involved, namely iron, vanadium and titanium. Table 2-14 delineates the various pyrometallurgical smelting methods associated with the processing of titaniferous ores as a summary of the overview.

Table 2-14: Delineation of smelting technologies associated with titaniferous materials

Type of furnace	Description	Operation	Type of Ti-ore
Blast furnace	Non-electrical	Shaft furnace	1, 3
Electric Arc Furnace (submerged arc)	AC circular furnace, 3 electrode	Covered bath, resistance heating	1
Electric Arc Furnace (open-arc)	AC, rectangular furnace, 6 electrodes in-line	Partially covered bath, energy supplied by arc	1, 2
Electric Arc Furnace (open-arc)	AC, circular furnace, 3 electrodes	Open or partially covered bath, energy supplied by arc	1, 2, 3
Electric Arc Furnace (open-arc)	DC, circular furnace (single electrode)	Open bath or partially covered bath, energy supplied by a single arc	1, 2, 3

1= Titaniferous magnetite 2=Ilmenite 3=Iron ore

The objective of the literature survey is to set a backdrop against which the feasibility of the proposed technology will be evaluated. The following insights are extracted:

- Smelting of titaniferous (and vanadiferous) magnetite ores are predominantly processed as an iron source with vanadium as a by-product from an ironmaking process. Titania is discarded as a waste slag from the smelting step.
- The majority of furnaces currently in operation are blast furnaces, and significant challenges are known to be associated in these furnaces. The feedstock is blended carefully with iron ore and fluxes to optimise the smelting regime in the blast furnace, primarily through dilution of the titanium oxide. If feasible, the ore is upgraded by removal of titania, but usually, the mineralogy limits this opportunity.
- Electric furnaces smelting of titanomagnetite ores are a relatively modern application, but the key objective has been to recover iron and vanadium as a by-product for strategic reasons (both entities had substantial government backing during inception). Both producers experienced process challenges, and a number of equipment and flowsheet changes were introduced to adapt to the challenges of processing this type of ore. Both producers operated with a fluxed smelting regime, but New Zealand Steel has always operated without a burden, thus operating closer to typical ilmenite smelters.

Table 2-15 presents a conceptual summary of the various smelting practices of ironmaking from iron ore, titanomagnetite ores and titania slag production, comparing these processes with fluxless smelting of titanomagnetite - as proposed via this research project. Ironmaking from highly oxides iron ore (typical) and ilmenite smelting to produce high-titania slag are compared to the current smelting practices associated with titanomagnetite processing.

The comparison is presented to contextualise, where fluxless smelting fits into the overall picture and aims to highlight the hybrid nature of titanomagnetite. The summary shows that the proposed fluxless method is more similar in concept to ilmenite smelting than the current ironmaking focus. The hypothesis is that processing titanomagnetite ores as an iron source limits the scope for comprehensive processing. The successful operation of ilmenite smelters worldwide and specifically DC smelting in South Africa poses an opportunity to rethink the need for fluxing and thus potentially allows for unlocking of this complex resource for future processing instead of creating a growing environmental legacy through diluted slag dumps. The various industrial processes for ironmaking and titania slags, as presented in the next table, illustrates where fluxless smelting of titaniferous magnetite fits within this broader context.

Table 2-15: Delineation of modern iron, titanomagnetite, and ilmenite smelting practices compared with a hypothetical fluxless vanadiferous titanomagnetite smelter

Primary Industry	**Ironmaking**				**Titania slag**
Feedstock	Iron ore	Vanadiferous titanomagnetite			Ilmenite
Simplified description of smelting step	Blast furnace	Blast furnace	Electric furnace (shielded arc)	Electric furnace (open-arc)	Electric furnace (open-arc)
	Fluxed	Fluxed, ore blending	Fluxed	Fluxless	Fluxless
Primary product	Iron	Iron, Vanadium		Iron, Vanadium Titania slag	Titania slag, Iron
Waste-product	Ironmaking slags	Diluted titania slags		-	-
Users	Global	China Russia	New Zealand South Africa	No current users	Canada, South Africa, Norway
Process features	• Iron ore processing bulk smelting (large furnaces as the economy of scale key to producing low-cost iron) • Ores and recipes hugely varied in composition • Ironmaking slags widely used in cement industry	• Blast furnace similar to ironmaking (economy of scale key to producing low-cost iron) • Processing associated with large volumes of slag dumps containing diluted titanium oxide and residual vanadium (poses an environmental risk) • Slags are not currently used or processed on large scale		• Recoveries optimised for metallurgical performance • Titania slag potential feed to pigment industry • Lower volumes of slag (no fluxing)	• Comprehensive use of ore to produce two products • Slag mainly used as feedstock to pigment industry

The proposed process, namely fluxless smelting of titaniferous magnetite ore, is based on the same principle as applied for the smelting of ilmenite. Fluxless smelting of titanomagnetite was also patented by Mintek in the early 90s (Boyd *et al.*, 1993), shortly after Mintek patented the DC smelting process for ilmenite smelting, but the technology was never commercialised (the patent protection has expired).

DC smelting of ilmenite has been proven in South Africa, and it is therefore likely that a local smelter processing titaniferous magnetite would benefit from the know-how of the local industry. If titaniferous magnetite ore is processed with the objective of recovering titanium (with iron and vanadium co-produced), the slag produced from this process will have to compete with higher grade furnace slag products produced from ilmenite deposits.

3 EXPERIMENTAL METHODOLOGY

In this section, a description of the equipment and raw materials, as well as the various experimental methods, are presented. A pilot-plant test is unlike a controlled laboratory experiment, as the intention is to simulate industrial operating conditions.

Pilot-plant smelting of a bulk sample of low-grade titaniferous ore was completed to evaluate the feasibility of upgrading low-grade titaniferous material via fluxless smelting. The main objective was to assess whether a titania-rich slag could be produced and to evaluate if the slag could potentially be a viable feedstock for pigment production.

Selection of technology is a complex process that entails evaluating a variety of techno-economic variables. New technology is associated with risk, and for all metallurgical processes, especially smelting processes, it is crucial to demonstrate the process at a significant scale to mitigate these risks. Pyrometallurgical testwork is also useful to benchmark a new technology or process flowsheet, often comparing the results against current processes. MINTEK's pilot furnace facilities are used to facilitate such comparisons and development work. Pilot-plant testwork addresses aspects of the process, such as product quality, recovery, and process parameters, thereby adding significant value to projects. The operational and metallurgical data from a pilot-plant test are processed and evaluated to provide input to feasibility and, ultimately, design studies.

Many factors influence the choice between laboratory and pilot-scale smelting testwork. Different types of results can be obtained from different scales. The scale depends on a number of factors, such as the stage of the project, affordability and access to feed materials (Geldenhuys & Jones, 2011). A pilot-plant test is favoured if new technology needs to be de-risked. The pilot DC smelting facility at Mintek mimics industrial practices and can be operated continuously for extended periods. A range of scale options is available, including operating power and furnace diameter, linked to aspects such as slag-to-metal ratio, metallurgical requirements such as feed recipes and operating temperatures, as well as off-gas volume. In essence, each project requires substantial engineering input from the researchers to specify the furnace for the installation.

The data collected from a pilot furnace operations are frequently used to specify key design parameters of a furnace and power supply design and is used as the primary input in design and feasibility studies by engineering companies.

Design of the experimental plan or the test programme takes into account the process requirements, slag properties, and mass flow rates, and the objective of the test. These factors are used to design the refractory installation, taphole designs, furnace diameter and the experimental plan. The next section provides a description of experimental techniques, the pilot-plant equipment design and set-up, as was designed to achieve the desired testwork outcomes, and characterisation work concluded on the raw materials prior to smelting.

A test program for a pilot smelting project consists of an elaborate experimental plan that includes a large number of potential variables. In order to achieve the desired experimental outcomes, it is essential to identify the most appropriate analytical techniques and sampling strategies for the various feed and product streams, as the matrices, the concentration of elements and properties of elements can influence the accuracy of a technique, as one example of the factors that need to be taken into account.

An important deliverable of a typical pilot-plant test is to demonstrate product grade specific to the ore tested, operating stability is therefore essential, and the operational strategy forms part of the scope to ensure enough stable data points are collected with reasonable confidence in the results. In order to evaluate grade-recovery relationships, feed and product streams are weighed and sampled during the test to produce an elemental mass balance used as the basis of the assessment of the experimental outcomes. The mass and energy balance is the crux of a pilot-plant test.

3.1 PILOT-PLANT EQUIPMENT DESCRIPTION

Demonstration-scale smelting testwork was conducted utilising a 2.5 m shell diameter DC electric arc furnace facility in the Pyrometallurgy Division at MINTEK. Auxiliary equipment includes a dedicated feed system, water-cooling circuits, an off-gas handling system, which includes a bag filter plant, and an integrated control system.

A description of the different aspects of the equipment as designed and used during the smelting campaign is described in the next sub-sections.

In Figure 3-1, a simplified diagram of the pilot-plant is shown. The facility is designed to demonstrate a process as close to industrial conditions as practically possible and therefor includes an integrated feed and off-gas handling system.

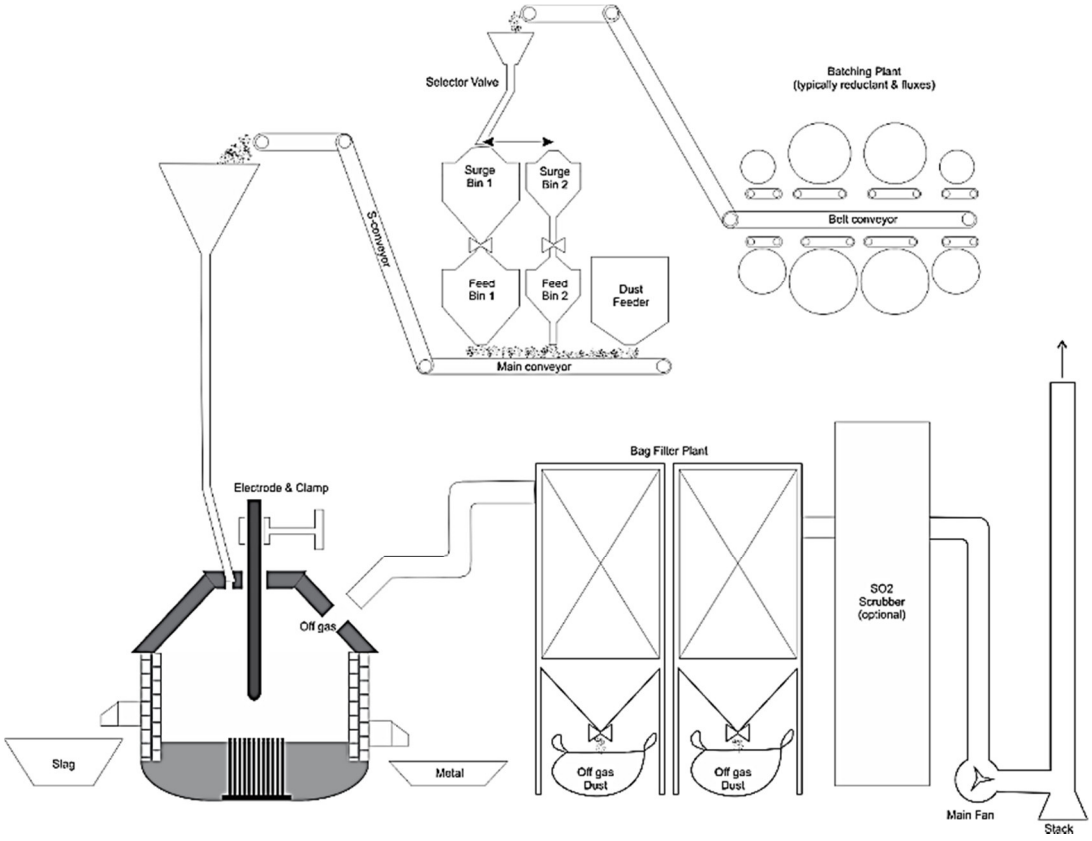

Figure 3-1: A schematic diagram of the pilot-plant facility

3.1.1 Description of the furnace installation

The installed pilot-plat furnace consists of a refractory-lined cylindrical shell, a domed base, a conical roof and a refractory roof plug resting on top of the conical roof. The furnace shell has an unlined internal diameter of 2.5 m (generally referred to as the shell diameter or "OD"). The conical roof design includes an off-gas port or opening to allow for the extraction of the process gasses. The shell has two openings, in which the taphole blocks are seated during the installation of the refractories. The conical roof and upper shell area are cooled by means of forced water-cooled circuits while the furnace lower shell is designed to utilise film water-cooling. Three water-cooled copper inserts were installed in the metal taphole, as part of the taphole design.

A single electrode located centrally to the furnace sidewalls serves as the cathode. The roof plug includes a mild steel electrode stuffing box, positioned centrally, to create a gas-seal around the graphite electrode. In addition, the roof plug contains two circular ports, one of which is utilised as a feed port while the second is generally used to inspect the furnace bath and take bath depth measurements by using a steel dip rod. Access to the roof is restricted by way of lock-out. The furnace off-gas port and the inspection port located in the roof were used during the testwork as inspection ports to evaluate the conditions of the bath.

The electrode clamp, roof and feed pipes are electrically isolated from the furnace. The return electrode (anode) consists of steel rods (20 mm diameter) connected at their lower ends to a steel plate welded to the dome of the furnace. The anode pins are embedded in the hearth refractory during installation. K-type thermocouples are installed for purposes of monitoring the temperature profile in the furnace, namely in the refractory lining in the lower shell area and in the hearth. The profile is used primarily during the furnace warm-up to manage the heating cycle of the various refractories, but are regarded as sacrificial. K-type thermocouples are used as the units are relatively inexpensive. A general view of the furnace is shown in Figure 3-2, the relative position of the various aspects described in this section annotated on the photograph for clarification.

Figure 3-2: A view the furnace in operation (photograph by author)

The refractory installation consisted of the hearth, sidewall and roof, each installed with an appropriate refractory type selected for each area in accordance with the purpose.

The domed base of the furnace was filled with high-magnesia ramming grit to a level of approximately 30 mm below the metal taphole (this constitutes the hearth). The magnesia ramming grit was tightly compacted during the installation process. Fourteen rows of magnesia bricks were required to line the sidewall. The installed sidewall thickness was approximately 230 mm while an average row consisted of 47 bricks (100 mm row height). The average lined operating diameter (ID) was 2010 mm. The conical roof refractory consisted of a high-alumina castable cast to a thickness of approximately 150 mm. The same castable refractory was used to cast the roof plug. Both the roof and roof plug were fired prior to installation. A schematic diagram, including the basic furnace dimensions, showing the refractory layout, is presented in Figure 3-3.

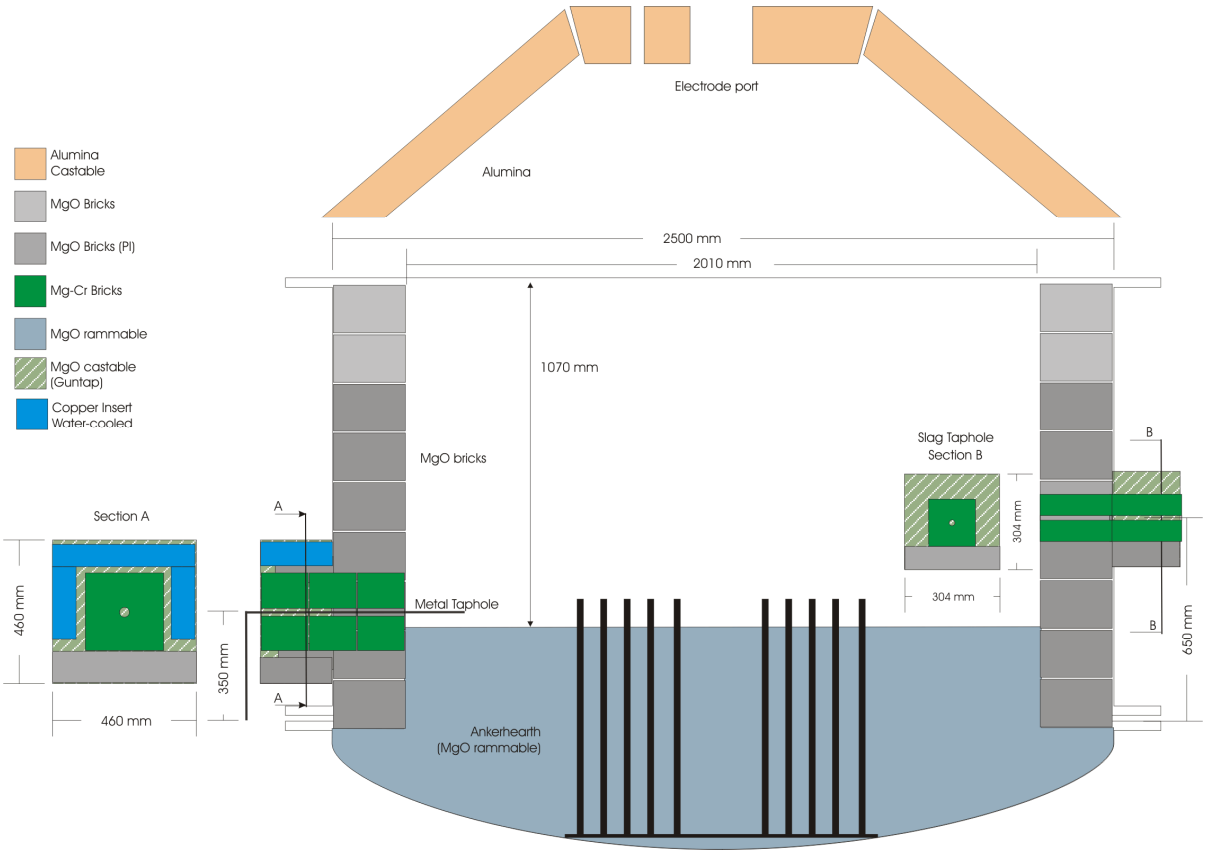

Figure 3-3: Schematic of furnace dimensions and refractory installation

Additional technical specifications and photographs of the installation process are provided in Appendix A, including the composition of the refractories.

3.1.2 Feed System

The feed system comprises a batching plant and a final feeder arrangement as well as a dedicated concentrate feeder suited to handle the fine feed materials. The final feed system arrangement includes two surge or storage bins and two final feeders, an S-conveyor, and a final transfer bin located above the furnace. The dust feeder feeds directly onto a dedicated conveyor belt linked to the S-conveyor and finally into the final transfer bin located above the furnace.

A feed pipe links the final transfer bin to the furnace. All the hoppers rest on load cells, connected to dedicated controllers. The feed rate targets of the controllers are entered into the control system and the supervisory control, and data acquisition system (commercial product, DeltaV) controls the relative rates accordingly. The batching plant consists of eight feed storage bins of varying size; each hopper delivers material to the primary conveyor belt via a dedicated controlled belt under each bin. The conveyor belt then transfers the material to a vertical pocket conveyor for elevating and discharging of the material into one of the two surge bins, as per the selection by the controller. Surge bin 1 and final feeder 1 was used to feed a proportioned addition of the low ash anthracite to achieve the desired degree of reduction matching the feed rate of the dust feeder (see Figure 3-1 for annotated diagram of the plant layout).

The surge bins and the feed hoppers utilised during the campaign, rest on load cells. All load cells were calibrated prior to the commencement of the campaign using standard weights. The various products (slag, metal, bag filter plant dust and off-gas cleanout) were weighed on a 4-ton scale that is regularly calibrated and maintained.

3.1.3 Off-gas handling

The pilot-plant facility includes an integrated off-gas handling system that can be linked to a number of different pilot test furnaces. Furnace gaseous products and dust were extracted through an off-gas port located on the furnace roof into the gas extraction system. The gas extraction system includes water-cooled ducting linking the furnace to the reverse-pulse bag filter plant, a fan and a stack — the water-cooled ducting transports the off-gas to the gas cleaning plant, consisting of two reverse-pulse bag filters. The bag filter plant is shown in Figure 3-4. The gas and dust stream enters the reverse-pulse gas filter, and the filtered gas stream exited from the side of the bag filter plant and was

exhausted to the environment via a stack, while the dust was collected at the bottom of the bag filter plant in bulk bags. The bags were changed at the end of a condition or when full. The dust was labelled according to the condition, weighed, sampled and stored.

MINTEK strives to operate all testwork projects in an environmentally responsible manner and operates all its facilities in accordance with South African standards and legal requirements for emissions. Emissions to the atmosphere are legislated by the National Environment Management Air Quality Act. A continuous SO_2 monitoring system is installed to monitor the SO_2 concentration in the stack during testwork campaigns. An independent specialist is contracted to measure carbon monoxide, carbon dioxide, nitrogen oxide and sulfur dioxide levels during smelting projects to ensure the facility adheres to the desired levels of emission. The procedure for "Determining Particulate Emissions" from steady processes is used for the measurement of the emission concentrations ("The International Standard ISO 9096 – 2004: Determination of concentration and mass flow rate of particulate material in gas carrying ducts").

Figure 3-4: The bag filter plant (left), and a close-up view of a full bulk bag of off-gas dust (right)

3.2 Definitions, Methods and Procedures

This section focuses on the general methodologies applied to achieve the testwork objectives, including sampling protocols, general descriptions of analytical techniques, and definitions used in the discussion of the results.

3.2.1 Mass balance techniques and definitions

The testwork mass balance is based on the law of conservation of elemental mass, stating that the mass of an element entering the system is equal to the sum of the mass of the element leaving the system and the accumulation of the element in the system.

$$m_{i,\,\mathrm{IN}} = m_{i,\,\mathrm{OUT}} + m_{i,\,\mathrm{ACC}} \qquad \text{Equation 1}$$

Where

$m_{i,\,\mathrm{IN}}$ = mass of element i in the stream entering the system
$m_{i,\,\mathrm{OUT}}$ = mass of element i in the streams leaving the system
$m_{i,\,\mathrm{ACC}}$ = mass of element accumulated in the system

The following diagram, Figure 3-5, illustrates the boundaries applied with respect to the mass balance. Several formulations of the mass balance are used to ensure that the data used to evaluate the results and specify the process design parameters, adequately represents the overall process or conditions. Uncertainties associated with weighing, sampling and assaying of raw materials and products are inevitable, and for a project of this scale, it is crucial to demonstrate that the results are based on substantive and reliable information. The mass balance techniques utilised during the current study are briefly summarised and defined for clarity and reference.

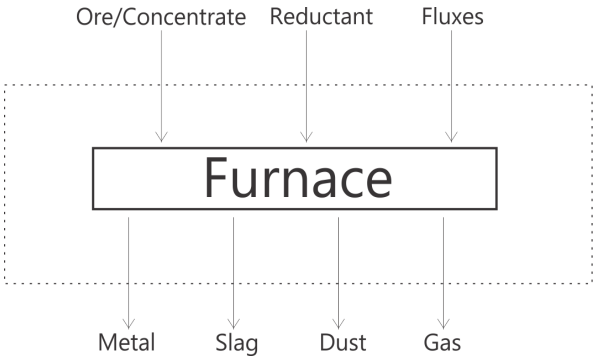

Figure 3-5: Diagram depicting mass balance boundaries

Overall Element Accountability: This denotes the percentage of the elements in the feed material that are recovered as products and is a useful tool for assessing the quality of the testwork and elemental mass balance. The overall accountability is generally affected by uncertainty in the analyses or masses of both the raw materials and the products. The overall accountability is based on the major elements present in the slag, metal and dust.

Cumulative Accountability: Cumulative accountability of major elements throughout the campaign is generally depicted in a graph. It presents the evolution of accountability throughout the campaign and is useful to highlight the accumulation of an element. It is one of the tools used to regulate/evaluate the furnace inventory, metal production rate and clearly illustrate refractory wear.

Element Recovery: Elemental recovery differs from accountability in that it quantifies the percentage of elements in the feed material that reports to, or is recovered to, a particular product (slag, metal or off-gas dust). It is also affected by analytical and weighing uncertainties of the raw materials and products. The recovery of the product of interest is of particular importance. For a test campaign on a pilot-plant facility, material recovered from the off-gas handling system is not recycled; while this could be the case on a commercial furnace. References to the recovery of an individual element to the metal phase – unless stated otherwise – is defined as per Equation 2. Recovery may also be expressed as elemental recovery to the slag phase.

$$Elemental\ recovery_{i,metal} = \frac{m_{i,metal}}{m_{i,in}} \qquad \text{Equation 2}$$

Element Distribution (also referred to as elemental deportment): The element distribution establishes the partition of total product mass of each element into the different product streams, e.g. metal, slag and dust. If conditions were ideal and masses and analyses were entirely accurate, and there was 100% accountability, the element distribution would be equivalent to the element recovery.

If the accountability of an element is good, the simplest expression for recovery of an element is the ratio between the elemental mass in the metal divided by the combined product mass, which is defined herein as elemental distribution or deportment (as per Equation 3) to the metal phase. For this definition, only solid product streams are taken into account.

$$Elemental\ distribution_{i,metal} = \frac{m_{i,alloy}}{m_{i,metal} + m_{i,slag} + m_{i,dust}} \qquad \text{Equation 3}$$

3.2.2 Description of sampling protocols and analytical techniques

Due to the scale of a pilot-plant, the average composition of the feed or head grade is determined via best-practice methods, constrained via practicality (time and cost) by preparing a representative sub-samples and preparing composites. The composition of the feed material is required as input to the overall mass balance. The general sampling strategy for feed materials is described, followed by a general description of the various analytical methods used for the test programme. Mintek's Analytical Laboratory is an accredited laboratory and operates in accordance with the ISO 17025 standard operating procedures.

Titaniferous concentrate: The bulk concentrate sample was delivered in drums (about 240 sealed 200-litre metal drums). On delivery, the concentrate was blended and sampled by de-drumming the concentrate onto a blending pad. It is always desirable to conduct testwork on a homogenous bulk sample. A representative head grade analysis was calculated from representative sub-samples from defined batched. The samples (10 of) were prepared and assayed to determine the composition of the low-grade titaniferous concentrate. The head grade analysis is used in calculations throughout this report. The following elements are included in the standard oxide package for ilmenite concentrate: Al_2O_3, SiO_2, CaO, TiO_2, V_2O_5, Cr_2O_3, MnO, FeO, MgO. In addition, C, S and P concentration was checked. An external analysis of the concentrate was also conducted to verify the in-house method; identical fractions were submitted to a commercial laboratory for validation. The following elements are included in the standard oxide package for concentrate: Al_2O_3, SiO_2, CaO, TiO_2, V_2O_5, Cr_2O_3, MnO, FeO, MgO (ICP-OES method).

Low-ash anthracite: The reductant was delivered to Mintek packaged in bulk bags, and was sampled upon arrival. The anthracite was delivered dry, and no further drying was required. Samples were taken from the bulk bags and collated to form a bulk sample. The four samples generated was assayed for total fixed C, S, P, and ash and volatile content as well as the calorific value. An ash analysis was also obtained for mass balance purposes.

All solid **furnace products** were sampled via suitable sampling methods to ensure representative samples are collected for each batch fed to the furnace. Spoon samples of metal and slag were taken during tapping by cross-cutting the fluid stream (metal or slag) flowing from the furnace. Slag and metal were tapped from separate tapholes, with the slag taphole approximately 300 mm higher than the metal taphole. At the same time, temperature measurement was taken, utilising an optical pyrometer. The samples were allowed to cool and the required sample mass selected for further preparation. The slag and the preliminary metal results were typically available within 4 to 6 hours of tapping the furnace.

Furnace off-gas dust is collected continuously at the bag plant during a test campaign (see section 3.1.3 for a description of the off-gas handling facility). The dust is collected in four bulk bags connected to four drop-out sections of the bag plant. For this test campaign bags were changed once full, the collected dust in the bag was sampled and weighed for mass balance purposes. Dust samples were submitted during regular working hours for analysis.

Online analyses, used for process control purposes, included the following elements (24-hours): *For slag:* MgO, Al_2O_3, CaO, V_2O_5, SiO_2, FeO, Cr_2O_3, MnO and TiO_2 (MXF, fused bead). Offline analysis of the metal, dust and slag sample included the following: S, C and P for the metal; Al_2O_3, SiO_2, CaO, TiO_2, V_2O_5, Cr_2O_3, MnO, FeO, MgO (MXF, Fused bead), S, C and P content of the dust; and S, C and P content of the slag. The following additional elements were analysed for all the metal samples: Si, Ti, V, Cr, Mn, Fe, Ni, Co (ICP-OES method).

The analytical techniques utilised to assay samples generated during the pilot test is summarised by the type of analyses.

Multi-channel X-ray fluorescence – Fused Bead (MXF): This method was used to analyse titania-concentrate, furnace slag and furnace dust. The specific technique provides a quick turnaround time on shift. The method utilised is briefly described in this section. The slag sample submitted for the assay was milled, and 0.25 g of the sample mixed with 6.75 g flux (LiB_4O_7). This mixture is fused into a glass bead in a furnace at 1050°C. The bead is analysed on a multi-channel X-

ray fluorescence (MXF) instrument which is calibrated against appropriately certified ilmenite concentrate and high-titania slag references, specifically SARMs (South African Reference Materials). The fusion of the sample into a glass bead ensures a uniform, mirror finish surface and a wholly homogenised dissolved sample for accurate analysis with no scatter of the X-rays.

Energy Dispersive X-ray – Pressed Pellet (EDX): Metal was analysed using a pressed pellet method (for control purposes). This analytical technique is utilised for the online analysis of metal due to the fast turnaround time, but each metal sample was subsequently assayed via ICP-OES for mass balance purposes. The quick turnaround time of this technique is preferred during the campaign, while the assay is not regarded as final; the method provides the desired information with regards to grade which is part of the process evaluation during the campaign. The metal sample is milled finely and pressed under 20 tons of pressure to render a smooth surface. The analysis is read by an Energy Dispersive X-ray (EDX) instrument. The elements analysed are majors and minor to major. Thus on such concentration levels, a wavelength dispersive X-ray instrument is not required as accuracy will not be compromised at percentage levels.

Carbon and Sulfur by LECO (via combustion): C and S content of feed and product samples were evaluated using standard combustion methods. Samples are heated in a combustion furnace, in oxygen, and the S is oxidized and detected as SO_2 by an infrared detector. Total carbon is analysed similarly and detected as CO_2.

Phosphorus (via colourimetry): P content of metal samples and composite slag and dust samples was determined. The product of the fusion with sodium peroxide and sodium carbonate is leached in water. After precipitating the P with ferrous iron, the precipitate is dissolved, and the P is complexed with an ammonium molybdate/vanadate reagent, forming a yellow complex. The complex is extracted into methyl isobutyl ketone (MIBK), and the P in the extract is determined spectrophotometrically (ultraviolet).

Inductively coupled plasma-optical emission spectroscopy (ICP-OES): Methods specific for concentrate, slag and off-gas dust and pig iron are used in each case. A known mass of the pulverised sample of interest is fused using a potent oxidising agent, such as sodium peroxide. The molten material is digested in acid and the solution assayed by ICP-OES using the appropriate accredited method for concentrate, slag or metal. Slag samples, metal, dust and feed samples were assayed via ICP-OES for mass balance purposes.

3.2.3 Product handling

The slag was tapped into mild steel ladles while the metal was tapped into refractory-lined ladles. The volume of the mild steel ladles was approximately 0.38 m³ while the volume of the refractory-lined ladles was approximately 0.12 m³. One slag ladle was used per slag tap while two to three refractory lined ladles were arranged in a cascade formation during metal taps.

Figure 3-6 shows a typical slag and metal tap in progress. The tapped products were allowed to solidify in the ladles, after which the ladles were taken by a forklift to a dedicated cooling area and allowed to cool for a further 8 to 12 hours, by which time the ladles were deemed safe to tip. Following this cooling period, the weighed, solidified slag, was tipped in a dedicated tipping area, and immediately sprayed with water mist, until cooled enough for safe handling by personnel. Each batch was bagged separately and the weight recorded. The slag product was stored in a dedicated slag storage area. Figure 3-7 shows an example of the slag product in the dedicated tipping area, prior to being bagged, and an example of a metal ingot removed from the ladle.

Figure 3-6: Slag and metal tapping in progress

Figure 3-7: Cooled products; slag (left), and a metal ingot (right)

3.2.4 Furnace control philosophy

The control system (DeltaV DCS, a programmable commercial system) is programmed and set up to allow the furnace and materials handling plant to be fully controlled from an operator user interface or partially controlled from a control desk located in the dedicated facility Control Room. The process is thus controlled and monitored, while the DeltaV interface provides a console for configuration of operating parameters, recipe management, alarm enunciation and data logging. Drives that were required to be started and stopped during the campaign, e.g. conveyors, feeders etc. were operated remotely via the DeltaV interface or manually via a local console consisting of a manual/automatic change over switch, control potentiometer (where appropriate) and start-stop buttons. The furnace was operated in what is informally referred to as 'Constant Current Mode' with a current and voltage target being entered into the control system to achieve the desired power outcome. The power supply control system thus strives to provide a constant current to the furnace and the power is then calculated as the product of the current and the voltage difference between the anode and the cathode. The voltage target is used to determine and control the position of the electrode tip, which changes the voltage difference between the anode and cathode (i.e. adjusted to achieve the desired arc length).

The power supply references the measured voltage between anode and cathode (as opposed to the voltage target) to calculate the power supplied. The arc length was periodically verified to ensure the desired arc length is achieved. Other parameters used for the purposes of controlling the furnace are the specific energy target (informally referred to as 'SER', kWh/kg), the estimated rate of energy loss (kWh/h) to the environment and the concentrate and reductant feed rates (kg/h). The SER is defined in Equation 4.

$$Specific\ Energy\ Requirement\ (SER, kWh/kg) = \frac{(Total\ Energy\ In - Total\ Energy\ Loss)}{Mass\ Fed} \qquad \text{Equation 4}$$

The control system calculates the achieved energy on an on-going basis, and this is used to determine whether the energy balance is on track (when compared to the target SER). Adjustments to the energy balance are usually made on the basis of tapping temperatures or if a process or plant incident disrupted the balance. The energy balance is managed batch-wise with the usable or, useful energy input (Energy In less Energy Lost), and the mass fed balanced at the end of each batch, referred to as the power-to-feed balance. Ideally, the power and feed input is balanced throughout any batch, but the control system is set up to make minor adjustments to the overcome energy or feed deficits. The energy input may be in deficit if electrode maintenance is required (addition of a section of the electrode). The importance of power-to-feed control in an open-arc furnace is described by Steinberg et al. (2011), as it pertained to the transition from submerged-arc to open-arc operations at Highveld Steel, and by Geldenhuys (2017), based on experiences operating DC furnaces.

The flow rate and temperature of the various water-cooling circuits were logged by the control system. The rate of energy loss (kWh/h) for individual circuits is calculated as follows: Rate of energy loss for a given circuit = m Cp ΔT (where, Cp = specific heat of water, m = mass flow rate, ΔT = change of water temperature. The total of all the measured losses, namely the sum of the losses calculated from the individual circuits, is used to estimate the rate of energy loss to the environment, a critical part of the control philosophy and thermal efficiency estimate for the furnace. Given that the entire furnace is not water-cooled, an additional factor for unmeasured losses to the environment is added to the total. A generic depiction of the water circuits utilised in the calculation of the total measured losses from the furnace is included in Appendix A, sub-section A3.

4 DESCRIPTION AND CHARACTERISATION OF RAW MATERIALS

The concentrate smelted during the pilot trial was explicitly produced for the test on the pilot furnace facility. Approximately 110 tons of concentrate, with an average of about 35% titanium dioxide, was secured to demonstrate the feasibility to smelt low-grade titaniferous ore in an open-arc DC smelter in the absence of fluxes. The as-received concentrate was blended prior to analyses; composite samples were prepared for purposes of characterising the bulk sample. The concentrate was characterised by a variety of methods including detailed chemistry, quantitative mineralogy, particle size analysis, phase chemical composition, and thermal analysis. The results are presented in this sub-section deals with the character of the feed, as well as relevant compositional aspects such as grade and mineralogy. A low-ash reductant was procured for the test, to minimise slag contamination via the ash. The chemical composition of the reductant is also presented. The anthracite arrived at Mintek pre-packaged in bulk bags. It was dry and required no further preparation. Pipe samples were taken from each bag; these were combined to produce four composite samples for analysis.

The bulk concentrate sample was blended and sampled in preparation for the pilot-plant test. The intention of blending the bulk sample is to minimise variability during the smelting test. A test of this nature can be disrupted by a number of undesirable process variations, and due to limited feed availability, process stability needs to be achieved as soon as practical. Blending the sample reduces the feed composition variability.

All raw materials were bagged in bottom-opening bulk bags (1m^3 bags) for purposes of storage and handling during the test campaign. The photographs in Figure 4-1 show the general appearance of the raw materials, namely the titaniferous concentrate (left) and the low-ash anthracite (right). A DC open-arc furnace allows for the use of finer materials, and thus the reductant could be selected based on chemical composition (low ash) rather than size grading.

Figure 4-1: General appearance of the titaniferous concentrate (left) and low-ash anthracite (right)

4.1 BULK CHEMICAL COMPOSITION OF THE REDUCTANT – LOW-ASH ANTHRACITE

The following table summarises the chemical composition of the anthracite (reductant) as used during the smelting test. The average results from four composite samples, submitted to two laboratories, are provided in Table 4-1 (individual sample results are included as in Appendix B). Using a low-ash reductant is crucial to minimise unnecessary contamination of the slag product. The reductant is a blended product provided by a local supplier, but the origins are unknown. In addition to the standard analysis, the ash was analysed separately and found to be dominated by FeO. The gross calorific value of 34.31 MJ/kg, was measured by a laboratory specialising in characterisation of coal and other reductants. The external laboratory's results are reported together with the average analysis by Mintek's own laboratory. The Mintek analysis was used for mass balance purposes.

Table 4-1: Average composition of the anthracite, mass %

Average	Fixed C	Volatile	Ash	Moisture	Total S	P_2O_5, ppm	Total	Ultimate assay (dry), %			
								C	H	N	O$^{\$}$
Mintek lab	79.0	10.7	8.62	1.68	<0.01	0.012	100	85.5	-	-	-
External Lab	78.9	12.2	8.63	0.30	0.01	-	100	87.0	3.65	0.09	0.35
Ash composition: FeO 7.10%, MgO 0.14%, CaO 0.30%, Al_2O_3 0.12%, SiO_2 0.35%											

($) oxygen content calculated; Ash analysed by Mintek laboratory

4.2 BULK CHEMICAL COMPOSITION OF THE TITANIFEROUS FEED

The chemical composition of the concentrate is based on the average composition of ten representative composite samples. Sub-fractions were submitted for analyses by two accredited laboratories. The MINTEK in-house laboratory analysis was used throughout for consistency, and the reaction products from the test were also analysed by the in-house laboratory. For purposes of the mass balance, the composition, as reported in Table 4-2, represents the average composition of the "as-processed" state of the raw material. This analysis was used as the basis for the mass balance.

Table 4-2: Bulk chemical analysis of concentrate, mass%

	$FeO^{\dagger}$	$TiO_2^{\dagger}$	MgO	Al_2O_3	SiO_2	CaO	V_2O_5	Cr_2O_3	MnO	TOTAL
$\bar{x}$	55.15	35.50	0.68	1.23	1.06	<0.05	0.44	0.08	0.59	94.7
± 95% CI	1.41	0.67	0.05	0.09	0.12	-	0.02	0.02	0.03	-
σ	2.28	1.08	0.09	0.15	0.19	-	0.04	0.03	0.05	2.32
σ^2	5.21	1.16	0.01	0.02	0.04	-	0.00	0.00	0.00	5.40
LOI (in argon, after drying) 0.5%, S 0.01%, C 0.05%, P 166 ppm, U <10 ppm Th <10ppm										

(†) Total Fe and Ti assayed, expressed as oxides

The oxidation states of Fe (namely Fe^0 and Fe^{2+}) was analysed via an external laboratory (Fe^{3+} was calculated by difference). The average ratio of Fe^{2+} to Fe^{3+} for the titaniferous concentrate was calculated to be 1.7.

A volatile component associated with the presence of clay minerals of approximately 0.5% was noted. Negative LOI values (approximately -2%) are consistent with the loss of volatile components combined with the gain in mass associated with the oxidation of Fe^{2+} to Fe^{3+} that is expected for this type of measurement.

Moisture content varied significantly from sample-to-sample (from 2% up to 10%). The average moisture content of the feed (as fed) was approximately 5%. The moisture capacity of material this finely sized feed is high, but it was not practical to undertake bulk drying on the sample prior to processing. The impact of the moisture content was assessed as part of the review of the overall results. Moisture does not participate in the chemical reactions but will contribute to energy consumption in the furnace. At industrial scale feed would be dried prior to feeding, but for a pilot test, some compromises are inevitable, due to limited access to drying facilities and resources.

4.3 THERMAL CHARACTERISTICS OF THE TITANIFEROUS CONCENTRATE

Thermal characterisation of the titaniferous composite sample is presented in this section. The tests consisted of heating the sample, in a thermo-balance at a constant rate (5°C/minute) to 1300°C while continuously recording the change in mass of the sample. The test was conducted first in air and repeated in an argon atmosphere. In air, decomposition of hydrated phases (clays and amphiboles) and the loss of volatiles from the decomposition of carbonates and similar minerals will occur. Relative to the mass loss from the decomposition reactions, oxidation reactions such as the conversion of FeO to Fe_2O_3 will occur under the same test conditions, but the latter will result in a mass gain. The final result thus represents the nett outcome (gain and loss). It is for this reason that the analysis is also conducted in argon to prevent the oxidation of Fe. This allows separating the decomposition reactions from oxidation reactions.

The thermal profiles for both atmospheres are shown in Figure 4-2. It can be seen from the profile that a distinct mass loss (under argon) occurs up to a temperature of 600°C. This is consistent with typical temperatures for dehydration reactions (decomposition of hydrated minerals). In air, the sample continues to gain mass, undoubtedly due to the oxidation of FeO, which simultaneously overwhelms the detection of any mass loss associated with the dehydration reaction. The magnitude of the final mass loss and gain give an indication of the relative proportions of the minerals associated with these mass changes, which in the case of FeO is consistent with the concentration of this species in the concentrate.

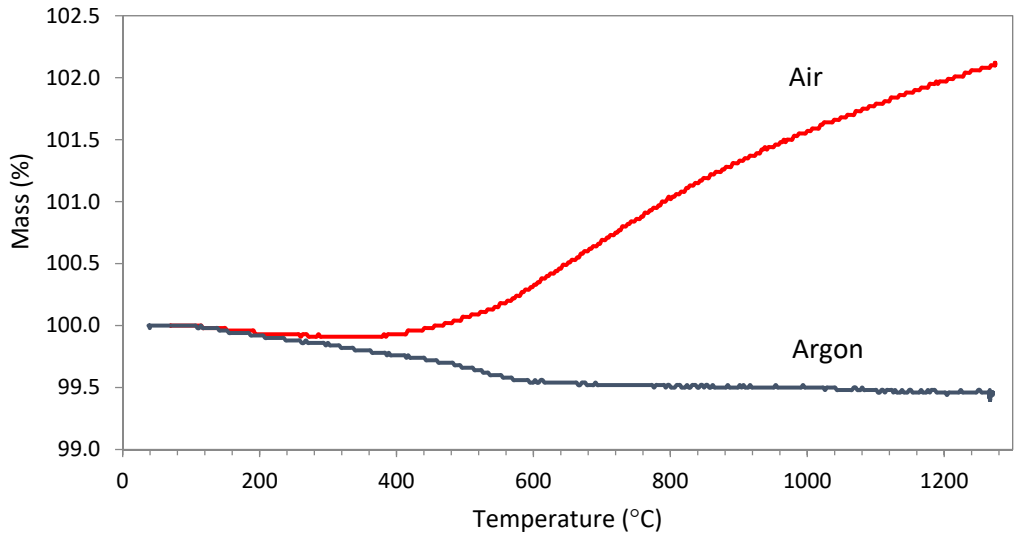

Figure 4-2: Thermogravimetric profile for heating of the concentrate in argon and air

4.4 Concentrate Particle Size Distribution and Associated Composition By Size

The particle size distribution of the sample of concentrate, randomly selected, was assessed, the results of which are presented in Table 4-3 and graphically in Figure 4-3. The sample was wet screened at 38 µm to remove the slimes fraction whereupon the dried +38 µm fraction was dry screened. The particle size appeared normally distributed with a D50 of approximately 120 µm.

Table 4-3: Particle size distribution of the concentrate, mass %

Screen Size, µm	Mass retained (%)				
	1	2	3	4	Average
600	0.38	0.35	0.35	0.41	0.37
425	5.04	5.26	5.26	5.40	5.24
300	14.79	14.82	14.81	15.24	14.91
212	17.65	17.76	17.77	17.59	17.69
150	21.37	20.92	20.92	21.46	21.16
106	16.84	16.44	16.44	17.18	16.73
75	19.33	13.07	13.08	12.05	14.38
53	2.13	6.22	6.22	6.39	5.24
38	1.89	2.75	2.75	2.50	2.47
pan	0.59	2.40	2.41	1.77	1.79
Total	100	100	100	100	100

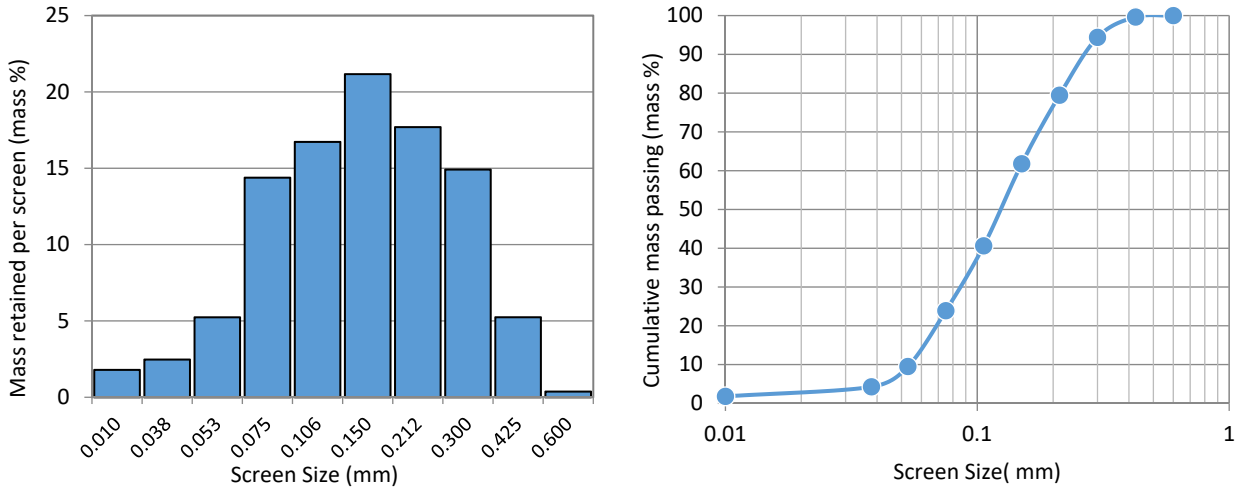

Figure 4-3: Discrete average particle size distribution (left) and cumulative average particle size distribution of the concentrate (right)

A single series of mass fractions, retained from the size evaluation, was submitted for chemical analysis by XRF. Table 4-4 presents the qualitative results by size fraction. The method of analysis is not consistent with previous methods, but the results were deemed acceptable from the point of view of demonstrating the trends that would be expected for the size-by-size analysis.

In terms of distribution, it would appear that the Fe (reported as total Fe) is more prevalent in the coarser size fraction than the TiO_2, which given the fact that magnetite and ilmenite are the predominant minerals in this sample, would suggest that the magnetite may be coarser than the ilmenite, as is typical of titaniferous magnetite ores. MgO appears to follow a similar distribution to TiO_2 suggesting an association of MgO with Ti, while Al_2O_3 appears to follow a similar trend to Fe and therefore could be associated with magnetite. SiO_2 appears to be concentrated in either a fine or coarse fraction suggesting 2 modes of occurrence which given the provenance of the sample could be related to a fine clay fraction and potentially a coarse silica-rich mineral possibly even quartz.

Table 4-4: Chemical composition of the individual mass fractions as determined by XRF, mass %

Mass (%)	Screen Size (µm)	Fe_{Total}	TiO_2	MgO	Al_2O_3	SiO_2	CaO	V_2O_5	Cr_2O_3	MnO
0.37	600	52.7	26.6	0.64	2.77	3.01	0.20	0.47	0.28	0.51
5.24	425	52.7	29.4	0.56	2.08	1.56	0.06	0.45	0.21	0.51
14.91	300	53.2	31.9	0.55	1.93	1.47	0.06	0.43	0.16	0.52
17.69	212	48.2	38.3	0.67	1.57	1.20	<0.05	0.37	0.13	0.52
21.16	150	43.2	47.1	0.86	1.25	1.17	<0.05	0.30	0.10	0.53
16.73	106	41.0	50.1	0.95	1.21	1.59	<0.05	0.27	0.08	0.55
14.38	75	40.9	50.4	0.93	1.03	1.85	0.05	0.27	0.10	0.56
5.24	53	40.7	50.9	0.96	1.07	1.83	0.08	0.26	0.09	0.57
2.47	38	41.7	49.2	0.90	1.26	1.79	0.08	0.25	0.17	0.59
1.79	-38	43.5	43.4	0.87	1.64	2.52	0.21	0.22	0.40	0.57
Weighted average		**45.3**	**43.4**	**0.79**	**1.42**	**1.49**	**0.06**	**0.32**	**0.12**	**0.54**

Figure 4-4 illustrates the distribution for Fe_{TOT}, TiO_2, MgO, SiO_2 and Al_2O_3, by size. From the chemical composition of the individual size fractions, it would appear that the magnetite is coarser than the ilmenite, a fact supported by the quantitative mineralogical results. No significant concentration of the gangue components (MgO, SiO_2 and Al_2O_3) in a particular size fraction was observed.

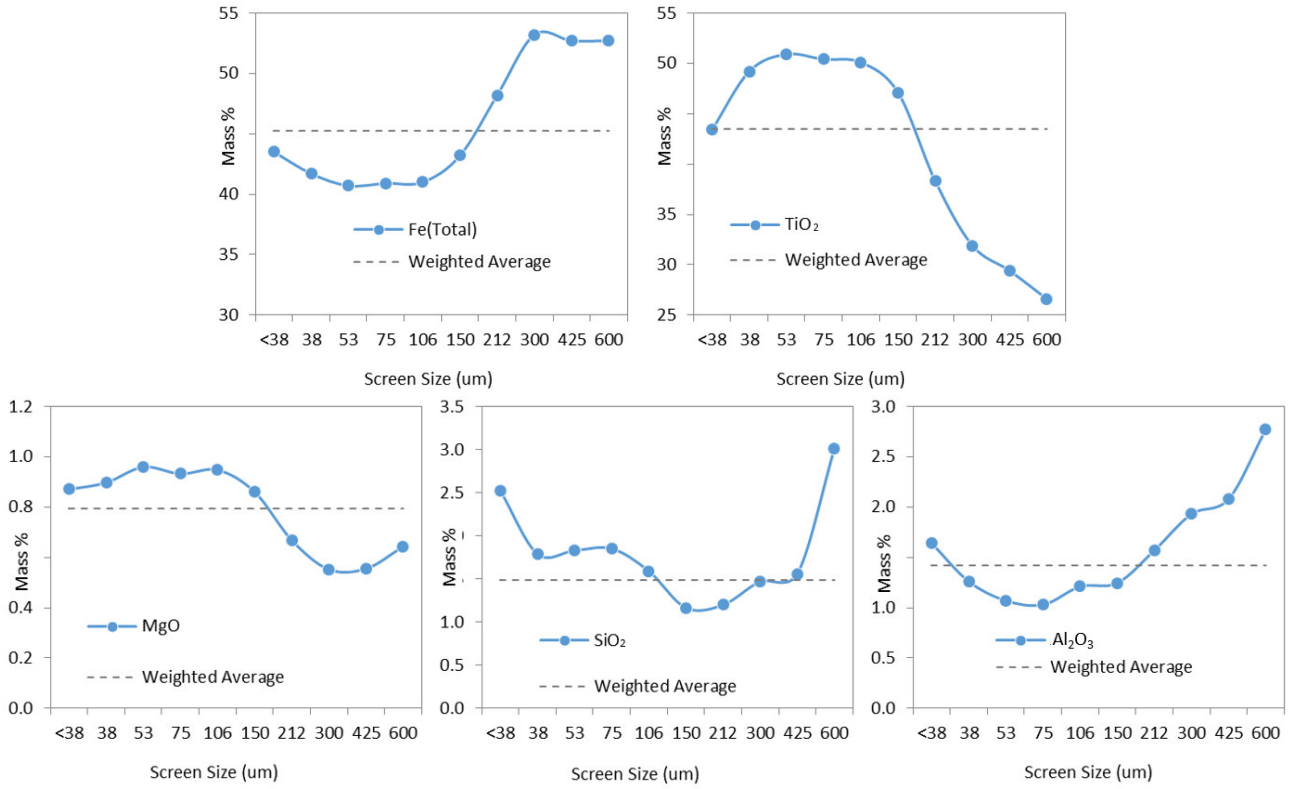

Figure 4-4: Graphs showing the distribution of particle size on a composition basis, mass %

4.5 PHASE CHEMICAL COMPOSITION OF THE CONCENTRATE

A polished section of a sub-sample of the concentrate was prepared and analysed by an Electron Microprobe using Wavelength Dispersive Spectroscopy (WDS) to determine the chemical composition of the major minerals present in the sample. WDS analysis is considered a more accurate technique than Energy Dispersive Spectrometry (EDS) which is typically employed by Scanning Electron Microscopes (SEM) allowing better resolution between elements and having a lower detection limit than EDS.

A number of individual microanalyses were performed on ilmenite (40) and magnetite (49) grains, the results of which are summarised in Table 4-5. The typical appearance of the titanomagnetite and ilmenite phases is illustrated by the backscattered electron image in Figure 4-5; the appearance is very typical of titaniferous magnetite deposits (Cawthorn *et al.*, 2005; Rohrmann, 1985).

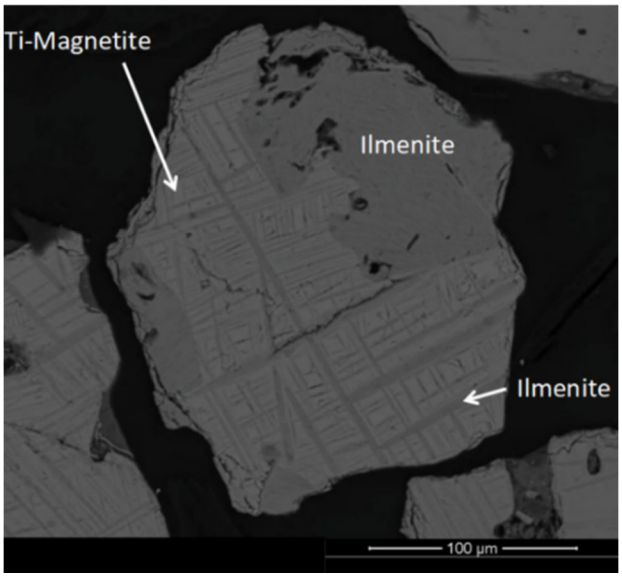

Figure 4-5: Backscattered electron image of the replacement texture of magnetite by ilmenite

Table 4-5: Summary of the composition as determined by WDS of the ilmenite and magnetite phases, mass %

Ilmenite	**MgO**	**Al_2O_3**	**SiO_2**	**TiO_2**	**V_2O_5**	**MnO**	**FeO**	**Total**
Mean	**1.12**	**0.08**	**0.07**	**52.77**	**0.00**	**0.59**	**44.21**	**98.84**
Max	1.47	0.35	0.14	57.92	0.00	1.10	46.78	100.38
Min	0.52	0.02	0.03	49.53	0.00	0.31	37.42	95.43
σ	0.21	0.07	0.02	1.64	0.00	0.13	2.22	1.20
Count	40							
Magnetite	MgO	Al_2O_3	SiO_2	TiO_2	V_2O_5	MnO	FeO	Total
Mean	**0.40**	**0.68**	**0.12**	**23.64**	**0.17**	**0.75**	**67.58**	**93.34[#]**
Max	0.98	1.15	0.23	32.57	1.82	4.94	83.86	96.03
Min	0.04	0.04	0.07	7.41	0.00	0.11	56.92	89.86
σ	0.22	0.21	0.04	5.15	0.40	0.95	5.29	1.17
Count	49							

(#) Low total due to the total Fe concentration being expressed as FeO

The composition of the ilmenite was found to be reasonably typical of ilmenite given known substitution with the end member phases Al_2O_3, $MgTiO_3$, Fe_2O_3 and $MnTiO_3$. The concentrate presented with the following stoichiometry: $(Fe_{0.94}Mg_{0.04}Mn_{0.01})^{2+}(Ti^{4+}_{1.01}Al^{3+}_{0.004})O_3$.

Similarly, the composition of the magnetite was consistent with known substitutions within the spinel mineral group and had the following stoichiometry: $(Fe_{1.65}Mg_{0.02}Mn_{0.03})^{2+}(Fe^{3+}_{0.57}Ti^{4+}_{0.70}\ Al^{3+}_{0.03})O_4$.

The phase chemical composition of the ilmenite indicates that approximately 1.1% MgO is contained in the ilmenite with a further 0.4% contained within the magnetite. The sample also contained MgO-bearing clay minerals. Approximately 52% of the sample is present as ilmenite and 44.2% as magnetite. Applying this weighting the two phases contribute 0.76% towards the overall MgO concentration in the concentrate which is similar to the MgO concentration as determined by chemical analysis of the bulk concentrate (presented in Table 4-2). The evaluation demonstrates that the MgO concentration in the concentrate is primarily determined by the major mineral chemistry.

Al_2O_3 is not as concentrated in the magnetite or ilmenite and is unlikely to contribute to more than 70% of the total Al_2O_3 concentration in the concentrate. MnO appears to be equally associated with magnetite and ilmenite while V_2O_5 is entirely associated with magnetite (within the context of these 2 phases).

A sub-sample of the titaniferous concentrate was analysed via an automated scanning electron microscope technique to determine the bulk mineralogy, ilmenite occurrence, grain size distribution, and mineral association and liberation characteristics.

The sample was split into two representative portions. One portion was screened into two size fractions (+75 µm and - 75 µm). Polished sections were prepared from representative portions of each fraction and analysed using an automated scanning electron microscope (AutoSEM). A second sub-sample was pulverised for X-Ray diffraction using qualitative X-Ray diffraction to determine the major minerals present, for verification of AutoSEM results. A Bruker D8 Advance Powder Diffractometer with Linxeye detector and Fe filtered Co-Kα radiation was employed. The method makes use of the net intensity of the main peaks of the phases, and identification was based on the crystal structure of crystalline phases which occur in amounts of >3 mass %. Amorphous phases were not identified. The phases were identified using Bruker Eva software.

The analysis chosen for this set of samples was a particle map analysis. The Mineral Liberation Analyser (MLA) is a scanning electron microscope (SEM) that combines backscattered electron images with X-ray analysis in an automated manner (Fandrich *et al.*, 2007).

The higher the average atomic number of a mineral, the brighter the backscattered electron intensity will be. The different phases are mapped as particles or grains (Figure 4-3). Particles and grains are distinguished on the basis of the differences in backscattered electron (BSE) intensity of minerals. In Picture B, Figure 4-3, grains 2 and 3 are the same mineral (and BSE intensity), but occur as separate grains and are counted separately. X-rays are then generated using energy dispersive spectrometry (EDS) to produce a spectrum from which the minerals of interest and associated gangue minerals can be identified.

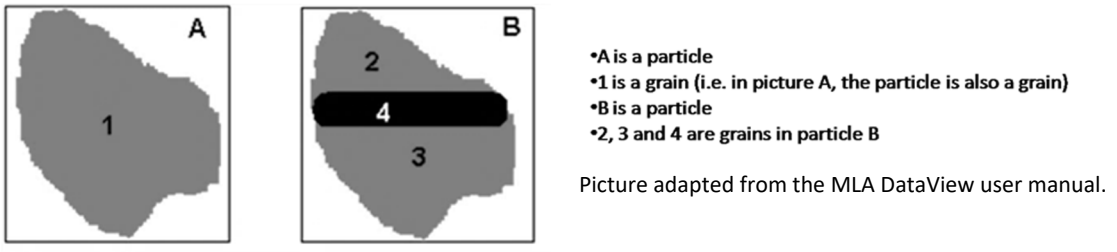

Figure 4-6: Explanation of the interpretation of the difference between a grain and a particle

A standards library was compiled for the different minerals present in the samples and applied to the analysis to identify the different phases and determine their size distribution.

The results are based on the combined data for all of the polished sections analysed for both size fractions. Note that in this measurement, using an AutoSEM will result in the grain size distributions being underestimated, as the data are gathered from sectioned grains and is not adjusted for stereological effects.

4.5.1 Modal distribution of the different phases of the concentrate

The dominant minerals present in the sample are ilmenite, titaniferous magnetite and magnetite (Table 4-6).

Table 4-6: Relative proportions of all the minerals in the concentrate

Mineral name	Density (g/cm^3)	Ideal chemical formula	Relative proportions (mass %)
Magnetite*	5.15	$Fe^{3+}_2Fe^{2+}O_4$	5.2
Titanomagnetite	5.20	$Fe(Fe,Ti)_2O_4$	39.0
Ilmenite	4.72	$FeTiO_3$	52.3
Rutile	4.25	TiO_2	0.4
Titanite	3.48	$CaTiSiO_5$	0.0
Zircon	4.65	$ZrSiO_4$	0.0
Leocoxene	3.60	$TiO_2 + SiO_2$	0.2
Plagioclase	2.69	$(Na,Ca)Si_3AlO_8$	0.0
Quartz	2.63	SiO_2	0.2
Amphibole	3.20	$NaCa_2(Mg,Fe)_4(Si_6Al_2O_{23})(OH)_2$	1.5
Clay	2.35	$(Na,Ca,Al,Mg)Si_4O_{10}(OH)_2{\cdot}4(H_2O)$	1.1
Total			100.0
* Some hematite might be present in this grouping			

Both hematite and magnetite were identified by X-Ray diffraction but were grouped together in the AutoSEM results as these two minerals have similar EDS spectra and cannot easily be distinguished. Ilmenite was distinguished from titaniferous magnetite on the basis of the Ti and Fe EDS peaks. (Note: Ilmenite will have similar peak heights for both Fe and Ti, whereas for titaniferous magnetite the Ti peak will be much lower than the Fe peak). The average titanium content in the titaniferous magnetite phase ranged between 1.4% and 6%. The gangue minerals all occurred in concentrations below 5% (mostly amphibole and clay minerals).

4.5.2 Grain size distribution and mineral associations

Minerals are considered as associated with each other when they share grain boundaries. The higher the degree of sharing of grain boundaries, the greater the degree of association. Free surface refers to the perimeter of the particle that is exposed and does not share a grain boundary with any mineral. An understanding of the association of minerals allows for assessing the upgrade potential via physical means. In the concentrate, magnetite is mostly associated with ilmenite, titanomagnetite, amphibole, clay and shows a free surface of 25%. The feed sample tested also presents with typical titanomagnetite features (Rohrmann, 1985), but the test sample had been optimised for titania, not iron, as for current smelting practices. The two microphotographs in Figure 4-7 illustrates the findings described in the current section.

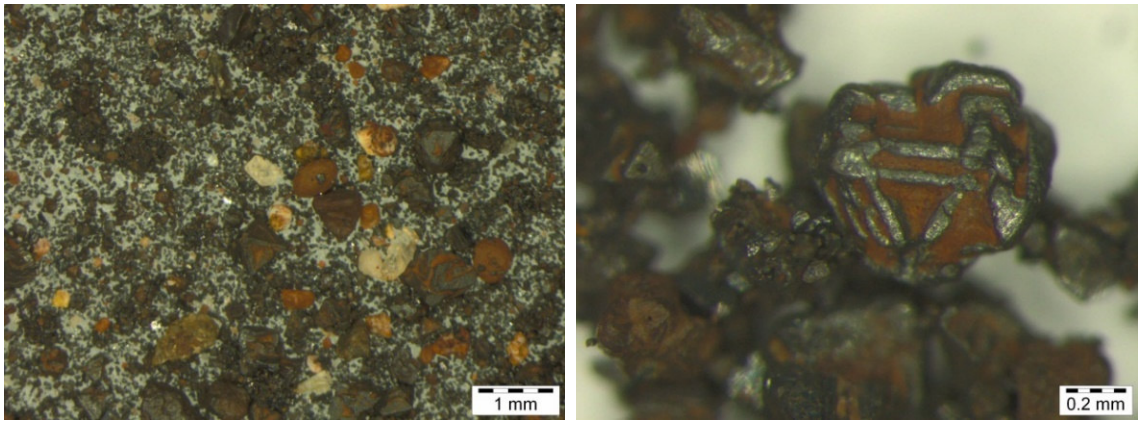

Figure 4-7: Microphotographs of the concentrate showing the presence of the gangue minerals and of clay and amphibole inclusion in the mineral particles at two magnification levels

Sizes are reported in terms of equivalent circle diameter (ECD), which is the diameter of a circle of the equivalent area to that of the grain of a two-dimensional surface. Approximately 52 mass % of the magnetite grains are classified in the size classes below 75 µm, whereas about 59% of titanomagnetite is found in the +150-600 µm size classes (Table 4-7). Ilmenite grains mostly reported to the -150+75 µm and -300+150 µm size classes.

Table 4-7: Grain size distribution of magnetite, titanomagnetite and ilmenite, %

Grain size distribution (µm)	**Magnetite**	**Titanomagnetite**	**Ilmenite**
+600	9.0	0.0	0.0
-600+300	5.7	19.6	0.9
-300+150	14.5	39.5	27.7
-150+75	19.1	23.8	43.1
-75+38	17.5	11.5	21.0
-38	34.1	5.7	7.3
Total	100.0	100.0	100.0

Phase chemically the ilmenite fraction was found to be relatively stoichiometric with substitution of mainly MgO (and MnO and Al_2O_3) into the crystal lattice. The MgO content of the ilmenite was found to be approximately 1%. Similar substitutions were found for the magnetite which is presented as more typically titaniferous magnetite containing approximately 24% TiO_2. About 0.4% of MgO was found to be present in this phase.

For the samples examined in this study, the combined MgO concentration of the ilmenite and titaniferous magnetite would contribute towards a concentrate composition having 0.76% MgO, which agrees well with bulk chemical assays. Overall, the sample was found to contain liberated ilmenite, but the liberated grains were finely sized, and there would be little benefit to target the fines separately as the titanomagnetite and ilmenite are strongly associated.

Two false colour maps are presented in Figure 4-8 and Figure 4-9. The images of two size fractions illustrate the mineral associations by grain size visually. The finer fraction shows definite liberation of the ilmenite from the matrix (via Figure 4-9) while the bulk of the sample (the +75 µm fraction, Figure 4-8) is strongly associated with the magnetite and gangue components.

The titanomagnetite grains were found to be associated with ilmenite, magnetite, amphibole and clay. Other than a significant free surface, ilmenite shared grain boundaries with titanomagnetite, magnetite, amphibole, clay, rutile and leucoxene. A summary of the mineral associations, as described, are presented in Table 4-8.

Table 4-8: Mineral grain boundary associations of magnetite, titanomagnetite and ilmenite, % association

Mineral	**Magnetite**	**Titanomagnetite**	**Ilmenite**
Magnetite		8	6
Titanomagnetite	28		40
Ilmenite	35	61	
Rutile	0	0	1
Leucoxene	0	0	1
Plagioclase	0	0	0
Quartz	0	0	0
Amphibole	4	3	3
Clay	8	3	2
Free surface	25	24	46
	100	99	99

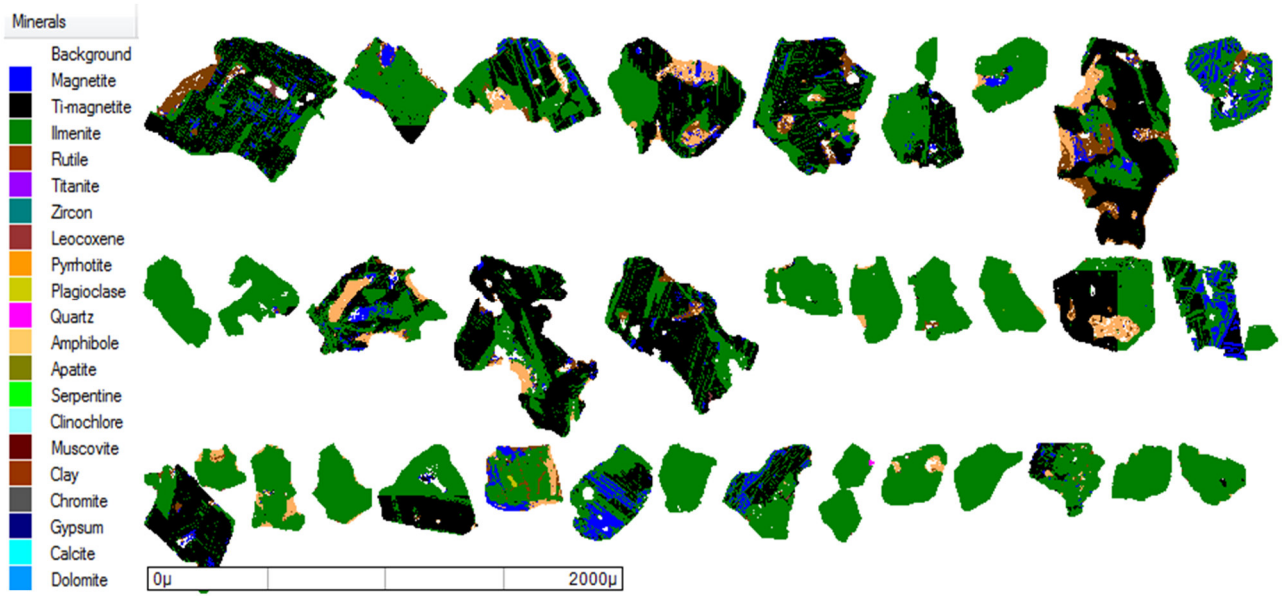

Figure 4-8: False colour map of the mineral grain occurrences in the >75 µm size fraction of the titaniferous magnetite concentrate

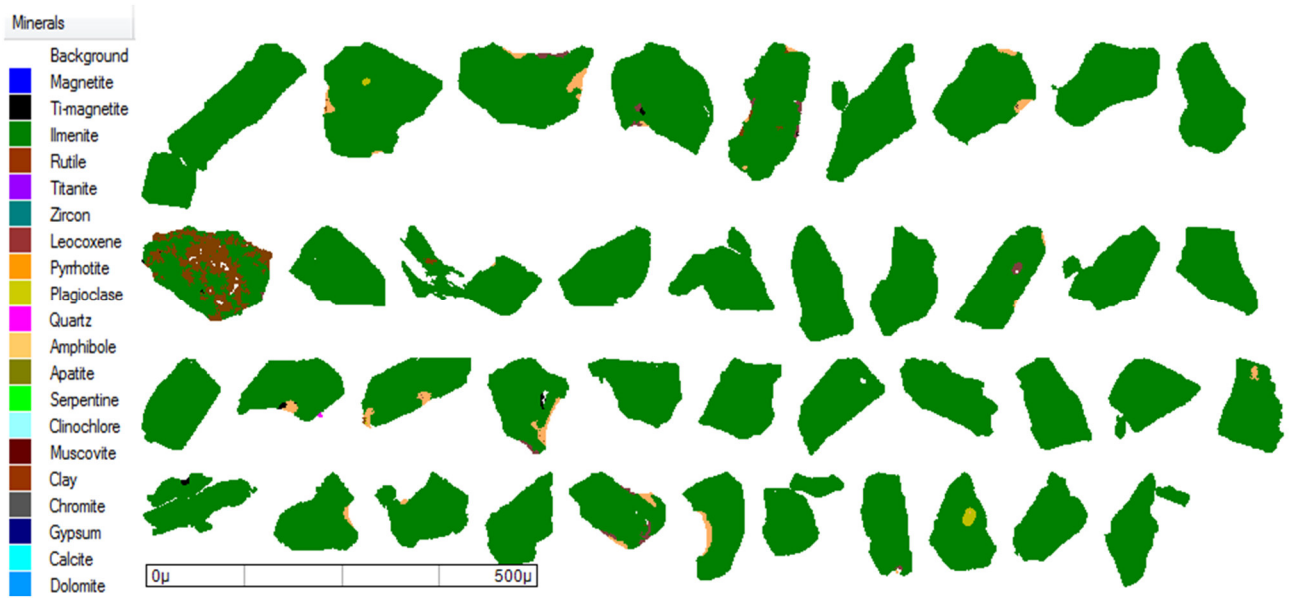

Figure 4-9: False colour map of the mineral grain occurrences in the <75 µm size fraction of the titaniferous magnetite concentrate

5 PILOT-PLANT SMELTING - OPERATIONAL OVERVIEW

A general summary of the testwork campaign in the context of the overall scope of work, testwork conditions and various test parameters and timelines are described in this section.

The progression of the testwork campaign, as summarised in this section, presents an overview of the progression of the testwork, while grouping the various batches into operating conditions for further evaluation. The section includes a summary of feed and product masses and reviews the operating targets and objectives for each period to establish a project timeline for reference purposes. Results are generally reported on a 'per tap' basis, which represents a discrete batch, fed over a predefined period, after which the furnace taphole or tapholes were opened to extract slag and/or metal.

5.1 Overall Material Balance

All materials fed and products collected from the furnace is outlined in this section. The furnace was operated continuously over a period of 17 days, including approximately a day of warm-up. During the test campaign, 54 batches of low-ash anthracite and titaniferous concentrate were fed to the furnace. Overall, about 108 tons of concentrate was fed together with about 20 tons of low-ash anthracite. A summary of the feed and product masses is presented in Table 5-1 via an overall material balance. During the assembly of the furnace, 1100 kg of iron scrap was placed in the furnace to serve as the start-up heel. In addition, about 50 kg of coke was added to the heel to prevent oxidation of the heel during the electrical warm-up of the furnace. The difference in mass between the total feed and total products can be attributed to the gaseous product, which is not accounted for by direct measurement. A simplified mass balance predicts approximately 0.3 kg of gas product per kg of concentrate.

Table 5-1: Overall material balance for the smelting campaign

FEED			**PRODUCTS**		
Concentrate, dry	102 126	kg	Slag	40 326	kg
Moisture from concentrate [c]	*5 375*	*kg*	Metal	46 705	kg
Heel (mild steel)	1 100	kg	Off-gas dust	6 431	kg
Anthracite (carbon) [a]	*18 304*	*kg*			
Anthracite (ash)	*1 727*	*kg*			
Electrode [b]	*495*	*kg*			
Total input	**129 127**	**kg**	**Total output**	**93 462**	**kg**
Total input (excluding a, b and c)	**104 953**	**kg**			

5.2 Operational Overview

Stable and sustained operating periods or conditions were identified to provide an overview of the smelting campaign. Objectives and significant events are summarised in accordance with the campaign timeline based on batches fed (numbered chronologically), typically associated with slag and/or metal tap. A detailed operational description is included as Appendix C, together with the operational targets and results per batch. Each batch consists of a discrete period during which the feed recipe, consisting of a targeted batch size of concentrate and reductant, was fed to the furnace at a specified feed rate. In subsequent sections, the use of 'batch' or 'tap' number is used interchangeably. The batch size and feed rate determine the duration of the feed period (the tap-to-tap time), which in turn is dependent on the volume of the furnace and the slag and metal volumes generated from the reaction.

During the batch, the furnace operation is managed carefully to ensure the feed and energy input is matched (the power-to-feed balance) to ensure that the desired reaction and operating temperatures can be achieved. Once the batch is fed, a tapping process starts, coordinated with the control room. Typically a slag and a metal tap were attempted due to the near 1:1 ratio of slag and metal make from this process. Each batch thus ended with a tap (the tap-to-tap period), and the slag and metal samples are associated with the sequential numbering system is linked to the number allocated to the batch preceding the tap.

For the current project, 54 batches were fed and tapped. The convention of number the batches are transferred to the slag and metal tap as the samples are associated with the specific conditions associated with the batch. Each batch represents a data point with energy, anthracite addition, tapping temperature and product compositions and masses. In essence, while the furnace is operated continuously, each tap represents a snapshot of the furnace conditions.

Stable conditions were identified as part of the post-campaign data evaluation of the data and are labelled chronologically (Period A to D) - each period includes a number of sequential batches. The operating conditions varied in accordance with the primary objective for each condition. Table 5-2 gives a summary of the recipe and operating power for the test conditions as identified. Operating power and anthracite addition were the primary testwork variables. The operational data summarised in Table 5-3, presents the experimental conditions targeted for each of the operating periods during the campaign. The targeted slag grade, namely slag containing about 85% TiO_2, was achieved at the conclusion of the warm-up and stabilisation condition - after completing 24 batches and stabilising the metallurgical operation.

Table 5-2: Summary of smelting campaign conditions

Condition Identifier	Description	Power (kW)	Batch or Taps in period
W	Warm-up and furnace conditioning - heating refractories and creating a molten pool in the furnace	800	1-6
A	Thermal and metallurgical stabilisation, mainly the systematic increase and optimisation of iron reduction	1200	7-24
B	Baseline condition to demonstrate the feasibility of smelting slag with TiO_2 content greater than 85%	1200	25-32
C	Smelting intensity increase, maintaining metallurgical stability at higher power levels	1300	33-51
D	Shutdown & electrical testing, including furnace excavation and refractory measurements	1300	52-54

Note: Batches are numbered sequentially (details of all the batches are included in Appendix C; Conditions A, B and C represents the primary metallurgical conditions

Table 5-3: Operational summary for primary metallurgical operating periods

Description **Period identifier**		**Warm-up** **W**	**Stabilisation** **A**	**Baseline** **B**	**High Power** **C**
Batches in the period		1-6	7-24	25-32	33-51
Number of batches processed		6	18	8	19
Duration of the period	h	87.2	102.5	52.0	117.7
Average power	kW	800	1200	1200	1300
Average voltage	V	218	230	250	250
Gross energy input	kWh	53.5	51.7	52.2	119.3
Feed					
Concentrate	t	15.8	30.4	16.5	38.9
Anthracite	t	2.3	5.6	3.3	7.6
Products					
Slag tapped	kg	5292	12 735	4082	12 724
Metal tapped	kg	4290	12 393	7613	16 101
Dust collected	kg	230	552	1075	4050

The evolution of the slag composition (presented through the FeO and TiO_2 content of the slag) as well as the anthracite addition and the cumulative Mg accountability for the entire campaign is graphically presented in Figure 5-1. The periods described in Table 5-2 and Table 5-3 are identified in the graphic to highlight the various transitions.

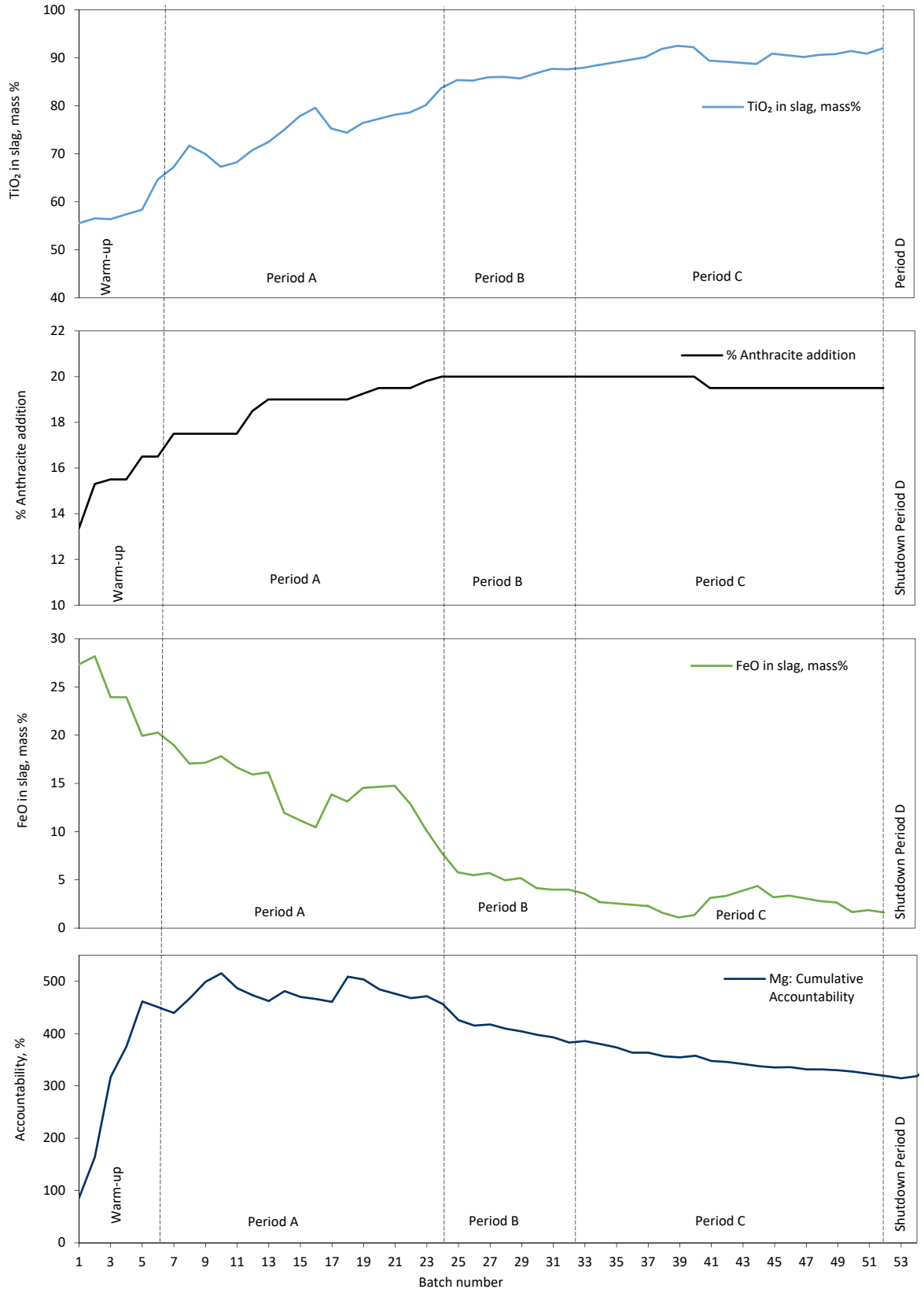

Figure 5-1: TiO_2 and FeO content in the slag, anthracite addition, and cumulative Mg accountability

6 RESULTS AND DISCUSSION

The results from the smelting campaign are reported and discussed in this section, generally referencing the various stable conditions identified in the previous sections. Slag, metal and off-gas dust compositions are reported and discussed. Furthermore, the process energy consumption, thermal efficiency of the furnace, refractory performance, electrical properties of the slag and arc, and electrode consumption are also assessed.

6.1 PRODUCTS

Slag and metal were removed from the furnace at set intervals. Slag was only tapped once the slag level in the furnace was deemed to consist of sufficient volume, typically at the end of a batch. The assessment consisted of a combination of inventory control and direct measurements of the bath-depth using a metal rod. During the removal of slag and metal from the furnace, a spoon sample method was used to sample the liquid stream. The off-gas dust bags were removed from the bag plant once the bags were full, and samples were taken upon removal.

The bulk chemical product compositions are reported as an average per condition, as well as an average for the entire smelting campaign. The tap-by-tap analyses are included in Appendix D, which includes compositions for all the slag, metal and off-gas dust samples collected during the test campaign.

During the course of the smelting campaign, samples of slag, metal and dust were collected for subsequent phase chemical investigation. The slag samples were from the latter part of the campaign when metallurgical stability had been achieved. These samples were water-quenched during the slag tap, directly poured from s slag sample spoon into a drum of water with an airline bubbler installed in the bottom. Metal samples and a dust sample, the latter collected at the end of the campaign, was also subjected to a phase chemical evaluation. The samples were examined through a combination of X-ray diffraction (XRD), Scanning electron Microscopy (SEM) and Electron Microprobe Analysis (EMPA). An overview of the results is presented in the following sub-sections.

The phase chemical investigation was primarily undertaken to determine whether the phase chemistry of the slag differs from that accepted for high-titania slags, the metal contains any inclusions, and if the baghouse dust sample contains a significant amount of volatile components.

As the primary objective of the test was to demonstrate that slag suitable for pigment production could be produced, detailed assessments of the slag characteristics are included.

6.1.1 Bulk chemical composition of the slag

A summary of average slag compositions, weighted and numerical, and the standard deviations for the various periods are presented in Table 6-1. Noteworthy trends in Table 6-1 are the changes in MgO, TiO_2 and FeO contents with the progress of the campaign.

The concentrations of MgO and FeO in the slag during the warm-up and stabilisation period (Period A), reflect the expected trends during the start-up of the furnace. During this period, adjustments were made to the energy and reductant addition based on the composition and temperature of the slag, specifically the FeO content. The degree of reduction is correlated to the concentration of FeO in the slag as this is the primary objective of the process.

Anthracite addition was systematically increased during the smelting campaign to evaluate the operability of the process under increasingly reducing conditions. As the FeO content in the slag decreased, the TiO_2 content in the slag increased relative to residual Fe content of the slag. FeO content in the slag of less than 5% was observed for most of the smelting campaign; FeO levels as low as about 1% was achieved intermittently.

The FeO content of the slag was used as the primary metallurgical control parameter, and the targeted FeO content in the slag was achieved by adjusting the anthracite addition. These adjustments were based on maintaining stable operating conditions in the furnace under highly reducing conditions (targeting low concentration of FeO in the slag); stability is directly related to properties of the slag in this instance. Factors considered include, amongst others, the ability to tap the slag on a regular basis. This objective was achieved for most of the campaign.

The principal objective of the testwork campaign was to demonstrate the production of high-titania slag from the low-grade concentrate, targeting a TiO_2 concentration of greater than 85%. High-grade slag was consistently produced from batch 25 onwards. In addition, slag with a TiO_2 concentration of greater than 90% was produced, exceeding the target of 85% significantly.

Table 6-1: Average slag analyses for the smelting campaign and sub-periods A to D, mass%

		MgO	Al_2O_3	SiO_2	CaO	TiO_2	V_2O_5	Cr_2O_3	MnO	FeO
Overall Batch 1 to 54	**W. Ave**	**5.53**	**3.40**	**2.14**	**0.18**	**80.28**	**0.79**	**0.16**	**0.93**	**9.43**
	$\bar{x}$	*5.52*	*3.41*	*2.18*	*0.18*	*80.61*	*0.80*	*0.15*	*0.94*	*9.40*
	σ	2.77	0.35	0.41	0.02	11.15	0.20	0.07	0.19	7.68
Warm-up Batch 1 - 6	**W. Ave**	**9.17**	**2.87**	**2.28**	**0.21**	**57.61**	**0.84**	**0.27**	**1.02**	**23.59**
	$\bar{x}$	*9.31*	*2.90*	*2.34*	*0.22*	*58.15*	*0.83*	*0.28*	*1.05*	*23.93*
	σ	1.33	0.11	0.18	0.02	3.32	0.03	0.04	0.17	3.44
Period A Stabilisation Batch 7 - 24	**W. Ave**	**7.52**	**3.15**	**2.43**	**0.19**	**74.82**	**1.00**	**0.19**	**1.00**	**13.78**
	$\bar{x}$	*7.49*	*3.18*	*2.42*	*0.19*	*74.65*	*0.99*	*0.19*	*1.00*	*14.17*
	σ	2.30	0.24	0.31	0.01	4.76	0.07	0.05	0.08	3.02
Period B Baseline Batch 25 - 32	**W. Ave**	**4.09**	**3.59**	**2.40**	**0.17**	**86.19**	**0.91**	**0.15**	**1.26**	**5.08**
	$\bar{x}$	*4.08*	*3.58*	*2.44*	*0.17*	*86.28*	*0.93*	*0.13*	*1.15*	*4.91*
	σ	0.56	0.10	0.19	0.00	0.95	0.06	0.02	0.19	0.76
Period C High power flux Batch 33 - 51	**W. Ave**	**3.25**	**3.71**	**1.84**	**0.17**	**90.39**	**0.58**	**0.09**	**0.76**	**2.58**
	$\bar{x}$	*3.26*	*3.71*	*1.84*	*0.17*	*90.26*	*0.58*	*0.09*	*0.76*	*2.70*
	σ	0.62	0.17	0.35	0.01	1.33	0.13	0.02	0.13	0.93
Period D Shutdown Batch 52 - 54	**W. Ave**	**2.70**	**3.78**	**1.62**	**0.17**	**91.08**	**0.61**	**0.13**	**0.77**	**1.90**
	$\bar{x}$	*2.69*	*3.67*	*1.61*	*0.17*	*91.50*	*0.62*	*0.12*	*0.80*	*1.73*
	σ	0.07	0.20	0.04	0.01	0.74	0.01	0.05	0.05	0.32

High-titania slag (exceeding the target of 85% TiO_2 substantially) with low FeO content was produced. High Fe recovery was achieved as a result, without compromising the product quality and operability of the furnace. Lower concentrations of FeO were associated with higher concentrations of TiO_2 in the slag, as would be expected. With increasing iron oxide reduction, via increased anthracite additions, the TiO_2 content of the slag is proportionally upgraded.

The high MgO content in the slag during the warm-up and stabilisation periods can be attributed to contamination due to refractory wear, which is usually experienced during start-up. The MgO content in the slag decreased as the smelting campaign progressed, which can be attributed to the formation and maintenance of a protective freeze lining which acts as a barrier between the melt and the refractory. The ability to maintain a freeze-lining is a positive outcome of the test.

A fair share of the refractory wear measured during the test campaign took place within the first six taps of the campaign, a period during which the FeO content in the slag was also above 20%. From batch 12 onwards, the accumulation of Mg (calculated via the elemental mass balance) stabilised, indicative of the formation of a freeze-lining. A freeze-lining (a layer of frozen slag) act as a barrier between the molten slag pool and the refractory lining thus minimises refractory wear. As the FeO content decreased, the cumulative Mg accountability stabilised, a consequence of the changed liquidus of the slag. Based on the thermal profile of the furnace, and the stabilisation of the Mg accountability, it was concluded that freeze-lining had formed. Mg accumulation was monitored as a measure of the freeze lining stability.

Figure 6-1 presents the evolution of FeO, TiO_2 and MgO for the duration of the test, relative to the anthracite additions for the five periods. It is clear from the graphs that during Period B and C, the primary metallurgical conditions, the MgO concentration was relatively stable.

The test demonstrated that it was possible to maintain the protective slag layer through the management of the power-to-feed balance while producing a high-grade (>85% titania) slag. The concentration of MgO in the slag and the cumulative accountability of Mg supports the premise that the operational stability minimised the refractory wear.

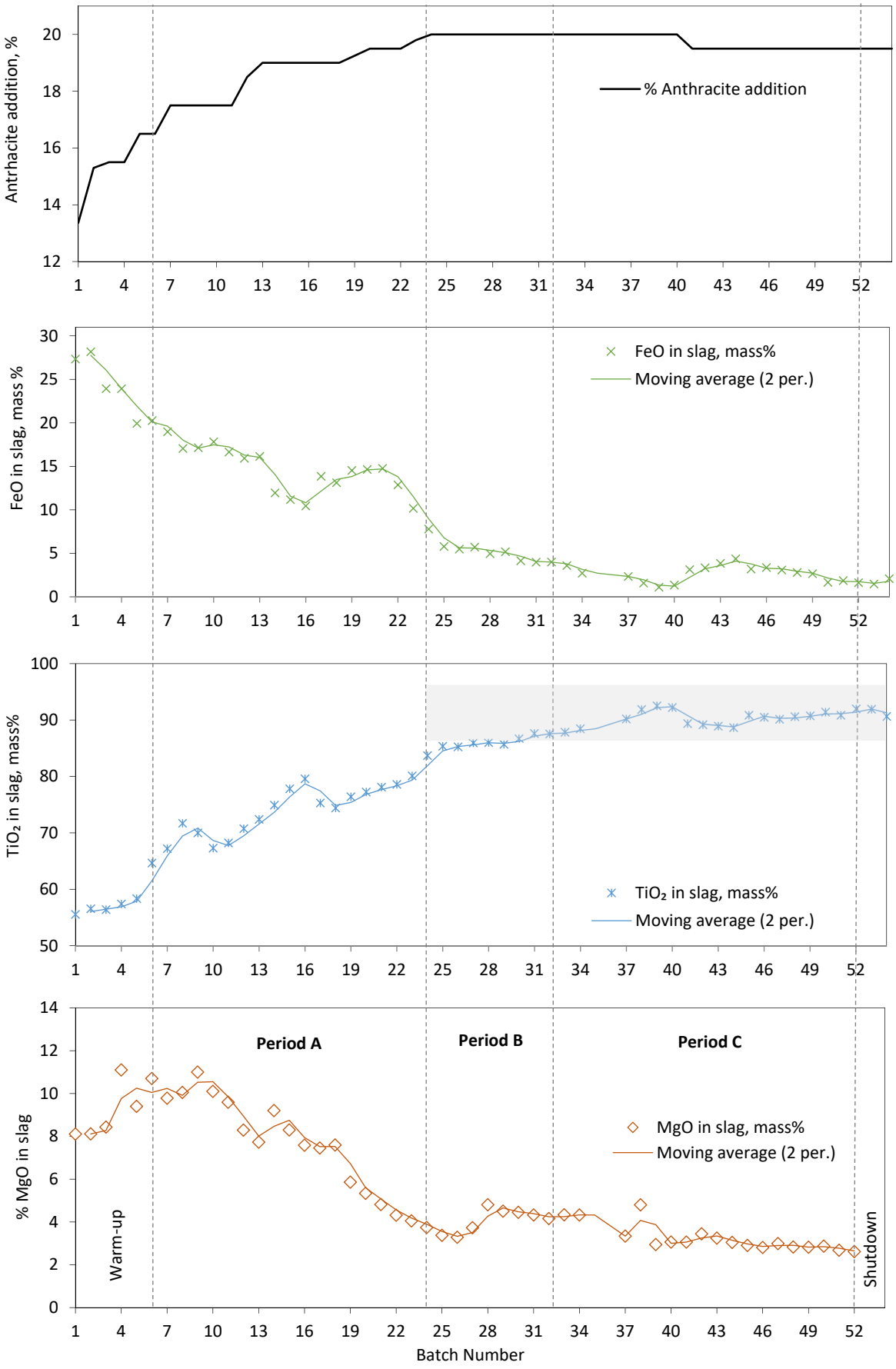

Figure 6-1: Evolution of TiO_2, FeO and MgO in the slag compared to anthracite addition

The linear trend plot for FeO and TiO_2 in slag, presented in Figure 6-2. As iron is removed from the slag via reduction, the remaining components, dominated by the titania, is proportionally upgraded. With the exception of minor elements such as sulfur, phosphorus, vanadium, and chromium, most impurities from the titaniferous ore, and the ash in the reductant are expected to report to the slag phase. This means that the slag purity is controlled by the ore (and reductant) purity. There is little or no scope to decrease impurity levels in slag. The proportional upgrade of TiO_2 as a function of FeO reduction is thus expected to be linear, as both are major components of the system.

Figure 6-3 presents a plot of Al_2O_3 and MgO in slag as a function of FeO concentration in the slag. As for TiO_2, the trend is expected to be linear if no contamination occurred. As indicated, the initial contamination of the slag with refractory components is expected.

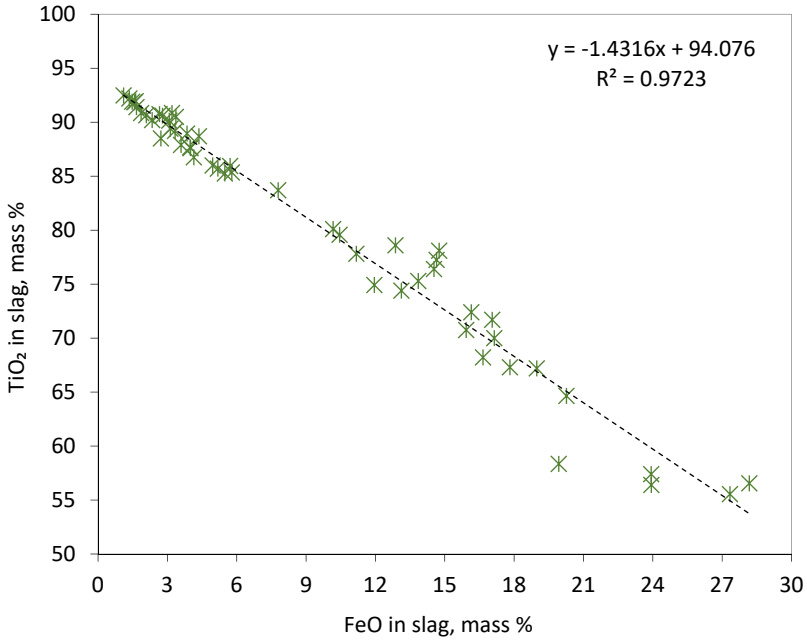

Figure 6-2: Plot of slag FeO content versus TiO_2 content

The same linear trend is expected for the other slag constituents, such as MgO and Al_2O_3. In the case of the alumina, the expected trend is observed. However, for the MgO data, the trend is not observed, mainly due to the fact that MgO was added to the system via refractory wear.

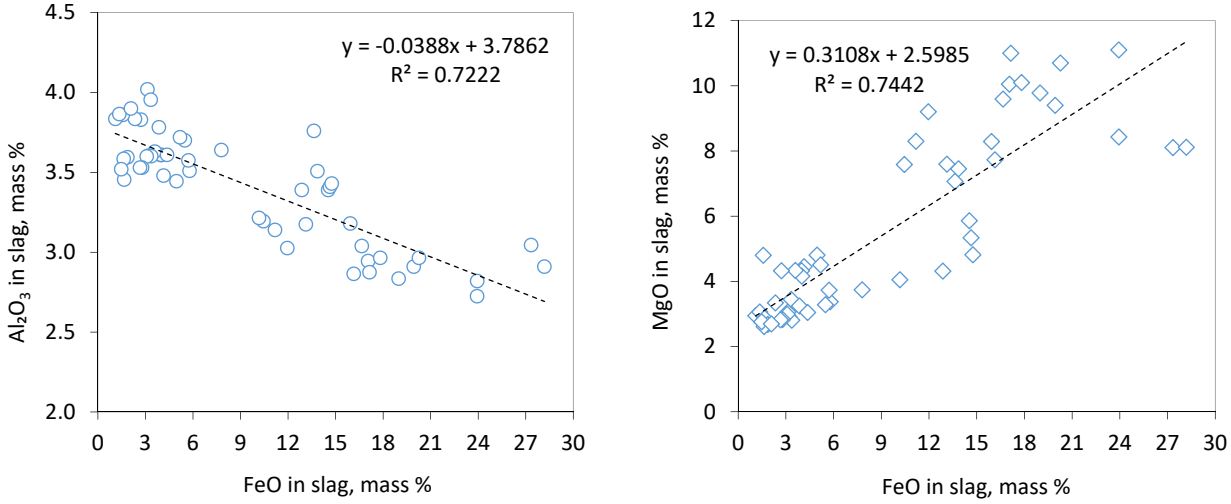

Figure 6-3: Plots of slag Al_2O_3 and MgO content per tap as a function of FeO in slag, mass %

6.1.2 Phase chemical evaluation of selected slag samples

Water-quenched slag samples were evaluated by XRD to determine major titanium-bearing phase stoichiometry, in particular, to distinguish between the presence of Ti_3O_5 and Ti_2O_3. SEM-based Energy Dispersive Spectrometry (EDS) microanalysis was used to gain a broad phase chemical understanding of the phases present in the slags. EMPA based Wavelength Dispersive Spectrometry (WDS) analysis of the main titanium-bearing phase was conducted to more accurately determine the composition of the titanium-bearing phase.

The examined slag samples appear to be dominated by the presence of the phase M_3O_5, which is not unexpected for the system (Zietsman & Pistorius, 2005). Small amounts of a silicate liquid are observed which are interstitial to the primary phase and small (approximately 10 µm) metal droplets are also observed. A typical view of the slag is shown in Figure 6-4. This appearance is consistent with the phase chemistry of most high-titania slags produced in South Africa. In terms of typical high-titania slag phase chemistry, the M_3O_5 contains a remarkably low level of FeO and high level of TiO_2 which is consistent with the bulk chemical composition of the slags. Titanium-oxy-carbide phases were not observed in the slags, which is a by-product of over reduction. All of the EDS and WDS analyses in this report express the Ti concentration of the phases as TiO_2, and as a result of this, most of the totals for the M_3O_5 phase will exceed 100%.

Generally, the M_3O_5 phase present in high-titania slag contains at most 90% TiO_2 together with 5 to 12% FeO. The low FeO concentrations for this phase would indicate that relatively reducing conditions existed in the furnace. The major impurities in the slag are MgO, Al_2O_3 and SiO_2. The average WDS analysis of the M_3O_5 phase for the various slag samples is summarised in Table 6-3. For a typical ilmenite slag FeO usually is the major impurity, while for the titaniferous magnetite feedstocks, the gangue constituents are not easily removed via physical means prior to smelting. At this level of reduction, it is likely that the dominant titanium-bearing phase would be Ti_2O_3; however, it appears that the presence of MgO, as an impurity, has to some extent stabilised the M_3O_5 phase.

Figure 6-4 shows the general appearance of the slag sample from Tap 50 (left) and showing the presence of M_3O_5 and interstitial silicate (dark grey phase, points 88 and 89) on the right. The micrograph for Tap 50 shows clear indications of metal entrainment, whereas slag samples from earlier taps appeared to be significantly cleaner. The phenomenon could be due to the increased smelting rate combined with the increase in viscosity, which is a consequence of the slag regime, exacerbated when the FeO concentration is low. The presence of droplets also may overestimate the Fe content reported as the analytical technique reports total Fe. Microanalysis of the highlighted points in Figure 6-4 (right), is presented in Table 6-2.

The average WDS analysis of the M_3O_5 phase for the slag samples evaluated is presented in Table 6-3 and for ease of reference the chemical composition of the slags, as tapped, is presented below.

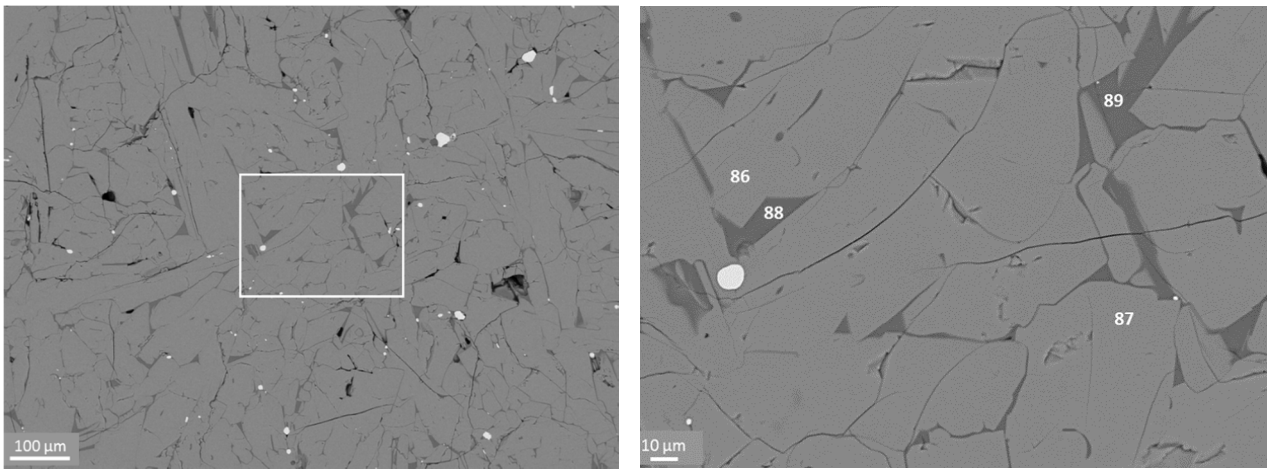

Figure 6-4: Backscattered electron micrographs of slag from batch 50 (left); higher magnification of highlighted zone (right)

Table 6-2: Microanalysis of M_3O_5 and silicate phases as per Figure 6-4, mass %

Identifier	MgO	Al_2O_3	SiO_2	CaO	TiO_2	MnO	Total	Comments
86	1.87	2.91			107.6		112.4	M_3O_5
87	1.94	2.87			107.6		112.4	M_3O_5
88	12.6	16.3	39.3	3.83	11.14	11.7	94.8	Silicate
89	13.0	15.6	37.2	3.67	11.75	11.5	92.6	Silicate

Table 6-3: Average WDS analysis of the M_3O_5 phase present in the slag samples, mass %

Batch	MgO	Al_2O_3	SiO_2	CaO	TiO_2	MnO	FeO	Total
32	3.33	3.11	0.18	0.03	95.4	0.29	1.45	103.8
33	3.20	3.12	0.23	0.02	96.3	0.29	1.15	104.3
38	1.86	3.00	0.09	0.01	100.2	0.14	0.26	105.6
39	1.79	3.15	0.09	0.02	99.9	0.14	0.25	105.3
50	2.20	3.23	0.22	0.03	98.8	0.25	0.74	105.5
58	2.21	3.05	0.12	0.02	97.2	0.22	1.08	103.9

Table 6-4: Bulk chemical compositions of selected water-quenched slag samples, mass %

Batch	MgO	Al_2O_3	SiO_2	CaO	TiO_2	MnO	FeO	Total
32	4.16	3.61	2.43	0.17	87.60	1.05	4.00	104.0
33	4.34	3.63	2.73	0.19	87.90	1.01	3.59	104.3
38	4.80	3.86	1.58	0.17	91.85	0.76	1.57	105.2
39	2.95	3.84	1.31	0.17	92.49	0.73	1.11	103.1
48	2.83	3.53	1.87	0.16	90.60	0.77	2.79	103.3
50	2.87	3.46	1.78	0.16	91.40	0.81	1.66	102.8

Detailed individual results, including micrographs of all the slag samples evaluated, is included in Appendix E.

The main conclusions from the phase chemical evaluation are as follows:

- The M_3O_5 phase contained low levels of FeO unlike typical titania slags produced from ilmenite, but instead, MgO and Al_2O_3 substitution were found.
- The presence of MgO appears to have somewhat stabilised the M_3O_5 phase, despite highly reducing conditions (low-FeO levels).

The slag produced from low-grade titaniferous ore is therefore not substantially different to slag produced from more typical ilmenite feedstock, and there appears to be some potential benefit with regards to the opportunity to operate with lower levels of FeO (higher Fe recovery) while maintaining operability.

6.1.3 Estimation of the Ti^{3+} content for the pilot-plant slags

The analytical methods used during the test reported slag results without differentiating oxidation state. The Ti^{3+} content of the slag is assumed to vary in agreement with a curve fit of data produced by Desrosiers et al. (Desrosiers *et al.*, 1980). The equation derived from the Desrosiers data is presented in Equation 5 (r^2=0.9798).

$$\frac{1}{y} = a + bx^3 \quad where\ a = 5.834\ and\ b = -5.059 \times 10^{-6}\ \left(y = \frac{Ti^{3+}}{Ti_{Total}}\ and\ x = \%TiO_2\right) \qquad \text{Equation 5}$$

Ti^{3+} is assumed to be in the form of Ti_3O_5 and a composite of Ti^{3+} and Ti^{4+} or $TiO_2.Ti_2O_3$ such that two moles of Ti^{3+} combines with one mole of Ti^{4+}. The Desrosiers correlation was derived from slag with greater than 78% TiO_2 content (Desrosiers *et al.*, 1980).

Pistorius (2002) published titania slag data, including Ti^{3+} content, for a number of industrial operations – specifically ilmenite smelters with TiO_2 content ranging from 66 to 92%). The data is reported to be collated from various sources and includes slag compositions for two commercial operations in South Africa (namely Richards Bay Minerals, which uses six-in-line alternating-current furnaces, Namakwa Sands, which uses a direct-current furnace), and the QIT plant in Canada (which uses similar furnaces to Richards Bay Minerals). The South African ores originate from beach sand

deposits while the Canadian ore is a hard rock deposit. In the case of the latter example, the resulting slags contain substantially higher concentrations of alkali earth components than slag produced from beach sand deposits (as was reviewed in the background).

The data from Pistorius was used to validate the equation derived from the data presented by Desrosiers et al. (1980). The analytical method used to determine slag composition during the pilot-plant test only reported total Ti content. In order to assess the slag quality in more depth, in the context of the potential application as feedstock to the pigment industry, an empirical approach was developed. A combination of Pistorius (2002) and Desrosier et al. (1980) data provided enough information to verify the empirical approach.

The graph below plots the calculated Ti^{3+}/Ti ratio for the data points published by Pistorius (2002). The ratio was calculated using Equation 5. The calculated ratio (which is based on the total Ti content of the industrial slags) was compared to the reported ratio from the Pistorius publication. The results are compared in Figure 6-5, and the correlation appears to be relatively robust for such a wide range of operations and compositions. This consistency is an intriguing and useful attribute of high-titania slags.

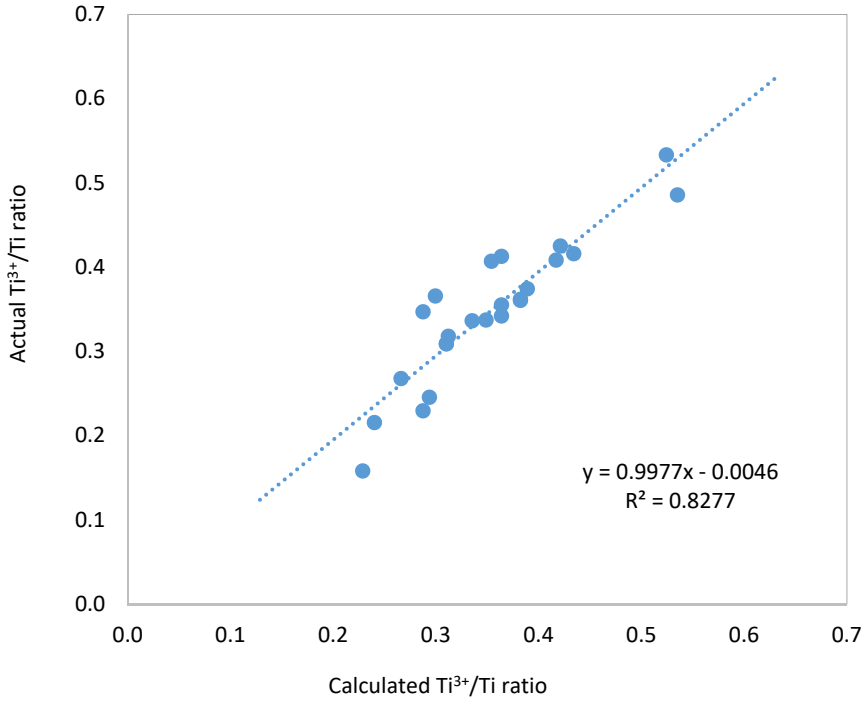

Figure 6-5: Calculated and actual Ti^{3+}/Ti ratios for slag compositions from Pistorius (2002)

Due to the strong indication that Equation 5 is a fair basis for estimating Ti^{3+} content, the relationship was used to estimate the Ti^{3+} content of the slag produced during the current study. The purpose is to compare the slag produced from the low-grade titaniferous ore with typical industrial high-titania slags to establish whether the current slag differs from typical ilmenite slags.

6.1.4 Relationship between Ti_2O_3 and FeO in the slag

Pistorius (1999) identified a relationship between FeO and Ti_2O_3 in industrial high-titania slags. This relationship has been investigated and described via several studies since the original publication (Pistorius, 2002, 2003, 2004; Pistorius & Coetzee, 2003). Pistorius presented slag compositions from South African and Canadian ilmenite smelters by plotting Ti_2O_3, FeO and the impurities relative to the total Ti, expressed as TiO_2, the comparison is shown in Figure 6-6 (left column features reproduced graphs from Zietsman (2004), while the column on the right, compares the current study slags with the data set evaluated by Pistorius).

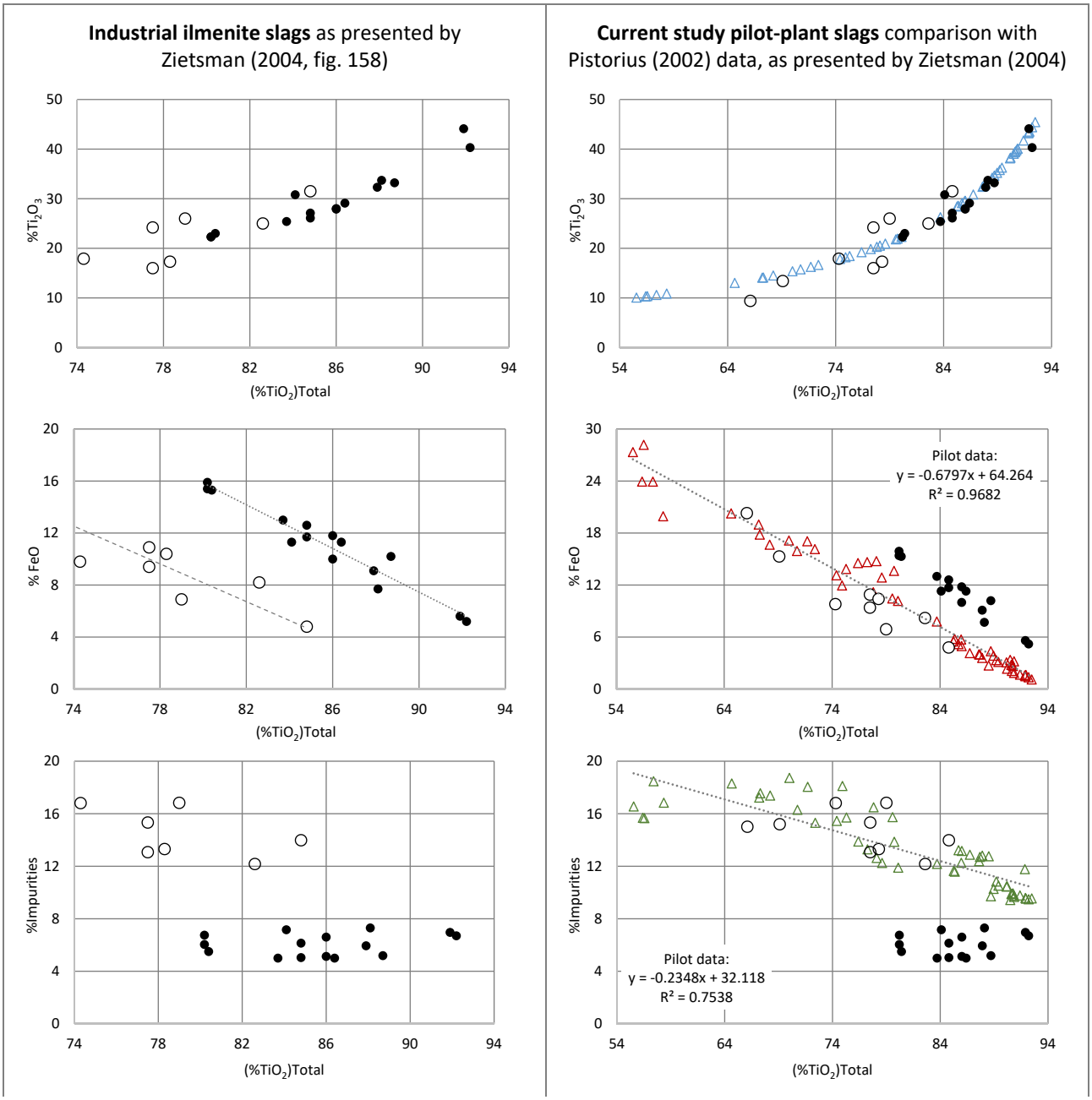

Figure 6-6: Compositional relationships in industrial ilmenite slags compared with slag from the current study (Data from Pistorius, 2002; graphs on the left reproduced from Zietsman, 2004)

Filled circles in Figure 6-6 indicate slags from South African ilmenites and empty circles slags from Canadian ilmenites, empty triangles indicate results from the current study. The horizontal axis for all the graphs indicates the total Ti content of the slag expressed as TiO_2.

The set of graphs on the right (in Figure 6-6) present the pilot data for the low-grade ore, together with the slag data as published by Pistorius (2002) - reproduced similarly to the Zietsman (2004) presentation on the right. According to Pistorius (2002), the observed pattern of the FeO-Ti_2O_3 relationship in ilmenite smelter slags, for different smelter furnace sizes and designs, is remarkably consistent.

The comparison (left to right in Figure 6-6) also illustrates the broader range of slag compositions from the current study, with respect to the titania content in the slag, if compared to the industrial examples. While very different, it is clear that there is a strong correlation. The observations appear to be only altered by the impurity content of the titaniferous feed and based on the results from the pilot test appears to apply to low-grade ore equally well. The current results are especially well-aligned with the Canadian examples presented by Pistorius. Pistorius concluded that given the deterministic nature of the relationship it implies that for a given degree of reduction (determined by the amount of reductant fed to the furnace), and the impurity content of the titaniferous ore and reductant, it, therefore, should be feasible to predict the composition of the slag (Pistorius, 2002).

The relationship between FeO and Ti_2O_3 is such that the composition of the slag follows M_3O_5 stoichiometry (Pistorius, 2002; Zietsman & Pistorius, 2005, 2006). The actual slag FeO and Ti_2O_3 contents can be converted to equivalent contents with the procedure used by Pistorius (2002). The slag composition can, therefore, be represented as $[(FeO, MgO, MnO).2(TiO_2)]x.[(Ti_2O_3, Cr_2O_3, V_2O_3, Al_2O_3).(TiO_2)]y$ with each divalent cation (Fe^{2+}, Mg^{2+} and Mn^{2+}) associated with two tetravalent Ti^{4+} cations in the slag, and each pair of trivalent cations (Ti^{3+}, Cr^{3+}, V^{3+}, Al^{3+}) associated with one tetravalent Ti^{4+} cation in the slag. Pistorius calculated the equivalent FeO content of the slag (the sum of all divalent oxides except CaO, expressed as a corresponding number of moles of FeO), and the equivalent Ti_2O_3 content (the sum of all trivalent oxides, expressed as a corresponding number of moles of Ti_2O_3).

The corresponding equations are as presented as equations 6(a) and 6(b) and the equivalent FeO and the equivalent Ti_2O_3 content is calculated as follows (Pistorius, 2002):

$$(\%FeO)_{eq} = (\%FeO) + \left(\frac{M_{FeO}}{M_{MgO}}\right)(\%MgO) + \left(\frac{M_{FeO}}{M_{MnO}}\right)(\%MnO) \qquad \text{Equation 6(a)}$$

$$(\%Ti_2O_3)_{eq} = (\%Ti_2O_3) + \left(\frac{M_{Ti_2O_3}}{M_{V_2O_5}}\right)(\%V_2O_5) + \left(\frac{M_{Ti_2O_3}}{M_{Cr_2O_3}}\right)(\%Cr_2O_3) + \left(\frac{M_{Ti_2O_3}}{M_{Al_2O_3}}\right)\left[(\%Al_2O_3) - \frac{(\%SiO_2)}{3}\right] \qquad \text{Equation 6(b)}$$

where M_i is the molar mass of oxide *i*, and the amounts of the oxides are in mass percentages.

In Equation 6(b), the vanadium content of slag is expressed as V_2O_5 since this is the convention for the analyses, although the vanadium is expected to be present in the trivalent form. Part of the Al_2O_3 is not taken into account when the equivalent Ti_2O_3 content is calculated, because some Al_2O_3 (a mass assumed to be one-third of that of the silica) reports to the separate silicate phases. CaO and SiO_2 are not included in this calculation, since these report to the silicate phases, and do not dissolve in the solid M_3O_5. The sum of $(\%FeO)_{eq}$, $(\%Ti_2O_3)_{eq}$ and $(\%TiO_2)$ is then normalized to 100%, where $(\%TiO_2)$ is the Ti^{4+} content of the slag, expressed as a mass of TiO_2 (Pistorius, 2002). The FeO and the calculated Ti_2O_3 contents of the pilot-plant slags were converted to equivalent content with the procedure used by Pistorius (2002) and normalized.

The liquidus diagram for the system TiO_2-$FeTiO_3$-Ti_2O_3 is presented in Figure 6-7 with the M_3O_5 equilibrium line highlighted (Zietsman, 2004). If this M_3O_5 solid solution is simply a mixture of the stoichiometric endmembers Ti_3O_5 and $FeTi_2O_5$, a simple linear relationship between the amounts of FeO and Ti_2O_3 in the solidified slag is expected.

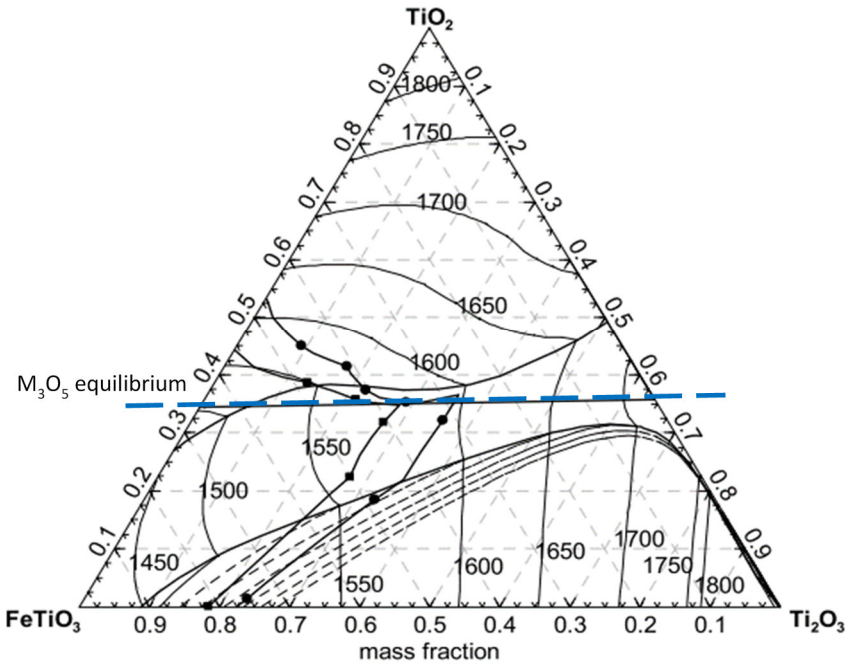

Figure 6-7: Liquidus diagram for the TiO_2-$FeTiO_3$-Ti_2O_3 system (Zietsman, 2004)

The results of the calculations, as per Equation 6, are presented in Figure 6-8. Filled circles in Figure 6-8 indicate slags from South African ilmenites and empty circles slags from Canadian ilmenites. The dashed line indicates the stoichiometric M_3O_5 composition, recreated from Pistorius (2002). The empty triangles represent the slag from the current study (stable metallurgical operation). The result of this evaluation shows that the pilot slags follow M_3O_5 stoichiometry, similarly to the data used by Pistorius - actual graph (a) and equivalent graph (b). The recalculated Ti_2O_3 vs FeO presented in graph most clearly displays the observed compositional invariance of industrial high-titania slags close to the stoichiometric M_3O_5 composition. The slags from South Africa and Canada and the pilot slags from the current study display the same trend. The reason for the significance of this relationship is the fact that some pigment manufacturers specify a maximum Ti_2O_3 content in slag. Understanding this relationship with respect to the titanomagnetite ores could assist in evaluating the quality of the slag produced from titanomagnetite ores.

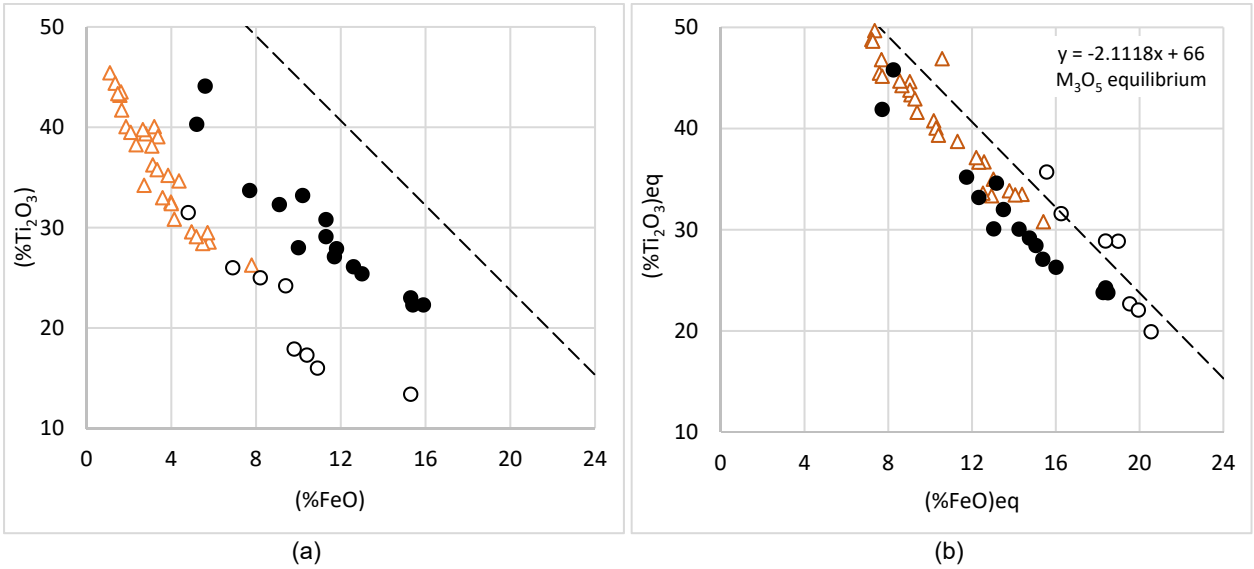

Note: Filled circles indicate slags from South African ilmenites and empty circles slags from Canadian ilmenites. The dashed line indicates the stoichiometric M_3O_5 composition.

Figure 6-8: The relationship between FeO and Ti_2O_3 in industrial high-titania slags and slags produced from low-grade titaniferous ore

6.1.5 Bulk chemical composition of the metal product

The primary objective of the test was to demonstrate the production of high-titania slag, but equally, to evaluate the quality of the metal product from the process.

Table 6-5 summarises the metal compositions averaged over the entire smelting campaign as well as over the operating conditions of interest. The Fe and C content of the metal product was relatively independent of the operating conditions, and that a reasonably consistent grade was achieved throughout the campaign. Noteworthy though is a marginal increase in concentrations of V, Mn, Si and Ti in the metal from Period B to Period C, likely a direct consequence of the higher degree of reduction achieved during the latter.

Table 6-5: Average metal analyses for each operating condition, mass%

		Fe	Ti	V	Cr	Mn	Si	C	P	S
Overall Batch 1 to 54	**W. Ave**	**96.80**	**0.06**	**0.26**	**0.02**	**0.06**	**0.16**	**2.49**	**0.02**	**0.01**
	$\bar{x}$	*97.05*	*0.05*	*0.20*	*0.02*	*0.05*	*0.12*	*2.40*	*0.02*	*0.01*
	σ	1.09	0.08	0.20	0.01	0.05	0.19	0.83	0.01	0.01
Warm-up Batch 1 - 6	**W. Ave**	**99.32**	**0.01**	**0.01**	**0.01**	**0.01**	**0.01**	**0.49**	**0.03**	**0.02**
	$\bar{x}$	*99.27*	*0.01*	*0.01*	*0.01*	*0.01*	*0.01*	*0.55*	*0.03*	*0.02*
	σ	0.36	0.00	0.00	0.00	0.00	0.00	0.35	0.01	0.01
Period A Stabilisation Batch 7 - 24	**W. Ave**	**97.39**	**0.01**	**0.04**	**0.02**	**0.01**	**0.01**	**2.43**	**0.03**	**0.01**
	$\bar{x}$	*97.40*	*0.01*	*0.04*	*0.02*	*0.01*	*0.01*	*2.42*	*0.03*	*0.01*
	σ	0.30	0.01	0.03	0.01	0.00	0.00	0.29	0.00	0.01
Period B Baseline Batch 25 - 32	**W. Ave**	**96.40**	**0.03**	**0.24**	**0.03**	**0.05**	**0.03**	**3.15**	**0.02**	**0.01**
	$\bar{x}$	*96.26*	*0.03*	*0.24*	*0.03*	*0.05*	*0.03*	*3.29*	*0.02*	*0.01*
	σ	0.36	0.01	0.07	0.01	0.02	0.02	0.38	0.00	0.01
Period C High power flux Batch 33 - 51	**W. Ave**	**96.08**	**0.12**	**0.43**	**0.03**	**0.10**	**0.30**	**2.73**	**0.02**	**0.01**
	$\bar{x}$	*96.20*	*0.13*	*0.43*	*0.03*	*0.10*	*0.32*	*2.70*	*0.02*	*0.01*
	σ	0.45	0.10	0.14	0.01	0.04	0.21	0.23	0.01	0.00
Period D Shutdown Batch 52 - 54	**W. Ave**	**96.23**	**0.11**	**0.46**	**0.03**	**0.13**	**0.40**	**2.57**	**0.02**	**0.01**
	$\bar{x}$	*96.20*	*0.12*	*0.46*	*0.03*	*0.13*	*0.41*	*2.59*	*0.02*	*0.01*
	σ	0.14	0.04	0.04	0.00	0.01	0.02	0.08	0.00	0.00

As FeO content decreased in the slag V and Mn content in the metal increased. While this is also applicable for C, the trend is not only associated with the degree of reduction as temperature effects may also play a role. The trend observed for the minor elements are expected, and despite the increased deportment, low levels of Ti were consistent. This could also be as a result of the higher Fe-ratio (compared to typical ilmenite ores), found in titanomagnetite ores.

Figure 6-9, Figure 6-10 and Figure 6-11 plot the relationship for C, V, and Mn content in the metal as a function of FeO content in the slag. Expected trends are observed. The relationships presented for these minor elements are useful predictors of the deportment ratios for these elements, expressed as a mass ratio relative to FeO in slag.

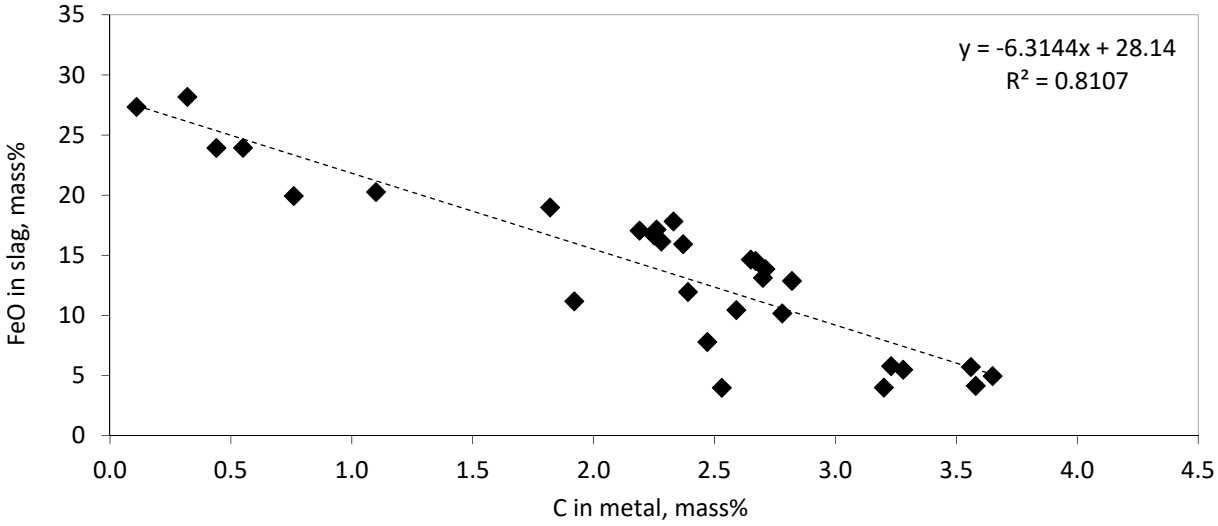

Figure 6-9: Plot of slag FeO content versus C content of the metal

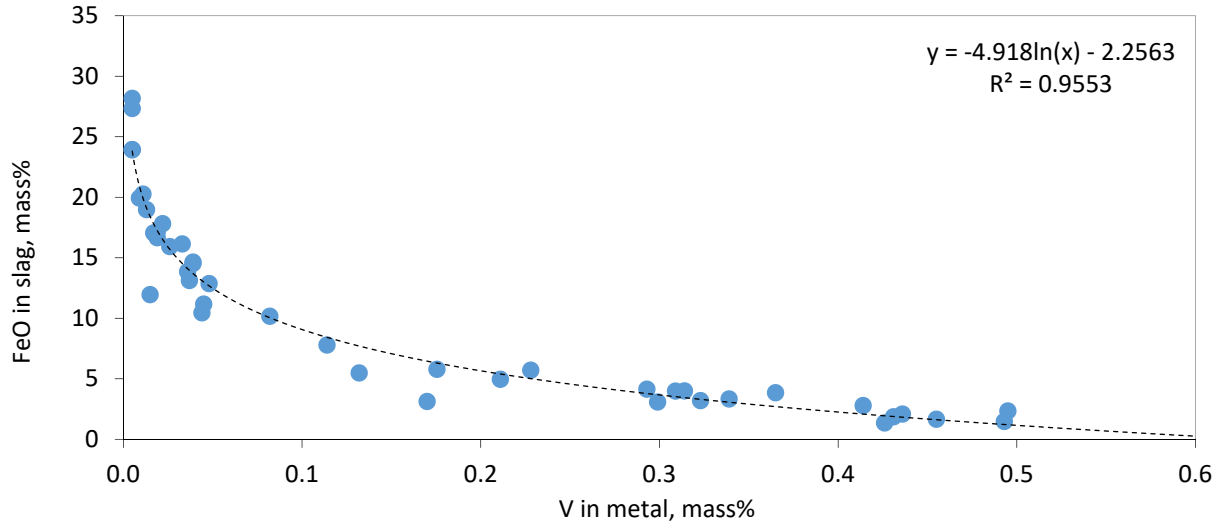

Figure 6-10: Plot of slag FeO content versus V content of the metal

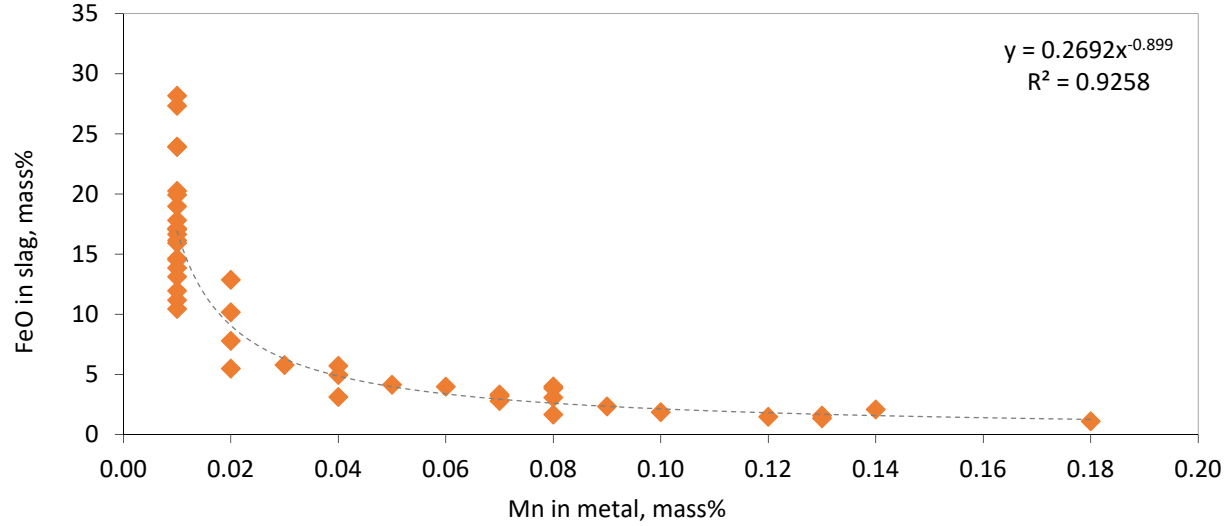

Figure 6-11: Plot of slag FeO content versus Mn content of the metal

6.1.6 Phase chemical evaluation of the metal product

The metal produced during the campaign was evaluated via SEM-based (EDS) microanalysis to identify the main metal phases and determine if any inclusions were present. EMPA based (WDS) analysis of the Fe-bearing phase to determine, more accurately, the composition of this phase.

The general appearance of three metal samples, via three micrographs, is shown via backscatter micrographs. It can be seen, via the microanalysis of highlighted points, that the metal generally consists of two distinct phases – an almost pure Fe alloy (bright phase in the image) and a carbon-bearing Fe alloy (as determined from the low totals for this phase and its slightly darker appearance in the backscattered image).

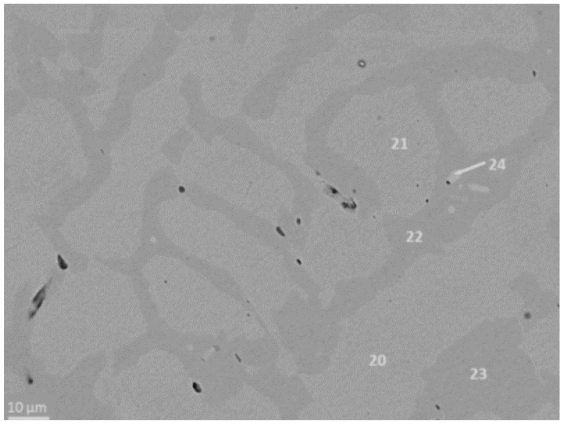

Metal Batch 9				
Identifier	Fe	V	Total	Comments
20	98.4		98.4	Fe-metal
21	98.9		98.9	Fe-metal
22	91.9		91.9	Fe-metal (C bearing)
23	91.8		91.8	Fe-metal (C bearing)
24	98.2		98.2	Fe-metal
25	100.3		100.3	Fe metal

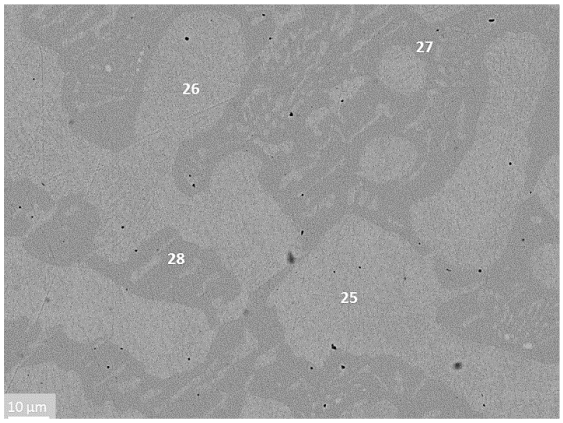

Metal Batch 27				
Identifier	Fe	V	Total	Comments
26	101.2		101.2	Fe metal
27	91.8		91.8	Fe metal (C-bearing)
28	91.8		91.8	Fe metal (C-bearing)

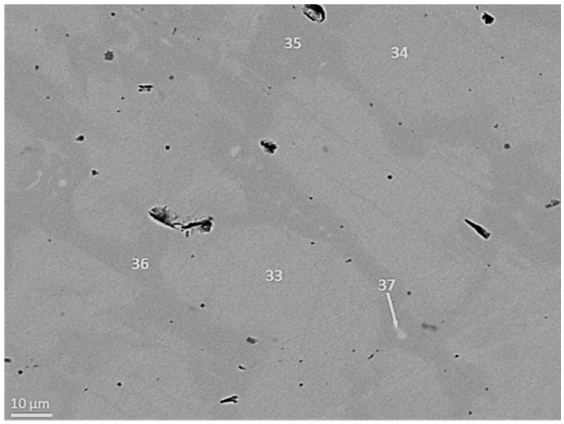

Metal Batch 50				
Identifier	Fe	V	Total	Comments
33	97.3		97.3	Fe metal
34	97.4		97.4	Fe metal
35	88.9	1.11	90.0	Fe metal (C-bearing)
36	89.5	1.90	91.4	Fe metal (C-bearing)

Figure 6-12: Backscattered electron micrographs showing the general appearance of metal and the microanalysis of highlighted points (batch 9, 27 and 50), mass %

A summary of the average WDS analyses of the two primary phases identified in four metal samples is presented in Table 6-6. The bulk chemical compositions of the corresponding metal taps are presented in Table 6-7 for ease of reference. The evaluation showed that V appears to be predominantly associated with the C-bearing phase.

Table 6-6: Average WDS analyses of the two distinct phases observed in the metal tap samples, mass %

	Fe-metal					C-bearing Fe-metal				
Batch	Si	Ti	V	Fe	Total	Si	Ti	V	Fe	Total
5	0.06	0	0.01	99.09	99.16	Not detected				
9	0.06	0.00	0.01	98.40	98.48	0.06	0.01	0.11	93.21	93.38
27	0.10	0.01	0.10	97.69	97.88	0.07	0.02	0.38	93.73	94.21
50	0.37	0.01	0.22	97.41	98.01	0.21	0.16	1.14	91.65	93.15

Table 6-7: Bulk chemical compositions of the selected metal samples, mass %

Batch	Al	Si	Ti	V	Cr	Mn	Fe	Ni	C	P	S	Total
5	0.01	0.01	0.01	0.01	0.01	0.01	99.00	0.03	0.76	0.041	0.03	99.91
9	0.01	0.01	0.01	0.02	0.02	0.01	97.60	0.03	2.26	0.029	0.01	99.99
27	0.01	0.01	0.02	0.23	0.03	0.04	96.00	0.01	3.56	0.020	0.01	99.93
50	0.01	0.27	0.08	0.46	0.03	0.08	96.10	0.01	2.86	0.021	0.01	99.92

A carbon-bearing phase was not observed in metal from batch 5, and it is correlated with the operating conditions, namely, during this period metallurgical stability had not been attained yet. The starting metal heel is also depleted of carbon. The conditions were not highly reducing and the start-up heel (metal inventory would have still been diluting the new metal make). The following main conclusions are highlighted:

- It is evident that V appears to partition to the metal phase.
- Very little Ti is observed in either phase which corresponds to the bulk chemical composition of the metals, suggesting that Ti-bearing inclusions are not present in the metal.
- Few inclusions were observed in the metal samples, an excellent outcome with respect to the quality of the metal product, especially since highly reducing conditions were tested.

Overall, it can be concluded that despite highly reducing conditions, the product quality did not appear to deteriorate significantly, and it is possible to recover vanadium to metal phase, despite low concentrations in the feed.

6.1.7 Bulk chemical composition and size distribution of off-gas dust

The off-gas dust consists of a combination of fine material particles carried over to the off-gas system and fumed constituents. Typically the formation of fumed constituents depends on the degree reduction and operating temperature, with higher temperatures favouring the formation of gaseous vapours. Overall, the dust composition and the mass collected during the campaign was in line with expectations for the type and scale of the test.

Each bag of off-gas dust collected from the off-gas handling plant was sampled and analysed. The rate of off-gas collection increased towards the latter part of the campaign, mainly due to inventory effects in the relatively large system. The dust collection system was operated for a week post-campaign to ensure all the dust that can be attributed to the test was collected. The chemical composition of the off-gas dust indicates that the bulk of the dust generated, as collected from the baghouse, is concentrate that by-passed the reaction zone and collected in the off-gas system. The overall collection of material from the off-gas handling facility was about 6% of the mass fed. The average dust composition for the test (weighted) is summarised in Table 6-8.

A sample of off-gas dust was subjected to a full element scan (a semi-quantitative pressed pellet scan), and the result is reported in

Appendix D, Table D6. The element scan is a useful tool to evaluate the potential presence of unwanted elements, but are not an accredited quantitative method.

Table 6-8: Average off-gas dust analyses for each operating condition, mass%

		MgO	Al_2O_3	SiO_2	CaO	TiO_2	V_2O_5	Cr_2O_3	MnO	FeO
Overall Batch 1 - 54	**W. Ave**	**4.86**	**2.09**	**7.20**	**0.28**	**36.18**	**0.44**	**0.55**	**1.82**	**40.66**
	$\bar{x}$	*4.80*	*2.09*	*7.09*	*0.30*	*35.65*	*0.43*	*0.57*	*1.92*	*41.11*
	σ	1.34	0.50	1.65	0.25	9.69	0.06	0.70	0.75	11.35

Eight randomly selected off-gas dust samples were selected for particle size characterisation. The samples were tested using Malvern Mastersizer 2000 instrument, suitable for samples with a top size below 1000 µm. The results presented in Figure 6-13, show that particle size distribution was reasonably consistent throughout the campaign. Dashed lines represent the size distribution of samples taken from stable operating periods, while the solid lines represent samples taken during stabilisation periods.

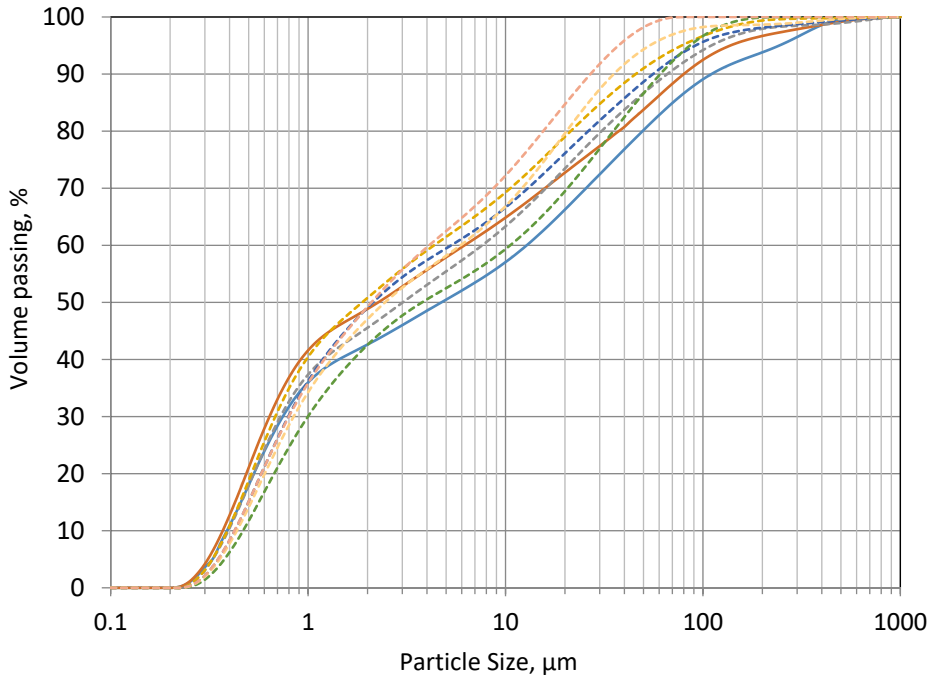

Figure 6-13: Particle size distribution of randomly selected off-gas dust samples

6.1.8 Phase chemical evaluation of the off-gas dust

The off-gas dust was evaluated via SEM-based (EDS) microanalysis only. The dust sample appeared to be a mixture of mainly molten feed droplets but did include what appears to be slag and metal droplets. Finer grained (<1 µm) particles were difficult to analyse, and it is possible that fumed products could make up a portion of the finer fraction. Reductant particles were not readily observable through the technique employed to examine the dust. Backscattered micrographs of the off-gas dust sample evaluated are shown in Figure 6-14. The microanalysis of each of the annotated points is presented in Table 6-9.

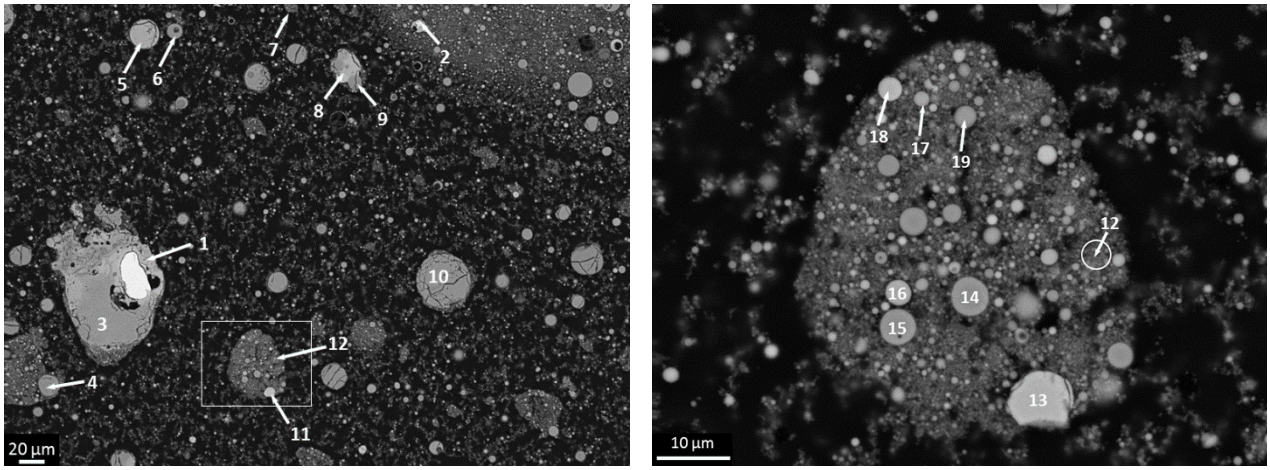

Figure 6-14: Backscattered electron micrograph of the off-gas dust; higher magnification (right)

Table 6-9: EDS microanalysis of phases identified in the dust sample, as per Figure 6-14, mass %

Point	Mg	Al	Si	Ti	Mn	Fe	Total
1				1.10		97.0	98.1
2				2.53		88.0	90.5
	MgO	**Al_2O_3**	**SiO_2**	**TiO_2**	**MnO**	**FeO**	**Total**
3	2.31	3.84	1.31	86.4	1.24	12.6	107.7
4	1.31	1.44	1.39	46.0	0.24	47.4	97.8
5	1.06	0.26	0.63	51.4	0.41	44.1	97.8
6	6.38	3.04	11.33	63.6	3.97	12.3	100.6
7	4.28	2.81	2.43	82.7	1.03	9.55	102.8
8	1.11	1.50	3.59	34.2	0.66	55.0	96.0
9	3.07	2.64	7.28	76.8	2.41	8.61	100.8
10	1.70	2.44	2.46	83.1	1.14	9.37	100.2
11	0.16	0.13	0.97	3.45	0.00	88.4	93.2
13	0.11	0.14	0.73	3.17	0.00	87.8	91.9
14	2.86	2.50	7.60	57.2	1.77	27.1	99.0
15	4.72	2.31	8.94	56.8	1.61	25.6	99.9
16	2.14	1.56	3.84	23.4	0.38	61.2	92.5
17	4.42	3.25	7.38	58.9	2.13	19.1	95.1
18	1.30	0.32	1.84	17.9	0.00	69.4	90.8
19	4.59	2.73	8.36	45.0	1.93	23.8	86.4

Noteworthy is the varied compositions (Table 6-9). The variations are identified as nominally feed and slag phases indicative that some partially altered feed is carried over to the off-gas, together with small droplets of slag, unreacted feed and fumed products. Only one sample was evaluated for the sake of completeness in the context of the current study, but as the method of capturing the dust is different to that of an industrial furnace, combined with the scale effects, it is not regarded as fully representative of solids that will be collected in an industrial situation.

Typically, dust losses can be minimised, and the solids are typically water quenched. The pilot facility is set-up to fully combust the CO-rich off-gas at the point of exit (via a gap between the furnace and the extraction system). This is mainly done for safety reasons to minimise the risk of CO explosions. This most definitely modifies the character of the dust and fume.

6.2 Elemental Mass Balance and Accountability

Elemental accountability is a useful tool to evaluate the quality of the test result, but are also used to assess recoveries and inventory trends. The elemental accountability (elemental mass balance) is summarised in Table 6-10. Moreover, the recovery and distribution of elements over the entire campaign are summarised in Table 6-12 and Table 6-13, respectively. Definitions defined in subsection 3.2 are applicable. The overall elemental mass balance is calculated using the compositions reported in section 4, and the feed and product masses, as well as product assays, are reported per batch ('tap') in Appendix C and Appendix D.

Table 6-10: Elemental mass balance and accountability

FEED		Elemental Mass Fed, kg								
Mass In		Fe	Ti	V	Cr	Mn	Ca	Mg	Al	Si
Concentrate	107 501	46084.3	21986.0	289.1	58.8	411.3	23.0	440.8	699.9	532.5
Anthracite	20 031	1105.4	-	-	-	-	42.9	16.9	12.7	32.8
Other	1 595	1100.0	-	-	-	-	-	-	-	-
Total Feed	129 127	48289.8	21986.0	289.1	58.8	411.3	66.0	457.7	712.6	565.2
PRODUCTS		Elemental Product Mass, kg								
Mass Out		Fe	Ti	V	Cr	Mn	Ca	Mg	Al	Si
Slag	40 326	3023.8	19397.6	176.4	42.4	285.4	50.6	1364.6	729.5	398.9
Metal	46 705	45152.7	29.2	120.7	11.7	29.3	-	-	3.4	76.5
Off-gas dust	6 431	2032.7	1394.8	15.8	24.4	90.6	12.7	188.3	71.3	216.4
Total Product	93 462	50209.2	20821.6	312.8	78.5	405.3	63.3	1553.0	804.2	691.9
		Unaccounted mass (feed less product), kg								
Element		Fe	Ti	V	Cr	Mn	Ca	Mg	Al	Si
Feed less products		-1919.5	1164.4	-23.8	-19.6	6.0	2.7	-1095.2	-91.6	-126.6
		Accountability, %								
Element		Fe	Ti	V	Cr	Mn	Ca	Mg	Al	Si
Product/Feed		104.0	94.7	108.2	133.4	98.5	95.8	339.3	112.9	122.4

Overall accountabilities were good. The mass balance is validated by evaluating the accountability of the two major components. Ti and Fe are reliable indicators of the overall mass balance as Ti is a major component of both the feed and the slag, and Fe as a major component of the feed and the metal.

The error in estimating the elemental masses is the sum of the squares of the uncertainties for all the steps involved in determining the elemental mass (weighing, sampling, operator and analytical errors all contribute to the combined uncertainty). Considering analytical and weighing uncertainties associated with bulk processing, the overall accountabilities for the current test is used as a measure of the combined uncertainty. Each potential source of an error has a specific magnitude. Some sources are positive, and others are negative, and some are larger in magnitude and others are smaller. The cumulative effect of these determinate errors is a net positive or negative error in accuracy or reliability of the measurement – in this scenario, the elemental accountability. In the context of a large-scale experiment, such as the current study, the overall mass balance (via the accountabilities) is used to calculate the cumulative error or uncertainty. As the majority of the elements can be accounted for with as 100% ±5%, the conclusion is that the data presented herein is sufficiently reliable.

The over-accounting of Fe (104%) can be attributed to potential unaccounted metal entrainment and additional mass from lance rods which is used during tapping and are not accounted for in the mass balance. A conservative estimate of the lance rod contamination, namely assuming an average consumption of 3 lance rods per tap, which accounts for at least 1000 kg of Fe from the lance rods over the entire duration of the smelting campaign.

The process of removing slag from the furnace during the dig-out is also associated with higher uncertainty than sampling and weighing from tapping slag as it is possible that the slag composition is varied (due to the freeze-lining)

and the weight of the sample could be over- or underestimated due to the nature of the dig-out process. A clean separation of the slag from the refractory materials is challenging. A significant quantity of high-titania slag was collected during the dig-out, which therefore may have contributed to the under-accounting of Ti. High accountabilities, close to 100%, for the major components, contribute to the confidence in the quality of the results.

6.2.1 Cumulative accountabilities

Cumulative accountability represents the evolution of accountability throughout the campaign and is useful to highlight the accumulation of an element (cumulative accountability = cumulative elemental feed mass minus cumulative elemental products mass). It is one of the tools used to regulate or evaluate the furnace inventory, metal production rate and refractory wear, or freeze-lining control. The inventory of the furnace is monitored for quality and operational reasons. The next series of graphs presents the cumulative accountability of elements of interest. The cumulative accountabilities represented in Figure 6-15 illustrates the evolution of accountability of six elements over the duration of the campaign, namely Ti, Fe, Mn, V, Si, and Ca.

The graphs also illustrate that process stability had been achieved after batch 24, represented in the graphs via the stable inventory. The increase at the end of the campaign is due to the attributed mass from the furnace dig-out (allocated as batch 55). The overall accountability of Mn and V, namely 98.5% and 108.2% respectively is excellent for minor elements. The accountabilities of Si, Cr and Ca are 122.4, 133.4 and 95.8%, respectively. The accountability of minor elements suffers from analytical measurement uncertainties as the concentration of trace elements are close to the detection limit of the analytical techniques deployed. Overall the accountabilities of both major and minor elements were high.

Noteworthy is the accountability of the elements associated with the refractories, specifically the furnace sidewall and roof (Mg and Al, respectively). The early slag compositions were characterized by indications of refractory pick-up, mainly MgO, which is typical for the pilot furnaces. A pilot-plant test provides an accelerated view of what is expected in terms of refractory wear. Some refractory wear from the roof, an alumina-based material, was observed towards the latter part of the test, likely due to the increase in power and the effects of an extended test campaign. The roof wear is typical for the scale and extent of the test campaign, especially since the refractory roof was specially installed for this project. The former is designed to install a new lining with a marginal excess of refractory and the roof refractory would likely have stabilised if the campaign had continued, due to fact that the roof is water-cooled.

The cumulative accountability for Mg and Al, shown in Figure 6-16, represents the accumulation of these elements over the duration of the campaign. Both elements, Al to a lesser extent, over account due to refractory wear. Mg, especially during the early part of the test, while a noticeable increase in accountability of Al, was observed during the shutdown phase of the test.

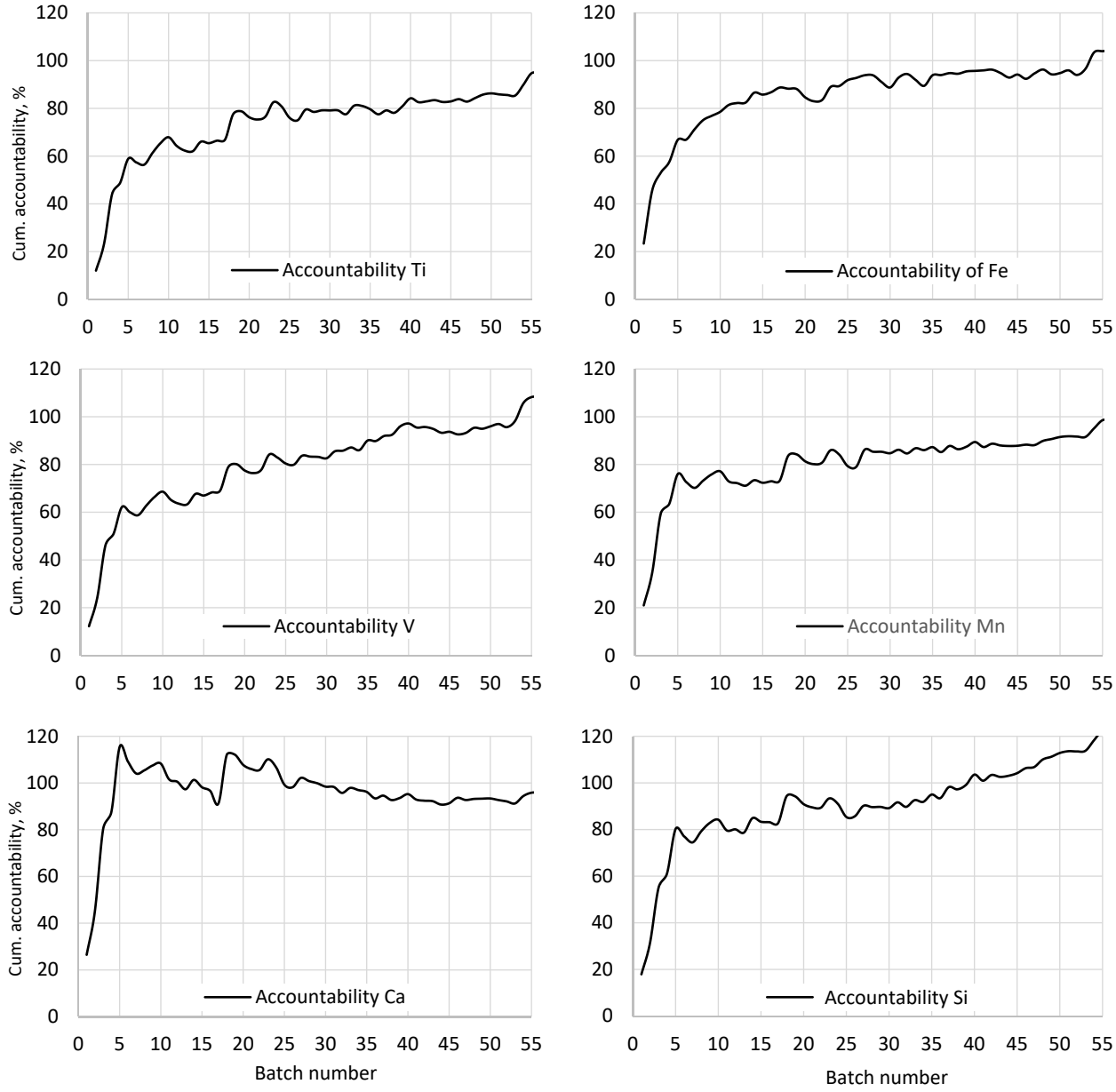

Figure 6-15: Plot of the evolution of the cumulative elemental accountability for Ti, Fe, V, Mn, Ca, and Si

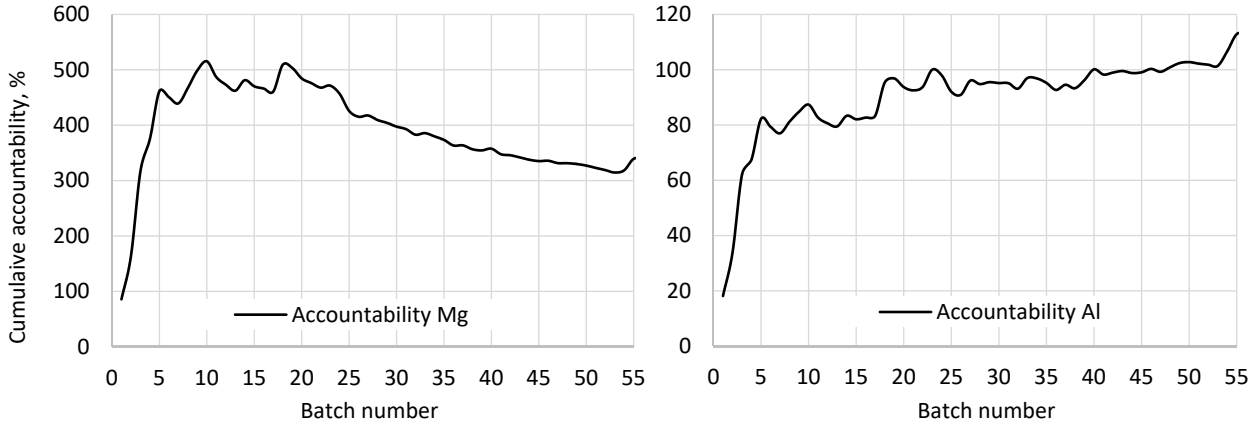

Figure 6-16: Plot of the evolution of the cumulative elemental accountability for Mg and Al

6.2.2 MgO reconciliation

MgO is the main component of the sidewall brick lining, as well as the refractory hearth material (95% and 77% respectively) – the composition of the various refractories used in the furnace is included in Appendix A, Table A1. Figure 6-17 graphically presents a comparison of the evolution of the Mg mass balance (accumulated excess Mg mass) and the cumulative Mg accountability (mass % ratio – as presented in Figure 6-16).

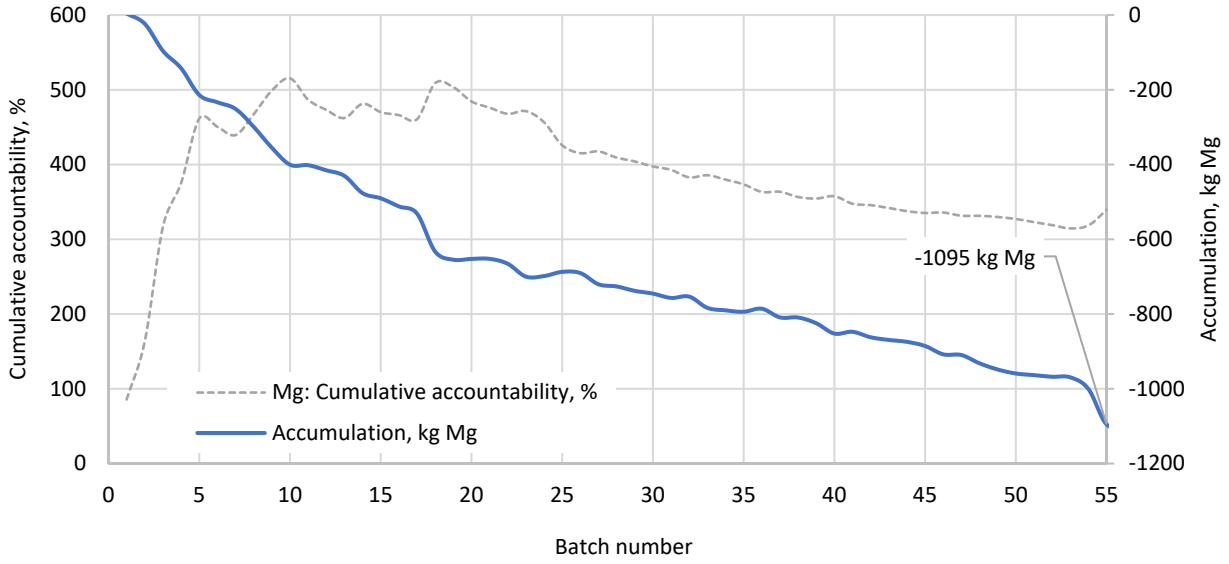

Figure 6-17: Accumulation (kg) and cumulative accountability of Mg, %

The overall accountability or cumulative accountability of Mg, namely 339%, implies that about 1095 kg of Mg (or 1815 kg of MgO) was removed from the furnace via the products (mainly slag) that cannot be accounted for by the feed materials (the overall material balance). The MgO accumulation is calculated from the mass of Mg fed minus the mass of Mg collected either via tapping or from the slag removed during the furnace excavation or as off-gas dust. Reconciliation is done to check whether the additional mass (about 1.8 tons of MgO), is sensible. The method estimates the mass of refractory wear based on the refractory wear profiles measured during the furnace excavation. The calculated volume loss is converted to a mass loss. It is plausible that the majority of the excess Mg presented by the mass balance may be due to refractory wear. It is likely that this is not the only contributor as other measurement errors would also contribute, but refractory wear is likely the major contributor.

Table 6-11 summarises the evaluation of the contribution of the refractory wear to the MgO mass balance. The calculation shows the reconciled overall MgO mass balance. Based on the detailed measurements taken prior to the furnace excavation a refractory volume loss was calculated on the basis of an average loss per brick (relative to the original brick volume determined by the brick dimensions). The average brick wear was estimated to be 8cm, which when converted to a volume loss (for all bricks) is equal to 0.586 m^3.

Table 6-11: Reconciliation of Mg mass balance, adjusted for furnace lining wear

Density of MgO	2970 kg/m^3
MgO content in bricks	95.0%
The total refractory mass associated with MgO (excl. hearth refractories)	1741 kg
Mg from refractory wear	998 kg
Mg excess mass from mass balance	-1095 kg
Mg (MgO) excess mass (by difference)	-97 kg (-169 kg)
MgO accountability, adjusted for refractory pick-up	*106.7%*
MgO accountability without refractory reconciliation	*339.3%*

The reconciliation provides a fair representation of the potential contribution of the refractory to the Mg mass balance, adding confidence to the overall mass balance and also provides a basis for recalculating the slag composition, to estimate the effect the dilution had on the product quality. The reconciliation thus provides additional validation for the overall confidence in the result.

Detailed profiles of the refractory wear are included in Appendix A: Furnace excavation measurements – profiles were constructed using post-test refractory measurements.

The condition of the metal and slag taphole areas before and after completion of the test is shown in Figure 6-18. The majority of refractory wear occurred in these two areas, which is not unexpected. MgO from the refractories is assimilated in the slag and is reported as total MgO in the slag analyses. The reconciliation adds to the confidence as to the reliability of the mass balance as the estimated MgO wear ties up well with the overall mass balance. The adjustment or reconciliation estimates that about 998 kg of Mg found in the slag can be linked to the observed refractory wear.

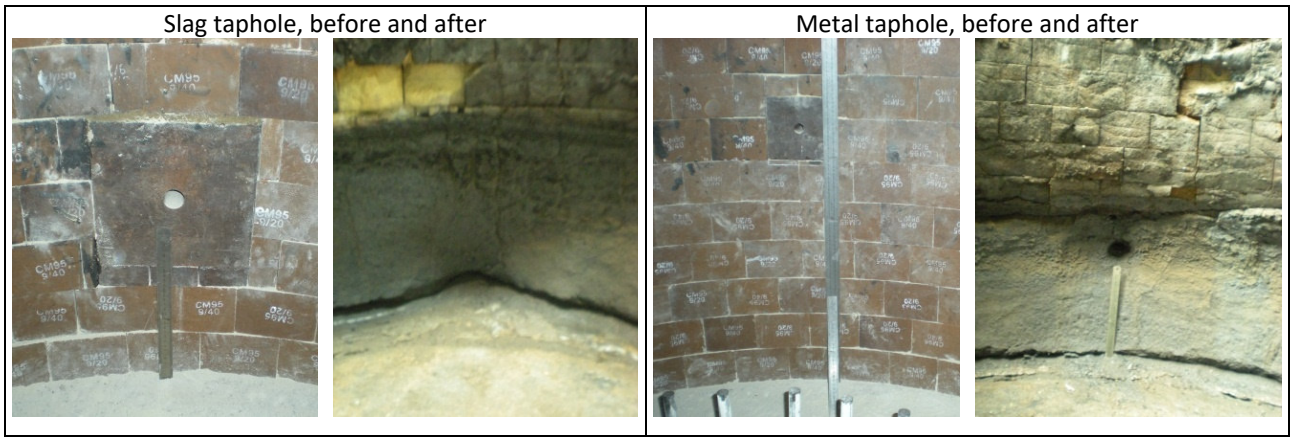

Figure 6-18: Views of the slag and metal taphole respectively, before and after the test campaign

6.2.3 Recovery and distribution of elements

The elemental recoveries and distribution of elements, from the mass balance, is summarised in Table 6-12 and Table 6-13, respectively.

Recovery of Fe to the metal phase is 93.5%; this is the proportion of Fe recovered as metal expressed as a ratio of the Fe in all the feed materials. Fe deportment is also considered, which expresses Fe recovery as a ratio of Fe recovered in the product streams; this normalised Fe recovery is about 90%.

Based on the number of data points and the various measurement uncertainties (weighing, sampling and analytical errors), the manner in which the recovery is calculated can be moderated by assessing and comparing the two calculation outcomes. Individual tap masses and analysis are included in the mass balance, while for the feed, a bulk composition is used. Therefore, depending on the variability of the feedstock, the uncertainty may be higher for the feed than for the products. If the overall accountability is high, then deportment and recovery should be similar, but if not, as was the case for Mg, for example, the deportment calculation is not a reliable indicator of the distribution of elements to various phases.

Table 6-12: Recovery of elements to products as a percentage of total mass fed, mass %

Recovered as:	Elemental distribution to the products, % of mass fed								
	Fe	Ti	V	Cr	Mn	Ca	Mg	Al	Si
Slag	6.3	88.2	61.0	72.1	69.4	76.6	298.1	102.4	70.6
Metal	93.5	0.1	41.7	19.8	7.1	-	-	0.5	13.5
Off-gas dust	4.2	6.3	5.5	41.5	22.0	19.2	41.1	10.0	38.3
Total Product	104.0	94.7	108.2	133.4	98.5	95.8	339.3	112.9	122.4

Table 6-13: Deportment of elements to products streams, mass %

Recovered as:	Elemental distribution to the products, % of product mass								
	Fe	Ti	V	Cr	Mn	Ca	Mg	Al	Si
Slag	6.0	93.2	56.4	54.0	70.4	80.0	87.9	90.7	57.7
Metal	89.9	0.1	38.6	14.9	7.2	-	-	0.4	11.1
Off-gas dust	4.0	6.7	5.0	31.1	22.4	20.0	12.1	8.9	31.3
Total Product	100	100	100	100	100	100	100	100	100

The recovery and distribution of the two primary components of the system, Fe and Ti, are evaluated by comparing differences between the conditions, namely the baseline condition and higher power intensity condition. The overall recovery of the major elements was good; however, inventory effects may impact the recovery calculations during sub-periods if substantial changes to the furnace inventory occurred during the sub-periods. Care has to be taken when evaluating the mass balance for interim conditions. Interim recoveries do not reflect the process distributions adequately due to inventory effects.

The average recovery is an average of the various operating conditions. The elemental distribution establishes the partition of the total product mass into the different product streams, for a specific element and to a degree neglects inventory, thus indicating a more accurate reflection of "recovery". If conditions were ideal, i.e. negligible inventory or lock-up and off-gas dust were fully recycled, masses and analyses were entirely accurate, and there was 100% accountability, the elemental distribution (deportment) would be equal to the elemental recovery.

6.3 Energy Consumption and Thermal Efficiency

The energy requirement for a given process describes the energy required to achieve the desired temperature, state, and reaction. During the test the operating power was systematically varied as part of the experimental programme, ultimately achieving broadly two operating regimes, namely the baseline conditions (Period B) and a high-power condition (Period C and D).

The furnace power input calculations are based on accurate feedback from the power supply (current and voltage measurements). The feed rates and masses fed to the furnace are also accurately recorded via the control system as all feed hoppers are installed with calibrated load cells. Albeit that the measured rate of energy loss to the environment is also continuously evaluated, there is a degree of uncertainty associated with the estimation as not all areas of the furnace are water-cooled, and the furnace is never perfectly in balance. A small additional factor for "unmeasured losses" is included in the estimation of total energy losses to the environment to correct for this. The estimate is based on a simplified heat transfer calculation (for the hearth) which is only cooled through natural convection and prior experience. In this case, the losses from the areas without water cooling was estimated to be about 10% of the total measured losses; thus about 40 kW to 50 kW. For the purposes of the energy balance management, the measured losses and the unmeasured factor is a control input and is not continuously adjusted during a batch. The set point in the system represents an average rate of loss for the batch or period. The terminology for this average estimated rate of energy loss (for a given batch of feed or period) is referred to as the 'Heatloss set point' or 'Heatlosses'.

Apart from the intrinsic measurement uncertainty, estimation of an average rate of energy loss also assumes that the furnace is always thermally balanced, which is never truly the case. In this section, gross energy consumption (total energy input ratio), specific energy requirement (average energy requirement excluding thermal efficiency), rate of energy loss, and thermal efficiency of the furnace are evaluated in the context of the smelting campaign. The power input as a function of feed rate is managed via what is referred to as the "power-to-feed balance" philosophy. The control philosophy is also described as part of the experimental procedure, summarised by the following relationship presented as Equation 7.

$$Power\ target = (SER\ target\ \times Desired\ feed\ rate) + Heatloss\ Set\ Point \qquad \text{Equation 7}$$

SER is herein defined as the specific or smelting energy requirement, kWh/kg feed (the SER excludes efficiency factors which are favoured as it excludes equipment efficiencies and is process specific). The relationship can be expressed as a ratio of the effective energy and the mass fed (Equation 8).

$$SER = \frac{Energy\ Input - Energy\ Loss}{Mass\ Fed} = \frac{Effective\ Energy}{Mass\ Fed} \qquad \text{Equation 8}$$

The gross energy consumption is the gross or total furnace energy input per batch as a ratio of the mass fed, kWh/kg feed. Gross energy consumption is equipment specific as the efficiency of a specific furnace design is included. To compare energy requirement SER excludes the energy losses. Equation 9 shows the calculation used for the gross energy consumption.

$$Gross\ Energy\ Consumption\ (GEC) = \frac{Energy\ Input}{Mass\ Fed} \qquad \text{Equation 9}$$

Note: The SER and GEC equations (Equation 8 and Equation 9) are expressed as a ratio of total feed (concentrate plus reductant) which is a choice of convention rather than for any specific purpose. It is also common to express this relationship as a ratio of the concentrate only or the metal product, for example.

Thermal efficiency is a function of the furnace design. Smaller furnaces are generally less thermally efficient. The pilot furnace is not explicitly designed for the process tested and is also relatively small. Yet, even at pilot scale, as throughput increases, smelting efficiency improves. For purposes of this discussion, thermal efficiency is defined as a ratio of the effective energy and total energy input; as per Equation 10.

$$\%\ Thermal\ Efficiency\ of\ the\ Operation = \frac{Effective\ Energy}{Total\ Energy\ Input} = \frac{SER}{GEC} \qquad \text{Equation 10}$$

The plot of gross energy consumption (kWh/kg total feed) for the pilot test is shown in Figure 6-19, as per Equation 9. The plot shows an inversely proportional relationship between throughput and energy consumption, illustrating the principle that thermal efficiency increases when the furnace is operated closer to the design throughput – a furnace operate more efficiently at higher smelting rates because the rate of energy loss does not increase proportionally with the smelting rate.

Specific energy (SER) for the smelting process can be evaluated by plotting average power as a function of average total feed rate per batch. The gradient of such a plot estimates the average SER for the smelting campaign or period. The y-axis intercept estimates the average rate of energy loss for the period of interest and should, in principle, agree with the measured average rate of energy loss. In Figure 6-20, this relationship is presented, both relative to the total average feed and the average concentrate feed rates per batch. From Figure 6-20, the average SER for the smelting campaign is 1.36 kWh/kg total feed or 1.63 kWh/kg concentrate, while the average rate of energy loss (kWh/h) converged on about 525kW.

The average SER estimated from the slope of the graph agrees very well with the targets used for the furnace control (power-to-feed balance) during the test campaign. The data shows that the increase in smelting intensity achieved the desired outcome of operating in different operating regions, which is required to enable establishing the linear relationship. The average rate of energy losses for the smelting campaign was 525 kW (determined through heat loss calculations). The average loss agrees very well with the average rate of energy loss of about 480 kW determined from the linear trend in Figure 6-20 (the y-intercept represents the average rate of energy loss for the campaign). This process allows for verification of the rate of energy loss calculated through the water-cooled circuits. As the majority of the furnace is water-cooled, the estimate used during the test is expected to be close to the intercept. An average rate of energy loss of about 500 kW is therefore assumed to be a fair approximation for all periods and the y-intercept is adapted as such. The excellent agreement between the estimated and the average rate of energy loss shows that the furnace was operated well and with minimal unplanned downtime.

Figure 6-21 shows the estimated thermal efficiency together with the gross energy consumption versus the average feed rate achieved per batch. The plot illustrates that an improvement in efficiency is achieved with increased throughput, even at a pilot-plant scale. The gross energy consumption approaches the average specific energy consumption with an increase in throughput, and the average SER serves as the horizontal asymptote of the gross energy consumption. Figure 6-21 illustrates the relationship between throughput and furnace thermal efficiency for this particular smelting campaign and equipment arrangement; increasing from about 35% to 57% as the intensity increased.

Figure 6-19 to Figure 6-21 summarises the overall energy assessment of the pilot test.

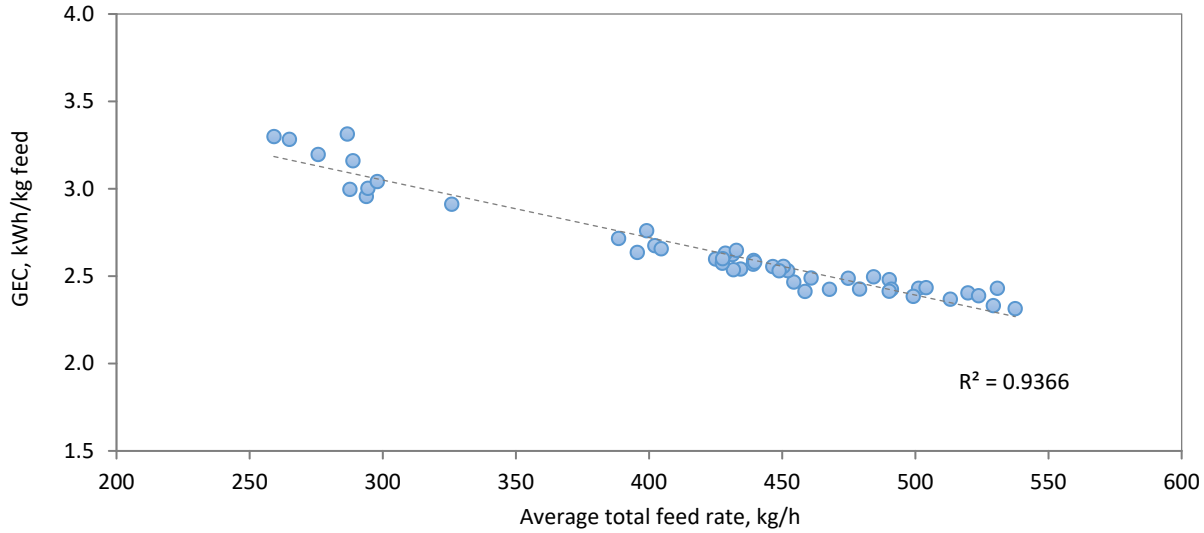

Figure 6-19: Gross energy consumption as a function of average total feed rate

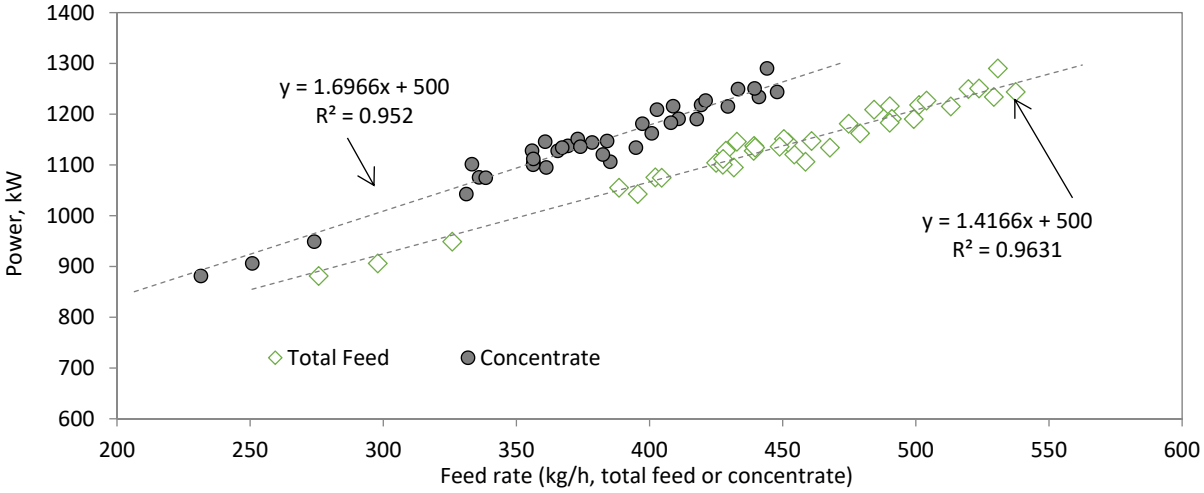

Figure 6-20: Average total power versus average feed rate

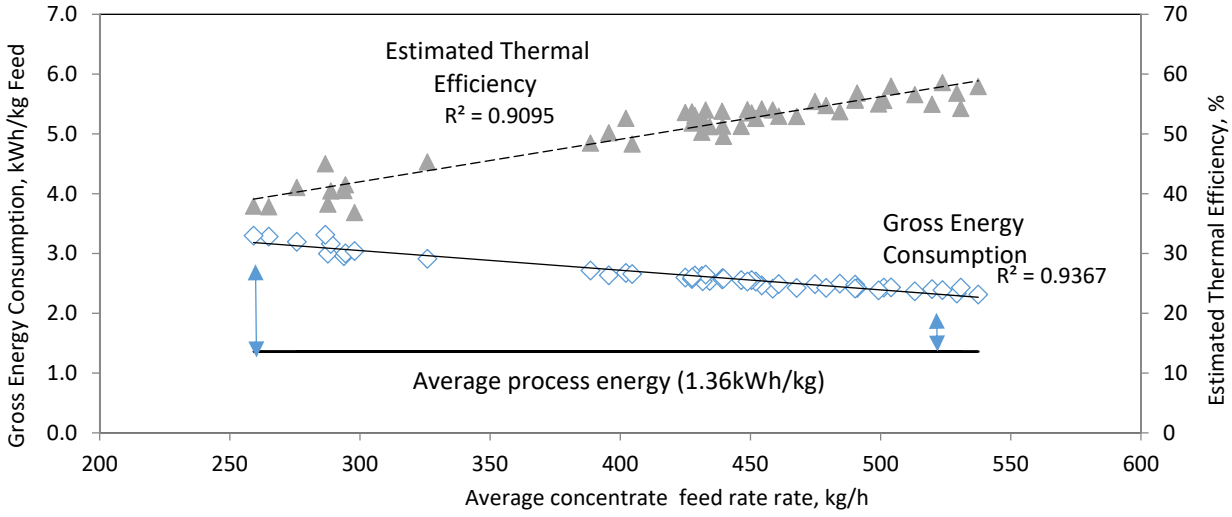

Figure 6-21: Energy consumption and thermal efficiency for the smelting campaign

6.4 ELECTRODE CONSUMPTION

Electrode consumption for the smelting campaign is calculated based on the overall electrode consumption, namely 495 kg, which is equivalent to about 5 ½ sections. The average mass of a new electrode section is about 90 kg, with a diameter of 200 mm. Pre-baked graphite electrodes are used for the pilot-scale furnace, with sections added during the operation when the length of the electrode string becomes inadequate through wear or breakage (the latter is a not a common occurrence).

Electrode consumption is tracked, as electrodes are a significant consumable cost for an electric smelting operation. The furnace is operated in open-arc mode; thus, the graphite is seldom in contact with the slag and tend to wear uniformly if the off-gas extraction is managed well. This is done to minimise unnecessary electrode wear. Natural wear of the electrode is expected, and periodically, a new section is added at the top of the string. The electrodes are procured with the necessary threaded fitting (male and female connections) to allow for additions during the operation of the furnace. The procedure to add a section includes a system of lock-outs to prevent access to the furnace roof if power is on. Sections are added manually by using a specially designed lifting mechanism that is hooked to an overhead crane. The process is part of the regular operation of any electric furnace.

Minimising downtime due to electrode additions or electrode breakages is part of the optimisation of the furnace operation. Electrode sections removed at the conclusion of the smelting campaign showed minimal wear, Figure 6-22. The overall electrode consumption for the smelting campaign was 1.4 kg graphite per MWh or 4.6 kg per ton of concentrate.

Figure 6-22: Condition of the electrode sections at the end of the project

6.5 SLAG AND ARC RESISTIVITY

The furnace operating voltage was in a range between 190 and 230V with a typical arc length between 10 and 20 cm. For this scale of operation, arc characteristic tests are typically performed by measuring the voltage with power on, and with the electrode at various known heights above the surface of the slag bath. A test may be carried out either with feed on or feed off and shows the behaviour of the voltage drop in the electric arc as a function of its length. Analysis of the data is possible in terms of the Bowman empirical model of the electrical behaviour of the arc (Reynolds & Jones, 2004).

Before commencement of the tests, the level of the bath was determined (the touchdown position or zero position). This position was established by lowering the electrode until physical contact was made between the electrode tip and the molten bath surface. The point of contact was confirmed visually. For the duration of the test, the furnace was operated at a constant current; as close as possible to the average operating current.

Slag resistivity measurements are conducted by lowering the graphite electrode into the slag bath, in increments of about 2.5cm, until a total depth of 30cm is reached, with a 30-second holding time at each position to allow the current and voltage to stabilise. The electrode was then raised in a similar fashion until it reached the original touchdown point (bath level). For the arc resistivity measurements, the electrode is raised above the molten slag bath, also by incrementally moving the hoist up by about 2.5cm, until a total height of about 30cm above the touchdown position was reached, with a 30-second holding time at each position. The electrode was then lowered in a similar fashion until it reached the touchdown point again. The shape and diameter of the electrode were evaluated post-campaign and the assumption for electrode diameter and shape is based on this evaluation.

Three tests were conducted during the campaign, two tests during batch 52 and one test during batch 54. The slag temperature before the tests was about 1790°C. The tests were therefore conducted at 5 kA. Table 6-15 summarises the results as estimated by using the measurements from the test data. Table 6-14 summarises the operating conditions and slag composition of the batches during which the tests were conducted as slag resistivity is a function of both temperature and composition.

Table 6-14: Operating conditions for the slag and arc characteristic tests

Batch No.	Test 1 Batch 52 (halfway through batch)	Test 2 Batch 52 (end of the batch)	Test 3 Batch 54 (halfway through batch)
Power target, kW	1300	1300	1300
Current Target, kA	5	5	5
Voltage target, V	260	260	260
Bath depth, mm	470	560	520
Mass % TiO_2 in slag	90.9	92.0	91.9
Mass % FeO in slag	1.9	1.6	1.5

Table 6-15: Summary of slag and arc characteristic results

Test No.	Batch No.	Slag resistivity (Ω.cm)	Arc resistivity (Ω.cm)	Slag Temperature (°C)
1	52 (halfway)	0.159	0.0181	1796
2	52 (end of batch)	0.165	0.0214	1790
3	54 (halfway)	0.171	0.0203	1784

The slag dip test results confirm that high-titania slags are very conductive, typically slag resistivity would be expected to be approximately 0.01 ohm.cm for high-titania slags. The slag resistivity results for the tests varied between 0.1 to 0.2 ohm.cm, which are at the very limits of the measurement technique. The high conductivity of high-titania slags means that the slag resistivity value is in principle for academic interest as it is not needed for the electrical design and scale-up for this regime. The arc resistivity results agreed well with typical values measured for this type of process, namely typical values used for CO atmosphere processes, namely, 0.0175 ohm.cm (Reynolds & Jones, 2004). While this measurement technique provides reasonable reference information, the method is prone to variability. The mere fact that a test is conducted causes an imbalance in temperature and slag condition, which may alter the outcome if significant. It is thus prudent to repeat the test, but this is not always practical.

6.6 MODELLING OF THE TEST RESULTS

Two sub-periods were identified for assessing the process by using (and updating) the semi-empirical models utilised for the preliminary mass and energy balance evaluations, completed prior to the smelting test as part of the preparation and planning for the test. The deportment correlations assumed for the preliminary study was evaluated in the context of the pilot-plant results and either applied directly or modified if the pilot results deviated substantially. A steady-state Pyrosim™ model was used to plan the pilot study, mainly to estimate raw material requirements and to estimate a starting point for energy requirement. It is useful to validate the steady-state model with the data collected from the pilot test, which then allows for additional refinement of the test results, or allows for assessing scenarios not tested during the experimental programme. Typically, limited time and material are available, and the test programme usually only allows for minimal variation of test parameters as it takes time to achieve stability or pseudo-steady state.

6.6.1 General description of the model

A general empirical model forms part of the Pyrosim software package, Mintek's in-house developed modelling software (Jones, 1987). The empirical model complements the existing predictive model, which is based on a multi-component multiphase equilibrium. The general empirical model allows the user to specify parameters for the process being modelled. The remaining process variables are then calculated from a set of simultaneous linear equations, and an energy balance can then calculated. Both the empirical and equilibrium Pyrosim model was used in the current work. The empirical model was used to estimate the mass and energy balance scenarios evaluated in the context of the test results. The equilibrium model was initially used to develop correlations for various deportment ratios that would be specified in the empirical model (Deneys & la Grange, 2001; Jones, 1987, 2011).

In the case of the empirical model, the number of variables to be calculated in a system is equal to the total number of chemical species in each phase, for example, in a system comprising five gas species, thirty species in the slag stream, and fifteen species in the metal stream, the number of variables to be calculated would be fifty. There are some built-in constraints on the system that result from the elemental mass balances. The number of constraints is equal to the number of elements present in the system. This means that the number of variables that are free to be specified is equal to the total number of species present minus the number of elements present. The specifications allowed by the program are of two types: namely ratios between pairs of species or percentages of species in a particular stream. A value can be specified for the mass ratio or molar ratio of any species in any stream to any other species in any other stream. For example, the molar ratio between CO and CO_2 in the gas can be specified, as can the mass ratio between Fe in the slag and Fe in the metal, or the mass ratio between TiO_2 in the slag and Ti in the metal or similarly the mass percentage of any species in any stream. For example, the content of C or Si in the metal can be specified (Deneys & la Grange, 2001; Jones, 1987, 2011).

Two scenarios were modelled, based campaign results. Two sets of data, namely sequential batches, identified as sufficiently stable and not severely affected by inventory effects, were selected to validate the models. The elemental balances for the two sub-periods are included for reference in Appendix F, the batch ranges and slag grades are as follows:

- Batch 27-35 – TiO_2 in slag ~ 87% - Scenario A
- Batch 48-53 – TiO_2 in slag ~ 91% - Scenario B

The overall results, for the two periods, are presented in Table 6-17 and Table 6-18, identified as the actual results in the first column of the tables. The results from these two periods were used to validate the model.

6.6.2 Model assumptions and definitions

The Ti^{3+} content of the slag was estimated previously based on the curve fit applied to the Desrosiers et al. (1980) – Equation 5. For purposes of the model, Ti^{3+} is assumed to be in the form of Ti_3O_5, thus two moles of Ti^{3+} combine with one mole of Ti^{4+} and by difference, the remainder is expressed as TiO_2. The composition of the concentrate, as used in the modelling, is summarised in Table 6-16.

Table 6-16: Summary of compositions assumed for the models, mass %

	Titaniferous concentrate	**Anthracite**
$H_2O^{\#}$	-	1.68
$LOI^{\$}$	0.50	-
C	0.02	-
Fixed C	-	79.0
Volatile	-	10.7
Ash	-	8.62
TiO_2	14.15	0.28
FeO	17.37	7.09
Fe_3O_4	20.14	-
Fe_2O_3	-	-
$FeTiO_3$	38.66	-
SiO_2	1.06	0.35
Al_2O_3	1.23	0.09
MgO	0.68	0.14
CaO	0.03	0.30
MnO	0.49	-
V_2O_5	0.48	-
Cr_2O_3	0.01	-
P_2O_5	0.072	-
K_2O	0.01	-
ZrO_2	0.25	
Total	95.22	99.63
Unaccounted	4.78	0.37

($^{\$}$) LOI refers to chemically bound water only (approximately 0.5%) – determined in an argon atmosphere
($^{\#}$) free moisture is excluded from the concentrate assay

It should be noted from the analyses that the iron and titanium contents have been re-proportioned to $FeTiO_3$ and $FeO.Fe_2O_3$ and TiO_2. This was done to more closely approximate the mineralogical and thereby obtain a more thermodynamically correct prediction of the reaction energy required. An average ratio of Fe^{3+}/Fe^{2+} = 0.766 was used to calculate the distribution. The re-calculated composition is summarised together with the anthracite composition as utilised for the model is presented in Table 6-16.

Water contributes significantly to energy consumption in a smelting process due to the unique properties of water. The average measured energy consumption for the pilot-plant test was higher than expected, and this typically indicates the presence of unwanted water. Due to a high surface area to weight ratio, finely sized ore has a high free moisture capacity, while not appearing wet. Water may be adsorbed at particle surfaces and as capillary-condensed water in small pores. It is also notoriously difficult to accurately assess the exact moisture content of a bulk sample of finely sized ore.

The average moisture content of the ore processed during the campaign was therefore evaluated indirectly as widely different values were measured via spot checks. The model was first assessed assuming there is no moisture in the concentrate and comparing the resulting energy requirement with the actual requirement achieved. To illustrate the contribution of water to energy, consider the following equation: $2H_2O(l) = 2H_2(g) + O_2(g)$. The equation represents water fed at 25°C and converted to hydrogen and oxygen in the reaction zone (at 1450°C). For these conditions, the energy required for this step is 5.45 kWh/kg H_2O. Assuming a 5% moisture content, this equates to about 0.27 kWh/kg of concentrate. It is thus plausible that the discrepancy in energy consumption may be explained by the contribution of water and the subsequent chemical reaction. It is also likely that some of the water is converted from liquid water to steam, which could account for about 1.56 kWh/kg H_2O. In an industrial application, moisture is not expected to be an

issue, as the concentrate is likely to be either flash-dried, preheated or prereduced prior to smelting. It is, however, worth noting the potential impact. Hydrogen also contributes significantly to the gas volume at these elevated temperatures and can impede the efficiency of off-gas handling systems.

The mass and energy balance calculated via the model was used to evaluate energy consumption measured during the test, taking into account the effect of water, and in addition to evaluate the effect of refractory pick-up on the slag composition.

Following the evaluation of the two pilot-plant conditions, the model was then applied to calculate the energy required for the process in the absence of moisture and for a slag product without refractory pick-up (steady-state industrial operation). In addition, scenarios with preheated feed (650°C and 850°C) and prereduced feed (mild prereduction of the concentrate) were also evaluated to illustrate the possible energy saving relative to a baseline scenario. Summary mass and energy balance flow sheets are presented as the final outcome of the section.

In order to predict a mass and energy balance for the smelting of TiO_2 concentrate to produce high-titania slag, the following assumptions apply to all the case studies:

- Furnace off-gas is assumed to consist of CO, CO_2, O_2, H_2 and N_2
- The following fumed components SiO, Mg and Mn are recovered as furnace dust as siO_2, MgO and MnO.
- Furnace operating temperature is based on simplistic FeO-TiO_2 binary liquidus data and the operating temperatures measured from the testwork campaign.
- Metal tapping temperature is 50°C below the operating temperature.
- Off-gas temperature assumed to be 200°C lower than the operating temperature.

6.6.3 Modelling validation and results

The mass and energy balance results for **Scenario A** are summarised in Table 6-17 (actual data and modelled):

- Actual results are presented in the first column (grey column). The results are representative of the general conditions targeted for Period B, with the batches included selected to ensure inventory effects are minimal for mass balance purposes.
- Model 1 simulated the pilot plant conditions represented by the actual results. The average metallurgical for Batch 27-35, including estimated MgO pick-up (based on the mass balance for the period, Appendix F) and the average rate of by-pass, namely 5% concentrate by-passing to the off-gas dust were included in the model. Deportment of Mg, Si and Mn to the off-gas adjusted based on average dust composition for the pilot test and expected equilibrium and experimental correlations.
- Model 2: Same as (Model 1) but adjusted to exclude Mg pick-up in the slag
- Model 3: Same as (Model 1) but with 3% feed-pass (reduced from 5%)

Three additional models were evaluated (using Model 3):

- Model 3.1: Preheated feed to the furnace at 650°C
- Model 3.2: Preheated feed to the furnace at 850°C
- Model 3.3: Prereduced concentrate fed to the furnace at 650°C, 25% Fe metallization assumed.

The mass and energy balance results for **Scenario B** are summarised in Table 6-18, based on the identical framework applied for Scenario A. The results from Model 4, 5 and 6 are presented in Table 6-18, together with the actual pilot results included in the first column for reference. Additional models were evaluated (based on Model 6), namely Model 6.1 and 6.2, preheated feed at 650°C and 850°C, respectively. This scenario is included to evaluate the impact relative to a more likely scenario, as embodied by Scenario A.

The main objective of modelling the various scenarios was to compare the test results with idealised smelting conditions. In the context of an industrial smelter these idealised conditions included, smelting dry feed, adjusted refractory wear and dust losses, the last two items being exaggerated at the pilot scale, and also the effect of hot feed on the energy requirement. It was possible to simulate the actual results from the pilot test with remarkable accuracy. The models confirmed the assertion that the moisture in the feed contributed to the energy consumption figures during the pilot plant.

In Table 6-17 and Table 6-18, the actual pilot plant results for the relevant period is presented in the first column and highlighted with a grey background. The model validation is presented in the second column, Model 1 and Model 4 respectively. Finally, two optimise scenarios are presented to demonstrate that the metallurgy is relatively unaffected due to the moisture.

Table 6-17: Summary of modelling results compared with pilot-plant results - Scenario A

Description	**Actual pilot-plant results**	Model 1	Model 2	Model 3
	Average results from batch 27-35	Simulated pilot conditions	Pilot conditions, dry feed & no MgO	3% by-pass, dry feed, no MgO
Degree of feed by-pass	5% by-pass	5% by-pass	5% by-pass	3% by-pass
Fe recovery, as metal	92.6%	91.9%	92.0%	93.8%
Ti recovery, as slag	92.7%	94.9%	94.9%	96.9%
Fe extraction	97.1%	98.5%	98.5%	98.5%
Ti_{Tot} as TiO_2 in feed	34.5%	34.5%	34.5%	34.5%
Ti_{Tot} as TiO_2 in slag	86.9%	87.0%	90.0%	90.0%
Dust make , % of conc.	6.2%	5.7%	**6.0%**	**3.9%**
Input (kg)				
Concentrate	1000.0	1000.0	1000.0	1000.0
Anthracite	200.7	200.0	200.0	200.0
Moisture	80.0	80	**0**	**0**
Estimated MgO pick-up	9.6	13.0	**0**	**0**
Excess Carbon (kg C)	-	34.5	30.2	27.6
SER, kWh/kg conc.				
Dry concentrate	-	1.150	1.130	1.140
5% moisture	-	1.423	1.403	1.413
8% moisture	1.630[$]	1.586	1.566	1.576
Output (kg)				
Slag	338.2	377.0	364.3	371.9
Metal	407.9	413.8	413.9	422.4
Dust	62.3	57.3	59.9	39.4
Gas	-	289.8	291.1	298.2
Slag-to-metal ratio	0.829	0.911	0.880	0.881
Slag mass %				
FeO	4.42	4.69	4.83	4.83
Al_2O_3	3.62	3.10	3.21	3.21
CaO	0.18	0.23	0.24	0.24
Cr_2O_3	0.13	0.02	0.02	0.02
MgO	4.24	4.12	1.48	1.48
MnO	1.18	1.01	1.04	1.04
P_2O_5	0.050	0.119	0.123	0.123
SiO_2	2.51	2.21	2.22	2.22
Ti_3O_5	47.44	47.60	58.01	58.06
TiO_2	36.05	35.97	27.85	27.82
V_2O_5	1.093	0.963	0.995	0.995
Metal, mass %				
Fe	96.01	96.47	96.48	96.48
C	3.04	3.04	3.04	3.04
Cr	0.03	0.005	0.005	0.005
Mn	0.08	0.07	0.07	0.07
Si	0.11	0.10	0.10	0.10
Ti	0.06	0.06	0.06	0.06
V	0.35	0.21	0.21	0.21
Dust*, mass %				
FeO	45.10	47.74	49.90	47.79
TiO_2	35.80	30.11	31.47	30.04
SiO_2	6.21	4.19	4.28	6.29
Al_2O_3	1.79	1.07	1.12	1.07
MgO	4.12	7.37	3.08	4.59
CaO	0.28	0.04	0.04	0.04
MnO	1.57	1.24	1.30	1.81
V_2O_5	0.52	0.42	0.44	0.42
Cr_2O_3	0.30	0.009	0.009	0.009
C	1.92	2.31	2.61	2.39

(*) Pilot-plant dust composition reported as the campaign average; ($) Average energy consumption for the entire campaign

Table 6-18: Summary of modelling results compared with pilot-plant results - Scenario B

Description	**Actual pilot-plant results**	Model 4	Model 5	Model 6
	Average results for batch 48-53	Simulated pilot conditions	Pilot conditions, dry feed & no MgO	3% by-pass, dry feed, no MgO
Degree of feed by-pass	5% by-pass	5% by-pass	5% by-pass	3% by-pass
Fe recovery, as metal	95.4%	93.7%	93.7%	95.6%
Ti recovery, as slag	94.0%	94.8%	94.8%	96.8%
Fe extraction	98.8%	98.5%	98.5%	98.5%
Ti_{Tot} as TiO_2 in feed	34.5%	34.5%	34.5%	34.5%
Ti_{Tot} as TiO_2 in slag	91.1%	93.9%	95.4%	95.4%
Dust make , % of conc.	5.0%	5.9%	5.7%	3.7%
Input (kg)	1000.0	1000.0	1000.0	1000.0
Concentrate	1000.0	1000.0	1000.0	1000.0
Anthracite	196.2	200.0	200.0	200.0
Moisture	50.0	50.0	-	-
Estimated MgO pick-up	3.4	5.0	0	0
Excess Carbon (kg C)	-	27.4	26.5	23.8
SER, kWh/kg conc.				
Dry concentrate	-	1.170	1.170	1.170
5% moisture	-	1.443	1.443	1.443
8% moisture	1.580[$]	1.606	1.606	1.606
Output (kg)				
Slag	327.0	348.9	343.5	350.7
Metal	463.1	422.4	422.4	431.0
Dust	50.3	58.6	56.9	36.5
Gas	-	307.2	310.1	317.3
Slag-to-metal ratio	0.706	0.826	0.813	0.814
Slag mass %				
FeO	2.16	2.29	2.32	2.32
Al_2O_3	3.53	3.35	3.40	3.40
CaO	0.16	0.25	0.26	0.25
Cr_2O_3	0.10	0.02	0.02	0.02
MgO	2.79	2.47	1.45	1.45
MnO	0.81	0.86	0.87	0.87
P_2O_5	0.030	0.141	0.143	0.143
SiO_2	1.77	1.71	1.72	1.72
Ti_3O_5	62.55	75.72	83.75	83.81
TiO_2	24.04	12.76	5.63	5.57
V_2O_5	0.600	0.322	0.327	0.327
Metal, mass %				
Fe	96.22	96.31	96.31	96.31
C	2.72	2.72	2.72	2.72
Cr	0.03	0.003	0.003	0.003
Mn	0.10	0.12	0.12	0.12
Si	0.25	0.25	0.24	0.24
Ti	0.10	0.10	0.10	0.10
V	0.45	0.48	0.48	0.48
Dust*, mass %				
FeO	45.10	46.73	48.12	45.08
TiO_2	35.80	29.47	30.35	28.34
SiO_2	6.21	5.51	5.62	8.31
Al_2O_3	1.79	1.05	1.08	1.01
MgO	4.12	5.73	3.68	5.44
CaO	0.28	0.04	0.04	0.04
MnO	1.57	2.15	2.21	3.24
V_2O_5	0.52	0.41	0.42	0.39
Cr_2O_3	0.30	0.009	0.009	0.008
C	1.92	3.48	2.90	2.85

(*) Pilot-plant dust composition reported as the campaign average; ($) Average energy consumption for the entire campaign

Table 6-19 and Table 6-20 summarise the energy consumption relative to Model 3 (Scenario A) and Model 6 (Scenario B) for a number of sub-conditions. The energy assessment shows the impact of preheating and prereduction, relative to the respective baseline condition.

The primary impact of free moisture, preheating, and prereduction is on energy consumption with the metallurgical outcomes, therefore relatively unaffected within the boundaries of the model variables. The various outcomes summarised in the two tables are graphically presented in Figure 6-23. The evaluation shows that for feed with 8% moisture excess energy consumption of 38% is expected, while 31% less energy will be consumed if the feed is fed at 650°C with 25% Fe metallization (a relatively low degree of metallization).

Table 6-19: Energy requirement evaluation for Scenario A

Scenario A	**Energy Requirement (model)**			Difference
	kWh/kg concentrate	kWh/kg slag	kWh/kg metal	Relative to Model 3, dry, 25°C feed
25% Fe metallization, 650°C	0.79	2.12	1.86	31.0%
Preheated Feed, 850°C	0.94	2.53	2.23	17.5%
Preheated Feed, 650°C	0.99	2.66	2.34	13.2%
Model 3[#], 25°C Dry feed	**1.14**	**3.07**	**2.70**	**0.0%**
Model 3, 25°C, 5% moisture	1.41	3.80	3.34	-23.9%
Model 3, 25°C, 8% moisture	1.58	4.24	3.73	-38.3%

([#]) Baseline flowsheet (Model 3) assumes 3% feed loss to off-gas dust and minimal refractory pick-up, pilot-plant concentrate and anthracite composition, specific energy reported – moisture and feed temperature is adjusted from this baseline

Table 6-20: Energy requirement evaluation for Scenario B

Scenario B	**Energy Requirement (model)**			Difference
	kWh/kg concentrate	kWh/kg slag	kWh/kg metal	Relative to Model 6, dry, 25°C feed
Preheated Feed, 850°C	0.98	2.79	2.27	16.4%
Preheated Feed, 650°C	1.03	2.94	2.39	12.0%
Model 6[#], 25°C, Dry feed	**1.17**	**3.34**	**2.71**	**0.0%**
Model 6, 25°C, 5% moisture	1.44	4.11	3.35	-23.3%
Model 6, 25°C, 8% moisture	1.61	4.58	3.73	-37.3%

([#]) Baseline flowsheet (Model 6) assumes 3% feed loss to off-gas dust and minimal refractory pick-up, pilot-plant concentrate and anthracite composition, specific energy reported – moisture and feed temperature is adjusted from this baseline

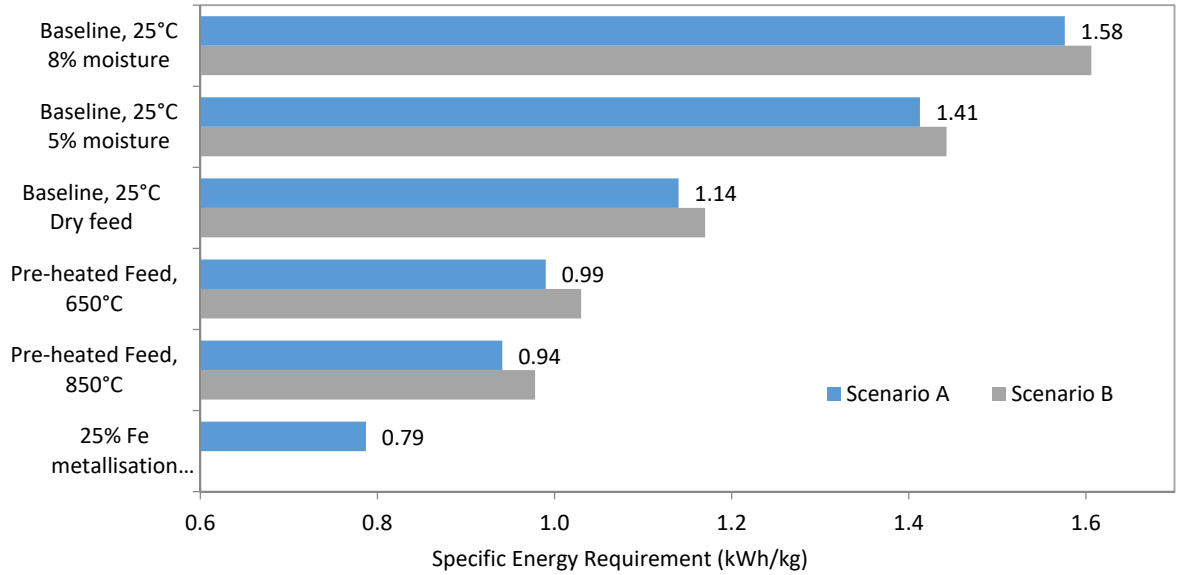

Figure 6-23: Summary of energy requirement evaluation for Scenario A and B

Four Pyrosim output reports, two per scenario, are included in Appendix G for reference. Numerous scenarios were assessed to establish the best outcomes. The review confirms that significant electrical energy savings can be achieved through feeding hot, prereduced feed, instead of cold concentrate.

6.6.4 Operational assessment

The pilot-plant smelting results were simulated using Mintek's in-house developed semi-empirical modelling software, Pyrosim, and methods developed by the author to specify mass ratio relationships for components in this current system.

Energy consumption for the selected baseline condition was shown to be very sensitive to (a) moisture content, (b) feed temperature and (c) degree of prereduction. This is not unexpected, especially for a process with relatively high operating temperatures and a high degree of reduction.

While the energy consumption measurement is a fairly accurate measurement, the average specific energy requirement (per kg concentrate) reflects the process energy consumption of the material 'as processed'. Energy requirement for smelting ilmenite (from beach sands) measured at similar scale (unpublished internal Mintek reports), is about 0.95 to 1.05 kWh/kg ilmenite which agrees well with the re-calculated energy requirement from the models, namely 1.13 to 1.15 kWh/kg concentrate. As the material is a low-grade ore, the higher energy requirement is not unexpected. The theoretical specific energy requirement published for the QIT process (production of Sorel slag) is 0.903 kWh/kg of ore (Guéguin & Cardarelli, 2007) to produce 80% TiO_2 and 9.7% FeO in the slag, 100% dry ore, also supports the recalculated SER for the process.

The variable and higher than the expected moisture content of the concentrate inflated the energy consumption during the pilot test, while the data is very accurate, the effect of moisture is not a characteristic of the process as moisture is minimised in any smelting process due to the unique properties of water (high heat capacity).

Although the test successfully demonstrated that the process was operable, even at low levels of FeO, this may not necessarily be a suitable operating regime due to the increase in unwanted side reactions, higher energy and reductant consumption, viscosity of the slag, and potential refractory wear; outcomes that follow when operating under highly reducing conditions. Despite the high degree of reduction achieved, especially during the latter part of the test, the impact of side reactions was not as severe as expected, but additional work would be required to evaluate the feasibility of such an operating regime as this period was relatively short. While the grade of the slag would be higher than 90% titania, the potential trade-offs that may be involved for downstream processing, the energy impact, and furnace operability may not justify this option.

Operational issues are challenging to quantify, and while the slag behaviours are similar there appear to be some operational benefits derived from the impurities, acting as in situ fluxes, thus allowing the lower-grade titanomagnetite operation to operate with lower FeO levels, if compared to the ilmenite smelters (Burger *et al.*, 2009; Gous, 2006).

Refractory wear, although well-managed within the constraints of the pilot-plant system, contributed to slag contamination (dilution) and the models were used to calculate a slag composition for the baseline condition which minimised the refractory contamination (as MgO) to represent a more realistic industrial equivalent.

The following table summarises the two compositions, together with the outcome of the modelling work. The mass balance for the two periods shows that refractory pick-up was about 9.6 kg MgO/t of concentrate for the period batch 27-35 and 3.4 kg MgO/t of concentrate for the period batch 48-53.

Table 6-21: Summary of slag compositions (actual and models) showing the effect of MgO contamination

mass %	Actual slag Batch 27-35	Model slag Model 2 [$]	Actual slag Batch 48-53	Model slag Model 5 [$]
FeO	4.42	4.83	2.16	2.32
Al_2O_3	3.62	3.21	3.53	3.40
CaO	0.18	0.24	0.16	0.26
Cr_2O_3	0.13	0.02	0.10	0.02
MgO	4.24	1.48	2.79	1.45
MnO	1.18	1.04	0.81	0.87
SiO_2	2.51	2.22	1.77	1.72
TiO_2[#]	86.9	90.0	91.1	95.4
V_2O_5	1.09	1.00	0.60	0.33

([#]) Total Ti expressed as TiO_2; ([$]) 5% feed by-pass assumed for both models; approximately the same dust make as the pilot-plant test

The modelled flowsheet matched the actual pilot results very well, including product compositions and energy requirements. The model can be used to assess various optimised scenarios for this specific concentrate and may be a useful tool for similar materials. For both scenarios, the additional models could be applied to evaluate the idealised operating conditions. The models confirmed the impact free moisture has on the overall energy consumption and as expected do not participate significantly in the primary process.

A model is a useful tool to evaluate mass and energy balance effects, as well as to consider the impact of refractory wear on the slag. The model was validated thoroughly with the pilot-plant results. The model and the methodology can be used to simulate a number of alternative scenarios, such as feed composition variation, optimising the slag grade, and so forth. The metallurgical behaviour of minor elements is also frequently not predicted well through simple equilibrium models. The deportment of these minor elements can be measured at pilot-scale, and deportment ratios can be developed for an empirical model.

The energy evaluation supports the premise that it is crucial for the process flowsheet to include a prereduction stage prior to smelting to minimise the electrical energy consumption. As fluxless smelting of titaniferous magnetite will always be a hybrid process (both iron and titania slag), economic viability will be strongly dependent on optimal prereduction. Most iron is produced in blast furnaces; thus, the cost of energy to produce iron via electric smelting needs to be considered carefully.

The benefit of the pilot-scale test is the extensive operability assessment that is achieved due to the scale and duration of the test, combined with the ability to validate this type of model. Most operability issues are practical and experiential.

6.7 Quality Considerations for the Slag

The phase chemical investigation of the slag produced during the pilot test, reported previously, was undertaken to determine whether the phase chemistry of the slag differs significantly from that of typical high-titania furnace slags produced from ilmenite feedstocks. The results show that the slag has the same appearance as typical ilmenite furnace slag. It is also accepted that the furnace slag cannot be upgraded in the smelting step beyond removing the iron, the final product grade (%TiO_2) is thus determined by the grade of the ore, and the contribution of contaminants from the reductant and potential refractory wear (which is minimised during normal operation). Ideally, pre-smelting upgrading potential would be beneficial to the process, but titaniferous magnetite is known for not being amenable to conventional upgrading methods (via physical means). Some physical upgrading potential can be leveraged, but this would need to be balanced in the context of the gains that could be made in terms of the grade of the product.

Contamination of the feedstock in the smelter by ash from the reductant could, for example, easily overshadow any minor upgrades, and efforts may be misplaced if not assessed holistically. The Sorel process includes various upgrading stages prior to smelting and would be an excellent example of appropriate effort. A roasting stage (thermal treatment of the ore after physical upgrading), prior to smelting, achieves an upgrade from 34% to 37% TiO_2 and lowering the total SiO_2 and Al_2O_3 content (Guéguin & Cardarelli, 2007). The QIT plant (Canada) uses a proprietary process to reduce the SiO_2, MgO and CaO contents of the standard furnace slag for the production of upgraded slag (UGS). This is done by grinding and sizing the slag, followed by roasting to produce heat-treated slag (HTS) to aid the subsequent leaching of the impurities. Leaching is carried out with hydrochloric acid and results in a product containing 92 to 95% TiO_2 (Gilman & Taylor, 2001). This upgraded slag is used as a feedstock to the chloride pigment process. Removal of the MgO and CaO is critical to creating a product suitable for use in the chloride pigment plants.

The pilot test results demonstrate that it is feasible to process low-grade titaniferous ore in a DC open-arc smelter to produce a high-grade slag. The concentrate tested is not regarded as typical ilmenite. The total TiO_2 content is below 38% and contains the following mineral associations, namely ilmenite, magnetite and titaniferous magnetite. This typical association would limit the upgrading potential via traditional physical separation techniques, but there are indications that a Sorel-type approach may be beneficial.

Typical titaniferous magnetite deposits contain from 1.5% to 38% TiO_2. Titanomagnetite ores are currently processed as iron ore, and many of these have an association with vanadium. It could at best, thus be described as low-grade titaniferous feedstock.

The feed from the Highveld Steel plant, titaniferous magnetite from the Bushveld Complex, illustrates this point well, with TiO_2 content ranging from about 12 to 20%. It is worth noting that the titaniferous magnetite feed for the Highveld process would not have been optimised for fluxless smelting; thus, there is likely some scope to improve the Ti-grade.

In Table 6-22 compositions, including the referenced Highveld Steel concentrate and concentrate from the Canadian QIT operation in Sorel, are presented with three examples of titaniferous magnetite concentrates originating from

different areas in South Africa ('Other Concentrate' A to C). There is most likely some scope to upgrade South African titaniferous magnetite, but how this can be achieved and what the objective of the upgrade should be is complicated due to the nature of these ores. An integrated study, to assess the various sensitivities would be required, but from a smelting perspective, the grade of the feed determines the quality of the slag. The grade is, however, not just a function of the TiO_2 content but is better represented via a ratio. The ratio of total TiO_2-to-impurities (total Ti expressed as TiO_2) is indicative of the upgrading potential via smelting – the potential is independent of the Fe-grade of the ore. The residual Fe in the slag is an operational target which impacts Fe recovery and potentially the quality of the metal product but can be independently manipulated by changing the reductant addition.

Table 6-22: Composition of various titaniferous concentrates, including the feed from the current pilot test, Highveld Steel and Canadian rock ilmenite concentrate, mass %

Description	TiO_2	FeO	MgO	SiO_2	Al_2O_3	V_2O_5	CaO	MnO	Cr_2O_3	ratio
Canadian hard rock concentrate $	37.6	60.1	2.70	0.80	0.80	0.30	0.20	0.10	0.10	7.5
Highveld Steel concentrate *	12.70	70.53	1.60	2.00	4.80	1.65	0.10	0.30	0.40	1.2
Other concentrate A	15.54	62.47	0.71	5.77	3.66	1.12	0.08	0.24	0.01	1.3
Other concentrate B	19.65	66.15	0.58	0.57	2.12	0.25	0.20	0.41	0.08	4.7
Other concentrate C	17.08	72.82	0.67	0.99	0.88	0.74	0.21	0.34	0.01	4.4
Concentrate from current study	34.12	55.15	0.68	1.06	1.23	0.48	0.03	0.49	0.01	8.6

(*) (Steinberg *et al.*, 2011); ($) (Guéguin & Cardarelli, 2007) (Other concentrates A, B and C) Concentrate compositions for three samples from different locations in the Bushveld Complex (unpublished data, 2006, 2013, 2014); ratio = TiO_2-to-total slag impurities

The following approach illustrates the upgrading potential for a range of titaniferous magnetite and titaniferous concentrates. By simplifying, and normalising the slag components into TiO_2, FeO and the sum of the impurities (slag formers), it becomes a simple calculation to estimate the slag composition ('via an upgrade factor'). Mass ratios can be used to compare different concentrates, without the effect of iron dilution. This allows for a balanced comparison of the various low-grade options. The comparisons are summarised Table 6-23.

A typical ilmenite smelter would operate with a higher residual iron concentration in the slag, but this is a function of the purity of the feedstock (low levels of MgO, Al_2O_3, and SiO_2). Low-grade titaniferous ores can operate with 1 to 2% FeO, due to the higher proportion of gangue components. The FeO acts as a slag modifier as it improves the slag viscosity, for example. The hypothetical three-component slags assume 5% residual FeO for purposes of the comparison summarised in Table 6-23.

Table 6-23: Normalised compositions of low-grade titaniferous concentrate, mass %

Description	Highveld Concentrate	Other Concentrate A	Other Concentrate B	Other Concentrate C	Concentrate - current study	Sorel Concentrate
Process	Ironmaking industrial	Examples of ore from potential deposits in South Africa			Current study	Industry pigment slag
Normalised three-component concentrate composition, mass %						
TiO_2 (total Ti)	13.5	17.3	18.2	21.8	36.6	36.6
Σ(Impurities)	11.5	12.9	4.1	4.7	4.3	4.9
FeO (total Fe)	75.0	69.8	77.7	73.5	59.2	58.5
Total	100	100	100	100	100	100
Concentrate ratios						
TiO_2/Σ(Impurities)	1.2	1.3	4.5	4.7	8.6	7.5
Fe/Ti	7.2	5.2	5.5	4.4	2.1	2.1
Normalised hypothetical three-component slag composition, mass %						
Residual FeO[b]	**5.0**	**5.0**	**5.0**	**5.0**	**5.0**	9.7[a]
Total impurities	43.8	40.6	17.4	16.8	9.9	10.1
TiO_2-grade	51.2	54.4	77.6	78.2	85.1	76.2

([a]) Residual FeO in accordance with published data; ([b]) 5% FeO assumed for other scenarios based on pilot results

The hypothetical slag composition for each of the concentrates (based on the three components defined earlier) illustrates the difference between the concentrates well. It is, however, not just the titania-grade that is of importance, but the content and composition of the impurities. Some impurities are less desirable than others, due to the impact of these impurities on the downstream process. Generally, impurities can potentially result in excessive and hazardous wastes.

Based on the assessment presented in Table 6-23, titanomagnetite concentrates can be grouped into three categories, namely low, medium and high-grade. The ratio that was found to be most useful is a mass ratio of titania and the total impurities in the concentrate; the Fe-to-Ti ratio is a good indication of the iron grade. As iron is removed from the slag as part of the upgrading process, it is not an indication of the grade of the slag. A titania-to-impurity ratio of at least 4.5 (medium grade), and ideally closer to 8 (high grade), will produce slags similar to that of existing ilmenite smelters, especially the hard rock ilmenite smelters. This is a useful target to use to assess the quality of the ore (physical or thermal upgrading can be used). Attempting to optimise iron or titania grade may be counterproductive.

Often during physical upgrading, a number of scenarios are feasible, and to optimise the grade for the intended purpose requires the minerals processing objectives to be quite clear. In the case of titaniferous magnetite, the system is very constrained due to the nature of the ore. If the aim is to comprehensively extract all three elements with economic value, namely Fe, V and Ti, the system becomes increasingly constrained as all three elements are somewhat associated with each other. During physical upgrading, there is limited scope due to the natural mineralisation of the ores to separate out ilmenite from the magnetite. Vanadium is generally not associated with a specific mineral phase. If there is scope to concentrate the ore, increasing the titania/impurity ratio correlates with the associated increase in predicted titania-slag grade. The graph below illustrates a proposed approach to assess the quality of concentrate (via a relative grading).

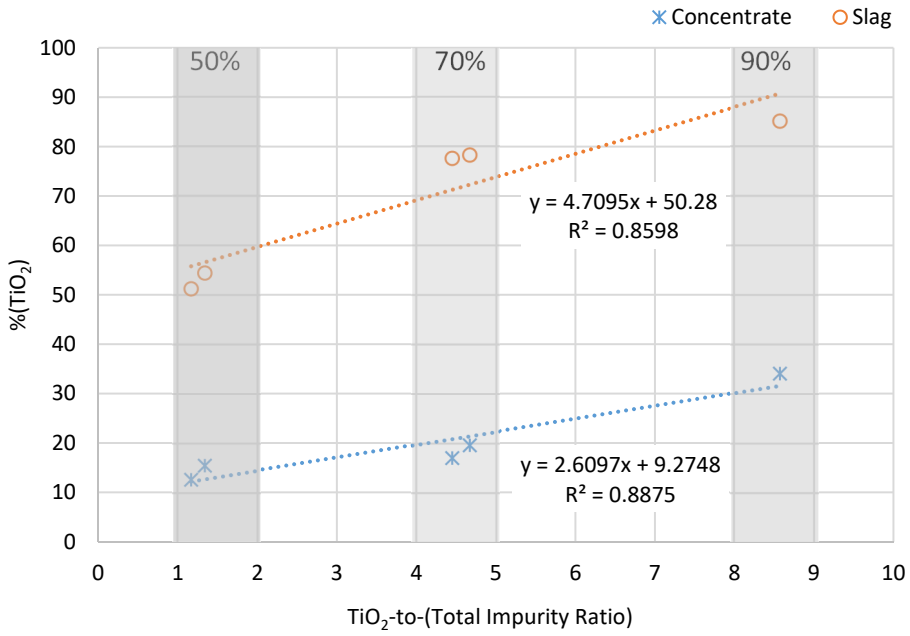

Figure 6-24: Projected slag grade based on titania-to-total impurities ratio – a guide

Typical specification for feedstocks processed via the chloride process has been evaluated by various authors (Fisher, 1997; Maharajh *et al.*, 2015; Stanaway, 1994a,b) and provide valuable insight into the impact of various impurities on the process and the product quality.

The sulfate process has the advantage of requiring lower initial capital expenditure, apart from the waste treatment steps. The main disadvantages of the sulfate process are the production of large volumes of acidic waste containing iron in solution and the associated requirements for effluent treatment facilities and waste disposal. The chloride process produces relatively low volumes of waste, mostly ferric chlorides, due to stringent requirements on impurity levels; hence this process favours higher quality feedstocks. Chlorine gas and titanium tetrachloride are very hazardous compounds to handle in a production facility. The capital costs of chloride plants can, therefore, be high due to the need for high performance, corrosion-resistant materials of construction. The process lends itself to a high degree of automation and can be scaled up significantly, which can offset the high cost of the equipment (Stanaway, 1994a,b).

Summaries of ideal compositional specifications of feedstock for the two processes are included for reference in Appendix H.

Furnaces slags compete with natural rutile, synthetic rutile, and upgraded slag as feedstock, especially to the chloride pigment process. These feedstocks contain more TiO_2 units than typical furnace slags (85-87% TiO_2). Production of a higher TiO_2 slag using a conventional smelting process, although beneficial to the chloride pigment producers, requires additional reductant, electricity, electrodes and increases the risks of operational challenges. The various gangue components and some specific minor elements influence the quality and cost of pigment production (Burger *et al.*, 2009; Moodley, Eric, Kucukkaragoz & Kale, 2012).

The need to reduce waste and operating cost, and to maintain product quality, translates to the drive by the pigment industry towards high-grade, low-impurity feedstocks. There will, therefore, always be a demand for slag producers to produce slag with higher TiO_2 content to remain competitive. It is clear that feedstock from a low-grade deposit will face stiff competition in the pigment industry. While it is technically feasible to upgrade the lower grade furnace slags directly via either the sulfate or chloride process, the availability of higher-grade (low impurity) feedstocks, make this approach not a viable tactic. For the chloride process, it is estimated that about thirteen kilograms less waste is generated for every percentage point increase in TiO_2 feedstock (Burger *et al.*, 2009). For example, a ton of 85% TiO_2 slag will generate 65 kilograms more waste when compared with a 90% TiO_2 slag. It would thus be essential to understand what market the lower grade slags will address and what alternative options may exist to upgrade the slag (similar to the UGS process, for example).

These factors translate into the need for detailed scenario analysis to evaluate what the best operating regime for titanomagnetite could be. Would it be for example be sensible to operate with low residual FeO which will maximise TiO_2-grade in the slag and maximise Fe recovery, or alternatively would it be more sensible to manipulate the slag chemistry to favour V deportment to the metal, while producing a lower-grade slag, that can be upgraded post-taphole. While there are many technically feasible options, the most economical regime will need to be selected through systematic evaluation. Titaniferous magnetite deposits are known to be widely varied in composition, which adds to the challenge of assessing the process options. It is clear that while the smelting stage is relatively simple, there remain a number of options to optimise the process flowsheet.

It is always challenging to evaluate the impact of various scenarios when some of the drivers may be detrimental to upstream processes, especially when the two operations are separate commercial entities. The value-in-use model presented by Maharajh et al. (2015) is an excellent example of the benefits of a holistic approach. Future work to construct a similar scenario model for the titanomagnetite slags would be invaluable to advance the proposed technology; especially in light of some of the insights gained about the opportunity titanomagnetite slags offer to lower the FeO content without significantly impacting the operability and/or product quality of the metal. The increased electricity costs and reductant consumption is likely to be inconsequential compared to the benefits of lower wastes generation and higher iron recovery, for example. In addition, upgrading via thermal methods, prior to smelting could enhance the ratio of Ti-to-impurities.

Table 6-24 compares the general composition of the titania slag produced from the current study with the specification for an ideal feedstock to the pigment industry; feedstock specification developed by Stanaway (1994a) and the detailed specifications are included in Appendix H as reference as it pertains to the interpretation in Table 6-24. The comparison is aimed at evaluating the potential value or benefit of the slag produced from titaniferous magnetite, in a competitive market where furnace slag is not in short supply.

Table 6-24: Evaluation of the quality of the high-titania slag produced from titaniferous magnetite ore

Aspect	Stanaway feedstock (1)	The case for titanomagnetite slag	The case against titanomagnetite slag
TiO_2	88 to 90%	Feed containing 35% TiO_2 & 5% impurities will result in slag with less than 90% TiO_2, and 2% residual FeO	Feed containing 18% TiO_2 and 10% impurities will result in slag with about 80% TiO_2 with only 2% residual FeO
Al_2O_3	< 1.50%	The titanomagnetite slag contained about 3.5% Al_2O_3, which consumes chlorine and coke and contributes to corrosion and sludge formation challenges - chloride process; addressed via UGS process.	
SiO_2	< 1.5%	Below 2% in titanomagnetite slags. UGS slags typically about 1.8% SiO_2	
MnO	< 2.0%	Typically about 1%	
MgO	< 1.0%	Titanomagnetite slags contain less MgO than Sorel slag about 3% versus 5.5%; Can be addressed via UGS process.	
CaO (2)	< 0.2%	Titanomagnetite slags contain similar levels of CaO as Sorel slag prior to upgrade (~0.5%)	
Cr_2O_3	< 0.25%	Cr_2O_3 reports preferentially to metal under greater than 90% Fe recovery conditions	
V_2O_5	< 0.60%	Note: V could be targeted during upgrading if needed, V detrimental to pigment colour.	V deportment to metal favoured for V recovery, but removal step may be required prior to pigment plant (40:60 slag: metal split is expected without fluxing).
U+Th	< 100 ppm ideally < 50 ppm	Not detected, <10 ppm in slag	
As, Sn	Minimise	Not detected	Confirmation required for Bushveld Complex
Fe	Minimise	5% FeO achieved with a minimal negative impact. Fe significant contributor to waste generation in pigment production.	
Nb_2O_5	<0.1% for sulfate process	Not detected	Confirmation required for Bushveld Complex
Size specifications and bulk density requirements particular to the chloride process not assessed.			

(1) (Stanaway, 1994a) (2) Alkali earth oxides form low-melting-point chlorides liquid at chlorination temperatures and can cause blockages and Ca prohibits crystal growth in the sulfate process.

An assessment of the impact of the various potential scenarios would be required to identify the best approach and if the technology is to be advanced. Based on the industrial operation in Canada, there is likely a practical (technical) and potential economical solution, to upgrade titanomagnetite furnace slags. The concentrate and slag produced during the pilot-plant test are similar in many aspects to Sorel slag produced at the Rio Tinto site in Canada. The Sorel slag is upgraded via a proprietary process from 77% to about 95% TiO_2.

To compete with the higher grade feedstocks, lowering FeO, and producing a slag with 90% TiO_2, may not be enough to entice pigment producers to use these slags, but a slag upgrade via a UGS-type process would definitely make these slags competitive, mainly if the slags are produced from medium- to high-grade titaniferous magnetite ores. The lower-grade titanomagnetite deposits, with titania-to-total impurity ratios below about four, maybe upgradable prior to smelting, but this would require an assessment of deposit specific mineralisation. From the evaluation, there is a strong case to subject the furnace slag produced from titaniferous magnetite ores to an upgrade step post-tapping. A number of advantages are highlighted if compared to ilmenite slags (based on the comparison in Table 6-24), namely:

- Lower FeO equivalent per unit of TiO_2 due to the composition of the gangue components (improved Fe recovery, and more iron units, as well as less iron waste in post-tapping processing)
- No radioactive associations that cause hazardous wastes
- Co-production of vanadium provides an economic benefit to the process

The low-grade titaniferous magnetite ore, with TiO_2-to-impurity ratio of greater than four, could, therefore, be feasible as feedstock to the pigment industry.

6.8 PROPOSED SMELTING FLOWSHEET

A basic flowsheet proposal is presented in the section, as an outcome of the background review and the proposed smelting regime tested during the smelting project. The current testwork only tested the feasibility of fluxless melting in a DC furnace, but it is clear that the process will need to be optimised with respect to energy consumption to be competitive with bulk smelting of magnetite in blast furnaces. The proposed flowsheet addresses the various feasibility issues evaluated in the current study, such as energy and potential downstream users for the slag. The current study focused on smelting of the slag, but in order to evaluate the overall feasibility, an understanding of the product requirements is needed as there is limited scope for removing impurities, other than iron, from the slag during the smelting process. The only practical interventions would be to improve on the grading prior to smelting (via physical upgrading, roasting and so forth), and finally to upgrade the slag post-tapping. In addition, as a bulk ore, and specifically an iron smelter, optimising the energy requirements are crucial. The testwork demonstrated that once stable operation is achieved, slag contamination from the slag can be minimised. This approach is common practice in ilmenite smelting furnaces.

Preheating and prereduction form part of the proposed flowsheet. From an energy perspective, the furnace off-gas could be used to facilitate heating or drying, and ideally highly metallized feed should be fed to the electric furnace. If a significant fraction of the Fe is prereduced, not only will less electrical energy be consumed, but the gas evolution in the furnace will also be lower. This could lower some of the typical operational issues experienced when smelting high-titania slags, specifically foaming (a viscous slag is known for foaming). Foam can be simply described as gas trapped in a viscous slag, which causes a slag volume expansion, typically quite rapidly, and generally unintended, although common practise in some industries).

The mass and energy balance for the smelting step, based on producing slag with at least 85% TiO_2, is presented in Figure 6-25. The flowsheet assumes 25% metallization of the feed (fed to the furnace at 650°C). The summary is presented on the basis of 1 ton per hour, to allow for easy conversion; via a relatively simple calculation, the annual capacity of a smelter, based on either metal or slag production, can be calculated.

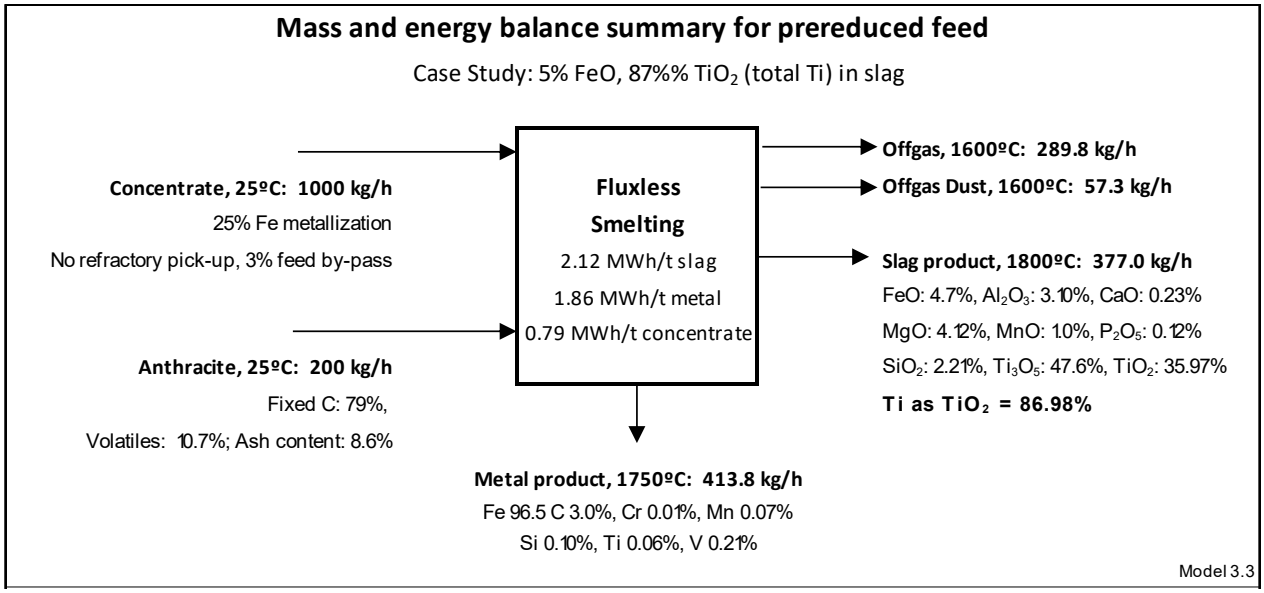

Figure 6-25: Smelting mass and energy balance for concentrate from the current study

A number of options for an idealised flowsheet for smelting titanomagnetite ore are presented in Figure 6-26, including various options for pretreatment. The grade and mineralisation of a deposit will determine the specific flowsheet best suited for the deposit.

The flowsheet (Figure 6-26) illustrates the potential to comprehensively extract iron, vanadium and titanium from a medium- to high-grade titanomagnetite ore.

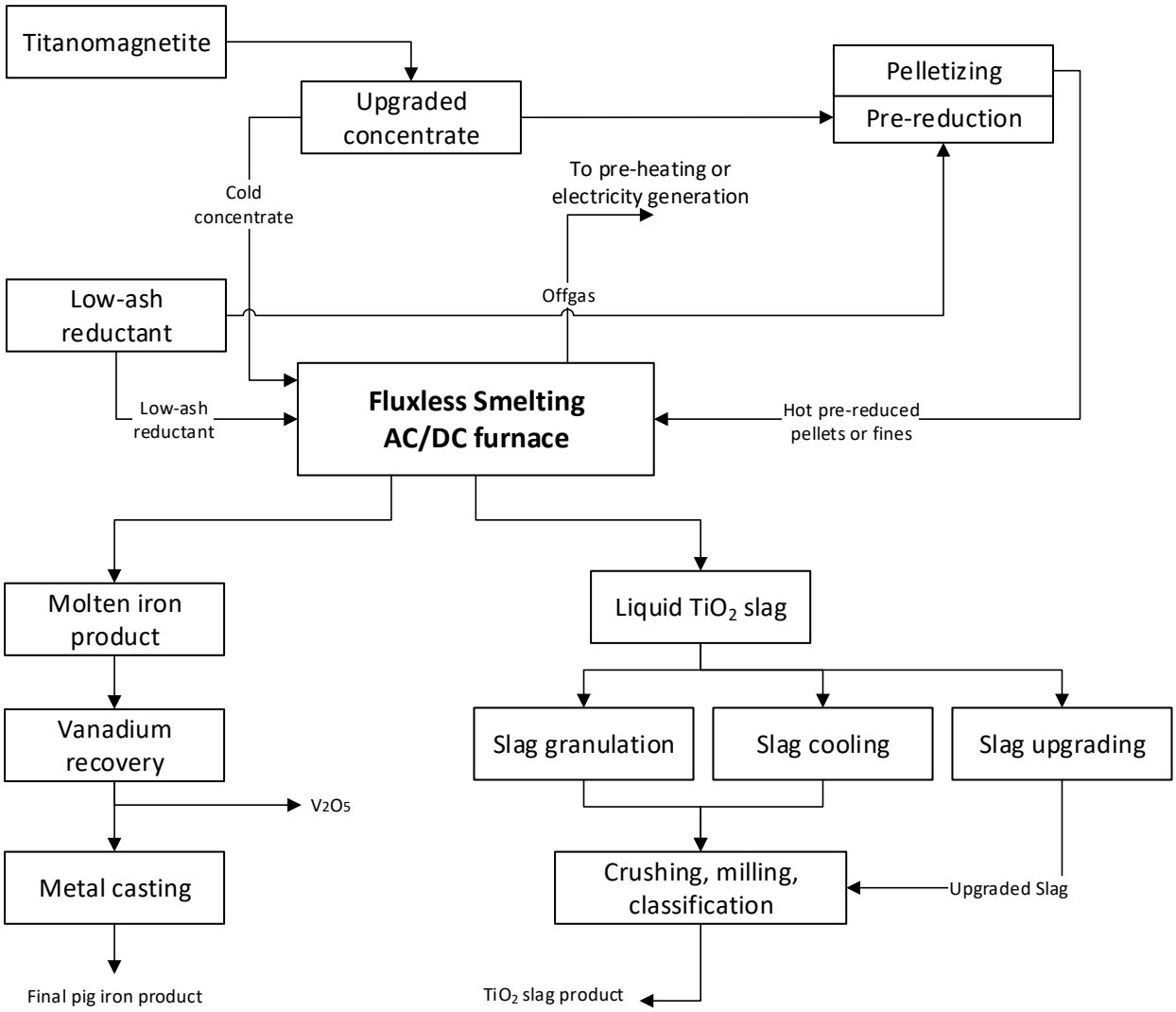

Figure 6-26: Fluxless smelting of titaniferous magnetite – flowsheet options

Extracting titanium from low-grade ores may not be economically viable, but the ore could be processed in the same way, that is via fluxless smelting, which may allow the slag to be processed in the future. The flowsheet options is a consolidated view of the smelting results, the background study, and draws on the various practices in industry to idealise an ideal process flowsheet for titanomagnetite. The preferred embodiment, due to the simplicity of a single electrode furnace would be a DC furnace but based on industrial practices, an AC furnace such as used by QIT and RBM (Rio Tinto) could be considered.

7 FINDINGS AND CONCLUSIONS

Fluxless smelting of titaniferous magnetite concentrate with about 35% TiO_2 content was successfully demonstrated. The smelting campaign produced about 40 tons of titania-slag of which the majority of data points exceeding 85% TiO_2 content. Smelting of the low-grade titaniferous concentrate in a DC furnace was shown to be a robust and flexible process able to achieve and maintain a high-grade slag product, producing slag with a TiO_2 content consistently exceeding 85%. An extended period during campaign produced slag with TiO_2 content in excess of 90%. A good quality iron-rich metal product was tapped throughout.

The testwork successfully demonstrated that a high-grade titania slag is achievable when smelting low-grade titaniferous concentrate in a DC furnace in the absence of fluxes. The test also demonstrated that slag composition by virtue of the degree of reduction could be optimised for the desired specification due to the added degree of freedom afforded by the open-arc operation. Recovery of Ti, as TiO_2 in the slag phase, was consistently greater than 93%, with losses primarily as a result of feed carry-over to the off-gas system.

The experimental programme also generated process information required for furnace design. These include the process energy requirement, smelting regime, slag and metal production rates, slag and metal quality as well as electrical properties of the slag. The process was operated with minimal operational disruptions despite the high-titania concept of the slag.

The process assessment also included evaluation of the quality of the metal product, energy, reductant, and electrode consumption, all in the context of fluxless smelting of titaniferous magnetite. Smelting of the low-grade concentrate involved a simple recipe which comprised of concentrate and anthracite fed to the furnace in the desired proportion to achieve the targeted metallurgical result, namely an undiluted titania-rich slag.

The concentrate was found to contain 52% ilmenite and 44% magnetite the balance being predominantly clay and amphibole minerals. The ilmenite, magnetite, and titaniferous magnetite phases are closely associated, with ilmenite liberation dominated in the ultrafine fractions.

Phase chemical evaluation of slag from the high-titania periods confirmed that the slag produced from titaniferous magnetite is consistent with the expected M_3O_5 substitution in terms of typical high-titania slag phase chemistry; the M_3O_5 phase contained remarkably low levels of FeO and high levels of TiO_2. A comparison with technical data from South African and Canadian ilmenite smelters also illustrated that the slag from the current study closely resembled ilmenite slags which is a positive outcome for the lower-grade titaniferous magnetite. It was concluded that in terms of typical high-titania slag phase chemistry, the M_3O_5 phase contained low levels of FeO and high level of TiO_2, which is consistent with the bulk chemical composition of the slags.

The refractory wear profiles indicated that a layer of frozen slag was maintained during the campaign and it is well-established that ilmenite smelters typically operate with such build-up. The smelting campaign data shows that once a freeze-lining had been established, it was possible to maintain it, even at elevated operating temperatures, which is a very positive outcome in terms of the feasibility study. The MgO-based refractory lining was sound, and the concept could be used for scale-up and design of a commercial furnace. A frozen layer of slag was maintained to protect the sidewalls from excessive slag attack after the initial expected refractory loss during the start-up. The water-cooled metal taphole design performed exceptionally well, while the slag taphole required no maintenance during the campaign.

The slag produced during the smelting test compares well with slag produced by industrial smelters. Generally, slags from titanomagnetite ores were shown to be amenable to upgrading via a smelting process, mainly through removal of the iron. The slags also compared favourably as a potential feedstock to the pigment industry, due to the low prevalence of undesirable elements in titaniferous magnetite deposits.

The electrode consumption measured for the test, namely 1.44 kg/MWh is comparable to industrial furnaces. Surface oxidation appears to be the dominant mechanism for consumption based on the condition of the electrode at the end of the campaign.

The process energy consumption for the campaign (excluding thermal efficiency) was shown to be about 1.63 kWh/kg concentrate. Notably, the energy balance indicated that the higher than expected energy consumption is due to about 5% free moisture in the finely sized feed. The free moisture resulted in higher energy consumption but did not adversely affect the metallurgical results. Based on the pilot-plant results, the specific energy requirement for dry feed would be 1.13 kWh/kg concentrate. The average specific energy requirement (1.63 kWh per kg concentrate) reflects the energy consumption for the material as processed during the pilot test, which includes the free moisture. The higher than expected moisture content of the concentrate inflated the energy consumption during the pilot test, while the data is very accurate, the effect of moisture is not a characteristic of the process as moisture is minimised in any smelting process due to the unique properties of water (high heat capacity).

The testwork mass balance was validated via high overall accountabilities as well as the validated model, which adds confidence to the overall findings and conclusions.

The slag produced during the pilot test did display increased viscosity during the ultra-low FeO periods, but generally, even with levels of below 3% FeO in slag, tapping had not been significantly constrained. The most stable operating conditions were achieved at 3% to 5% FeO in the slag.

Refractory wear, although minimized during the test, contributed to slag contamination and the model was used to calculate a slag composition for the baseline condition which excludes the refractory contamination (as MgO) and uncontaminated slag, with FeO of about 1.5% MgO versus 4.5% achieved during the middle period (batch 27 to 35) and 2.5% MgO achieved during the latter part of the campaign (batch 48 to 53). The impact of Mg contamination is exaggerated at pilot scale due to the short duration of the project, relative to a stable commercial smelting operation.

A titaniferous magnetite system is complex, and constrained, due to a number of interdependencies. A number of deterministic relationships are consistent and applicable across a wide range of feedstocks, including the concentrate tested during the current study. These ores have a complex mineralogical profile with a wide range of potential mineral substitutions. The characteristic mineralisation of ilmenite as finely dispersed layers in the magnetite, as well as the fact that vanadium is not strongly associated with a particular mineral, limits the upgrading potential by traditional physical means; thus a smelting step is required to extract the inherent value. Fluxless smelting was shown to unlock the potential of this complex resource efficiently.

Titanomagnetite ores are a potential source of titanium, iron and vanadium and the pilot smelting test demonstrated that it is feasible to produce a high-grade slag in the absence of fluxes. A generalised flowsheet is proposed, but due to the complexities each ore body, due to the high variability, needs to be assessed for potential unique opportunities to upgrade the ores.

8 FINAL REMARKS AND RECOMMENDATIONS

Fluxless smelting of titaniferous magnetite concentrate at pilot scale demonstrated the concept successfully. Titania-rich slag (ranging from 85% to 90% TiO_2) was produced from concentrate with about 35% titania content. The pilot-scale slag was compared with slags from industrial smelters, as is typically produced from titaniferous ilmenite ores, and compared relatively favourably. There appears to be a strong technical case for medium and high-grade titaniferous magnetite ores as feedstock to the pigment industry. The absence of radioactive element association could be an advantage, for example.

Due to the complex nature of the ore, a number of process scenarios and processing approaches may be feasible to optimise a process flowsheet aimed at extracting iron, vanadium and titanium from vanadiferous titanomagnetite deposits, such as is found in the South African Bushveld Complex. These options include preconcentration via thermal treatment possibly including prereduction, selective fluxing to optimise post-taphole slag upgrading, if deemed favourable, and to selectively deportment vanadium to either slag or metal. As these ores are likely to contain significant alkali earth elements, even post-upgrading, it is also more than likely that a slag upgrading process will be required to allow for use in the current chloride or sulfate processes for pigment production. It is also expected that the titania-rich slags produced from titaniferous magnetite could be used in titanium metal production, and future research to establish the application of the slags for the production of titanium metal is recommended.

The motivation for smelting titaniferous magnetite ores despite being regarded as a problematic ore to process is the co-production of vanadium as a by-product from the ironmaking process. Current practices favour the primary recovery of vanadium from the metal, but this is not necessarily the only viable option. Vanadium deportment to the slag impacts the slag quality, and it may be a nuisance or contaminant to address, or it could be an opportunity to comprehensively extract residual vanadium by recovering the vanadium from both metal and slag streams.

The comprehensive utilisation of titaniferous magnetite ores remains the ultimate objective, as current practices, such as blast furnace smelting, is creating large stockpiles of waste slags with enormous environmental liabilities for future generations. The proposed flowsheet comprehensively process the ore, and extract maximum value, with a significant reduction in the waste stream. In light of the fact that feedstock materials for the pigment industry are not in short supply, there needs to be an additional incentive for a pigment producer to select the product from a titanomagnetite smelter as feedstock. One of the highlighted advantages of titanomagnetite is the fact that these deposits are typically not associated with radioactive elements, a challenge for pigment producers as it adds complexity to the waste management of the chloride and sulfate processes. An assessment of this advantage would be required to establish the potential impact.

A detailed feasibility study to evaluate operating and capital costs for the proposed approach is advisable and would be required to assess the competitiveness of the proposed process. A combination of current practices, New Zealand Steel (pretreatment of the titaniferous magnetite) and Rio Tinto's QIT in Canada (upgrading of the slag produced from rock ilmenite), would provide a reasonable approach for an engineering study. This would allow for relatively reliable assessment of the case for the Bushveld Complex's lower-grade ores.

There are opportunities to optimise preconcentration and slag upgrading, but this is likely unique to specific deposits due to the nature of the ore. In order to progress the technology, a base case study is needed to establish reasonableness and opportunities for refinement, but the pilot plan results are encouraging, and a useful step in advancing the case for comprehensive utilisation of titaniferous magnetite. A process flowsheet selector tool may be a useful development to support comprehensive utilisation of titaniferous magnetite deposits.

REFERENCES

Avertana. 2017. *Avertana Technology*. [Online], Available: http://avertana.com/technical-details/ [accessed 20 April 2017].

Badmatsyrenova, R. & Orsoev, D. 2005. Origin of titanomagnetite-ilmenite mineralization, Arsentyev gabbro-syenite massif, Transbaikalia, Russia. In Berlin, Heidelberg: Springer Berlin Heidelberg *Mineral Deposit Research: Meeting the Global Challenge*. 725–727.

Bauer, G., Güther, V., Hess, H., Otto, A., Roidl, O., Roller, H. & Sattelberger, S. 2012. Vanadium and Vanadium Compounds. In Vol. 38. Weinheim, Germany: Wiley-VCH Verlag GmbH & Co. KGaA *Ullmann's Encyclopedia of Industrial Chemistry*. 49–69.

Bleloch, W. 1949. The Electric Smelting of Iron Ores For Production of Alloy Irons and Steels and Recovery of Chromium and Vanadium. *Journal of the Chemical, Metallurgical and Mining Society of South Africa*. (March):363–402.

Boyd, M.D., Schoukens, A.F.S. & Denton, G.M. 1993. *Patent No. 93/4619*. South Africa.

Burger, H., Bessinger, D. & Moodley, S. 2009. Technical considerations and viability of higher titania slag feedstock for the chloride process. In The Southern African Institute of Mining and Metallurgy *The 7th International Heavy Minerals Conference "What next"*. 187–194.

Cawthorn, R.G., Barnes, S., Ballhaus, C. & Malitch, K.N. 2005. Platinum group element, chromium and vanadium deposits in mafic and ultramafic rocks. In Vol. 100th Anni. Society of Economic Geologists *Economic Geology 100th Anniversary Volume*. 215–249.

Chen, S. & Chu, M. 2014a. Metalizing reduction and magnetic separation of vanadium titano-magnetite based on hot briquetting. *International Journal of Minerals Metallurgy and Materials*. 21(3):225–233.

Chen, S. & Chu, M. 2014b. A new process for the recovery of iron, vanadium, and titanium from vanadium titanomagnetite. *Journal of the Southern African Institute of Mining and Metallurgy*. 114(6):481–487.

Chen, D.S., Song, B., Wang, L.N., Qi, T., Wang, Y. & Wang, W.J. 2011. Solid state reduction of Panzhihua titanomagnetite concentrates with pulverized coal. *Minerals Engineering*. 24(8):864–869.

Chen, S., Fu, X., Chu, M., Liu, Z. & Tang, J. 2015. Life cycle assessment of the comprehensive utilisation of vanadium titano-magnetite. *Journal of Cleaner Production*. 101:122–128.

Cloete, K. 2014. *R242m Namakwa Sands cogen plant delivers results*. [Online], Available: http://www.engineeringnews.co.za/article/r242m-namakwa-sands-cogen-plant-delivers-results-2014-10-16 [accessed 28 December 2018].

Connelly, D., Reed, C. & Palmer, R. 2008. Trends with Titaniferous Magnetite Processing for Vanadium Extraction. In Perth *Metallurgical Plant Design and Operating Strategies (MetPlant 2008)*. 18–19.

Deneys, A. & la Grange, G. 2001. [Online], Available: http://www.mintek.co.za/Pyromet/Pyrosim/PyroMan.htm [accessed 22 September 2019].

Desrosiers, R., Ajersch, F. & Grau, A.E. 1980. Electrical conductivity of industrial slags of high titania content. In *Proceedings International Symposium on Metallurgical Slags, Part of the 19th Annual Conference of Metallurgists*.

Dippenaar, R. 2005. Industrial uses of slag (the use and re-use of iron and steelmaking slags). *Ironmaking & Steelmaking*. 32(1):35–46.

"Editorial: So long sulphur". 2009. *Nature Chemistry*. 1(5):333–333.

EVRAZ Highveld Steel and Vanadium. 2015. *Business Rescue*. [Online], Available: http://www.evrazhighveld.co.za/businessrescue.asp [accessed 18 February 2017].

Fandrich, R., Gu, Y., Burrows, D. & Moeller, K. 2007. Modern SEM-based mineral liberation analysis. *International Journal of Mineral Processing*. 84(1–4):310–320.

Filippou, D. & Hudon, G. 2009. Iron removal and recovery in the titanium dioxide feedstock and pigment industries. *JOM*. 61(10):36–42.

Fischer, R.P. 1975. Vanadium resources in titaniferous magnetite deposits. *U.S. Geological Survey Professional Paper*. 926-B:1–9.

Fisher, J.R. 1997. Developments in the TiO2 pigment industry which will drive demand for TiO2 mineral feedstocks. In

Heavy Minerals 1997. 207–218.

Fu, W.G. & Xie, H.E. 2011. Progress in Technologies of Vanadium-Bearing Titanomagnetite Smelting in PanGang. *Steel Research International*. 82(5):501–504.

Fu, W., Wen, Y. & Xie, H. 2011. Development of Intensified Technologies of Vanadium-Bearing Titanomagnetite Smelting. *Journal of Iron and Steel Research, International*. 18(4):7–18.

Gambogi, J. & Gerdemann, S.J. 2013. Titanium Metal: Extraction to Application. In San Diego: TMS (The Minerals, Metals & Materials Society) *Review of Extraction, Processing, Properties & Applications of Reactive Metals*. 175–210.

Geldenhuys, I.J. 2017. The Exact Art and Subtle Science of DC Smelting: Practical Perspectives on the Hot Zone. *JOM*. 69(2):343–350.

Geldenhuys, I.J. & Jones, R.T. 2011. What Scale Should Your Smelting Testwork Be Done At, And What Do You Get For The Money You Spend? In The Southern African Institute of Mining and Metallurgy *6th Southern African Base Metals Conference 2011*. 477–492.

Gilman, S.K. & Taylor, R.K.A. 2001. The Future for Ilmenite Beneficiation Technologies. In Fremantle: AusIMM *International Heavy Minerals Conference*. 18–19.

Goldberg, I., Hammerbeck, E.C.I., Labuschagne, L.S. & Rossouw, C. 1992. *Minerals Inventory: Summary Report - Vanadium*. [Online], Available: https://pubs.usgs.gov/circ/1992/0930k/report.pdf.

Goso, X.C., Nell, J. & Petersen, J. 2016. Review of liquidus surface and phase equilibria in the TiO2-SiO_2-Al2O3-MgO-CaO slag system at PO2 applicable in fluxed titaniferous magnetite smelting. In R.G. Reddy et al. (eds.). TMS (The Minerals, Metals & Materials Society) *Advances in Molten Slags, Fluxes, and Salts: Proceedings of The 10th International Conference on Molten Slags, Fluxes and Salts (MOLTEN16)*. 105–114.

Gous, M. 2006. An overview of the Namakwa Sands ilmenite smelting operations. *Journal of the Southern African Institute of Mining and Metallurgy*. 106(6):379–384.

Guéguin, M. & Cardarelli, F. 2007. Chemistry And Mineralogy Of Titania-Rich Slags. Part 1—Hemo-Ilmenite, Sulphate, And Upgraded Titania Slags. *Mineral Processing and Extractive Metallurgy Review*. 28(1):1–58.

Guo, Y., Liu, S., Jiang, T., Qiu, G. & Chen, F. 2014. A process for producing synthetic rutile from Panzhihua titanium slag. *Hydrometallurgy*. 147–148:134–141.

Hassell, D.J., Obern, J.K., Molloy, S.D.J., Ibrahim, S.O.Z.E.M. & Ali, M.S. 2016. *Patent No. WO/2016/007021*. [Online], Available: http://www.sumobrain.com/patents/WO2016007021A1.html.

Hu, T., Lv, X., Bai, C., Lun, Z. & Qiu, G. 2013. Reduction behavior of Panzhihua titanomagnetite concentrates with coal. *Metallurgical and Materials Transactions B: Process Metallurgy and Materials Processing Science*. 44(2):252–260.

Hukkanen, E. & Walden, H. 1985. The production of vanadium and steel from titanomagnetites. *International Journal of Mineral Processing*. 15(1–2):89–102.

Infomine Research Group. 2014. *JSC "Evraz NTMK" (Russia) (company business profile)*. [Online], Available: www.infomine.ru; [accessed 07 December 2018].

Ivanic, T.J., Wingate, M.T.D., Kirkland, C.L., Van Kranendonk, M.J. & Wyche, S. 2010. Age and significance of voluminous mafic–ultramafic magmatic events in the Murchison Domain, Yilgarn Craton. *Australian Journal of Earth Sciences*. 57(5):597–614.

James, H., Brothers, I., Grime, G.W. & Swann, C.P. 2002. Albemarle Iron Works (1771-1772): Why did this operation fail? *Nuclear Instruments and Methods in Physics Research, Section B: Beam Interactions with Materials and Atoms*. 189(1–4):340–343.

Jones, R.T. 1987. Computer Simulation of Pyrometallurgical Processes. In Vol. 2 *APCOM 87, Proceedings of the Twentieth International Symposium on the Application of Mathematics and Computers in the Minerals Industries, Volume 2: Metallurgy*. 265–279.

Jones, R.T. 2011.

Jones, R.T. & Geldenhuys, I.J. 2011. The pros and cons of reductive matte smelting for PGMs. *Minerals Engineering*. 24(6):495–498.

Jones, T. & Egerton, T.A. 2012. Titanium Compounds, Inorganic. In *Kirk-Othmer Encyclopedia of Chemical Technology*. 1–62.

Jones, R., Reynolds, Q., Curr, T. & Sager, D. 2011. Some myths about DC arc furnaces. In R. Jones & P. den Hoed (eds.) *Southern African Pyrometallurgy 2011*. 15–32.

Kelly, B.F. 1993. Kelly Ironmaking at BHP New Zealand Steel Limited, Glenbrook. New Zealand. In Victoria, Australia: Australasian Institute of Mining and Metallurgy *AUSTRALASIAN mining and metallurgy : The Sir Maurice Mawby Memorial Volume (2nd ed.). (Monograph series (Australasian Institute of Mining and Metallurgy), 19). (1993). Parkville, Vic.: AusIMM.* 348–353.

Killick, D. & Fenn, T. 2012. Archaeometallurgy: The Study of Preindustrial Mining and Metallurgy. *Annual Review of Anthropology*. 41(1):559–575.

Killick, D. & Miller, D. 2014. Smelting of magnetite and magnetite-ilmenite iron ores in the northern Lowveld, South Africa, ca. 1000 CE to ca. 1880 CE. *Journal of Archaeological Science*. 43(1):239–255.

Langslow, D.R. 1988. Sulphur or sulfur? A tale of two spellings. *British Medical Journal*. 297(6664):1697–1699.

Lazutkin, S.E., Yusfin, Y.S., Zinyagin, G.A., Pchelkin, S.A., Lazutkin, S.S. & Krasil'nikov, A.O. 2001. Improving a Technology for the Direct Production of Iron and Vanadium-Bearing Products Based on the Midrex Process. *Metallurgist*. 45(9):354–359.

Lepinski, J.A. 2000. Iron by Direct Reduction. In Hoboken, NJ, USA: John Wiley & Sons, Inc. *Kirk-Othmer Encyclopedia of Chemical Technology*. 1–15.

Li, C., Liang, B., Guo, L. hong & Wu, Z. b. 2006. Effect of mechanical activation on the dissolution of Panzhihua ilmenite. *Minerals Engineering*. 19(14):1430–1438.

Liu, X., Gai, G., Yang, Y., Sui, Z., Li, L. & Fu, J. 2008. Kinetics of the leaching of TiO_2 from Ti-bearing blast furnace slag. *Journal of China University of Mining and Technology*. 18(2):275–278.

Maharajh, S., Muller, J. & Zietsman, J.H. 2015. Value-in-use model for chlorination of titania feedstocks. *Journal of the Southern African Institute of Mining and Metallurgy*. 115(05):385–394.

Manamela, M.M. & Pistorius, P.C. 2005. Ore size does affect direct reduction of titaniferous magnetite. *Journal of the Southern African Institute of Mining and Metallurgy*. 105(3):183–185.

Mcrae, L.B., Pothas, E., Jochens, P. & Howat, D. 1969. Physico-Chemical Properties of Titaniferous Slags. *Journal of the Southern African Institute of Mining and Metallurgy African Institute of Mining and Metallurgy*. 69(June):578–594.

Moodley, S., Eric, R.H., Kucukkaragoz, C. & Kale, A. 2012. Chlorination of titania feedstocks. In T. Jiang et al. (eds.). The Minerals, Metals and Materials Society (TMS) *3rd International Symposium on High-Temperature Metallurgical Processing*. 93–104.

Moskalyk, R.R. & Alfantazi, A.M. 2003. Processing of vanadium: a review. *Minerals Engineering*. 16(9):793–805.

New Zealand Steel. 2018. *The History of Ironsand*. [Online], Available: https://www.nzsteel.co.nz/new-zealand-steel/the-story-of-steel/the-history-of-ironsand/ [accessed 02 December 2018].

Pang, K.N., Zhou, M.F., Qi, L., Shellnutt, G., Wang, C.Y. & Zhao, D. 2010. Flood basalt-related Fe-Ti oxide deposits in the Emeishan large igneous province, SW China. *Lithos*. 119(1–2):123–136.

Pariser, H.H., Backeberg, N.R., Masson, O.C.M. & Bedder, J.C.M. 2018. Changing nickel and chromium stainless steel markets - a review. *Journal of the Southern African Institute of Mining and Metallurgy*. 118(6):25–28.

Park, E. & Ostrovski, O. 2003. Reduction of Titania – Ferrous Ore by Carbon Monoxide. *ISIJ International*. 43(9):1316–1325.

Peck, D.C. & Huminicki, M.A.E. 2016. Value of mineral deposits associated with mafic and ultramafic magmatism: Implications for exploration strategies. *Ore Geology Reviews*. 72:269–298.

Perks, C. 2018. *Technical issue at Cristal's Saudi slag project to keep high-grade titanium feedstocks tight in 2019*. [Online], Available: https://www.indmin.com/Article/3841697/Technical-issue-at-Cristals-Saudi-slag-project-to-keep-high-grade-titanium-feedstocks-tight-in-2019.html [accessed 15 January 2019].

Pistorius, P.C. 1999. Limits on energy and reductant inputs in the control of ilmenite smelters. In R.G. Stimson (ed.). Johannesburg, South Africa: The South African Institute of Mining and Metallurgy (SAIMM) *Heavy Minerals 1999*. 183–188.

Pistorius, P.C. 2002. The relationship between FeO and Ti2O3 in ilmenite smelter slags. *Scandinavian Journal of Metallurgy*. 31(2):120–125.

Pistorius, P.C. 2003. Fundamentals of freeze lining behaviour in ilmenite smelting. *Journal of The South African Institute of Mining and Metallurgy*. 103(8):509–514.

Pistorius, P.C. 2004. Equilibrium interactions between freeze lining and slag in ilmenite smelting. *Journal of The South African Institute of Mining and Metallurgy*. 104(7):417–422.

Pistorius, P.C. 2008. Ilmenite smelting: The basics. *Journal of the Southern African Institute of Mining and Metallurgy*. 108(1):35–43.

Pistorius, P.C. & Coetzee, C. 2003. Physicochemical aspects of titanium slag production and solidification. *Metallurgical and Materials Transactions B*. 34(5):581–588.

Pistorius, P.C. & Kotzé, H. 2009. Role of silicate phases during comminution of titania slag. *Minerals Engineering*. 22(2):182–189.

PowerOptimal. 2015. *Eskom tariff increases vs inflation since 1988*. [Online], Available: http://www.poweroptimal.com/infographic-eskom-tariff-increases-vs-inflation-since-1988/ [accessed 05 May 2017].

Reynolds, I.M. 1985. The nature and origin of titaniferous magnetite-rich layers in the upper zone of the Bushveld complex: a review and synthesis. *Economic Geology*. 80(4):1089–1108.

Reynolds, Q.G. & Jones, R.T. 2004. Semi-empirical modelling of the electrical behaviour of DC-arc smelting furnaces. *Journal-South African Institute of Mining and Metallurgy*. 104(6):345–351.

Richards, S.R. & Davies, C.E. 1980. Smelting Alternatives for New Zealand Titaniferous Minerals. In The Australian Institute of Mining and Metallurgy *The Aus. I. M. M. Conference*. 237–253.

Rio Tinto. 2016. [Online], Available: http://www.riotinto.com/documents/201601_RBM_Fact_sheet.pdf [accessed 29 August 2019].

Rohrmann, B. 1985. Vanadium in South Africa. *J. S. Afr. Inst. Min. Metall.* 85(5):141–150.

Rosenqvist, T. 1992. Ilmenite smelting. *Transactions of the Technical University of Košice*. 2(Special Issue):40–46.

Roskill Information Services. 2010. *Vanadium: Global industry markets and outlook*. 12th ed. London: Roskill Information Services Ltd. [Online], Available: www.roskill.com.

Singewald, J.T. 1913. *The Titaniferous Iron Ores of the United States Their Composition and Economic Value*.

Smirnov, L.A., Tret'yakov, M.A. & Gladyshev, V.I. 2000. *Processing vanadium-bearing and titanomagnetite iron ores*. Vol. 44.

Stanaway, K.J. 1994a. A titanium pigment feedstock overview. In Albuquerque, New Mexico *SME Annual Meeting*. 1–6.

Stanaway, K.J. 1994b. Overview of titanium dioxide feedstocks. *Mining Engineering*. 46(December 1994):1367–1370.

Steinberg, W., Geyser, W. & Nell, J. 2011. The history and development of the pyrometallurgical processes at Evraz Highveld steel & vanadium. *Journal of the Southern African Institute of Mining and Metallurgy*. 111(10):705–710.

Sun, H., Wang, J., Dong, X. & Xue, Q. 2012. A literature review of titanium slag metallurgical processes. *Metalurgia International*. 17:49–56.

Taylor, D.J.C., Page, D.C. & Geldenhuys, P. 1988. Iron and steel in South Africa. *J.S.Afr. Inst. Min. Metall.* 88(3):73–95.

Taylor, P.R., Shuey, S.A., Edgar E. Vidal, Wang, W. & Gomez, J.C. 2005. Extractive Metallurgy of Vanadium Containing Titaniferous Magnetite Ores : a Review. *2005 SME Annual Meeting*. (May):1–9.

U.S. Geological Survey. 2014. *2014 Minerals Yearbook Titanium [Advance Release]: U.S. Geological Survey*. [Online], Available: https://minerals.usgs.gov/minerals/pubs/commodity/titanium/myb1-2014-titan.pdf [accessed 20 April 2017].

U.S. Geological Survey. 2016. *Mineral Commodity Summaries 2016: U.S. Geological Survey*. U.S. Government Printing Office.

U.S. Geological Survey. 2017. *Mineral Commodity Summaries 2017: U.S. Geological Survey*. U.S. Government Printing Office.

Vanitec. 2017. *Vanadium in Energy Storage*. [Online], Available: http://vanitec.org/vanadium/article/vanadium-redox-flow-battery-vrfb [accessed 27 April 2017].

Williams, G.E. & Steenkamp, J.D. 2006. Heavy Mineral Processing at Richards Bay Minerals. In R.T. Jones (ed.). South African Institute of Mining and Metallurgy *Southern African Pyrometallurgy 2006*. 5–8.

World Steel Association. 2018. *World Steel in Figures 2018*. [Online], Available: www.worldsteel.org [accessed 10 July 2018].

Yuan, Z. fu, Pan, Y. fang, Zhou, E., Xu, C. & Li, S. qing. 2007. Comprehensive Utilization of Complex Titania Ore. *Journal of Iron and Steel Research International*. 14(1):1–6.

Zhang, L., Zhang, L.N., Wang, M.Y., Li, G.Q. & Sui, Z.T. 2007. Recovery of titanium compounds from molten Ti-bearing blast furnace slag under the dynamic oxidation condition. *Minerals Engineering*. 20(7):684–693.

Zhang, W., Zhu, Z. & Cheng, C.Y. 2011. A literature review of titanium metallurgical processes. *Hydrometallurgy*. 108(3–4):177–188.

Zhou, G., Peng, T., Sun, H. & Xian, H. 2015. Chemical and Mineralogical Characterizations of High Ti-Bearing Blast Furnace Slag in Panzhihua, China. In F. Dong (ed.). Springer International Publishing *Proceedings of the 11th International Congress for Applied Mineralogy*. 521–530.

Zietsman, J.H. 2004. Interactions Between Freeze Lining and Slag Bath in Ilmenite Smelting. University of Pretoria.

Zietsman, J.H. & Pistorius, P.C. 2005. Process mechanisms in ilmenite smelting. *Journal of the South African Institute of Mining and Metallurgy*. 105(December):229–235.

Zietsman, J.H. & Pistorius, P.C. 2006. Modelling of an ilmenite-smelting DC arc furnace process. *Minerals Engineering*. 19:262–279.

APPENDIX A PILOT-PLANT FURNACE

A1 Furnace installation

The photographs in this section show the individual sections of the pilot furnace, prior to complete installation.

Figure A1: Unlined conical roof (left) and roof plug (right)

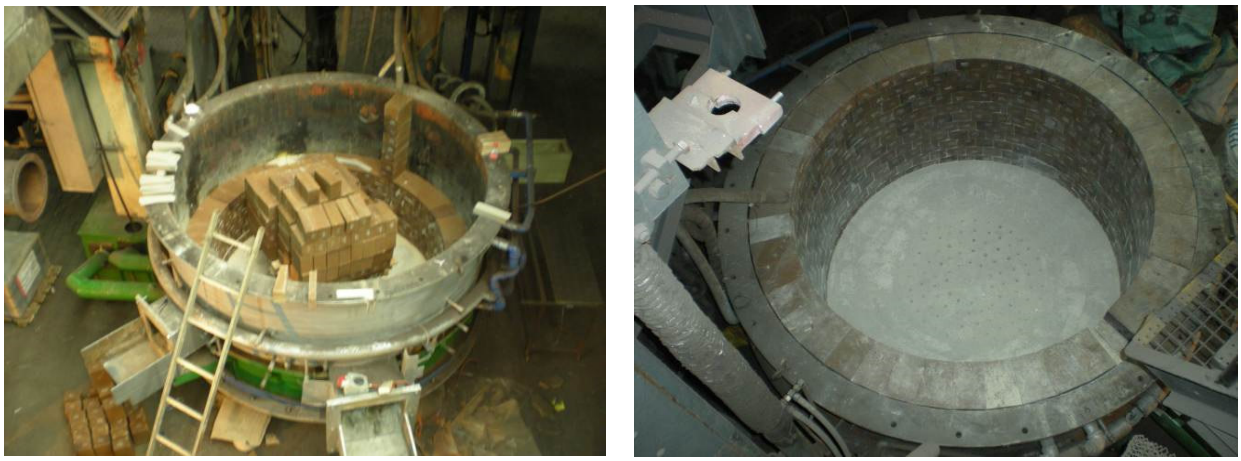

Figure A2: Refractory installation in progress (left) and completed refractory lining (right)

Figure A3: Shell and pins prior to lining installation (left) and ramming of the hearth (right)

Figure A4 shows the positions of the four thermocouples installed in the hearth refractory (photograph of thermocouples installed prior to installation of hearth refractory) – with an overhead view presented in Figure A3 (left). The four thermocouples installed in the hearth, are identified according to the labels allocated to each in the data system. Thermocouple 304 was located approximately mid-point between the slag and metal tapholes, while thermocouples 262, 263 and 264 were located in the area underneath the arc attachment zone. Temperature profiles

are used to evaluate hearth wear or hearth build-up, and a heating rate is also a valuable tool during the warm-up and stabilisation of the furnace.

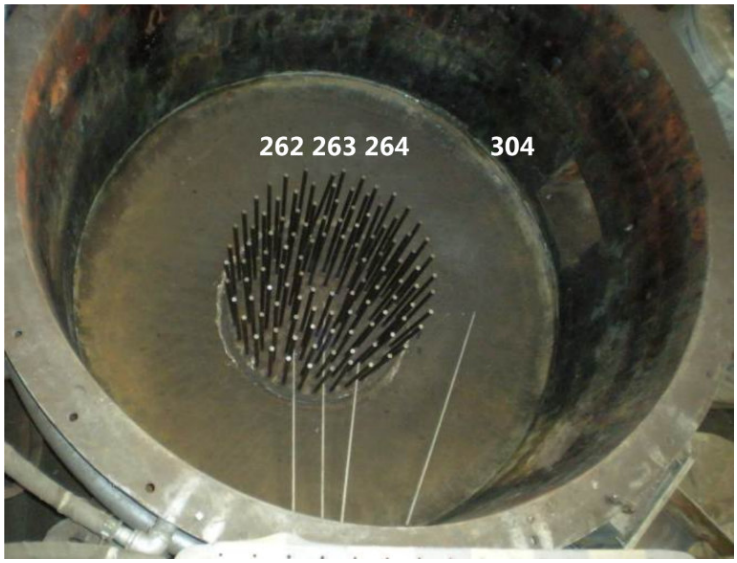

Figure A4: Position and identity of the four hearth thermocouples

The next graph shows the hearth thermocouple temperatures as recorded during the campaign. The plot shows a fairly steady increase in temperature throughout the campaign, with a delayed response due to the fact that these thermocouples are seated deep in the hearth refractory.

The fact that the temperatures remained relatively low agrees well with the significant metal heel found in the furnace during the excavation. In general, the furnace hearth was in excellent condition at the end of the test.

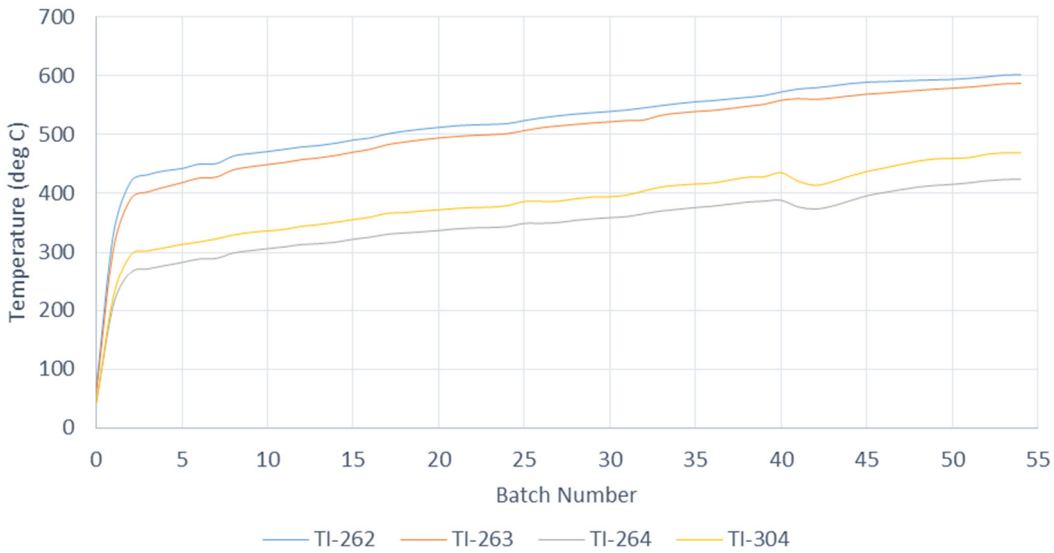

Figure A5: Hearth temperature profile for the duration of the test campaign

A2 Composition of refractories

The chemical composition and brand names of the refractories used during the installation of the furnace are summarised below.

Table A1: Chemical composition of refractory materials, mass %

Commercial Product Name	CERAMAC 95	GUNTAP	VEROKAST 1800	ANKER-HARTH	D50 C5
Use	**Sidewalls**	**Taphole**	**Roof**	**Hearth**	**Taphole**
Type	**Brick**	**Ramming**	**Castable**	**Ramming**	**Brick**
SiO_2	<2.0	4.0	0.2	0.7	1.6
Al_2O_3	-	1.2	93.5	0.5	8.6
Fe_2O_3	-	1.7	0.2	3.5	12.2
TiO_2	-	-	0.0	-	-
CaO	-	2.2	5.4	18	1.2
MgO	>95	89.0	0.1	77.0	47.4
Cr_2O_3	-	-	-	-	28.6
$Na_2O + K_2O$	-	-	0.6	-	-

A3 Furnace water-cooling

The diagram below, not to scale, illustrates the relevant dimensions and location of the three main water-cooled areas of the furnace, namely the conical roof, upper sidewall (or top ring) and lower sidewall areas. Surface areas for each of these zones were calculated and used to estimate the average heat flux, based on the measured rate of energy loss for each circuit.

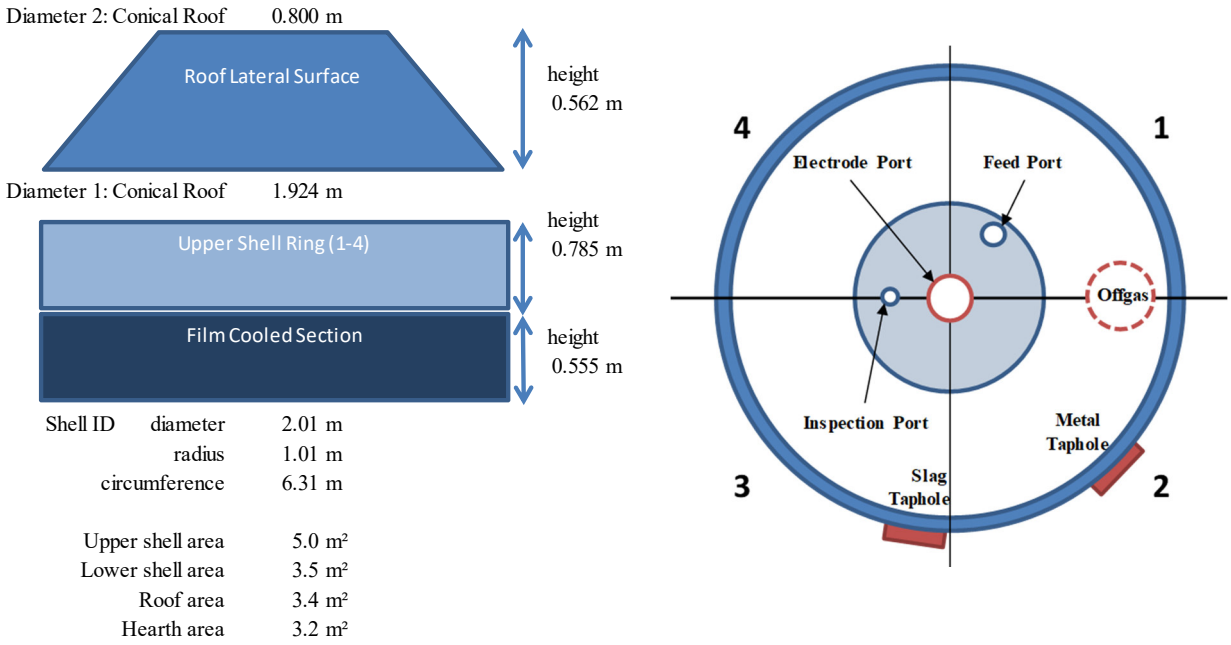

Figure A6: Representation of the relative positions of the various water-cooled areas

The following photographs show the various stages of the refractory installation, highlighting the details of the taphole installations. Table A1 summarises the chemical composition of the refractory design for the pilot furnace.

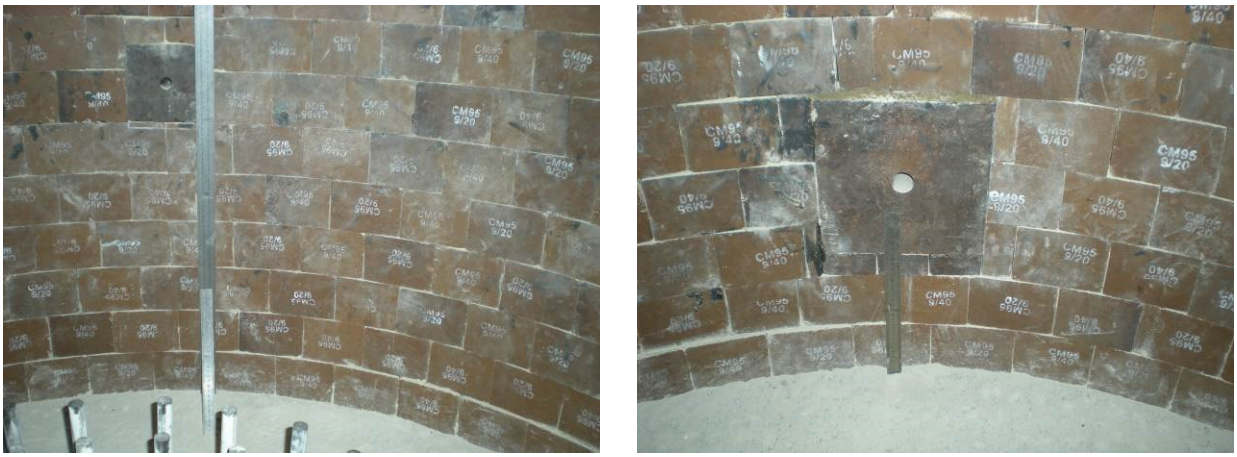

Figure A7: Slag (left) and metal (right) tapholes; the position relative to the hearth indicated

Figure A8: Slag (left) and metal (right) taphole and launder installation

A4 Furnace excavation measurements

At the conclusion of the testwork, the furnace was allowed to cool down for a couple of days. Furnace shell-cooling water circuits were active during this period to expedite the cooling process. Once the furnace had cooled down adequately, it was dismantled. The metal and slag tapholes and the furnace off-gas were selected as reference positions as refractory wear is expected. Eight measurement positions, as shown in Figure A9, were deemed adequate to render a representative profile of the furnace. Profiles were drawn from measurements taken at each of the positions of interest to evaluate refractory wear and are represented via four diagrams (via views E-A, F-B, G-C, H-D).

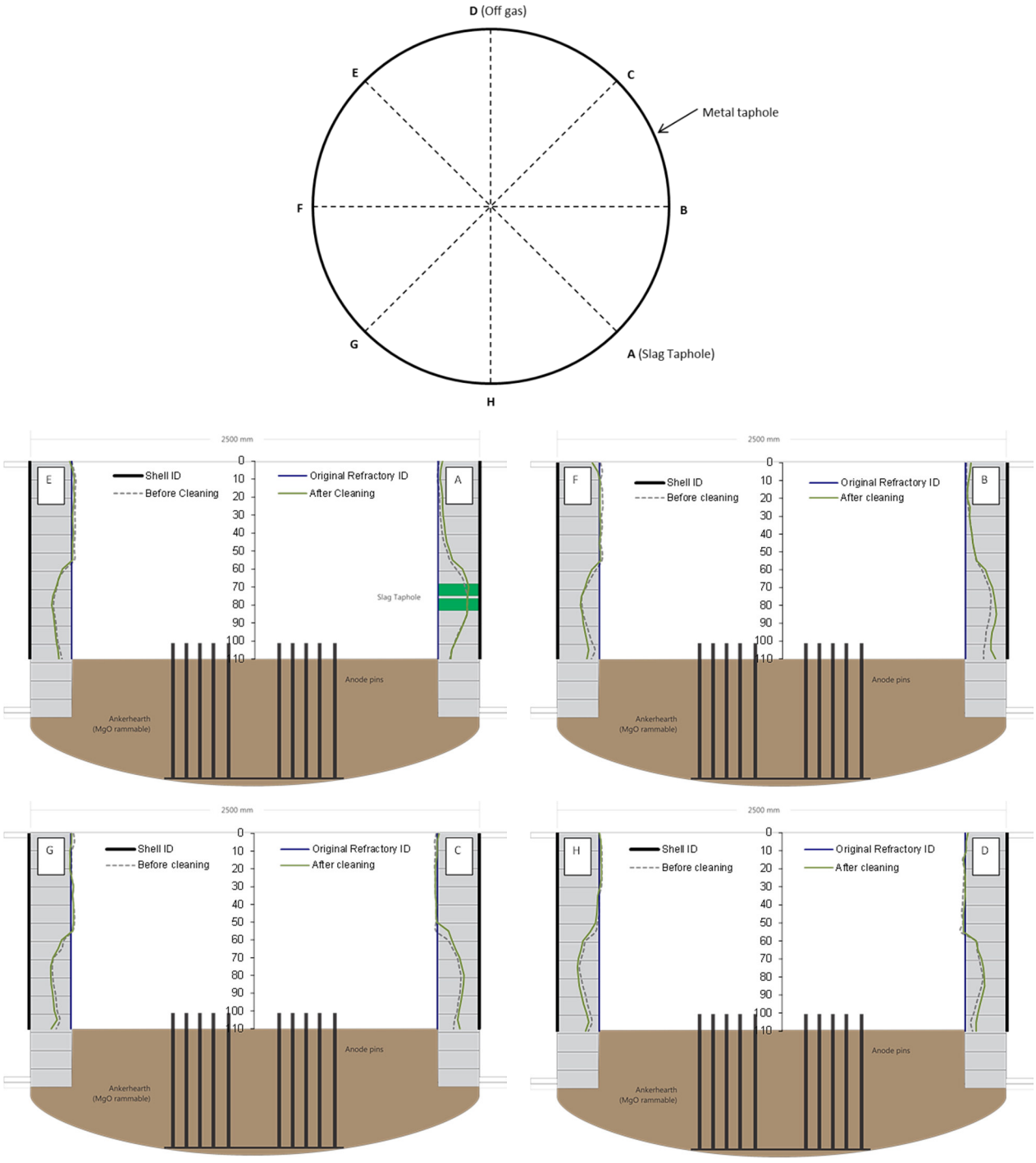

Figure A9: Measurement positions and reconstructed wear profiles for the furnace.

The diagrams show that refractory wear occurred around the slag-metal interface, as established earlier. The freeboard saw minimal refractory wear as expected.

APPENDIX B RAW MATERIAL DATA

Four representative samples of the bulk anthracite were characterised with the full set of data presented below.

Table B1: Chemical composition of anthracite composite samples, mass %

	Mintek Laboratory				*External Laboratory*			
	Sample 1	Sample 2	Sample 3	Sample 4	Sample 1	Sample 2	Sample 3	Sample 4
Fixed Carbon	79.1	78.9	79.4	78.7	79.0	78.9	78.8	78.7
Volatile	9.8	10.7	11.2	11.0	12.1	12.3	12.3	12.2
Ash	8.84	8.47	8.50	8.66	8.60	8.50	8.60	8.80
Moisture	2.30	1.89	0.95	1.58	0.30	0.30	0.30	0.30
Total S	<0.01	<0.01	<0.01	<0.01	0.01	0.01	0.01	0.01
Total	100.0	100.0	100.1	99.9	100.0	100.0	100.0	100.0
P as P_2O_5 (ppm)	-	123	124	-				
Gross Calorific Value (MJ/kg)	-	-	-	-	34.3	34.5	34.4	34.1
Ultimate assay (dry basis):								
Total carbon content	86.3	85.1	85.0	85.6	87.3	87.1	86.8	86.7
Hydrogen content	-	-	-	-	3.70	3.67	3.63	3.61
Nitrogen content	-	-	-	-	0.06	0.08	0.09	0.11
Oxygen content (calculated)	-	-	-	-	0.07	0.34	0.50	0.47

Ash composition, mass %				
FeO	7.07	6.96	7.13	7.26
MgO	0.15	0.14	0.14	0.14
CaO	0.37	0.31	0.24	0.27
Al_2O_3	0.17	0.11	0.11	0.09
SiO_2	0.37	0.34	0.34	0.34
Total	**8.14**	**7.85**	**7.96**	**8.10**

The bulk chemical composition of ten composite concentrate samples (Composition Sample 1 to 10) was determined. Representative sub-fractions from each of the composited bags of concentrate were submitted to two laboratories, namely MINTEK's in-house analytical services section, as well as an independent commercial laboratory, designated as 'Laboratory A'. Samples were assayed as received, that is containing some free moisture. In general the average TiO_2 grade range between 34.5 and 38.3% with a Fe (total Fe) of between 41 and 43%.

Laboratory A was able to report the oxidation states of Fe (Fe^0 and Fe^{2+}, Fe^{3+} was calculated by difference). The average ratio of Fe^{2+} to Fe^{3+} for the titaniferous concentrate was calculated to be 1.7.

A volatile component associated with the presence of clay minerals of approximately 0.5% was noted. LOI values of -2% are consistent with the loss of volatile components combined with the gain in mass associated with the oxidation of Fe^{2+} to Fe^{3+} that is expected for this type of measurement.

Table B2: Bulk chemical analysis of concentrate analysed by the MINTEK laboratory, mass%

	MgO	Al_2O_3	SiO_2	CaO	TiO_2	V_2O_5	Cr_2O_3	MnO	FeO [†]	TOTAL
$\bar{x}$	0.68	1.23	1.06	<0.05	35.50	0.44	0.08	0.59	55.15	94.7
± 95% CI	0.05	0.09	0.12	-	0.67	0.02	0.02	0.03	1.41	-
Sample Number										
1	0.59	1.18	1.24	<0.05	36.50	0.39	0.07	0.602	51.80	92.4
2	0.53	1.30	1.13	<0.05	35.00	0.44	0.15	0.600	54.29	93.4
3	0.58	0.92	1.13	<0.05	36.00	0.40	0.08	0.592	51.99	91.7
4	0.71	1.12	0.79	<0.05	35.00	0.48	0.07	0.640	55.98	94.8
5	0.71	1.28	0.82	<0.05	35.20	0.47	0.06	0.633	55.60	94.8
6	0.74	1.20	0.79	<0.05	35.50	0.45	0.06	0.635	54.95	94.3
7	0.75	1.36	1.14	<0.05	35.80	0.45	0.06	0.626	54.83	95.0
8	0.72	1.46	1.28	<0.05	34.00	0.48	0.06	0.619	55.08	93.7
9	0.79	1.15	1.20	<0.05	37.70	0.38	0.08	0.498	57.46	99.3
10	0.65	1.32	1.10	<0.05	34.30	0.49	0.09	0.490	59.46	97.9

(†) Total Fe assayed, expressed as FeO

Table B3: Bulk chemical analysis of as-received concentrate samples analysed by Laboratory A, mass %

	MgO	Al_2O_3	SiO_2 [$]	CaO	TiO_2	V_2O_5	Cr_2O_3	MnO	FeO [‡]	Fe_2O_3[‡]	TOTAL[$]
$\bar{x}$	0.65	1.6		0.01	34.48	0.48	0.01	0.49	19.60	37.46	94.7
± 95% CI	0.13	0.16		-	0.61	0.04	-	0.01	1.75	3.57	-
Sample Number											
1	0.81	1.80		0.01	35.09	0.42	0.01	0.50	23.0	30.9	92.6
2	0.65	1.73		0.01	34.60	0.45	0.01	0.45	21.5	33.5	92.9
3	0.73	1.74		0.01	32.50	0.46	0.01	0.49	21.0	33.6	88.8
4	0.74	1.79		0.01	34.40	0.52	0.01	0.52	20.5	38.9	97.4
5	0.78	1.50		0.01	34.20	0.43	0.01	0.50	19.2	34.5	91.1
6	0.80	1.50		0.01	36.40	0.43	0.01	0.51	21.5	33.3	94.5
7	0.78	1.39		0.01	34.70	0.43	0.01	0.49	21.1	34.6	93.5
8	0.21	1.45		0.01	34.00	0.57	0.01	0.48	18.5	42.5	97.7
9	0.32	1.10		0.01	34.90	0.50	0.01	0.49	15.7	45.2	98.2
10	0.64	2.01		0.01	34.00	0.59	0.01	0.51	14.0	47.6	99.4

(‡) Fe total and Fe^{2+} measured, and Fe^{3+} calculated by difference; ($) SiO_2 result excluded due to confirmed laboratory error

Table B4: Comparison of TiO_2 of the blended concentrate, detailing TiO_2, mass%

Composite	MINTEK laboratory	External Laboratory A
$\bar{x}$ ± 95% CI	35.4 ±0.7	34.5 ±0.6
σ	1.08	0.99
σ^2	1.17	0.98

(*) Calculated average based on the individual analysis of bags provided by the owner

APPENDIX C OPERATIONAL OVERVIEW AND DATA

An overview of the pilot-plant progression is provided for background and context. During the pilot test, detailed logs of the operation is maintained via logbooks, data sheets, and an electronic data sheet (spreadsheet). The latter is continuously updated with the latest chemical assays and operational data, which is used to assess progress, as decision support, and to track the condition of the furnace.

Warm-up and metallurgical stabilisation period

Approximately 46 tons of concentrate was processed during the warm-up and stabilisation. The main objective of these batches was to first warm-up the furnace after which metallurgical stabilisation could commence. The furnace was initially operated at a lower power after which the power was increased steadily from about 100 kW to 900 kW over a period of about 24 hours. During this period, the refractories and metal inventory was heated up. Small quantities of anthracite were sporadically added to minimise oxidation of the molten metal in the furnace. Regular furnace inspection was carried out to assess the warm-up progress and the formation of a molten pool. At the conclusion of the warm-up period, the heel was molten, and slow feeding of the concentrate recipe commenced. Reductant addition was initially conservatively adjusted as the reactivity and smelting behaviour of the anthracite was not known. A number of small batches were slowly fed to the furnace while periodic inspections were carried out to assess the bath condition. The first slag and metal taps were carried out at the end of the first batch. Upon completion of batch 6, the furnace warm-up was deemed complete, after which metallurgical stability was prioritised.

The operational objective of the stabilisation period was to establish a regular tapping regime, stabilise temperatures and achieve thermal stability. The primary metallurgical objectives of this period were to evaluate the performance of the anthracite and upgrade the TiO_2 content of the slag to about 85%. Anthracite addition was systematically increased from 13.4% to 20% (anthracite-to-concentrate mass ratio) while the slag composition was monitored to evaluate the anthracite performance.

The systematic increase in reduction (associated with the increased reductant addition and stabilisation of the operation) also resulted in an increase in energy consumption – as would be expected. The furnace warm-up commenced with an SER target of 1.2 kWh/kg total feed, and by the conclusion of the stabilisation period, the target had been increased to 1.36 kWh/kg total feed. The power-to-feed balance was adjusted based on both metallurgical and operational performance, including tapping temperatures, the conditions of the furnace bath and general operability.

Baseline Condition, Tap 25 to 32 (Period B)

The primary objective of the baseline condition was to achieve stable operating and metallurgical conditions; that is an operation that consistently reproduces a slag product with a TiO_2 content of approximately 85%. Minimal adjustments were made to the targets during these batches as the focus was on maintaining the stable conditions achieved towards the latter part of Period A.

Anthracite addition was 20% while the slag composition was monitored carefully to evaluate reproducibility. The SER target remained at 1.36 kWh/kg total feed for the duration of this period. The main challenges during this condition were to maintain stable operating conditions (metallurgically and thermally) while tapping slag and metal regularly. During Period B anthracite additions of about 20%, resulted in slags with a TiO_2 content consistently greater than 85%, and the FeO content below 10%. A freeze lining was maintained throughout this period as confirmed via the cumulative Mg accountability.

Smelting Intensity Condition, Tap 33 to 51 (Period C)

Following the metallurgical stabilisation and successful demonstration of the baseline condition, a secondary baseline condition with higher power followed. The main objective of this condition was to maintain the metallurgical targets but operate the furnace at higher average power. Systematic increases in smelting intensity form part of the experimental methodology to evaluate the energy requirement as accurately as possible. The average power for this period was about 100kW higher than for the Period B. The relatively conservative increase in power was to reduce risk and in an effort to maintain the freeze lining. The power flux for Period B was 380kW/m^2 while the power flux for the higher power period was about 410kW/m^2 (power flux is the power input expressed as a ratio of the hearth area and represents smelting intensity; smelting intensity is a design parameter that is used to determine the design diameter for a scaled-up furnace).

MgO and FeO concentration remained low in the slag, which indicates that the freeze lining was at least partially intact, despite the increase in smelting intensity. The increase in throughput (about 14% from Period B to C) and optimisation of the extraction from the furnace, most likely contributed to higher reductant efficiencies, a phenomenon often observed on pilot-plant furnaces. Deportment of minor elements to the metal phase also increased during this

condition; some elements were initially below the detection limits of the analytical techniques. The increased smelting intensity could have resulted in an increase in fuming of SiO(g) or Mg(g) due to the relatively high operating temperatures, combined with excess carbon may also have contributed to the variations that were observed. The raw materials were unfortunately mostly consumed and limited time was available to optimise the operating regime.

The anthracite addition was adjusted slightly from 20% to 19.5% about halfway through this condition, but this had minimal impact on the grade of the slag as the slag retained an average grade in excess of 90% TiO_2. The SER target remained at 1.36 kWh/kg total feed for the bulk of this operating period and was only decreased slightly towards the end of this condition to match the minor adjustment to the reductant addition.

Campaign Shutdown Condition, Tap 52 to 54 (Period D)

The final batches were used to conduct final measurements; primarily electrical properties and due to these interruptions, the final taps are excluded from the metallurgical condition. At the end of batch 54, the furnace was emptied. The objective was to drain the furnace as completely as possible. The furnace was subsequently allowed to cool, and the roof was removed after about 48 hours of cooling. Profile measurements of the wear and build-up were recorded, although much of the slag had decrepitated and minimal build-up remained on the sidewalls. Upon completion, the remaining slag and metal were removed together with the refractories and hand sorted for mass balance purposes.

Table C1: Feed and product masses, kg

Tap	Total Mass Fed	Concentrate Mass Fed	Anthracite Mass Fed (kg)	Spare Mass Fed	Electrode	Iron Scrap Fed	Total Products	Slag Tapped	Metal Tapped	Off-gas dust
1	7960.3	7004.3	936.0	20.0	180	1100	1382	518	864	0
2	2002.4	1736.7	265.7		0	0	1839	717	1122	0
3	2020.4	1749.7	270.7		90	0	2048	1571	477	0
4	2021.2	1750.3	270.9		0	0	1353	802	551	0
5	2039.4	1767.4	272.0		0	0	2310	1266	814	230
6	2039.2	1752.0	287.2		0	0	880	418	462	0
7	2047.9	1750.2	297.7		0	0	1280	428	852	0
8	2056.3	1750.3	306.0		0	0	1722	914	808	0
9	2056.6	1775.1	281.5		0	0	1607	954	653	0
10	2056.5	1750.6	305.9		0	0	1541	868	673	0
11	2057.2	1751.6	305.6		0	0	1098	152	946	0
12	2085.7	1760.8	324.9		0	0	1092	215	567	310
13	2083.6	1750.5	333.1		0	0	1095	480	615	0
14	1724.8	1452.0	272.8		90	0	1982	942	1040	0
15	2087.3	1755.4	331.9		0	0	952	427	525	0
16	2061.3	1730.8	330.5		0	0	1411	634	777	0
17	2083.4	1750.5	332.9		0	0	1545	596	949	0
18	2083.4	1753.8	329.6		0	0	2747	2236	269	242
19	2083.8	1752.0	331.8		0	0	1406	828	578	0
20	2094.5	1753.4	341.1		0	0	178	166	12	0
21	1048.9	878.2	170.7		0	0	125	125	0	0
22	2092.1	1750.7	341.4		0	0	1482	794	688	0
23	2093.7	1755.9	337.8		0	0	3389	1710	1679	0
24	2100.5	1739.5	361.0		0	0	1027	266	761	0
25	4219.9	3524.1	695.8		90	0	2197	186	2011	0
26	2263.9	1891.4	372.5		0	0	1441	259	870	312
27	2220.0	1850.0	370.0		0	0	2577	1415	872	290
28	2220.4	1848.2	372.2		0	0	1178	347	715	116
29	2220.7	1843.6	377.1		0	0	723	723	0	0
30	2220.2	1850.9	369.3		0	0	685	569	116	0
31	2220.2	1850.2	370.0		0	0	2557	405	1795	357
32	2220.4	1850.4	370.0		0	0	1412	178	1234	0
33	2220.7	1846.9	373.8		90	0	1453	1449	4	0
34	2269.5	1891.7	377.8		0	0	577	564	13	0
35	2244.5	1871.9	372.6		0	0	2526	0	2064	462
36	2261.9	1885.0	376.9		0	0	836	0	836	0
37	2404.2	2003.6	400.6		0	0	2257	832	995	430
38	2400.3	2000.3	400.0		0	0	1086	308	778	0
39	2400.0	2000.0	400.0		-90	0	2562	1344	1218	0
40	1880.2	1609.5	270.7		180	0	2286	1263	663	360
41	3227.1	2700.1	527.0		0	0	1613	369	1244	0
42	2390.7	1997.2	393.5		0	0	1806	573	875	358
43	2390.6	2005.8	384.8		0	0	1097	804	293	0
44	2394.0	2003.5	390.5		0	0	565	233	4	328
45	2393.6	2003.1	390.5		0	0	2132	623	1297	212
46	2390.5	2000.4	390.1		0	0	1142	855	1	286
47	2194.6	1832.9	361.7		0	0	2044	131	1675	238
48	2754.8	2304.9	449.9		0	0	3058	1029	1549	480
49	2754.7	2305.1	449.6		0	0	1417	1127	0	290
50	2749.5	2300.5	449.0		0	0	2237	757	1128	352
51	2749.4	2300.7	448.7		90	0	2181	463	1464	254
52	2749.6	2300.5	449.1		0	0	771	503	0	268
53	2749.6	2288.7	460.9		0	0	2922	634	2250	38
54	1695.7	1417.7	278.0		0	0	6285	2251	4000	34
55*	0.0						2348	2105	59	184

Table C2: Tapping temperature, availability and energy data

Tap	Slag tap Temp (°C)	Metal tap Temp (°C)	Total Energy Input (kWh)	Total Energy Loss (kWh)	Effective Energy (kWh)	Downtime (h)	Duration Tap-to-tap (h)	Power target (kW)	Average power (kW)	Losses estimate (kW)
1	1575	1546	22013	12633	9380	1.66	49.3	900	447	450
2	1494	1500	6000	3704	2296	0.61	7.6	900	793	490
3	1583	1683	5973	3552	2421	0.38	7.3	900	824	490
4	1754	1652	6069	3551	2518	0.20	7.1	900	860	520
5	1632	1666	6695	4164	2532	0.31	8.0	900	836	520
6	1651	1551	6727	4176	2551	0.17	8.0	900	837	520
7	1640	1682	6472	3854	2618	0.33	7.4	1000	873	520
8	1673	1624	5225	2549	2676	0.17	4.9	1200	1065	520
9	1691	1558	5395	2682	2713	0.39	5.2	1200	1045	520
10	1685	1651	5254	2561	2693	0.32	4.9	1200	1066	520
11	1650	1545	5587	2879	2708	0.25	5.5	1200	1008	520
12	1670	1607	5057	2381	2676	0.29	4.7	1200	1066	500
13	1679	1652	5027	2312	2715	0.08	4.6	1200	1086	500
14	1740	1556	5246	3313	1933	0.84	6.6	1200	791	500
15	1650	1725	6078	3324	2754	0.25	6.7	1200	914	500
16	1728	1668	6589	3884	2704	0.30	7.8	1200	848	500
17	1701	1483	8384	5611	2773	1.43	11.2	1200	747	500
18	1686	1701	5138	2355	2784	0.13	4.7	1200	1090	500
19	1697	1634	5397	2628	2769	0.52	5.3	1200	1026	500
20	1720	1720	5302	2513	2789	0.38	5.0	1200	1057	500
21	1705		2765	1377	1388	0.12	2.8	1200	999	500
22	1722	1746	5307	2523	2784	0.20	5.1	1200	1051	500
23	1713	1584	5440	2525	2915	0.12	5.1	1200	1077	500
24	1635	1666	5368	2496	2873	0.34	5.0	1200	1074	500
25	1782	1791	11647	6995	4652	3.56	14.1	1200	824	500
26	1775	1681	6055	2870	3185	0.12	5.7	1200	1054	500
27	1793	1593	5714	2647	3067	0.11	5.3	1200	1078	500
28	1761	1677	5703	2635	3068	0.22	5.3	1200	1081	500
29	1786	1800	5844	2743	3101	0.30	5.5	1200	1066	500
30	1750	1790	5878	2704	3174	0.29	5.4	1200	1085	500
31	1790	1693	5619	2582	3037	0.23	5.2	1200	1086	500
32	1778	1659	5750	2716	3034	0.03	5.4	1200	1057	500
33	1793	1693	5543	2566	2977	0.54	5.1	1300	1082	500
34	1800	1728	5456	2458	2999	0.57	4.9	1300	1106	500
35		1762	5566	2463	3103	0.35	4.9	1300	1129	500
36		1710	5235	2202	3032	0.20	4.4	1300	1187	500
37	1810	1762	5985	2815	3170	0.42	5.6	1300	1062	500
38	1773	1828	5596	2417	3179	0.30	4.8	1300	1157	500
39	1799	1725	6240	3007	3234	0.41	6.0	1300	1037	500
40	1783	1840	10769	10304	465	7.22	20.6	1300	522	500
41	1766	1694	7843	3483	4361	0.52	7.0	1300	1128	500
42	1765	1740	5819	2444	3375	0.16	4.9	1300	1188	500
43	1776	1742	5709	2364	3345	0.17	4.7	1300	1205	500
44	1786		5670	2463	3207	0.26	4.9	1300	1150	500
45	1786	1772	5806	2506	3300	0.13	5.0	1300	1161	500
46	1760	1795	5947	2651	3296	0.28	5.3	1300	1119	500
47	1770	1690	5662	2854	2808	0.73	5.7	1300	990	500
48	1792	1765	6696	3063	3633	0.36	5.5	1300	1206	500
49	1813		6552	2810	3742	0.23	6.2	1300	1056	500
50	1790	1681	6671	3019	3652	0.30	6.0	1300	1104	500
51	1796	1685	6556	2950	3606	0.38	5.9	1300	1113	500
52	1790		7305	3776	3529	0.77	7.6	1300	965	500
53	1784	1685	6637	2944	3693	0.29	5.9	1300	1125	500
54	1791	1685	5618	3090	2529	0.27	6.2	1300	909	500

Table C3: Average feed rates, anthracite addition and SER

Tap	Average total feed rate (kg/h)	Anthracite Addition Target (%)	Achieved Anthracite Addition (%)	Power flux (kW/m2)	SER, per ton of total feed (MWh/t)	Total energy consumption, per ton of total feed (MWh/t)	Conc. Feed rate flux (kg/m2)
1	167	13.4	13.4	146	1.230	2.772	46
2	288	15.3	15.3	272	1.140	2.996	79
3	294	15.5	15.5	274	1.200	2.956	80
4	294	15.5	15.5	279	1.250	3.002	80
5	265	16.5	15.4	274	1.240	3.283	72
6	259	16.5	16.4	269	1.250	3.299	70
7	289	17.5	17.0	288	1.280	3.160	78
8	434	17.5	17.5	348	1.300	2.541	117
9	431	17.5	15.9	357	1.320	2.623	117
10	446	17.5	17.5	359	1.310	2.555	120
11	389	17.5	17.4	333	1.320	2.716	104
12	468	18.5	18.5	357	1.280	2.425	124
13	459	19.0	19.0	349	1.300	2.413	121
14	298	19.0	18.8	286	1.120	3.041	79
15	326	19.0	18.9	299	1.320	2.912	86
16	276	19.0	19.1	278	1.310	3.196	73
17	213	19.0	19.0	270	1.330	4.024	56
18	454	19.0	18.8	353	1.340	2.466	121
19	439	19.3	18.9	359	1.330	2.590	116
20	452	19.5	19.5	361	1.350	2.531	119
21	396	19.5	19.4	329	1.360	2.636	104
22	432	19.5	19.5	345	1.330	2.537	114
23	425	19.8	19.2	348	1.390	2.598	112
24	450	20.0	20.8	363	1.370	2.556	118
25	399	20.0	19.7	347	1.102	2.760	105
26	402	20.0	19.7	339	1.410	2.675	106
27	428	20.0	20.0	347	1.380	2.574	112
28	439	20.0	20.1	355	1.380	2.568	115
29	429	20.0	20.5	355	1.400	2.632	112
30	433	20.0	20.0	361	1.430	2.648	114
31	449	20.0	20.0	358	1.370	2.531	118
32	410	20.0	20.0	335	1.370	2.590	108
33	484	20.0	20.2	381	1.340	2.496	127
34	520	20.0	20.0	394	1.320	2.404	137
35	490	20.0	19.9	383	1.380	2.480	129
36	537	20.0	20.0	392	1.340	2.314	141
37	461	20.0	20.0	362	1.320	2.489	121
38	529	20.0	20.0	389	1.320	2.331	139
39	428	20.0	20.0	350	1.350	2.600	112
40	140	20.0	16.8	253	0.250	5.728	38
41	501	19.5	19.5	384	1.350	2.430	132
42	504	19.5	19.7	387	1.410	2.434	133
43	524	19.5	19.2	394	1.400	2.388	138
44	513	19.5	19.5	383	1.340	2.368	135
45	491	19.5	19.5	375	1.380	2.425	129
46	475	19.5	19.5	372	1.380	2.488	125
47	440	19.5	19.7	357	1.280	2.580	116
48	531	19.5	19.5	407	1.320	2.431	140
49	461	19.5	19.5	345	1.360	2.378	122
50	479	19.5	19.5	366	1.330	2.426	126
51	499	19.5	19.5	375	1.310	2.385	132
52	405	19.5	19.5	339	1.280	2.657	107
53	490	19.5	20.1	373	1.340	2.414	129
54	287	19.5	19.6	299	1.490	3.313	76

APPENDIX D CHEMICAL COMPOSITION OF PRODUCTS

Table D1: Individual slag tap compositions, mass%

Tap	MgO	Al_2O_3	SiO_2	CaO	TiO_2	V_2O_5	Cr_2O_3	MnO	FeO	C	P	S	Total
1	8.11	3.05	2.65	0.25	55.55	0.78	0.34	1.38	27.34	0.03	0.001	0.01	99.4
2	8.11	2.91	2.25	0.21	56.55	0.82	0.30	1.06	28.17	0.02	0.001	0.01	100.4
3	8.43	2.82	2.14	0.21	56.40	0.83	0.27	1.00	23.94	0.02	0.001	0.01	96.0
4	11.10	2.73	2.38	0.22	57.40	0.84	0.27	0.94	23.93	0.04	0.001	0.01	99.8
5	9.40	2.91	2.24	0.21	58.35	0.87	0.25	0.96	19.93	0.02	0.001	0.01	95.1
6	10.70	2.97	2.41	0.21	64.65	0.85	0.23	0.94	20.26	0.01	0.013	0.01	103.2
7	9.78	2.84	2.32	0.21	67.20	0.89	0.25	0.95	18.98	0.02	0.003	0.01	103.4
8	10.05	2.95	2.69	0.19	71.70	0.92	0.29	0.97	17.05	0.02	0.008	0.01	106.8
9	11.00	2.88	2.52	0.19	70.00	0.92	0.28	0.95	17.14	0.03	0.006	0.01	105.9
10	10.10	2.97	2.26	0.20	67.30	0.89	0.24	0.91	17.82	0.02	0.009	0.01	102.7
11	9.59	3.04	2.46	0.20	68.22	0.92	0.22	0.96	16.65	0.02	0.002	0.01	102.3
12	8.29	3.18	2.47	0.18	70.75	0.98	0.21	0.98	15.93	0.02	0.009	0.01	103.0
13	7.73	2.87	2.36	0.17	72.40	0.98	0.22	0.98	16.15	0.03	0.012	0.01	103.9
14	9.20	3.03	3.51	0.23	74.92	1.09	0.18	0.88	11.95	0.03	0.024	0.01	105.0
15	8.30	3.14	2.65	0.18	77.81	1.00	0.13	1.09	11.17	0.02	0.003	0.01	105.5
16	7.58	3.19	2.43	0.17	79.58	1.11	0.13	1.12	10.45	0.02	0.019	0.01	105.8
17	7.45	3.51	2.43	-	75.29	1.06	0.16	1.10	13.85	0.02	0.005	0.01	104.9
18	7.60	3.18	2.35	0.20	74.40	0.98	0.14	1.01	13.12	0.03	0.017	0.01	103.0
19	5.86	3.39	2.21	0.21	76.40	1.02	0.19	1.00	14.53	0.02	0.020	0.01	104.8
20	5.34	3.41	2.20	0.20	77.25	1.00	0.19	0.95	14.64	0.30	0.021	0.01	105.2
21	4.82	3.43	2.19	0.20	78.10	0.91	0.18	0.91	14.76	0.03	0.005	0.01	105.5
22	4.32	3.39	2.11	0.19	78.60	1.06	0.16	1.03	12.87	0.02	0.003	0.01	103.7
23	4.05	3.22	2.18	0.19	80.10	1.05	0.15	1.05	10.17	0.02	0.028	0.01	102.2
24	3.74	3.64	2.35	0.18	83.70	1.00	0.13	1.14	7.79	0.05	0.020	0.01	103.7
25	3.38	3.51	2.34	0.18	85.35	0.97	0.12	1.09	5.79	0.02	0.012	0.01	102.7
26	3.28	3.70	2.23	0.17	85.25	1.01	0.12	1.12	5.48	0.02	0.026	0.01	102.4
27	3.73	3.58	2.14	0.17	85.95	0.84	0.19	1.61	5.71	0.02	0.038	0.01	103.9
28	4.81	3.45	2.51	0.17	86.00	0.96	0.14	1.13	4.96	0.02	0.035	0.01	104.1
29	4.51	3.72	2.65	0.17	85.70	0.97	0.13	1.07	5.18	0.02	0.007	0.01	104.1
30	4.45	3.48	2.68	0.17	86.75	0.92	0.12	1.05	4.14	0.02	0.013	0.01	103.8
31	4.33	3.61	2.51	0.17	87.68	0.91	0.12	1.06	3.98	0.02	0.025	0.01	104.4
32	4.16	3.61	2.43	0.17	87.60	0.86	0.11	1.05	4.00	0.02	0.003	0.01	104.0
33	4.34	3.63	2.73	0.19	87.90	0.81	0.10	1.01	3.59	0.01	0.012	0.01	104.3
34	4.33	3.83	2.55	0.20	88.50	0.78	0.09	0.98	2.72	0.02	0.028	0.01	104.0
37	3.34	3.84	1.66	0.16	90.20	0.61	0.07	0.80	2.34	0.03	0.006	0.01	103.0
38	4.80	3.86	1.58	0.17	91.85	0.55	0.06	0.76	1.57	0.02	0.012	0.01	105.2
39	2.95	3.84	1.31	0.17	92.49	0.51	0.05	0.73	1.11	0.02	0.011	0.01	103.1
40	3.06	3.87	1.40	0.17	92.20	0.40	0.07	0.52	1.35	0.03	0.011	0.01	103.0
41	3.06	4.02	1.72	0.19	89.40	0.62	0.11	0.80	3.13	0.02	0.023	0.01	103.0
42	3.45	3.96	1.78	0.20	89.20	0.60	0.10	0.76	3.33	0.02	0.011	0.01	103.4
43	3.25	3.78	1.80	0.18	88.95	0.51	0.09	0.67	3.85	0.04	0.020	0.01	103.1
44	3.05	3.61	1.82	0.17	88.70	0.42	0.08	0.58	4.36	0.06	0.030	0.01	102.8
45	2.91	3.61	1.89	0.17	90.85	0.37	0.08	0.64	3.20	0.01	0.010	0.01	103.7
46	2.81	3.60	1.74	0.16	90.50	0.38	0.11	0.64	3.37	0.02	0.014	0.01	103.3
47	2.99	3.60	2.02	0.17	90.15	0.71	0.11	0.85	3.08	0.02	0.014	0.01	103.7
48	2.83	3.53	1.87	0.16	90.60	0.62	0.09	0.77	2.79	0.02	0.014	0.01	103.3
49	2.82	3.53	1.84	0.15	90.75	0.66	0.11	0.82	2.66	0.02	0.011	0.01	103.3
50	2.87	3.46	1.78	0.16	91.40	0.61	0.08	0.81	1.66	0.02	0.011	0.01	102.8
51	2.68	3.60	1.77	0.17	90.85	0.65	0.06	0.83	1.86	0.02	0.016	0.01	102.5
52	2.62	3.59	1.63	0.16	91.95	0.63	0.06	0.85	1.63	0.02	0.016	0.01	103.1
53	2.76	3.52	1.57	0.16	91.90	0.61	0.17	0.79	1.48	0.02	0.014	0.01	103.0
54	2.70	3.90	1.64	0.18	90.65	0.61	0.13	0.75	2.09	0.02	0.031	0.01	102.6
55*	7.07	3.76	1.71	0.05	79.73	0.58	0.12	0.57	13.63	0.23	0.018	0.01	107.2

*Dig-out slag

Table D2: Semi-quantitative full element XRF scan of selected slag samples

		Tap 18 Slag	Tap 52 Slag	Tap 18 Slag	Tap 52 Slag
Al	%	<0.010	<0.009	<0.8	<0.9
Si	%	0.492	0.410	0.866	0.499
P	%	<0.005	<0.005	<0.5	<0.5
S	%	0.053	0.040	0.090	0.077
Cl	%	0.01	0.01	0.7	0.3
K	%	<0.01	<0.01	<0.012	<0.013
Ca	%	0.17	0.16	0.44	0.43
Ti	%	16.32	15.76	36.65	49.53
V	%	0.341	0.33	0.412	0.169
Cr	%	<0.006	<0.006	<0.7	<0.5
Mn	%	0.34	0.34	0.75	0.61
Fe	%	39.04	38.12	10.63	1.60
Co	ppm	527	431	334	311
Ni	ppm	<16.0	<16.0	9.9	14.6
Cu	ppm	297.5	277.8	91.7	68.1
Zn	ppm	440.8	457.5	45.9	39.1
Ga	ppm	45.6	45.7	17.2	16.4
Ge	ppm	<2.9	<2.6	<1.9	<1.9
As	ppm	5.10	<2.800	1.1	4.5
Se	ppm	<2.6	<2.5	1.2	1.0
Br	ppm	2.50	4.00	4.6	3.8
Rb	ppm	3.60	<2.100	<0.6	<0.6
Sr	ppm	4.90	3.50	8.0	8.6
Y	ppm	6.00	6.50	13.4	14.9
Zr	ppm	507.1	539.0	1282	1668
Nb	ppm	132.2	143.9	308.9	117.1
Mo	ppm	19.00	17.00	4.7	<6.4
Ag	ppm	<1.000	<1.200	<0.9	1.7
Cd	ppm	2.10	1.90	1.3	1.8
In	ppm	<0.7	<0.7	1.0	1.3
Sn	ppm	6.70	6.60	<0.8	<0.8
Sb	ppm	4.80	4.90	<1.0	2.8
Te	ppm	<1.1	<1.2	<1.1	<1.1
I	ppm	<2.3	<2.2	<2.1	1.5
Cs	ppm	4.60	<3.80	<3.7	<3.6
Ba	ppm	13.30	9.40	19.8	26.4
La	ppm	11.60	<7.80	12.1	17.3
Ce	ppm	<11.0	9.9	16.7	20.3
Hf	ppm	<28.0	<28.0	28.3	54.3
Ta	ppm	31.0	<31.0	24.4	22.6
W	ppm	<19.0	<18.0	23.9	27.8
Hg	ppm	9.40	<4.3	<3.0	<3.4
Tl	ppm	<4.6	<4.9	<2.7	1.8
Pb	ppm	16.7	25.7	8.2	4.1
Bi	ppm	<10.0	<11.0	<4.7	<2.6
Th	ppm	<9.7	<10.0	14.6	19.5
U	ppm	<5.8	<7.9	<6.7	<5.3

Table D3: Metal composition per tap, mass %

TAP	Al	Si	Ti	V	Cr	Mn	Fe	Ni	C	P	S	Total
1	0.01	0.01	0.01	0.01	0.01	0.01	99.70	0.05	0.11	0.033	0.02	99.96
2	0.01	0.01	0.01	0.01	0.01	0.01	99.50	0.04	0.32	0.028	0.02	99.95
3	0.01	0.01	0.01	0.01	0.01	0.01	99.30	0.03	0.55	0.036	0.02	99.99
4	0.01	0.01	0.01	0.01	0.01	0.01	99.40	0.03	0.44	0.026	0.01	99.95
5	0.01	0.01	0.01	0.01	0.01	0.01	99.00	0.03	0.76	0.041	0.03	99.91
6	0.01	0.01	0.01	0.01	0.01	0.01	98.70	0.03	1.10	0.029	0.01	99.92
7	0.01	0.01	0.01	0.01	0.01	0.01	98.00	0.02	1.82	0.030	0.01	99.94
8	0.01	0.01	0.01	0.02	0.02	0.01	97.50	0.07	2.19	0.028	0.03	99.88
9	0.01	0.01	0.01	0.02	0.02	0.01	97.60	0.03	2.26	0.029	0.01	99.99
10	0.01	0.01	0.01	0.02	0.02	0.01	97.50	0.01	2.33	0.026	0.01	99.94
11	0.01	0.01	0.01	0.02	0.01	0.01	97.60	0.01	2.25	0.024	0.01	99.95
12	0.01	0.01	0.01	0.03	0.02	0.01	97.50	0.01	2.37	0.028	0.01	99.99
13	0.01	0.01	0.01	0.03	0.02	0.01	97.60	0.01	2.28	0.031	0.01	100.01
14	0.01	0.01	0.01	0.02	0.01	0.01	97.50	0.01	2.39	0.027	0.01	99.99
15	0.01	0.01	0.01	0.05	0.02	0.01	97.90	0.01	1.92	0.028	0.01	99.96
16	0.01	0.01	0.01	0.04	0.02	0.01	97.20	0.01	2.59	0.023	0.01	99.92
17	0.01	0.01	0.01	0.04	0.02	0.01	97.10	0.01	2.71	0.039	0.01	99.96
18	0.01	0.01	0.01	0.04	0.02	0.01	97.10	0.01	2.70	0.020	0.01	99.92
19	0.01	0.01	0.01	0.04	0.01	0.01	97.20	0.01	2.67	0.024	0.01	99.99
20	0.01	0.01	0.01	0.04	0.01	0.01	97.20	0.01	2.65	0.021	0.01	99.97
21												
22	0.01	0.01	0.01	0.05	0.02	0.02	97.00	0.01	2.82	0.028	0.01	99.97
23	0.01	0.01	0.04	0.08	0.03	0.02	97.00	0.01	2.78	0.030	0.01	100.02
24	0.01	0.01	0.01	0.11	0.03	0.02	97.30	0.02	2.47	0.022	0.01	100.02
25	0.01	0.01	0.02	0.18	0.02	0.03	96.50	0.01	3.23	0.021	0.01	100.03
26	0.01	0.01	0.01	0.13	0.03	0.02	96.40	0.01	3.28	0.021	0.01	99.93
27	0.01	0.01	0.02	0.23	0.03	0.04	96.00	0.01	3.56	0.020	0.01	99.93
28	0.01	0.02	0.02	0.21	0.03	0.04	96.00	0.01	3.65	0.018	0.01	100.02
29												
30	0.01	0.04	0.04	0.29	0.03	0.05	95.90	0.01	3.58	0.020	0.01	99.97
31	0.01	0.05	0.05	0.31	0.03	0.06	96.90	0.01	2.53	0.022	0.01	99.97
32	0.01	0.05	0.04	0.31	0.04	0.08	96.10	0.05	3.20	0.022	0.03	99.92
33												
34												
35	0.01	0.26	0.11	0.50	0.04	0.13	96.00	0.01	2.94	0.018	0.01	100.01
36	0.02	0.45	0.15	0.50	0.04	0.09	95.90	0.01	2.83	0.025	0.01	100.02
37	0.01	0.34	0.14	0.50	0.04	0.09	96.40	0.01	2.44	0.012	0.01	99.97
38	0.02	0.57	0.40	0.66	0.03	0.13	95.30	0.01	2.83	0.017	0.01	99.97
39	0.01	0.78	0.28	0.68	0.04	0.18	95.40	0.01	2.54	0.019	0.01	99.94
40	0.01	0.58	0.17	0.43	0.03	0.13	96.50	0.01	2.09	0.010	0.01	99.95
41	0.01	0.06	0.03	0.17	0.02	0.04	96.90	0.01	2.64	0.026	0.01	99.91
42	0.08	0.24	0.10	0.34	0.03	0.07	96.30	0.01	2.72	0.021	0.01	99.92
43	0.01	0.19	0.09	0.37	0.03	0.08	96.40	0.01	2.77	0.022	0.01	100.01
44												0.00
45	0.01	0.16	0.07	0.32	0.02	0.07	96.50	0.01	2.81	0.018	0.01	99.99
46												
47	0.01	0.13	0.05	0.30	0.02	0.08	96.40	0.01	2.92	0.030	0.01	99.95
48	0.01	0.13	0.03	0.41	0.03	0.07	96.70	0.01	2.56	0.026	0.01	99.98
49												
50	0.01	0.27	0.08	0.46	0.03	0.08	96.10	0.01	2.86	0.021	0.01	99.92
51	0.01	0.32	0.12	0.43	0.02	0.10	96.00	0.01	2.90	0.017	0.01	99.93
52												
53	0.01	0.42	0.15	0.49	0.03	0.12	96.10	0.01	2.64	0.017	0.01	99.99
54	0.01	0.39	0.09	0.44	0.03	0.14	96.30	0.01	2.53	0.020	0.01	99.95

Greyed out cells indicate the following: Al <0.005%, Si <0.01%, Ti < 0.005%, V < 0.005%, Cr < 0.01%, Mn < 0.01%, Ni < 0.01%
Not all batches resulted in a successful metal tap. The blank lines represent such events.

Table D4: Off-gas dust composition, mass %

Tap	MgO	Al_2O_3	SiO_2	CaO	TiO_2	V_2O_5	Cr_2O_3	MnO	FeO	C	P	S	Total
5	5.23	1.57	5.73	0.58	15.70	0.28	1.47	0.837	61.75	3.76	0.14	0.02	97.06
12	5.61	1.47	3.78	0.30	18.00	0.35	0.34	1.03	62.84	2.53	0.14	0.03	96.42
18	4.50	0.81	4.56	1.18	22.60	0.44	0.44	1.06	59.95	1.41	0.13	0.09	97.17
26	3.27	1.62	4.52	0.24	27.05	0.45	0.24	1.08	56.60	1.56	0.11	0.04	96.77
27	3.46	1.58	4.85	0.32	24.50	0.42	0.42	1.03	57.14	2.04	0.12	0.11	95.98
28	5.28	1.35	5.70	0.42	19.50	0.40	0.60	1.08	58.49	2.04	0.13	0.11	95.09
31	4.13	1.95	6.55	0.24	41.20	0.61	0.19	1.79	40.40	1.54	0.10	0.02	98.72
35	4.25	1.92	6.93	0.26	42.80	0.55	0.23	1.87	37.82	2.10	0.10	0.04	98.86
37	5.75	1.89	8.94	0.24	41.60	0.46	0.15	2.28	35.51	1.39	0.09	0.04	98.33
40	5.13	2.23	8.56	0.05	42.85	0.47	0.13	1.86	32.98	1.54	0.10	0.05	95.94
42	5.19	2.26	8.63	0.05	41.00	0.37	0.14	2.54	33.74	0.85	0.08	0.02	94.86
44	4.72	2.67	7.18	0.05	40.80	0.44	0.42	1.96	34.28	1.31	0.08	0.02	93.94
45	6.87	2.41	8.61	0.45	35.45	0.42	1.72	1.86	34.69	1.99	0.07	0.02	94.55
46	9.48	2.80	10.60	0.72	27.70	0.38	3.10	1.84	35.63	1.13	0.09	0.08	93.55
47	5.09	2.61	8.38	0.24	35.80	0.46	0.77	1.83	36.53	1.39	0.09	0.03	93.23
48	5.00	2.40	8.00	0.13	40.40	0.44	1.05	1.87	34.10	1.20	0.08	0.03	94.71
49	4.07	2.66	7.16	0.13	42.60	0.43	0.44	1.61	33.20	2.97	0.08	0.05	95.40
50	3.52	2.17	7.68	0.21	43.40	0.44	0.13	2.04	34.28	1.50	0.09	0.02	95.48
51	4.38	2.31	7.78	0.21	42.10	0.41	0.12	2.45	33.83	1.74	0.08	0.01	95.42
52	3.84	2.39	7.50	0.21	44.10	0.40	0.13	2.04	32.39	1.94	0.07	0.03	95.04
53	3.44	2.24	7.15	0.22	45.00	0.44	0.17	3.12	33.65	1.46	0.08	0.04	97.02
54	3.85	2.33	6.71	0.23	44.00	0.46	0.20	3.64	33.38	1.18	0.09	0.02	96.08
55	4.40	2.43	7.56	0.16	41.70	0.40	0.46	3.34	32.30	1.95	0.07	0.02	94.78

Note: The 'Tap' number reflects the timing of the removal of the full bag and thus represents the composition of the dust produced during the preceding period. In some cases, bags were removed prior to commencing of a new operating regime.

Table D5: Average off-gas dust analyses for each operating condition, mass%

		MgO	Al_2O_3	SiO_2	CaO	TiO_2	V_2O_5	Cr_2O_3	MnO	FeO
Overall Batch 1 - 54	**W. Ave**	**4.86**	**2.09**	**7.20**	**0.28**	**36.18**	**0.44**	**0.55**	**1.82**	**40.66**
	$\bar{x}$	*4.80*	*2.09*	*7.09*	*0.30*	*35.65*	*0.43*	*0.57*	*1.92*	*41.11*
	σ	1.34	0.50	1.65	0.25	9.69	0.06	0.70	0.75	11.35
Period A Stabilisation Batch 7 - 24	**W. Ave**	**5.12**	**1.18**	**4.12**	**0.69**	**20.02**	**0.39**	**0.39**	**1.04**	**61.58**
	$\bar{x}$	*5.05*	*1.14*	*4.17*	*0.74*	*20.30*	*0.40*	*0.39*	*1.04*	*61.40*
	σ	0.78	0.47	0.56	0.62	3.25	0.06	0.07	0.03	2.05
Period B Baseline Batch 25 - 32	**W. Ave**	**3.82**	**1.69**	**5.41**	**0.28**	**30.25**	**0.49**	**0.31**	**1.30**	**51.57**
	$\bar{x}$	*4.03*	*1.63*	*5.40*	*0.30*	*28.06*	*0.47*	*0.36*	*1.24*	*53.16*
	σ	0.91	0.25	0.91	0.08	9.30	0.10	0.18	0.37	8.54
Period C High power flux Batch 33 - 51	**W. Ave**	**5.24**	**2.32**	**8.18**	**0.21**	**40.08**	**0.45**	**0.66**	**1.98**	**34.84**
	$\bar{x}$	*5.37*	*2.36*	*8.24*	*0.23*	*39.49*	*0.44*	*0.75*	*1.96*	*34.80*
	σ	1.62	0.30	1.04	0.20	4.75	0.05	0.92	0.25	1.46
Period D Shutdown Batch 52 - 54	**W. Ave**	**4.13**	**2.36**	**7.55**	**0.20**	**42.92**	**0.41**	**0.21**	**2.60**	**32.95**
	$\bar{x}$	*3.98*	*2.34*	*7.34*	*0.20*	*43.38*	*0.42*	*0.22*	*2.92*	*33.11*
	σ	0.41	0.07	0.42	0.03	1.41	0.03	0.14	0.66	0.72

Table D6: Semi-quantitative full element XRF scan of selected dust samples

		Dust 23/03 Sample A	**Dust 23/03 Sample B**
Al	%	<0.050	<0.011
Si	%	1.663	1.992
P	%	<0.5	<0.5
S	%	0.101	0.084
Cl	%	0.025	0.016
K	%	<0.20	<0.012
Ca	%	0.364	0.358
Ti	%	18.75	18.33
V	%	0.334	0.245
Cr	%	0.026	0.021
Mn	%	1.281	1.592
Fe	%	26.1	25.5
Co	ppm	371	401
Ni	ppm	75.0	61.5
Cu	ppm	722	640
Zn	ppm	6136	4849
Ga	ppm	106.9	88.1
Ge	ppm	6.9	7.1
As	ppm	27.8	19.9
Se	ppm	3.1	3.1
Br	ppm	6.7	7.4
Rb	ppm	5.4	4.9
Sr	ppm	6.0	5.9
Y	ppm	8.3	8.8
Zr	ppm	606.8	578.4
Nb	ppm	138.9	90.0
Mo	ppm	10.1	9.9
Ag	ppm	1.4	<1.0
Cd	ppm	2.1	2.4
In	ppm	4.3	2.6
Sn	ppm	24.3	21.5
Sb	ppm	6.8	4.6
Te	ppm	1.7	0.8
I	ppm	1.8	<2.3
Cs	ppm	5.6	<4.0
Ba	ppm	15.4	13.0
La	ppm	8.1	10.9
Ce	ppm	<3.0	<11.0
Hf	ppm	18.0	<31.0
Ta	ppm	41	<35.0
W	ppm	<2.0	<33.0
Hg	ppm	<2.0	<4.1
Tl	ppm	2.9	<5.0
Pb	ppm	158.4	128.5
Bi	ppm	<2.0	<6.8
Th	ppm	<2.0	<5.1
U	ppm	<2.0	<6.1

APPENDIX E PHASE CHEMICAL EVALUATION OF SELECTED SLAG SAMPLES

The results of the phase chemical evaluation of selected water-quenched slag samples are presented in this section. A summary is included in the main body of the report.

In the case of a naturally occurring concentrate, the presence of the impurities Mg and Al in particular and to some extent V, see the formation of a solid solution member phase referred to as M_3O_5. This phase can have the following stoichiometry: $(Fe^{2+},Mg^{2+},Ti^{4+})(Al^{3+},Ti^{3+},V^{3+})_2O_5$. Ti can exist in this phase in two oxidation states, that is as Ti^{4+} (e.g. TiO_2), and Ti^{3+} (e.g. Ti_2O_3). The analytical techniques employed do not distinguish between these two states. As a result analysis of the M_3O_5 phase expresses the total Ti concentration in this phase as TiO_2, which is not strictly correct and leads to a total for the analysis of this phase that exceeds 100%.

Table E1: Illustration of the impact of oxidation state on the analysis

Phase	Ti	O	Fe	Total Ti as TiO_2
TiO_2	59.9	40.1		100.0
Ti_3O_5	64.2	35.8		107.1
$FeTi_2O_5$	41.3	34.5	24.2	100.0
Ti_2O_3	66.6	33.3		111.1

E1 Slag sample from batch 32

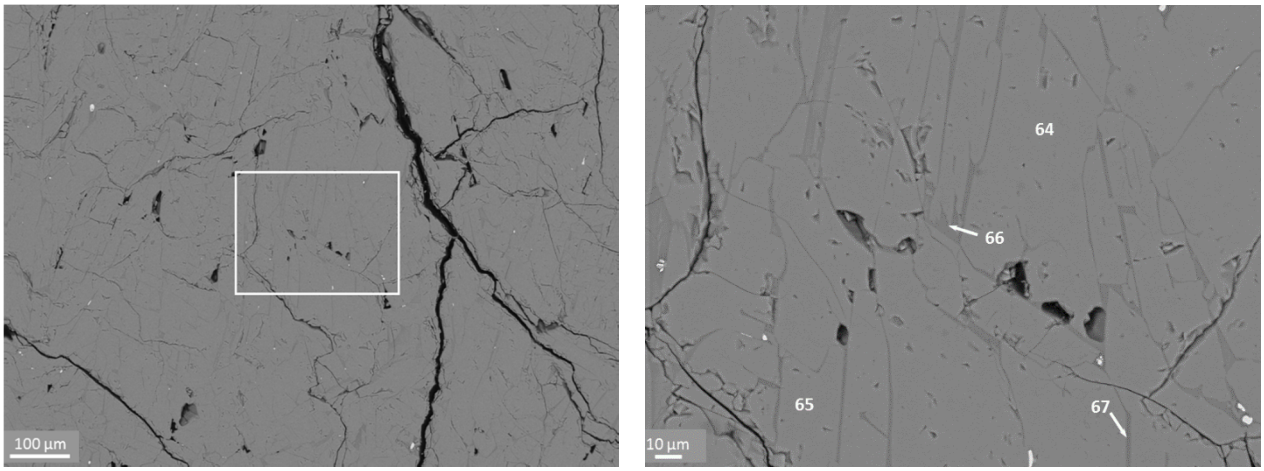

Figure E1: Backscattered electron micrographs of the slag from batch 32

The point analyses, for the points highlighted in Figure E1 (from the higher magnification of the zone highlighted on the left), is presented in Table E2.

Table E2: Microanalysis for slag from batch 32 and the average M_3O_5 composition, mass %

Point	MgO	Al_2O_3	SiO_2	CaO	TiO_2	Cr_2O_3	MnO	FeO	Total	Comments
64	3.22	3.09			103.2			0.98	110.5	M_3O_5
65	3.17	3.04			103.1			1.20	110.5	M_3O_5
66	8.70	10.4	28.9	1.91	17.0		8.73	22.9	98.4	Silicate
67	8.58	9.40	22.6	1.56	37.5		6.41	17.6	103.7	Silicate
Average WDS analyses of the M_3O_5 phase in slag from batch 32										
n=30	MgO	Al_2O_3	SiO_2	CaO	TiO_2		MnO	FeO	Total	
mean	3.33	3.11	0.18	0.03	95.37		0.29	1.45	103.76	
σ	0.23	0.16	0.32	0.03	1.46		0.12	0.54	0.75	

E2 Slag sample from batch 33

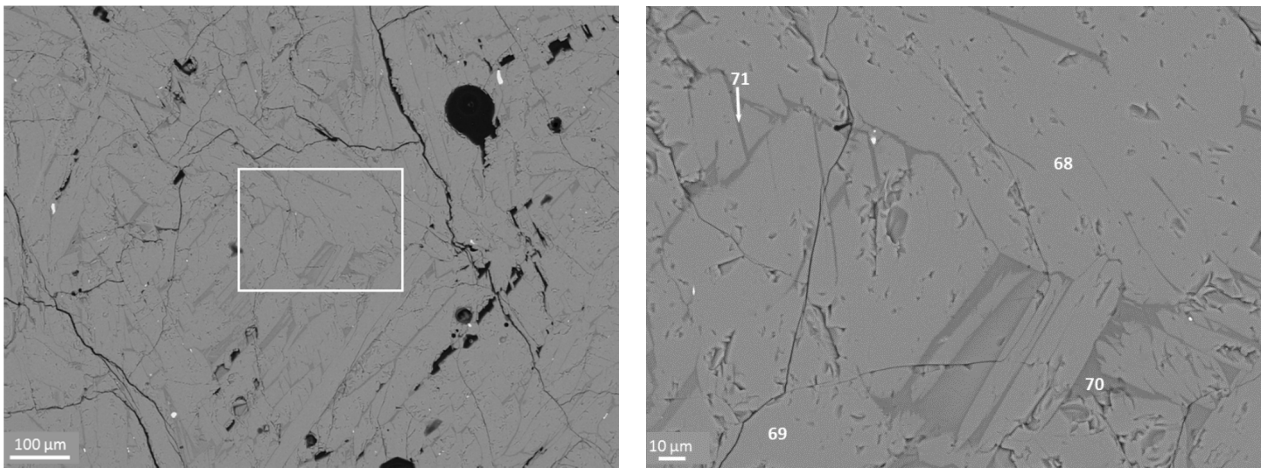

Figure E2: Backscattered electron micrographs of the slag from batch 33

The point analyses, for the points highlighted in Figure E2 (from the higher magnification of the zone highlighted on the left), is presented in Table E3.

Table E3: Microanalysis for slag from batch 33 and average M_3O_5 composition, mass %

Point	MgO	Al_2O_3	SiO_2	CaO	TiO_2	Cr_2O_3	MnO	FeO	Total	Comments
68	2.61	3.02			106.4			0.52	112.6	M_3O_5
69	3.12	3.00			106.2			0.83	113.2	M_3O_5
70	11.7	11.9	31.1	2.28	21.5		8.82	15.4	102.7	Silicate
71	9.45	10.1	24.0	1.56	35.5		7.35	14.6	102.6	Silicate
Average WDS analyses of the M_3O_5 phase in slag from batch 33										
n=27	MgO	Al_2O_3	SiO_2	CaO	TiO_2		MnO	FeO	Total	
Average	3.20	3.12	0.23	0.02	96.26		0.29	1.15	104.28	
σ	0.28	0.16	0.35	0.02	1.53		0.12	0.39	0.56	

E3 Slag sample from batch 38

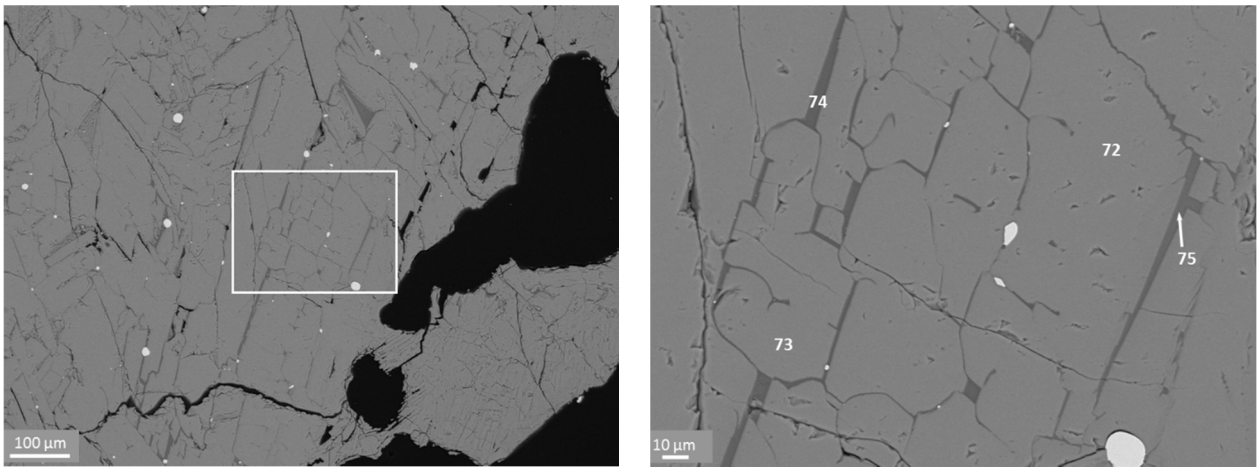

Figure E3: Backscattered electron micrographs of the slag from batch 38

The point analyses, for the points highlighted in Figure E3 (from the higher magnification of the zone highlighted on the left), is presented in Table E4.

Table E4: Microanalysis for the slag from batch 38 and average M_3O_5 composition, mass %

Point	MgO	Al_2O_3	SiO_2	CaO	TiO_2	Cr_2O_3	MnO	FeO	Total	Comments
72	1.88	3.08			107.6			0.25	112.8	M_3O_5
73	1.78	2.79			107.2			0.22	111.9	M_3O_5
74	18.6	18.3	25.9	3.00	26.9		10.1	-	102.8	Silicate
75	13.2	16.4	31.2	3.47	14.8		10.4	-	89.4	Silicate
Average WDS analyses of the M_3O_5 phase in slag from batch 38										
n=32	MgO	Al_2O_3	SiO_2	CaO	TiO_2		MnO	FeO	Total	
Average	1.86	3.00	0.09	0.01	100.24		0.14	0.26	105.59	
σ	0.41	0.54	0.05	0.01	0.88		0.06	0.09	1.05	

E4 Slag sample from batch 39

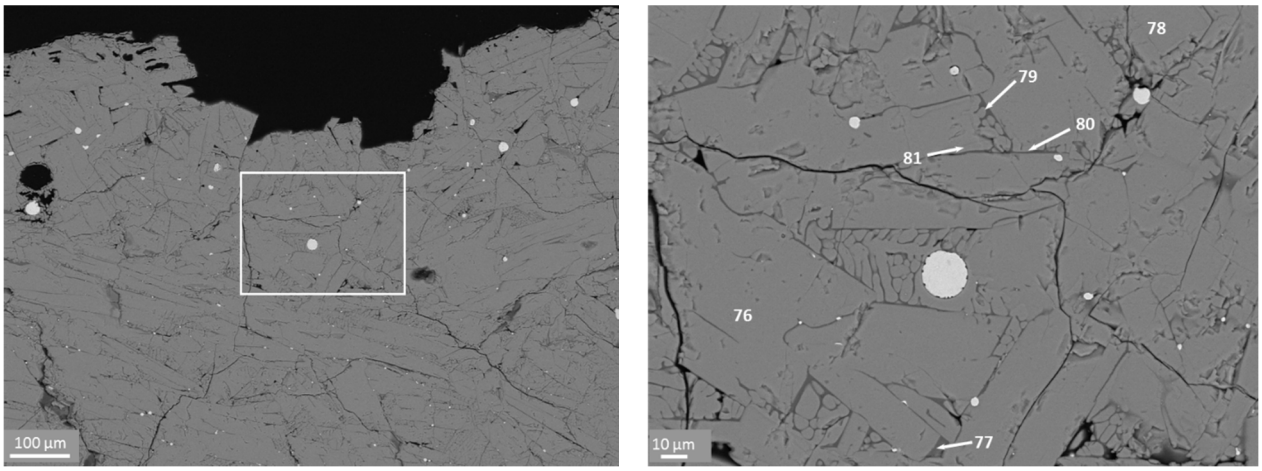

Figure E4: Backscattered electron micrographs of the slag from batch 39

The point analyses, for the points highlighted in Figure E4 (from the higher magnification of the zone highlighted on the left), is presented in Table E5.

Table E5: Microanalysis for slag from batch 39 and average M_3O_5 composition, mass %

Point	MgO	Al_2O_3	SiO_2	CaO	TiO_2	Cr_2O_3	MnO	FeO	Total	Comments
76	1.66	2.93	0.30		106.9				111.8	M_3O_5
77	14.7	22.0	29.8	4.07	16.0		8.85		95.4	Silicate
78	1.81	3.13	0.35		106.4				111.7	M_3O_5
79	10.8	19.3	25.2	3.69	23.2		7.49		89.6	Silicate
80	5.34	2.87	0.36		102.1		1.38		112.0	M_3O_5
81	6.62	3.71	1.36		99.4		1.88		113.0	M_3O_5
Average WDS analyses of the M_3O_5 phase in slag from batch 39										
n=32	MgO	Al_2O_3	SiO_2	CaO	TiO_2		MnO	FeO	Total	
Average	1.79	3.15	0.09	0.02	99.89		0.14	0.25	105.33	
σ	0.31	0.24	0.07	0.01	2.60		0.07	0.15	2.51	

E5 Slag sample from batch 48

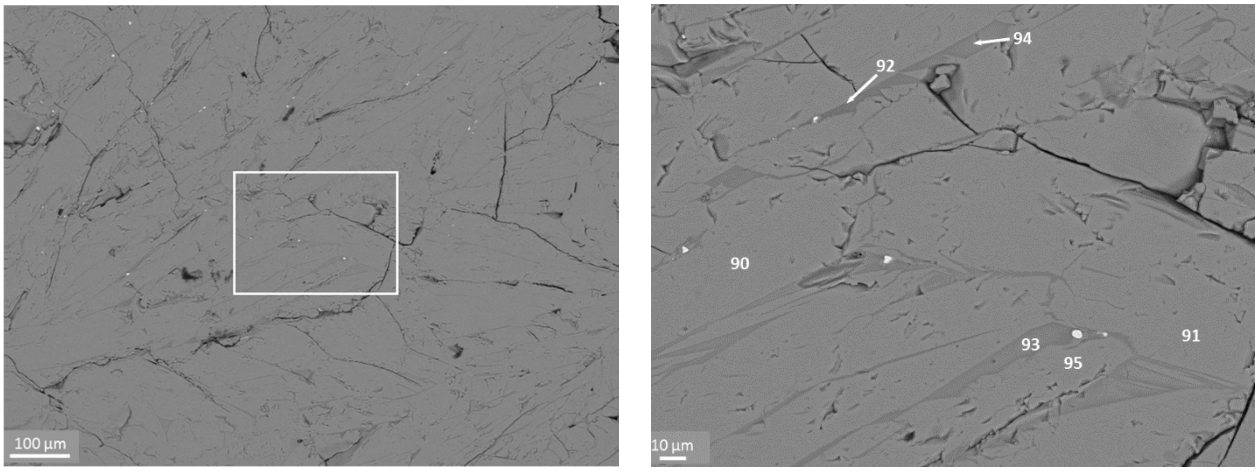

Figure E5: Backscattered electron micrographs of the slag from batch 48

The point analyses, for the points highlighted in Figure E5 (from the higher magnification of the zone highlighted on the left), is presented in Table E6.

Table E6: Microanalysis for slag from batch 48 and average M_3O_5 composition, mass %

Point	MgO	Al_2O_3	SiO_2	CaO	TiO_2	Cr_2O_3	MnO	FeO	Total	Comments
90	2.38	3.19	0.28		105.7				111.6	M_3O_5
91	2.50	3.21			102.8				108.5	M_3O_5
92	7.88	12.7	34.7	3.39	16.0		11.5		86.2	Silicate
93	6.18	10.2	27.7	2.68	22.3		9.18		78.2	Silicate
94	6.29	11.9	32.1	2.62	15.1		9.01		77.0	Silicate
95	6.08	11.1	28.4	2.46	17.0		8.92		74.0	Silicate
Average WDS analyses of the M_3O_5 phase in slag										
n=34	MgO	Al_2O_3	SiO_2	CaO	TiO_2		MnO	FeO	Total	
Average	2.21	3.05	0.12	0.02	97.24		0.22	1.08	103.94	
σ	0.59	0.56	0.15	0.02	1.73		0.15	0.73	1.77	

E6 Slag sample from batch 50

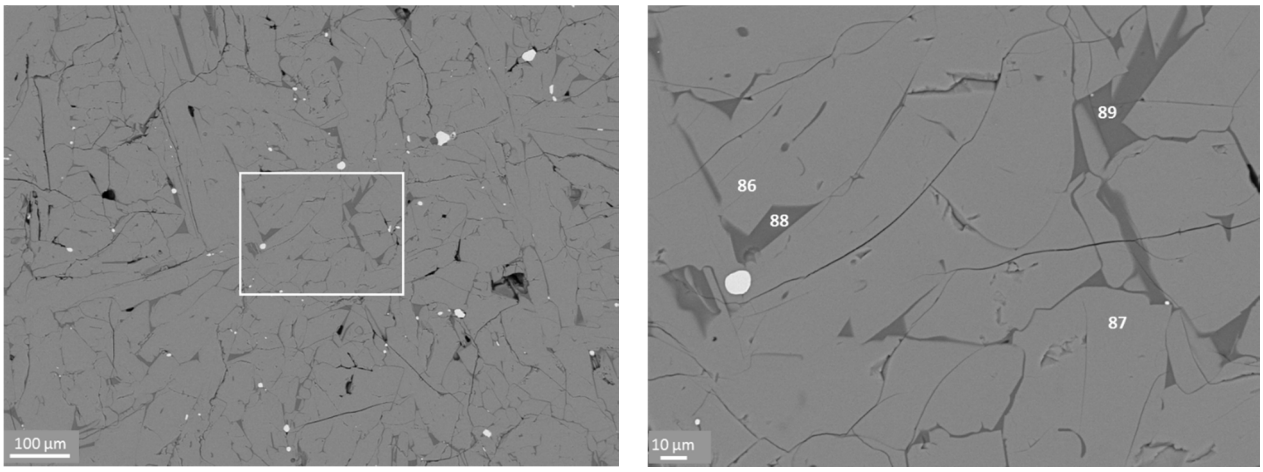

Figure E6: Backscattered electron micrographs of the slag from batch 50

The point analyses, for the points highlighted in Figure E6 (from the higher magnification of the zone highlighted on the left), are presented in Table E7.

Table E7: Microanalysis for slag from batch 50 and average M_3O_5 composition, mass %

Point	MgO	Al_2O_3	SiO_2	CaO	TiO_2	Cr_2O_3	MnO	FeO	Total	Comments
86	1.87	2.91			107.6				112.4	M_3O_5
87	1.94	2.87			107.6				112.4	M_3O_5
88	12.6	16.3	39.3	3.83	11.14		11.7		94.8	Silicate
89	13.0	15.6	37.2	3.67	11.75		11.5		92.6	Silicate
Average WDS analyses of the M_3O_5 phase in slag										
n=28	MgO	Al_2O_3	SiO_2	CaO	TiO_2		MnO	FeO	Total	
Average	2.20	3.23	0.22	0.03	98.81		0.25	0.74	105.48	
σ	0.45	0.31	0.54	0.05	2.02		0.20	0.33	0.63	

APPENDIX F ELEMENTAL MASS BALANCES FOR SUB-PERIODS

In order to minimise the effects of dust hold-up in the system, the overall weighted average dust composition was used for both periods. The overall dust mass collected was apportioned equally to all periods.

Table F1: Elemental mass balance and recovery of elements Tap 27 to 35

	Mass IN	Elemental Mass Fed, kg								
	kg	Mg	Al	Si	Ca	Ti	V	Cr	Mn	Fe
Concentrate	16704	68.5	108.7	82.7	3.6	3416.3	44.9	9.1	63.9	7160.7
Anthracite	3353	2.8	2.1	5.5	7.2					185.0
Other	90									
Total		71.3	110.9	88.2	10.8	3416.3	44.9	9.1	63.9	7345.8

	Mass OUT	Elemental Product Mass, kg								
	kg	Mg	Al	Si	Ca	Ti	V	Cr	Mn	Fe
Slag	5650	144.41	108.2	66.24	7.29	2944.1	27.35	5.08	51.74	194.1
Metal	6813		0.34	7.16		3.9	23.52	2.37	5.44	6541.4
Off gas dust	1041	29.57	11.4	34.52	1.95	227.1	2.58	0.71	14.31	331.1
Total		174.0	120.0	107.9	9.2	3175.1	53.4	8.2	71.5	7066.6
Unaccounted	kg	-102.7	-9.1	-19.7	1.5	241.2	-8.5	1.0	-7.6	279.2
Accountability	%	243.9	108.2	122.3	85.8	92.9	119.0	89.2	111.9	96.2

		Recovery and Distribution, %								
		Mg	Al	Si	Ca	Ti	V	Cr	Mn	Fe
Recovery [@]			0.3	8.1		0.1	52.4	25.9	8.5	89.1
Distribution [*]	Slag	83.0	90.2	61.4	78.9	92.7	51.2	62.2	72.4	2.7
	Metal		0.3	6.6		0.12	44.0	29.0	7.6	92.6
	Dust	17.0	9.5	32.0	21.1	7.2	4.8	8.7	20.0	4.7
Total		100.0	100.0	100.0	100.0	100.0	100.0	100.0	100.0	100.0

Slag	Mass	MgO	Al_2O_3	SiO_2	CaO	TiO_2	V_2O_5	Cr_2O_3	MnO	FeO
W. Ave	5650	4.24	3.62	2.51	0.18	86.93	0.9	0.13	1.18	4.42
Average	628	4.33	3.61	2.52	0.18	87.01	0.88	0.13	1.12	4.29

Metal	Mass	Ti	V	Cr	Mn	Fe	C	P	S	Total
W. Ave	6813	0.06	0.35	0.03	0.08	96.01	3.036	0.020	0.009	99.72
Average	852	0.05	0.31	0.03	0.07	96.15	3.24	0.020	0.009	99.88

Dust	Mass	MgO	Al_2O_3	SiO_2	CaO	TiO_2	V_2O_5	Cr_2O_3	MnO	FeO
W. Ave	1041	4.71	2.07	7.10	0.26	36.38	0.44	0.10	1.78	40.91
Average	116	4.71	2.07	7.10	0.26	36.38	0.44	0.10	1.78	40.91

([@]) Recovery to metal = metal/feed ; ([*]) slag/(metal+slag+dust) or metal/(metal+slag+dust)

Table F2: Elemental mass balance and recovery of elements Tap 48 to 53

	Mass IN	Elemental Mass Fed, kg								
	kg	Mg	Al	Si	Ca	Ti	V	Cr	Mn	Fe
Concentrate	19637	80.5	127.8	97.3	4.2	4016.1	52.8	10.7	75.1	8418.1
Anthracite	3850	3.2	2.4	6.3	8.3					212.4
Other	90									
Total		83.8	130.3	103.6	12.5	4016.1	52.8	10.7	75.1	8630.5

	Mass OUT	Elemental Product Mass, kg								
	kg	Mg	Al	Si	Ca	Ti	V	Cr	Mn	Fe
Slag	6122	103.55	114.98	50.94	6.99	3339.0	19.57	4.21	36.33	116.7
Metal	9364	0.00	0.47	23.45	0.00	8.09	38.15	2.37	8.40	9015.9
Off gas dust	1041	29.57	11.41	34.52	1.95	227.1	2.58	0.71	14.31	331.14
Total		133.1	126.9	108.9	8.9	3574.2	60.3	7.3	59.0	9463.7
Unaccounted	kg	-49.3	3.4	-5.4	3.5	441.9	-7.5	3.5	16.1	-833.2
Accountability	%	158.9	97.4	105.2	71.8	89.0	114.2	67.8	78.6	109.7

		Recovery and Distribution, %								
		Mg	Al	Si	Ca	Ti	V	Cr	Mn	Fe
Recovery [@]			0.4	22.6		0.2	72.2	22.0	11.2	104.5
Distribution [*]	Slag	77.8	90.6	46.8	78.2	93.4	32.5	57.7	61.5	1.2
	Metal		0.4	21.5		0.23	63.3	32.5	14.2	95.3
	Dust	22.2	9.0	31.7	21.8	6.4	4.3	9.8	24.2	3.5
Total		100.0	100.0	100.0	100.0	100.0	100.0	100.0	100.0	100.0

Slag	Mass	MgO	Al_2O_3	SiO_2	CaO	TiO_2	V_2O_5	Cr_2O_3	MnO	FeO
W. Ave	6122	2.80	3.55	1.78	0.16	90.99	0.6	0.10	0.77	2.45
Average	680	2.81	3.56	1.79	0.16	90.99	0.58	0.10	0.78	2.41

Metal	Mass	Ti	V	Cr	Mn	Fe	C	P	S	Total
W. Ave	9364	0.09	0.407	0.025	0.090	96.28	2.77	0.02	0.01	99.69
Average	1040	0.08	0.40	0.025	0.087	96.30	2.78	0.02	0.01	99.70

Dust	Mass	MgO	Al_2O_3	SiO_2	CaO	TiO_2	V_2O_5	Cr_2O_3	MnO	FeO
W. Ave	1041	4.71	2.07	7.10	0.26	36.38	0.44	0.10	1.78	40.91
Average	116	4.71	2.07	7.10	0.26	36.38	0.44	0.10	1.78	40.91

([@]) metal/feed ; ([*]) slag/(metal+slag+dust) or metal/(metal+slag+dust)

APPENDIX G PYROSIM OUTPUT REPORT

Pilot-plant Simulation - Batch 27 to 35

PILOT-PLANT MODEL for Batch 27-35

FLOWRATES

	FLOWRATE (kg/h)	TEMPERATURE (øC)
FEED 1		
##2TiMagConc-35%	10000	25
##1Anthracite	2000	25
Refractory	130	25
PRODUCTS 1		
Solids	345	1800
Slag	3770	1800
Metal	4138	1750
TO NEXT UNIT		
Gas	2971	1600
Dust	500	1600
FEED 2		
PRODUCTS 2		
Gas	2898	1600
Slag	573	1600

OPERATION

UNIT 1

General Empirical model allows the user to specify ratios and percentages in streams
ELEMENTS: C O H Mg Mn N Si S Al Ca Cr Fe K Na P V Zr Ti Ni
Gas: CO CO2 H2 Mg Mn N2 O2 SiO SO2 VOL.
Slag: Al2O3(l) CaO(l) Cr2O3 Fe FeO K2O MgO(l) MnO Na2O P4O10 S SiO2(l) V2O5 ZrO2
Ti3O5(l) TiO2(l) NiO
Metal: C Cr Fe Mn P S Si Ti V Ni
Solids (pure phases): C

1.500% O2 in Gas
0.001% VOL. in Gas
0.500% Fe in Slag
0.010% S in Slag
3.040% C in Metal
0.025% P in Metal
0.009% S in Metal
0.060% Ti in Metal

CO2 in Gas / CO in Gas (mass ratio) = .0001
FeO in Slag / Fe in Metal (molar ratio) = .0297
V in Metal / V2O5 in Slag (mass ratio) = .2946
Cr2O3 in Slag / Cr in Metal (molar ratio) = 1.0718
Mn in Metal / MnO in Slag (molar ratio) = .1049
MnO in Slag / Mn in Gas (molar ratio) = 8.1
SiO in Gas / SiO2(l) in Slag (molar ratio) = .2237
Si in Metal / SiO2(l) in Slag (molar ratio) = .1079
Mg in Gas / MgO(l) in Slag (molar ratio) = .25
Ti3O5(l) in Slag / TiO2(l) in Slag (mass ratio) = 1.3233

Operating temperature = 1800øC
Operating pressure = 1.00 atm
Dust loss = 0%
Slag : Metal ratio = 0.91

UNIT 2

Equilibrium model calculates multi-phase multi-reaction equilibrium
ELEMENTS: C O H K N S Al Ca Cr Fe Mg Mn P Si Ti V Zr
Gas: CO CO2 H2 K N2 SO2 VOL.
Slag: Al2O3(l) C CaO(l) Cr2O3 Fe2O3 MgO(l) MnO P S SiO2(l) TiO2 V2O5 ZrO2

Operating temperature = 1600øC
Operating pressure = 1.00 atm

ENERGY

UNIT 1 requires 11500 kWh (41300 MJ) per hour of operation, including a rate of energy loss of 0 kW
This is 2.78 MWh per ton of Metal produced in this unit
UNIT 2 requires -400 kWh (-1440 MJ) per hour of operation, including a rate of energy loss of 0 kW

ANALYSES
(MASS %)

	Al	Al2O3	Al2O3(l)	C	CaCO3	CaO	CaO(l)	CO	CO2	Cr	Cr2O3
FEED 1											
##2TiMagConc-35%	.....	1.230	.....	0.020	.....	0.030	.....	.....	.....	.....	0.010
##1Anthracite	.....	.....	.....	79.000	.....	0.300	.....	.....	.....	.....	.....
Refractory	.....	.....	.....	.....	.....	.....	.....	.....	.....	.....	.....
PRODUCTS 1											
Solids	.....	.....	.....	100.000	.....	.....	.....	.....	.....	.....	.....
Slag	.....	.....	3.099	.....	.....	.....	0.233	.....	.....	.....	0.017
Metal	.....	.....	.....	3.040	.....	.....	.....	.....	.....	0.005	.....
TO NEXT UNIT											
Gas(vol %)	.....	.....	.....	.....	.....	.....	.....	86.406	0.005	.....	.....
Gas	.....	.....	.....	.....	.....	.....	.....	95.100	0.010	.....	.....
Dust	.....	1.230	.....	3.180	.....	0.042	.....	.....	.....	.....	0.010
FEED 2											
PRODUCTS 2											
Gas(vol %)	.....	.....	.....	.....	.....	.....	.....	88.195	0.023	.....	.....
Gas	.....	.....	.....	.....	.....	.....	.....	97.862	0.040	.....	.....
Slag	.....	.....	1.073	2.312	.....	.....	0.037	.....	.....	.....	0.009

	CrO	Fe	Fe2O3	Fe3C	Fe3O4	Fe3Si	FeO	FeS	FeTiO3	H2	H2O
FEED 1											
##2TiMagConc-35%	.....	.....	.....	.....	20.144	.....	17.386	.....	38.664	.....	1.000
##1Anthracite	.....	.....	.....	.....	.....	.....	7.090	.....	.....	.....	1.680
Refractory	.....	.....	.....	.....	.....	.....	.....	.....	.....	.....	.....
PRODUCTS 1											
Solids	.....	.....	.....	.....	.....	.....	.....	.....	.....	.....	.....
Slag	.....	0.500	.....	.....	.....	.....	4.046	.....	.....	.....	.....
Metal	.....	96.472	.....	.....	.....	.....	.....	.....	.....	.....	.....

TO NEXT UNIT											
Gas(vol %)	.....	.....	.....	.....	.....	.....	.....	.....	.....	10.155	.....
Gas	.....	.....	.....	.....	.....	.....	.....	.....	.....	0.806	.....
Dust	.....	.....	.....	.....	20.141	.....	17.667	.....	38.659	.....	1.067
FEED 2											
PRODUCTS 2											
Gas(vol %)	.....	.....	.....	.....	.....	.....	.....	.....	.....	10.660	.....
Gas	.....	.....	.....	.....	.....	.....	.....	.....	.....	0.853	.....
Slag	.....	.....	53.056	.....	.....	.....	.....	.....	.....	.....	.....

	K	K2O	Mg	MgCO3	MgO	MgO(l)	Mn	MnO	MnO2	N2	Na
FEED 1											
##2TiMagConc-35%	.....	.....	.....	.....	0.680	.....	.....	0.490	.....	.....	.....
##1Anthracite	.....	.....	.....	.....	0.140	.....	.....	.....	.....	.....	.....
Refractory	.....	.....	.....	.....	97.500	.....	.....	.....	.....	.....	.....
PRODUCTS 1											
Solids	.....	.....	.....	.....	.....	.....	.....	.....	.....	.....	.....
Slag	.....	.....	.....	.....	.....	4.119	.....	1.005	.....	.....	.....
Metal	.....	.....	.....	.....	.....	.....	0.074	.....	.....	.....	.....
TO NEXT UNIT											
Gas(vol %)	.....	.....	0.825	.....	.....	.....	0.056	.....	.....	1.084	.....
Gas	.....	.....	0.788	.....	.....	.....	0.122	.....	.....	1.193	.....
Dust	.....	.....	.....	.....	0.686	.....	.....	0.490	.....	.....	.....
FEED 2											
PRODUCTS 2											
Gas(vol %)	.....	.....	.....	.....	.....	.....	.....	.....	.....	1.122	.....
Gas	.....	.....	.....	.....	.....	.....	.....	.....	.....	1.245	.....
Slag	.....	.....	.....	.....	.....	7.372	.....	1.244	.....	.....	.....

	Na2O	O2	P	P4O10	S	Si	SiO	SiO2	SiO2(l)	SO2	SO3
FEED 1											
##2TiMagConc-35%	.....	.....	.....	0.072	0.010	.....	.....	1.060	.....	.....	.....
##1Anthracite	.....	.....	.....	.....	0.005	.....	.....	0.350	.....	.....	.....
Refractory	.....	.....	.....	.....	.....	.....	.....	2.500	.....	.....	.....
PRODUCTS 1											
Solids	.....	.....	.....	.....	.....	.....	.....	.....	.....	.....	.....
Slag	.....	.....	.....	0.119	0.010	.....	.....	.....	2.209	.....	.....
Metal	.....	.....	0.025	.....	0.009	0.101	.....	.....	.....	.....	.....
TO NEXT UNIT											
Gas(vol %)	.....	1.193	.....	.....	.....	.....	0.266	.....	.....	0.008	.....
Gas	.....	1.500	.....	.....	.....	.....	0.460	.....	.....	0.020	.....
Dust	.....	.....	.....	0.072	0.010	.....	.....	1.074	.....	.....	.....
FEED 2											
PRODUCTS 2											
Gas(vol %)	.....	.....	.....	.....	.....	.....	.....	.....	.....	.....	.....
Gas	.....	.....	.....	.....	.....	.....	.....	.....	.....	.....	.....
Slag	.....	.....	0.027	.....	0.061	.....	.....	.....	4.187	.....	.....

	Ti	Ti2O3	Ti3O5	Ti4O7	Ti5O9	Ti6O11	Ti7O13	Ti8O15	TiC	TiO	TiO2
FEED 1											
##2TiMagConc-35%	.....	.....	.....	.....	.....	.....	.....	.....	.....	.....	14.145
##1Anthracite	.....	.....	.....	.....	.....	.....	.....	.....	.....	.....	0.280
Refractory	.....	.....	.....	.....	.....	.....	.....	.....	.....	.....	.....
PRODUCTS 1											
Solids	.....	.....	.....	.....	.....	.....	.....	.....	.....	.....	.....
Slag	.....	.....	.....	.....	.....	.....	.....	.....	.....	.....	.....
Metal	0.060	.....	.....	.....	.....	.....	.....	.....	.....	.....	.....
TO NEXT UNIT											
Gas(vol %)	.....	.....	.....	.....	.....	.....	.....	.....	.....	.....	.....
Gas	.....	.....	.....	.....	.....	.....	.....	.....	.....	.....	.....
Dust	.....	.....	.....	.....	.....	.....	.....	.....	.....	.....	14.154
FEED 2											
PRODUCTS 2											
Gas(vol %)	.....	.....	.....	.....	.....	.....	.....	.....	.....	.....	.....
Gas	.....	.....	.....	.....	.....	.....	.....	.....	.....	.....	.....
Slag	.....	.....	.....	.....	.....	.....	.....	.....	.....	.....	30.108

	V	V2O3	V2O4	V2O5	V4O7	VO	VO2	VOL.	Zr	ZrO	ZrO2
FEED 1											
##2TiMagConc-35%	.....	.....	.....	0.480	.....	.....	.....	0.500	.....	.....	0.110
##1Anthracite	.....	.....	.....	.....	.....	.....	.....	10.700	.....	.....	.....
Refractory	.....	.....	.....	.....	.....	.....	.....	.....	.....	.....	.....
PRODUCTS 1											
Solids	.....	.....	.....	.....	.....	.....	.....	.....	.....	.....	.....
Slag	.....	.....	.....	0.793	.....	.....	.....	.....	.....	.....	0.277
Metal	0.213	.....	.....	.....	.....	.....	.....	.....	.....	.....	.....
TO NEXT UNIT											
Gas(vol %)	.....	.....	.....	.....	.....	.....	.....	0.001	.....	.....	.....
Gas	.....	.....	.....	.....	.....	.....	.....	0.001	.....	.....	.....
Dust	.....	.....	.....	0.480	.....	.....	.....	0.928	.....	.....	0.110
FEED 2											
PRODUCTS 2											
Gas(vol %)	.....	.....	.....	.....	.....	.....	.....	.....	.....	.....	.....
Gas	.....	.....	.....	.....	.....	.....	.....	.....	.....	.....	.....
Slag	.....	.....	.....	0.419	.....	.....	.....	.....	.....	.....	0.096

	Ti2O3(l)	Ti3O5(l)	TiO2(l)	Ni	NiO	SO3
FEED 1						
##2TiMagConc-35%	.....	.....	.....	.....	.....	.....
##1Anthracite	.....	.....	.....	.....	.....	.....
Refractory	.....	.....	.....	.....	.....	.....
PRODUCTS 1						
Solids	.....	.....	.....	.....	.....	.....
Slag	.....	47.601	35.972	.....	.....	.....
Metal	.....	.....	.....	.....	.....	.....
TO NEXT UNIT						
Gas(vol %)	.....	.....	.....	.....	.....	.....
Gas	.....	.....	.....	.....	.....	.....
Dust	.....	.....	.....	.....	.....	.....
FEED 2						
PRODUCTS 2						
Gas(vol %)	.....	.....	.....	.....	.....	.....
Gas	.....	.....	.....	.....	.....	.....
Slag	.....	.....	.....	.....	.....	.....

ELEMENTAL ANALYSES
(MASS %) Slag constituents are shown as oxides; all others as elements

	Al/Al2O3	C	Ca/CaO	Cr/Cr2O3	Fe/FeO	H	K/K2O	Mg/MgO	Mn/Mn2O3	N	Na/Na2O
PRODUCTS 1											
Gas	.....	40.783	.....	.....	.....	0.804	.....	0.788	0.122	1.193	.....
Dust	0.651	3.595	0.030	0.007	42.535	0.154	.....	0.413	0.379	0.127	.....
Solids	.....	100.000	.....	.....	.....	.....	.....	.....	.....	.....	.....
Slag	3.099	.....	0.233	0.017	4.689	.....	.....	4.120	1.119	.....	.....
Metal	.....	3.040	.....	0.005	96.472	.....	.....	.....	0.074	.....	.....
PRODUCTS 2											
Gas	.....	41.975	.....	.....	.....	0.851	.....	.....	.....	1.245	.....
Slag	1.073	2.312	0.037	0.009	47.740	.....	.....	7.373	1.384	.....	.....

	Ni	O	P/P2O5	S	Si/SiO2	Ti/TiO2	V/V2O5	Zr/ZrO2
PRODUCTS 1								
Gas	.....	56.006	.....	0.010	0.293	.....	.....	.....
Dust	.....	30.526	0.031	0.010	0.502	20.689	0.269	0.081
Solids	.....	.....	.....	.....	.....	.....	.....	.....
Slag	.....	37.387	0.119	0.010	2.208	86.977	0.793	0.277
Metal	.....	.....	0.025	0.009	0.101	0.060	0.213	.....
PRODUCTS 2								
Gas	.....	55.928	.....	.....	.....	.....	.....	.....
Slag	.....	34.169	0.063	0.061	4.186	30.108	0.419	0.096

DISTRIBUTION OF ELEMENTS

PRODUCTS 1	Gas	Dust	Solids	Slag	Metal	Matte
Al:	.....	5.000%	.....	95.000%	.....	.....
C :	71.263%	1.057%	20.280%	.....	7.400%	.....
Ca:	.....	2.333%	.....	97.667%	.....	.....
Cr:	.....	5.000%	.....	64.780%	30.220%	.....
Fe:	.....	4.898%	.....	3.165%	91.937%	.....
H :	96.887%	3.113%	.....	.....	.....	.....
Mg:	19.653%	1.735%	.....	78.612%	.....	.....
Mn:	9.548%	5.000%	.....	77.339%	8.113%	.....
N :	98.242%	1.758%	.....	.....	.....	.....
O :	51.577%	4.732%	.....	43.691%	.....	.....
P :	.....	5.000%	.....	62.072%	32.928%	.....
S :	27.232%	4.636%	.....	34.274%	33.858%	.....
Si:	16.023%	4.619%	.....	71.629%	7.729%	.....
Ti:	.....	4.994%	.....	94.887%	0.120%	.....
V :	.....	5.000%	.....	62.257%	32.743%	.....
Zr:	.....	5.000%	.....	95.000%	.....	.....

PRODUCTS 2	Gas	Dust	Solids	Slag	Metal	Matte
Al:	.....	.....	.....	100.000%	.....	.....
C :	98.922%	.....	.....	1.078%	.....	.....
Ca:	.....	.....	.....	100.000%	.....	.....
Cr:	.....	.....	.....	100.000%	.....	.....
Fe:	.....	.....	.....	100.000%	.....	.....
H :	100.000%	.....	.....	.....	.....	.....
Mg:	.....	.....	.....	100.000%	.....	.....
Mn:	.....	.....	.....	100.000%	.....	.....
N :	100.000%	.....	.....	.....	.....	.....
O :	89.219%	.....	.....	10.781%	.....	.....
P :	.....	.....	.....	100.000%	.....	.....
S :	.....	.....	.....	100.000%	.....	.....
Si:	.....	.....	.....	100.000%	.....	.....
Ti:	.....	.....	.....	100.000%	.....	.....
V :	.....	.....	.....	100.000%	.....	.....
Zr:	.....	.....	.....	100.000%	.....	.....

PYROSIM v1.57 Copyright 26-JUL

Moderated refractory wear and feed by-pass for Scenario A (Batch 27 to 35)

```
PILOT-PLANT MODEL for Batch 27 to 35; 3% by-pass scenario, moderated refractory wear

     FLOWRATES
                          FLOWRATE (kg/h)      TEMPERATURE (øC)
          FEED  1
          ##4TiMagConc-35%    10000.000               25
          ##1Anthracite        2000.000               25
          Refractory              0.001               25
          PRODUCTS 1
          Solids               300.771              1800
          Slag                3718.955              1800
          Metal               4223.523              1750
          TO NEXT UNIT
          Gas                 3042.799              1600
          Dust                 308.002              1600
          FEED  2
          PRODUCTS 2
          Gas                 3006.083              1600
          Slag                 344.718              1600
     OPERATION
     UNIT 1
          General Empirical model allows the user to specify ratios and percentages in streams
          ELEMENTS:  C   O   H   Mg  Mn  N   Si  S   Al  Ca  Cr  Fe  K   Na  P   V   Zr  Ti  Ni
          Gas:       CO  CO2 H2  Mg  Mn  N2  O2  SiO  SO2  VOL.
          Slag:      Al2O3(l)  CaO(l)  Cr2O3  Fe  FeO  K2O  MgO(l)  MnO  Na2O  P4O10  S  SiO2(l)  V2O5  ZrO2
                     Ti3O5(l)  TiO2(l)  NiO
          Metal:     C  Cr  Fe  Mn  P  S  Si  Ti  V  Ni
          Solids (pure phases):  C

            1.100% O2       in Gas
            0.001% VOL.     in Gas
            0.500% Fe       in Slag
            0.010% S        in Slag
            3.040% C        in Metal
            0.025% P        in Metal
            0.009% S        in Metal
            0.060% Ti       in Metal
          CO2 in Gas / CO in Gas (mass ratio) = .0001
          FeO in Slag / Fe in Metal (molar ratio) = .0297
          V in Metal / V2O5 in Slag (mass ratio) = .2946
          Cr2O3 in Slag / Cr in Metal (molar ratio) = 1.0718
          Mn in Metal / MnO in Slag (molar ratio) = .1049
          MnO in Slag / Mn in Gas (molar ratio) = 8.1
          SiO in Gas / SiO2(l) in Slag (molar ratio) = .2237
          Si in Metal / SiO2(l) in Slag (molar ratio) = .1079
          Mg in Gas / MgO(l) in Slag (molar ratio) = .25
          Ti3O5(l) in Slag / TiO2(l) in Slag (mass ratio) = 2.087

          Operating temperature = 1800øC
          Operating pressure = 1.00 atm
          Dust loss = 0%
          Slag : Metal ratio =  0.88

     UNIT 2
          Equilibrium model calculates multi-phase multi-reaction equilibrium
          ELEMENTS:  C   O   H   K   N   S   Al  Ca  Cr  Fe  Mg  Mn  P   Si  Ti  V   Zr
          Gas:       CO  CO2  H2  K  N2  SO2  VOL.
          Slag:      Al2O3(l)  C  CaO(l)  Cr2O3  Fe2O3  MgO(l)  MnO  P  S  SiO2(l)  TiO2  V2O5  ZrO2

          Operating temperature = 1600øC
          Operating pressure = 1.00 atm
     ENERGY
          UNIT 1 requires  11400 kWh ( 40900 MJ) per hour of operation, including a rate of energy loss of 0 kW
                 This is 2.70 MWh per ton of Metal produced in this unit
          UNIT 2 requires -244 kWh (-877 MJ) per hour of operation, including a rate of energy loss of 0 kW
     ANALYSES
     (MASS %)
                              Al     Al2O3  Al2O3(l)   C     CaCO3    CaO    CaO(l)    CO      CO2       Cr     Cr2O3
          FEED 1
          ##4TiMagConc-35%  .....   1.230   .....   0.020   .....   0.030   .....   .....   .....   .....   0.010
          ##1Anthracite     .....   .....   .....  79.000   .....   0.300   .....   .....   .....   .....   .....
          Refractory        .....   .....   .....   .....   .....   .....   .....   .....   .....   .....   .....
          PRODUCTS 1
          Solids            .....   .....   ..... 100.000   .....   .....   .....   .....   .....   .....   .....
          Slag              .....   .....   3.208   .....   .....   .....   0.238   .....   .....   .....   0.018
          Metal             .....   .....   .....   3.040   .....   .....   .....   .....   .....   0.005   .....
          TO NEXT UNIT
          Gas(vol %)        .....   .....   .....   .....   .....   .....   .....  87.408   0.006   .....   .....
          Gas               .....   .....   .....   .....   .....   .....   .....  96.065   0.010   .....   .....
          Dust              .....   1.198   .....   5.149   .....   0.049   .....   .....   .....   .....   0.010
          FEED 2
          PRODUCTS 2
          Gas(vol %)        .....   .....   .....   .....   .....   .....   .....  88.580   0.022   .....   .....
          Gas               .....   .....   .....   .....   .....   .....   .....  97.939   0.039   .....   .....
          Slag              .....   .....   1.070   2.390   .....   .....   0.044   .....   .....   .....   0.009

                             CrO      Fe     Fe2O3    Fe3C    Fe3O4   Fe3Si    FeO     FeS    FeTiO3    H2      H2O
          FEED 1
          ##4TiMagConc-35%  .....   .....   .....   .....  20.144   .....  17.386   .....  38.664   .....   1.000
          ##1Anthracite     .....   .....   .....   .....   .....   .....   7.090   .....   .....   .....   1.680
          Refractory        .....   .....   .....   .....   .....   .....   .....   .....   .....   .....   .....
          PRODUCTS 1
          Solids            .....   .....   .....   .....   .....   .....   .....   .....   .....   .....   .....
          Slag              .....   0.500   .....   .....   .....   .....   4.186   .....   .....   .....   .....
          Metal             .....  96.475   .....   .....   .....   .....   .....   .....   .....   .....   .....
          TO NEXT UNIT
          Gas(vol %)        .....   .....   .....   .....   .....   .....   .....   .....   .....  10.038   .....
          Gas               .....   .....   .....   .....   .....   .....   .....   .....   .....   0.796   .....
          Dust              .....   .....   .....   .....  19.621   .....  17.395   .....  37.660   .....   1.083
          FEED 2
          PRODUCTS 2
```

Gas(vol %)	.....	.....	.....	.....	.....	.....	.....	.....	.....	10.312	.....
Gas	.....	.....	.....	.....	.....	.....	.....	.....	.....	0.822	.....
Slag	.....	.....	53.111	.....	.....	.....	.....	.....	.....	.....	.....

	K	K2O	Mg	MgCO3	MgO	MgO(l)	Mn	MnO	MnO2	N2	Na
FEED 1											
##4TiMagConc-35%	.....	.....	.....	.....	0.680	.....	.....	0.490	.....	.....	.....
##1Anthracite	.....	.....	.....	.....	0.140	.....	.....	.....	.....	.....	.....
Refractory	.....	.....	.....	.....	97.500	.....	.....	.....	.....	.....	.....
PRODUCTS 1											
Solids	.....	.....	.....	.....	.....	.....	.....	.....	.....	.....	.....
Slag	.....	.....	.....	.....	.....	1.479	.....	1.040	.....	.....	.....
Metal	.....	.....	.....	.....	.....	.....	0.074	.....	.....	.....	.....
TO NEXT UNIT											
Gas(vol %)	.....	.....	0.286	.....	.....	.....	0.056	.....	.....	1.064	.....
Gas	.....	.....	0.273	.....	.....	.....	0.122	.....	.....	1.169	.....
Dust	.....	.....	.....	.....	0.671	.....	.....	0.477	.....	.....	.....
FEED 2											
PRODUCTS 2											
Gas(vol %)	.....	.....	.....	.....	.....	.....	.....	.....	.....	1.085	.....
Gas	.....	.....	.....	.....	.....	.....	.....	.....	.....	1.200	.....
Slag	.....	.....	.....	.....	.....	4.588	.....	1.812	.....	.....	.....

	Na2O	O2	P	P4O10	S	Si	SiO	SiO2	SiO2(l)	SO2	SO3
FEED 1											
##4TiMagConc-35%	.....	.....	.....	0.072	0.010	.....	.....	1.060	.....	.....	.....
##1Anthracite	.....	.....	.....	.....	0.005	.....	.....	0.350	.....	.....	.....
Refractory	.....	.....	.....	.....	.....	.....	.....	2.500	.....	.....	.....
PRODUCTS 1											
Solids	.....	.....	.....	.....	.....	.....	.....	.....	.....	.....	.....
Slag	.....	.....	.....	0.123	0.010	.....	.....	.....	2.216	.....	.....
Metal	.....	.....	0.025	.....	0.009	0.098	.....	.....	.....	.....	.....
TO NEXT UNIT											
Gas(vol %)	.....	0.876	.....	.....	.....	.....	0.257	.....	.....	0.008	.....
Gas	.....	1.100	.....	.....	.....	.....	0.445	.....	.....	0.021	.....
Dust	.....	.....	.....	0.070	0.010	.....	.....	1.055	.....	.....	.....
FEED 2											
PRODUCTS 2											
Gas(vol %)	.....	.....	.....	.....	.....	.....	.....	.....	.....	.....	.....
Gas	.....	.....	.....	.....	.....	.....	.....	.....	.....	.....	.....
Slag	.....	.....	0.027	.....	0.101	.....	.....	.....	6.291	.....	.....

	Ti	Ti2O3	Ti3O5	Ti4O7	Ti5O9	Ti6O11	Ti7O13	Ti8O15	TiC	TiO	TiO2
FEED 1											
##4TiMagConc-35%	.....	.....	.....	.....	.....	.....	.....	.....	.....	.....	14.145
##1Anthracite	.....	.....	.....	.....	.....	.....	.....	.....	.....	.....	0.280
Refractory	.....	.....	.....	.....	.....	.....	.....	.....	.....	.....	.....
PRODUCTS 1											
Solids	.....	.....	.....	.....	.....	.....	.....	.....	.....	.....	.....
Slag	.....	.....	.....	.....	.....	.....	.....	.....	.....	.....	.....
Metal	0.060	.....	.....	.....	.....	.....	.....	.....	.....	.....	.....
TO NEXT UNIT											
Gas(vol %)	.....	.....	.....	.....	.....	.....	.....	.....	.....	.....	.....
Gas	.....	.....	.....	.....	.....	.....	.....	.....	.....	.....	.....
Dust	.....	.....	.....	.....	.....	.....	.....	.....	.....	.....	13.796
FEED 2											
PRODUCTS 2											
Gas(vol %)	.....	.....	.....	.....	.....	.....	.....	.....	.....	.....	.....
Gas	.....	.....	.....	.....	.....	.....	.....	.....	.....	.....	.....
Slag	.....	.....	.....	.....	.....	.....	.....	.....	.....	.....	30.043

	V	V2O3	V2O4	V2O5	V4O7	VO	VO2	VOL.	Zr	ZrO	ZrO2
FEED 1											
##4TiMagConc-35%	.....	.....	.....	0.480	.....	.....	.....	0.500	.....	.....	0.110
##1Anthracite	.....	.....	.....	.....	.....	.....	.....	10.700	.....	.....	.....
Refractory	.....	.....	.....	.....	.....	.....	.....	.....	.....	.....	.....
PRODUCTS 1											
Solids	.....	.....	.....	.....	.....	.....	.....	.....	.....	.....	.....
Slag	.....	.....	.....	0.820	.....	.....	.....	.....	.....	.....	0.287
Metal	0.213	.....	.....	.....	.....	.....	.....	.....	.....	.....	.....
TO NEXT UNIT											
Gas(vol %)	.....	.....	.....	.....	.....	.....	.....	0.001	.....	.....	.....
Gas	.....	.....	.....	.....	.....	.....	.....	0.001	.....	.....	.....
Dust	.....	.....	.....	0.468	.....	.....	.....	1.182	.....	.....	0.107
FEED 2											
PRODUCTS 2											
Gas(vol %)	.....	.....	.....	.....	.....	.....	.....	.....	.....	.....	.....
Gas	.....	.....	.....	.....	.....	.....	.....	.....	.....	.....	.....
Slag	.....	.....	.....	0.418	.....	.....	.....	.....	.....	.....	0.096

	Ti2O3(l)	Ti3O5(l)	TiO2(l)	Ni	NiO	SO3
FEED 1						
##4TiMagConc-35%	.....	.....	.....	.....	.....	.....
##1Anthracite	.....	.....	.....	.....	.....	.....
Refractory	.....	.....	.....	.....	.....	.....
PRODUCTS 1						
Solids	.....	.....	.....	.....	.....	.....
Slag	.....	58.056	27.818	.....	.....	.....
Metal	.....	.....	.....	.....	.....	.....
TO NEXT UNIT						
Gas(vol %)	.....	.....	.....	.....	.....	.....
Gas	.....	.....	.....	.....	.....	.....
Dust	.....	.....	.....	.....	.....	.....
FEED 2						
PRODUCTS 2						
Gas(vol %)	.....	.....	.....	.....	.....	.....
Gas	.....	.....	.....	.....	.....	.....
Slag	.....	.....	.....	.....	.....	.....

ELEMENTAL ANALYSES
(MASS %) Slag constituents are shown as oxides; all others as elements

	Al/Al2O3	C	Ca/CaO	Cr/Cr2O3	Fe/FeO	H	K/K2O	Mg/MgO	Mn/Mn2O3	N	Na/Na2O
PRODUCTS 1											
Gas	.....	41.197	.....	.....	.....	0.794	.....	0.272	0.122	1.169	.....
Dust	0.634	5.679	0.035	0.007	41.578	0.165	.....	0.405	0.370	0.162	.....
Solids	.....	100.000	.....	.....	.....	.....	.....	.....	.....	.....	.....
Slag	3.208	.....	0.238	0.018	4.829	.....	.....	1.479	1.158	.....	.....
Metal	.....	3.040	.....	0.005	96.475	.....	.....	.....	0.074	.....	.....
PRODUCTS 2											
Gas	.....	42.008	.....	.....	.....	0.821	.....	.....	.....	1.200	.....
Slag	1.070	2.390	0.044	0.009	47.791	.....	.....	4.588	2.017	.....	.....

	Ni	O	P/P2O5	S	Si/SiO2	Ti/TiO2	V/V2O5	Zr/ZrO2
PRODUCTS 1								
Gas	.....	56.152	.....	0.010	0.283	.....	.....	.....
Dust	.....	29.933	0.031	0.010	0.493	20.158	0.262	0.079
Solids	.....	.....	.....	.....	.....	.....	.....	.....
Slag	.....	36.925	0.123	0.010	2.216	90.027	0.820	0.287
Metal	.....	.....	0.025	0.009	0.098	0.060	0.213	.....
PRODUCTS 2								
Gas	.....	55.971	.....	.....	.....	.....	.....	.....
Slag	.....	34.303	0.063	0.101	6.291	30.042	0.418	0.096

DISTRIBUTION OF ELEMENTS

PRODUCTS 1	Gas	Dust	Solids	Slag	Metal	Matte
Al:	.....	3.000%	.....	97.000%	.....	.....
C :	73.728%	1.029%	17.692%	.....	7.552%	.....
Ca:	.....	1.667%	.....	98.333%	.....	.....
Cr:	.....	3.000%	.....	66.144%	30.856%	.....
Fe:	.....	2.949%	.....	3.215%	93.836%	.....
H :	97.944%	2.056%	.....	.....	.....	.....
Mg:	19.416%	2.921%	.....	77.663%	.....	.....
Mn:	9.749%	3.000%	.....	78.967%	8.284%	.....
N :	98.621%	1.379%	.....	.....	.....	.....
O :	53.831%	2.905%	.....	43.264%	.....	.....
P :	.....	3.000%	.....	63.393%	33.607%	.....
S :	28.817%	2.818%	.....	33.809%	34.556%	.....
Si:	16.316%	2.876%	.....	72.938%	7.870%	.....
Ti:	.....	2.997%	.....	96.881%	0.122%	.....
V :	.....	3.000%	.....	63.568%	33.432%	.....
Zr:	.....	3.000%	.....	97.000%	.....	.....

PRODUCTS 2	Gas	Dust	Solids	Slag	Metal	Matte
Al:	.....	.....	.....	100.000%	.....	.....
C :	99.352%	.....	.....	0.648%	.....	.....
Ca:	.....	.....	.....	100.000%	.....	.....
Cr:	.....	.....	.....	100.000%	.....	.....
Fe:	.....	.....	.....	100.000%	.....	.....
H :	100.000%	.....	.....	.....	.....	.....
Mg:	.....	.....	.....	100.000%	.....	.....
Mn:	.....	.....	.....	100.000%	.....	.....
N :	100.000%	.....	.....	.....	.....	.....
O :	93.433%	.....	.....	6.567%	.....	.....
P :	.....	.....	.....	100.000%	.....	.....
S :	.....	.....	.....	100.000%	.....	.....
Si:	.....	.....	.....	100.000%	.....	.....
Ti:	.....	.....	.....	100.000%	.....	.....
V :	.....	.....	.....	100.000%	.....	.....
Zr:	.....	.....	.....	100.000%	.....	.....

PYROSIM v1.57 Copyright 26-JUL

Pilot-plant Simulation - Batch 48 to 53

```
PILOT-PLANT MODEL Simulation of Period Batch 48-53

        FLOWRATES
                                FLOWRATE (kg/h)      TEMPERATURE (øC)
                FEED  1
                ##2TiMagConc-35%      10000.0                 25
                ##1Anthracite         2000.0                 25
                Refractory              50.0                 25
                PRODUCTS 1
                Solids                 274.0                1800
                Slag                  3489.3                1800
                Metal                 4223.5                1750
                TO NEXT UNIT
                Gas                   3157.2                1600
                Dust                   500.1                1600
                FEED  2
                PRODUCTS 2
                Gas                   3071.8                1600
                Slag                   585.5                1600

        OPERATION
        UNIT 1
                General Empirical model allows the user to specify ratios and percentages in streams
                ELEMENTS:  C   O   H   Mg  Mn  N   Si  S   Al  Ca  Cr  Fe  K   Na  P   V   Zr  Ti  Ni
                Gas:       CO  CO2  H2  Mg  Mn  N2  O2  SiO  SO2  VOL.
                Slag:      Al2O3(l)  CaO(l)  Cr2O3  Fe  FeO  K2O  MgO(l)  MnO  Na2O  P4O10  S  SiO2(l)  V2O5  ZrO2
                           Ti3O5(l)  TiO2(l)  NiO
                Metal:     C  Cr  Fe  Mn  P  S  Si  Ti  V  Ni
                Solids (pure phases):  C

                  1.100% O2       in Gas
                  0.001% VOL.     in Gas
                  0.500% Fe       in Slag
                  0.010% S        in Slag
                  2.719% C        in Metal
                  0.020% P        in Metal
                  0.005% S        in Metal
                  0.100% Ti       in Metal
                CO2 in Gas / CO in Gas (mass ratio) = .0001
                FeO in Slag / Fe in Metal (molar ratio) = .011
                V in Metal / V2O5 in Slag (mass ratio) = 2.2
                Cr2O3 in Slag / Cr in Metal (molar ratio) = 2
                Mn in Metal / MnO in Slag (molar ratio) = .22
                MnO in Slag / Mn in Gas (molar ratio) = 2.945
                SiO in Gas / SiO2(l) in Slag (molar ratio) = .45
                Si in Metal / SiO2(l) in Slag (molar ratio) = .37
                Mg in Gas / MgO(l) in Slag (molar ratio) = .35
                Ti3O5(l) in Slag / TiO2(l) in Slag (mass ratio) = 5.9361

                Operating temperature = 1800øC
                Operating pressure = 1.00 atm
                Dust loss = 0%
                Slag : Metal ratio =  0.83
        UNIT 2
                Equilibrium model calculates multi-phase multi-reaction equilibrium
                ELEMENTS:  C   O   H   K   N   S   Al  Ca  Cr  Fe  Mg  Mn  P   Si  Ti  V   Zr
                Gas:       CO  CO2  H2  K  N2  SO2  VOL.
                Slag:      Al2O3(l)  C  CaO(l)  Cr2O3  Fe2O3  MgO(l)  MnO  P  S  SiO2(l)  TiO2  V2O5  ZrO2

                Operating temperature = 1600øC
                Operating pressure = 1.00 atm

        ENERGY
                UNIT 1 requires  11700 kWh ( 42100 MJ) per hour of operation, including a rate of energy loss of 0 kW
                       This is 2.77 MWh per ton of Metal produced in this unit
                UNIT 2 requires -378 kWh (-1360 MJ) per hour of operation, including a rate of energy loss of 0 kW

        ANALYSES
        (MASS %)
                                  Al    Al2O3  Al2O3(l)   C     CaCO3    CaO    CaO(l)    CO     CO2      Cr    Cr2O3
                FEED 1
                ##2TiMagConc-35%  .....   1.230   .....   0.020   .....   0.030   .....   .....   .....   .....   0.010
                ##1Anthracite     .....   .....   .....  79.000   .....   0.300   .....   .....   .....   .....   .....
                Refractory        .....   .....   .....   .....   .....   .....   .....   .....   .....   .....   .....
                PRODUCTS 1
                Solids            .....   .....   ..... 100.000   .....   .....   .....   .....   .....   .....   .....
                Slag              .....   .....   3.349   .....   .....   .....   0.252   .....   .....   .....   0.022
                Metal             .....   .....   .....   2.719   .....   .....   .....   .....   .....   0.003   .....
                TO NEXT UNIT
                Gas(vol %)        .....   .....   .....   .....   .....   .....   .....  87.369   0.006   .....   .....
                Gas               .....   .....   .....   .....   .....   .....   .....  95.528   0.010   .....   .....
                Dust              .....   1.230   .....   3.180   .....   0.042   .....   .....   .....   .....   0.010
                FEED 2
                PRODUCTS 2
                Gas(vol %)        .....   .....   .....   .....   .....   .....   .....  88.807   0.017   .....   .....
                Gas               .....   .....   .....   .....   .....   .....   .....  97.992   0.029   .....   .....
                Slag              .....   .....   1.050   3.482   .....   .....   0.036   .....   .....   .....   0.009

                                   CrO      Fe    Fe2O3    Fe3C   Fe3O4   Fe3Si    FeO     FeS    FeTiO3    H2     H2O
                FEED 1
                ##2TiMagConc-35%  .....   .....   .....   .....  20.144   .....  17.386   .....  38.664   .....   1.000
                ##1Anthracite     .....   .....   .....   .....   .....   .....   7.090   .....   .....   .....   1.680
                Refractory        .....   .....   .....   .....   .....   .....   .....   .....   .....   .....   .....
                PRODUCTS 1
                Solids            .....   .....   .....   .....   .....   .....   .....   .....   .....   .....   .....
                Slag              .....   0.500   .....   .....   .....   .....   1.650   .....   .....   .....   .....
                Metal             .....  96.305   .....   .....   .....   .....   .....   .....   .....   .....   .....
                TO NEXT UNIT
                Gas(vol %)        .....   .....   .....   .....   .....   .....   .....   .....   .....   9.619   .....
                Gas               .....   .....   .....   .....   .....   .....   .....   .....   .....   0.759   .....
                Dust              .....   .....   .....   .....  20.141   .....  17.667   .....  38.659   .....   1.067
```

FEED 2											
PRODUCTS 2											
Gas(vol %)	.....	.....	.....	.....	.....	.....	.....	.....	.....	10.112	.....
Gas	.....	.....	.....	.....	.....	.....	.....	.....	.....	0.805	.....
Slag	.....	.....	51.936	.....	.....	.....	.....	.....	.....	.....	.....

	K	K2O	Mg	MgCO3	MgO	MgO(l)	Mn	MnO	MnO2	N2	Na
FEED 1											
##2TiMagConc-35%	.....	.....	.....	.....	0.680	.....	.....	0.490	.....	.....	.....
##1Anthracite	.....	.....	.....	.....	0.140	.....	.....	.....	.....	.....	.....
Refractory	.....	.....	.....	.....	97.500	.....	.....	.....	.....	.....	.....
PRODUCTS 1											
Solids	.....	.....	.....	.....	.....	.....	.....	.....	.....	.....	.....
Slag	.....	.....	.....	.....	.....	2.465	.....	0.855	.....	.....	.....
Metal	.....	.....	.....	.....	.....	.....	0.120	.....	.....	.....	.....
TO NEXT UNIT											
Gas(vol %)	.....	.....	0.606	.....	.....	.....	0.116	.....	.....	1.027	.....
Gas	.....	.....	0.575	.....	.....	.....	0.249	.....	.....	1.122	.....
Dust	.....	.....	.....	.....	0.686	.....	.....	0.490	.....	.....	.....
FEED 2											
PRODUCTS 2											
Gas(vol %)	.....	.....	.....	.....	.....	.....	.....	.....	.....	1.064	.....
Gas	.....	.....	.....	.....	.....	.....	.....	.....	.....	1.175	.....
Slag	.....	.....	.....	.....	.....	5.727	.....	2.149	.....	.....	.....

	Na2O	O2	P	P4O10	S	Si	SiO	SiO2	SiO2(l)	SO2	SO3
FEED 1											
##2TiMagConc-35%	.....	.....	.....	0.072	0.010	.....	.....	1.060	.....	.....	.....
##1Anthracite	.....	.....	.....	.....	0.005	.....	.....	0.350	.....	.....	.....
Refractory	.....	.....	.....	.....	.....	.....	.....	2.500	.....	.....	.....
PRODUCTS 1											
Solids	.....	.....	.....	.....	.....	.....	.....	.....	.....	.....	.....
Slag	.....	.....	.....	0.141	0.010	.....	.....	.....	1.714	.....	.....
Metal	.....	.....	0.020	.....	0.005	0.245	.....	.....	.....	.....	.....
TO NEXT UNIT											
Gas(vol %)	.....	0.881	.....	.....	.....	.....	0.364	.....	.....	0.012	.....
Gas	.....	1.100	.....	.....	.....	.....	0.626	.....	.....	0.031	.....
Dust	.....	.....	.....	0.072	0.010	.....	.....	1.074	.....	.....	.....
FEED 2											
PRODUCTS 2											
Gas(vol %)	.....	.....	.....	.....	.....	.....	.....	.....	.....	.....	.....
Gas	.....	.....	.....	.....	.....	.....	.....	.....	.....	.....	.....
Slag	.....	.....	0.027	.....	0.092	.....	.....	.....	5.515	.....	.....

	Ti	Ti2O3	Ti3O5	Ti4O7	Ti5O9	Ti6O11	Ti7O13	Ti8O15	TiC	TiO	TiO2
FEED 1											
##2TiMagConc-35%	.....	.....	.....	.....	.....	.....	.....	.....	.....	.....	14.145
##1Anthracite	.....	.....	.....	.....	.....	.....	.....	.....	.....	.....	0.280
Refractory	.....	.....	.....	.....	.....	.....	.....	.....	.....	.....	.....
PRODUCTS 1											
Solids	.....	.....	.....	.....	.....	.....	.....	.....	.....	.....	.....
Slag	.....	.....	.....	.....	.....	.....	.....	.....	.....	.....	.....
Metal	0.100	.....	.....	.....	.....	.....	.....	.....	.....	.....	.....
TO NEXT UNIT											
Gas(vol %)	.....	.....	.....	.....	.....	.....	.....	.....	.....	.....	.....
Gas	.....	.....	.....	.....	.....	.....	.....	.....	.....	.....	.....
Dust	.....	.....	.....	.....	.....	.....	.....	.....	.....	.....	14.154
FEED 2											
PRODUCTS 2											
Gas(vol %)	.....	.....	.....	.....	.....	.....	.....	.....	.....	.....	.....
Gas	.....	.....	.....	.....	.....	.....	.....	.....	.....	.....	.....
Slag	.....	.....	.....	.....	.....	.....	.....	.....	.....	.....	29.473

	V	V2O3	V2O4	V2O5	V4O7	VO	VO2	VOL.	Zr	ZrO	ZrO2
FEED 1											
##2TiMagConc-35%	.....	.....	.....	0.480	.....	.....	.....	0.500	.....	.....	0.110
##1Anthracite	.....	.....	.....	.....	.....	.....	.....	10.700	.....	.....	.....
Refractory	.....	.....	.....	.....	.....	.....	.....	.....	.....	.....	.....
PRODUCTS 1											
Solids	.....	.....	.....	.....	.....	.....	.....	.....	.....	.....	.....
Slag	.....	.....	.....	0.265	.....	.....	.....	.....	.....	.....	0.299
Metal	0.482	.....	.....	.....	.....	.....	.....	.....	.....	.....	.....
TO NEXT UNIT											
Gas(vol %)	.....	.....	.....	.....	.....	.....	.....	0.001	.....	.....	.....
Gas	.....	.....	.....	.....	.....	.....	.....	0.001	.....	.....	.....
Dust	.....	.....	.....	0.480	.....	.....	.....	0.928	.....	.....	0.110
FEED 2											

PRODUCTS 2											
Gas(vol %)	.....	.....	.....	.....	.....	.....	.....	.....	.....	.....	.....
Gas	.....	.....	.....	.....	.....	.....	.....	.....	.....	.....	.....
Slag	.....	.....	.....	0.410	.....	.....	.....	.....	.....	.....	0.094

	Ti2O3(l)	Ti3O5(l)	TiO2(l)	Ni	NiO	SO3
FEED 1						
##2TiMagConc-35%	.....	.....	.....	.....	.....	.....
##1Anthracite	.....	.....	.....	.....	.....	.....
Refractory	.....	.....	.....	.....	.....	.....
PRODUCTS 1						
Solids	.....	.....	.....	.....	.....	.....
Slag	.....	75.722	12.756	.....	.....	.....
Metal	.....	.....	.....	.....	.....	.....
TO NEXT UNIT						
Gas(vol %)	.....	.....	.....	.....	.....	.....
Gas	.....	.....	.....	.....	.....	.....
Dust	.....	.....	.....	.....	.....	.....
FEED 2						
PRODUCTS 2						
Gas(vol %)	.....	.....	.....	.....	.....	.....
Gas	.....	.....	.....	.....	.....	.....
Slag	.....	.....	.....	.....	.....	.....

ELEMENTAL ANALYSES
(MASS %) Slag constituents are shown as oxides; all others as elements

	Al/Al2O3	C	Ca/CaO	Cr/Cr2O3	Fe/FeO	H	K/K2O	Mg/MgO	Mn/Mn2O3	N	Na/Na2O
PRODUCTS 1											
Gas	.....	40.967	.....	.....	.....	0.757	.....	0.575	0.249	1.123	.....
Dust	0.651	3.595	0.030	0.007	42.535	0.154	.....	0.413	0.379	0.127	.....
Solids	.....	100.000	.....	.....	.....	.....	.....	.....	.....	.....	.....
Slag	3.349	.....	0.252	0.022	2.293	.....	.....	2.465	0.952	.....	.....
Metal	.....	2.719	.....	0.003	96.305	.....	.....	.....	0.120	.....	.....
PRODUCTS 2											
Gas	.....	42.028	.....	.....	.....	0.803	.....	.....	.....	1.175	.....
Slag	1.050	3.483	0.036	0.009	46.733	.....	.....	5.728	2.392	.....	.....

	Ni	O	P/P2O5	S	Si/SiO2	Ti/TiO2	V/V2O5	Zr/ZrO2
PRODUCTS 1								
Gas	.....	55.916	.....	0.015	0.399	.....	.....	.....
Dust	.....	30.526	0.031	0.010	0.502	20.689	0.269	0.081
Solids	.....	.....	.....	.....	.....	.....	.....	.....
Slag	.....	36.568	0.141	0.010	1.714	93.893	0.265	0.299
Metal	.....	.....	0.020	0.005	0.245	0.100	0.482	.....
PRODUCTS 2								
Gas	.....	55.994	.....	.....	.....	.....	.....	.....
Slag	.....	33.821	0.061	0.092	5.514	29.472	0.410	0.094

DISTRIBUTION OF ELEMENTS

PRODUCTS 1	Gas	Dust	Solids	Slag	Metal	Matte
Al:	.....	5.000%	.....	95.000%	.....	.....
C :	76.072%	1.057%	16.116%	.....	6.755%	.....
Ca:	.....	2.333%	.....	97.667%	.....	.....
Cr:	.....	5.000%	.....	76.000%	19.000%	.....
Fe:	.....	4.898%	.....	1.432%	93.669%	.....
H :	96.887%	3.113%	.....	.....	.....	.....
Mg:	25.183%	2.867%	.....	71.950%	.....	.....
Mn:	20.684%	5.000%	.....	60.915%	13.401%	.....
N :	98.242%	1.758%	.....	.....	.....	.....
O :	55.272%	4.779%	.....	39.949%	.....	.....
P :	.....	5.000%	.....	68.115%	26.885%	.....
S :	44.445%	4.636%	.....	31.721%	19.198%	.....
Si:	23.563%	4.700%	.....	52.363%	19.374%	.....
Ti:	.....	4.994%	.....	94.803%	0.204%	.....
V :	.....	5.000%	.....	19.279%	75.721%	.....
Zr:	.....	5.000%	.....	95.000%	.....	.....

PRODUCTS 2	Gas	Dust	Solids	Slag	Metal	Matte
Al:	.....	.....	.....	100.000%	.....	.....
C :	98.445%	.....	.....	1.555%	.....	.....
Ca:	.....	.....	.....	100.000%	.....	.....
Cr:	.....	.....	.....	100.000%	.....	.....
Fe:	.....	.....	.....	100.000%	.....	.....
H :	100.000%	.....	.....	.....	.....	.....
Mg:	.....	.....	.....	100.000%	.....	.....
Mn:	.....	.....	.....	100.000%	.....	.....
N :	100.000%	.....	.....	.....	.....	.....
O :	89.675%	.....	.....	10.325%	.....	.....
P :	.....	.....	.....	100.000%	.....	.....
S :	.....	.....	.....	100.000%	.....	.....
Si:	.....	.....	.....	100.000%	.....	.....
Ti:	.....	.....	.....	100.000%	.....	.....
V :	.....	.....	.....	100.000%	.....	.....
Zr:	.....	.....	.....	100.000%	.....	.....

PYROSIM v1.57 Copyright 26-JUL

Moderated refractory wear and feed by-pass for Scenario B (Batch 48 to 53)

```
PILOT-PLANT MODEL for Batch 48-53; 3% by-pass scenario, moderated refractory wear

          FLOWRATES
                              FLOWRATE (kg/h)      TEMPERATURE (øC)
                FEED  1
                ##4TIMAGCONC-35%  10000.000                  25
                ##1Anthracite      2000.000                  25
                Refractory            0.001                  25
                PRODUCTS 1
                Solids              238.223                1800
                Slag               3507.237                1800
                Metal              4310.196                1750
                TO NEXT UNIT
                Gas                3230.393                1600
                Dust                308.002                1600
                FEED  2
                PRODUCTS 2
                Gas                3172.946                1600
                Slag                365.436                1600

          OPERATION
          UNIT 1
                General Empirical model allows the user to specify ratios and percentages in streams
                ELEMENTS:  C   O   H   Mg  Mn  N   Si  S   Al  Ca  Cr  Fe  K   Na  P   V   Zr  Ti  Ni
                Gas:       CO  CO2  H2  Mg  Mn  N2  O2  SiO  SO2  VOL.
                Slag:      Al2O3(l)  CaO(l)  Cr2O3  Fe  FeO  K2O  MgO(l)  MnO  Na2O  P4O10  S  SiO2(l)  V2O5  ZrO2
                           Ti3O5(l)  TiO2(l)  NiO
                Metal:     C  Cr  Fe  Mn  P  S  Si  Ti  V  Ni
                Solids (pure phases):  C

                  1.100% O2       in Gas
                  0.001% VOL.     in Gas
                  0.500% Fe       in Slag
                  0.010% S        in Slag
                  2.719% C        in Metal
                  0.020% P        in Metal
                  0.005% S        in Metal
                  0.100% Ti       in Metal
                CO2 in Gas / CO in Gas (mass ratio) = .0001
                FeO in Slag / Fe in Metal (molar ratio) = .011
                V in Metal / V2O5 in Slag (mass ratio) = 2.2
                Cr2O3 in Slag / Cr in Metal (molar ratio) = 2
                Mn in Metal / MnO in Slag (molar ratio) = .22
                MnO in Slag / Mn in Gas (molar ratio) = 2.945
                SiO in Gas / SiO2(l) in Slag (molar ratio) = .45
                Si in Metal / SiO2(l) in Slag (molar ratio) = .37
                Mg in Gas / MgO(l) in Slag (molar ratio) = .35
                Ti3O5(l) in Slag / TiO2(l) in Slag (mass ratio) = 15.0485

                Operating temperature = 1800øC
                Operating pressure = 1.00 atm
                Dust loss = 0%
                Slag : Metal ratio =  0.81

          UNIT 2
                Equilibrium model calculates multi-phase multi-reaction equilibrium
                ELEMENTS:  C   O   H   K   N   S   Al  Ca  Cr  Fe  Mg  Mn  P   Si  Ti  V   Zr
                Gas:       CO  CO2  H2  K  N2  SO2  VOL.
                Slag:      Al2O3(l)  C  CaO(l)  Cr2O3  Fe2O3  MgO(l)  MnO  P  S  SiO2(l)  TiO2  V2O5  ZrO2

                Operating temperature = 1600øC
                Operating pressure = 1.00 atm
          ENERGY
                UNIT 1 requires  11700 kWh ( 42300 MJ) per hour of operation, including a rate of energy loss of 0 kW
                       This is 2.71 MWh per ton of Metal produced in this unit
                UNIT 2 requires -295 kWh (-1060 MJ) per hour of operation, including a rate of energy loss of 0 kW

          ANALYSES
          (MASS %)

                                    Al     Al2O3  Al2O3(l)   C      CaCO3    CaO    CaO(l)    CO      CO2       Cr     Cr2O3
                FEED 1
                ##4TIMAGCONC-35%  .....   1.230   .....    0.020   .....   0.030   .....   .....   .....   .....   0.010
                ##1Anthracite     .....   .....   .....   79.000   .....   0.300   .....   .....   .....   .....   .....
                Refractory        .....   .....   .....    .....   .....   .....   .....   .....   .....   .....   .....
                PRODUCTS 1
                Solids            .....   .....   ..... 100.000   .....   .....   .....   .....   .....   .....   .....
                Slag              .....   .....   3.402    .....   .....   .....   0.252   .....   .....   .....   0.022
                Metal             .....   .....   .....    2.719   .....   .....   .....   .....   .....   0.003   .....
                TO NEXT UNIT
                Gas(vol %)        .....   .....   .....    .....   .....   .....   .....  87.748   0.006   .....   .....
                Gas               .....   .....   .....    .....   .....   .....   .....  95.810   0.010   .....   .....
                Dust              .....   1.198   .....    5.149   .....   0.049   .....   .....   .....   .....   0.010
                FEED 2
                PRODUCTS 2
                Gas(vol %)        .....   .....   .....    .....   .....   .....   .....  89.127   0.020   .....   .....
                Gas               .....   .....   .....    .....   .....   .....   .....  98.049   0.035   .....   .....
                Slag              .....   .....   1.010    2.853   .....   .....   0.041   .....   .....   .....   0.008

                                     CrO      Fe    Fe2O3    Fe3C   Fe3O4   Fe3Si    FeO     FeS    FeTiO3    H2      H2O
                FEED 1
                ##4TIMAGCONC-35%  .....   .....   .....    .....  20.144   .....  17.386   .....  38.664   .....   1.000
                ##1Anthracite     .....   .....   .....    .....   .....   .....   7.090   .....   .....   .....   1.680
                Refractory        .....   .....   .....    .....   .....   .....   .....   .....   .....   .....   .....
                PRODUCTS 1
                Solids            .....   .....   .....    .....   .....   .....   .....   .....   .....   .....   .....
                Slag              .....   0.500   .....    .....   .....   .....   1.675   .....   .....   .....   .....
                Metal             .....  96.308   .....    .....   .....   .....   .....   .....   .....   .....   .....
                TO NEXT UNIT
                Gas(vol %)        .....   .....   .....    .....   .....   .....   .....   .....   .....   9.517   .....
                Gas               .....   .....   .....    .....   .....   .....   .....   .....   .....   0.749   .....
```

Dust	.....	.....	.....	.....	19.621	.....	17.395	.....	37.660	.....	1.083
FEED 2											
PRODUCTS 2											
Gas(vol %)	.....	.....	.....	.....	.....	.....	.....	.....	.....	9.819	.....
Gas	.....	.....	.....	.....	.....	.....	.....	.....	.....	0.779	.....
Slag	.....	.....	50.100	.....	.....	.....	.....	.....	.....	.....	.....

	K	K2O	Mg	MgCO3	MgO	MgO(l)	Mn	MnO	MnO2	N2	Na
FEED 1											
##4TIMAGCONC-35%	.....	.....	.....	.....	0.680	.....	.....	0.490	.....	.....	.....
##1Anthracite	.....	.....	.....	.....	0.140	.....	.....	.....	.....	.....	.....
Refractory	.....	.....	.....	.....	97.500	.....	.....	.....	.....	.....	.....
PRODUCTS 1											
Solids	.....	.....	.....	.....	.....	.....	.....	.....	.....	.....	.....
Slag	.....	.....	.....	.....	.....	1.452	.....	0.869	.....	.....	.....
Metal	.....	.....	.....	.....	.....	.....	0.120	.....	.....	.....	.....
TO NEXT UNIT											
Gas(vol %)	.....	.....	0.351	.....	.....	.....	0.116	.....	.....	1.009	.....
Gas	.....	.....	0.333	.....	.....	.....	0.248	.....	.....	1.101	.....
Dust	.....	.....	.....	.....	0.671	.....	.....	0.477	.....	.....	.....
FEED 2											
PRODUCTS 2											
Gas(vol %)	.....	.....	.....	.....	.....	.....	.....	.....	.....	1.034	.....
Gas	.....	.....	.....	.....	.....	.....	.....	.....	.....	1.137	.....
Slag	.....	.....	.....	.....	.....	5.442	.....	3.234	.....	.....	.....

	Na2O	O2	P	P4O10	S	Si	SiO	SiO2	SiO2(l)	SO2	SO3
FEED 1											
##4TIMAGCONC-35%	.....	.....	.....	0.072	0.010	.....	.....	1.060	.....	.....	.....
##1Anthracite	.....	.....	.....	.....	0.005	.....	.....	0.350	.....	.....	.....
Refractory	.....	.....	.....	.....	.....	.....	.....	2.500	.....	.....	.....
PRODUCTS 1											
Solids	.....	.....	.....	.....	.....	.....	.....	.....	.....	.....	.....
Slag	.....	.....	.....	0.143	0.010	.....	.....	.....	1.719	.....	.....
Metal	.....	.....	0.020	.....	0.005	0.242	.....	.....	.....	.....	.....
TO NEXT UNIT											
Gas(vol %)	.....	0.882	.....	.....	.....	.....	0.359	.....	.....	0.012	.....
Gas	.....	1.100	.....	.....	.....	.....	0.616	.....	.....	0.031	.....
Dust	.....	.....	.....	0.070	0.010	.....	.....	1.055	.....	.....	.....
FEED 2											
PRODUCTS 2											
Gas(vol %)	.....	.....	.....	.....	.....	.....	.....	.....	.....	0.000	.....
Gas	.....	.....	.....	.....	.....	.....	.....	.....	.....	0.000	.....
Slag	.....	.....	0.026	.....	0.146	.....	.....	.....	8.315	.....	.....

	Ti	Ti2O3	Ti3O5	Ti4O7	Ti5O9	Ti6O11	Ti7O13	Ti8O15	TiC	TiO	TiO2
FEED 1											
##4TIMAGCONC-35%	.....	.....	.....	.....	.....	.....	.....	.....	.....	.....	14.145
##1Anthracite	.....	.....	.....	.....	.....	.....	.....	.....	.....	.....	0.280
Refractory	.....	.....	.....	.....	.....	.....	.....	.....	.....	.....	.....
PRODUCTS 1											
Solids	.....	.....	.....	.....	.....	.....	.....	.....	.....	.....	.....
Slag	.....	.....	.....	.....	.....	.....	.....	.....	.....	.....	.....
Metal	0.100	.....	.....	.....	.....	.....	.....	.....	.....	.....	.....
TO NEXT UNIT											
Gas(vol %)	.....	.....	.....	.....	.....	.....	.....	.....	.....	.....	.....
Gas	.....	.....	.....	.....	.....	.....	.....	.....	.....	.....	.....
Dust	.....	.....	.....	.....	.....	.....	.....	.....	.....	.....	13.796
FEED 2											
PRODUCTS 2											
Gas(vol %)	.....	.....	.....	.....	.....	.....	.....	.....	.....	.....	.....
Gas	.....	.....	.....	.....	.....	.....	.....	.....	.....	.....	.....
Slag	.....	.....	.....	.....	.....	.....	.....	.....	.....	.....	28.340

	V	V2O3	V2O4	V2O5	V4O7	VO	VO2	VOL.	Zr	ZrO	ZrO2
FEED 1											
##4TIMAGCONC-35%	.....	.....	.....	0.480	.....	.....	.....	0.500	.....	.....	0.110
##1Anthracite	.....	.....	.....	.....	.....	.....	.....	10.700	.....	.....	.....
Refractory	.....	.....	.....	.....	.....	.....	.....	.....	.....	.....	.....
PRODUCTS 1											
Solids	.....	.....	.....	.....	.....	.....	.....	.....	.....	.....	.....
Slag	.....	.....	.....	0.269	.....	.....	.....	.....	.....	.....	0.304
Metal	0.482	.....	.....	.....	.....	.....	.....	.....	.....	.....	.....
TO NEXT UNIT											
Gas(vol %)	.....	.....	.....	.....	.....	.....	.....	0.001	.....	.....	.....
Gas	.....	.....	.....	.....	.....	.....	.....	0.001	.....	.....	.....
Dust	.....	.....	.....	0.468	.....	.....	.....	1.182	.....	.....	0.107
FEED 2											
PRODUCTS 2											
Gas(vol %)	.....	.....	.....	.....	.....	.....	.....	.....	.....	.....	.....
Gas	.....	.....	.....	.....	.....	.....	.....	.....	.....	.....	.....
Slag	.....	.....	.....	0.394	.....	.....	.....	.....	.....	.....	0.090

	Ti2O3(l)	Ti3O5(l)	TiO2(l)	Ni	NiO	SO3
FEED 1						
##4TIMAGCONC-35%	.....	.....	.....	.....	.....	.....
##1Anthracite	.....	.....	.....	.....	.....	.....
Refractory	.....	.....	.....	.....	.....	.....
PRODUCTS 1						
Solids	.....	.....	.....	.....	.....	.....
Slag	.....	83.813	5.570	.....	.....	.....
Metal	.....	.....	.....	.....	.....	.....
TO NEXT UNIT						
Gas(vol %)	.....	.....	.....	.....	.....	.....
Gas	.....	.....	.....	.....	.....	.....
Dust	.....	.....	.....	.....	.....	.....
FEED 2						
PRODUCTS 2						
Gas(vol %)	.....	.....	.....	.....	.....	.....
Gas	.....	.....	.....	.....	.....	.....
Slag	.....	.....	.....	.....	.....	.....

ELEMENTAL ANALYSES
(MASS %) Slag constituents are shown as oxides; all others as elements

	Al/Al2O3	C	Ca/CaO	Cr/Cr2O3	Fe/FeO	H	K/K2O	Mg/MgO	Mn/Mn2O3	N	Na/Na2O
PRODUCTS 1											
Gas	.....	41.088	.....	.....	.....	0.748	.....	0.333	0.248	1.102	.....
Dust	0.634	5.679	0.035	0.007	41.578	0.165	.....	0.405	0.370	0.162	.....
Solids	.....	100.000	.....	.....	.....	.....	.....	.....	.....	.....	.....
Slag	3.402	.....	0.252	0.022	2.318	.....	.....	1.452	0.967	.....	.....
Metal	.....	2.719	.....	0.003	96.308	.....	.....	.....	0.120	.....	.....
PRODUCTS 2											
Gas	.....	42.054	.....	.....	.....	0.777	.....	.....	.....	1.137	.....
Slag	1.010	2.854	0.041	0.008	45.081	.....	.....	5.443	3.599	.....	.....

	Ni	O	P/P2O5	S	Si/SiO2	Ti/TiO2	V/V2O5	Zr/ZrO2
PRODUCTS 1								
Gas	.....	56.074	.....	0.016	0.393	.....	.....	.....
Dust	.....	29.933	0.031	0.010	0.493	20.158	0.262	0.079
Solids	.....	.....	.....	.....	.....	.....	.....	.....
Slag	.....	36.222	0.143	0.010	1.719	95.377	0.269	0.304
Metal	.....	.....	0.020	0.005	0.242	0.100	0.482	.....
PRODUCTS 2								
Gas	.....	56.031	.....	0.000	.....	.....	.....	.....
Slag	.....	34.413	0.059	0.146	8.314	28.339	0.394	0.090

DISTRIBUTION OF ELEMENTS

PRODUCTS 1	Gas	Dust	Solids	Slag	Metal	Matte
Al:	.....	3.000%	.....	97.000%	.....	.....
C :	78.065%	1.029%	14.012%	.....	6.893%	.....
Ca:	.....	1.667%	.....	98.333%	.....	.....
Cr:	.....	3.000%	.....	77.600%	19.400%	.....
Fe:	.....	2.949%	.....	1.455%	95.595%	.....
H :	97.944%	2.056%	.....	.....	.....	.....
Mg:	25.169%	2.921%	.....	71.910%	.....	.....
Mn:	21.120%	3.000%	.....	62.197%	13.683%	.....
N :	98.621%	1.379%	.....	.....	.....	.....
O :	57.070%	2.905%	.....	40.025%	.....	.....
P :	.....	3.000%	.....	69.563%	27.437%	.....
S :	45.706%	2.818%	.....	31.884%	19.592%	.....
Si:	24.014%	2.876%	.....	53.365%	19.745%	.....
Ti:	.....	2.997%	.....	96.795%	0.208%	.....
V :	.....	3.000%	.....	19.685%	77.315%	.....
Zr:	.....	3.000%	.....	97.000%	.....	.....

PRODUCTS 2	Gas	Dust	Solids	Slag	Metal	Matte
Al:	.....	.....	.....	100.000%	.....	.....
C :	99.225%	.....	.....	0.775%	.....	.....
Ca:	.....	.....	.....	100.000%	.....	.....
Cr:	.....	.....	.....	100.000%	.....	.....
Fe:	.....	.....	.....	100.000%	.....	.....
H :	100.000%	.....	.....	.....	.....	.....
Mg:	.....	.....	.....	100.000%	.....	.....
Mn:	.....	.....	.....	100.000%	.....	.....
N :	100.000%	.....	.....	.....	.....	.....
O :	93.394%	.....	.....	6.606%	.....	.....
P :	.....	.....	.....	100.000%	.....	.....
S :	0.044%	.....	.....	99.956%	.....	.....
Si:	.....	.....	.....	100.000%	.....	.....
Ti:	.....	.....	.....	100.000%	.....	.....
V :	.....	.....	.....	100.000%	.....	.....
Zr:	.....	.....	.....	100.000%	.....	.....

PYROSIM v1.57 Copyright 26-JUL

APPENDIX H TYPICAL SPECIFICATIONS FOR TITANIA FEEDSTOCK

The tables (Table H1 & Table H2) summarise the technical specifications for the sulfate and chloride pigment production processes.

Table H1: Typical specifications for feedstocks used in the chloride process

Compound	Specification	Comment
Al_2O_3	< 1.50%	A consumer of chlorine and coke. Causes corrosion and sludge formation. A process to convert aluminium impurities to solids is typically required.
SiO_2	< 2.00%	Silica can prevent efficient chlorination. Silica and zirconia can build-up and block the reactor. Unblocking or purging is expensive. SiO_2 also condenses partly with $TiCl_4$ and requires separation.
MnO	< 2.00%	Some users specify a combined maximum (MnO+MgO) MnO (and FeO) consume coke and increase gas volumes.
MgO	< 1.20%	Alkali earth oxides form low-melting-point chlorides liquid at chlorination temperatures and can cause blockages
CaO	< 0.13%	
Cr_2O_3	< 0.25%	Chromium and vanadium as both can cause potential toxicity of iron chloride waste. V_2O_5 follows $TiCl_4$ and requires additional steps to remove.
V_2O_5	< 0.60%	
U+Th	< 100 ppm	U+Th is concentrated in waste and process streams
As, Sn	Minimise	Concentrates in $TiCl_4$ (after distillation) and thus needs to be minimized in feedstock
Fe	Minimise	To minimise waste generation, lower iron content is favoured. MnO and FeO forms solid/liquid phases chlorides sludge that blocks ducting
Other		Bulk density and particle size distribution critical to fluidisation, and to minimise fines losses. Cr and V contribute to the hazardous rating of effluents and wastes.

(Fisher, 1997; Maharajh *et al.*, 2015; Stanaway, 1994a,b)

Table H2: Typical specifications for feedstocks used in the sulfate process

Compound	Specification	Comment
rutile	avoided	Rutile is insoluble in sulfuric acid (H_2SO_4), and the use of natural and synthetic rutile and pseodorutile are excluded as feedstock
Fe	'low'	Low iron is desired as it minimises waste disposal requirements, reagent consumption and supports optimisation of plant capacity. Ferric iron is undesirable while some ferrous iron facilitates TiO_2 precipitation.
P_2O_5	<0.05%	Calcium and phosphorous negatively impact crystal development.
CaO	<0.20%	
Cr_2O_3	<0.1%	Minimise due to impact on product quality (discolouration of white pigment). Cr and V can potentially increase disposal costs of hazardous waste.
V_2O_5	'low'	
Nb_2O_5	<0.1%	
U+Th	<100 ppm	Limit input as it concentrates in product and waste streams (preferred levels below <50 ppm)
		Cr and V contributes to the hazardous rating of effluents and wastes

(Stanaway, 1994a,b)